

Images from red cells

Edited by

Giampaolo Minetti, Paola Bianchi, Lars Kaestner and
Anna Bogdanova

Published in

Frontiers in Physiology



FRONTIERS EBOOK COPYRIGHT STATEMENT

The copyright in the text of individual articles in this ebook is the property of their respective authors or their respective institutions or funders. The copyright in graphics and images within each article may be subject to copyright of other parties. In both cases this is subject to a license granted to Frontiers.

The compilation of articles constituting this ebook is the property of Frontiers.

Each article within this ebook, and the ebook itself, are published under the most recent version of the Creative Commons CC-BY licence. The version current at the date of publication of this ebook is CC-BY 4.0. If the CC-BY licence is updated, the licence granted by Frontiers is automatically updated to the new version.

When exercising any right under the CC-BY licence, Frontiers must be attributed as the original publisher of the article or ebook, as applicable.

Authors have the responsibility of ensuring that any graphics or other materials which are the property of others may be included in the CC-BY licence, but this should be checked before relying on the CC-BY licence to reproduce those materials. Any copyright notices relating to those materials must be complied with.

Copyright and source acknowledgement notices may not be removed and must be displayed in any copy, derivative work or partial copy which includes the elements in question.

All copyright, and all rights therein, are protected by national and international copyright laws. The above represents a summary only. For further information please read Frontiers' Conditions for Website Use and Copyright Statement, and the applicable CC-BY licence.

ISSN 1664-8714
ISBN 978-2-83251-459-7
DOI 10.3389/978-2-83251-459-7

About Frontiers

Frontiers is more than just an open access publisher of scholarly articles: it is a pioneering approach to the world of academia, radically improving the way scholarly research is managed. The grand vision of Frontiers is a world where all people have an equal opportunity to seek, share and generate knowledge. Frontiers provides immediate and permanent online open access to all its publications, but this alone is not enough to realize our grand goals.

Frontiers journal series

The Frontiers journal series is a multi-tier and interdisciplinary set of open-access, online journals, promising a paradigm shift from the current review, selection and dissemination processes in academic publishing. All Frontiers journals are driven by researchers for researchers; therefore, they constitute a service to the scholarly community. At the same time, the *Frontiers journal series* operates on a revolutionary invention, the tiered publishing system, initially addressing specific communities of scholars, and gradually climbing up to broader public understanding, thus serving the interests of the lay society, too.

Dedication to quality

Each Frontiers article is a landmark of the highest quality, thanks to genuinely collaborative interactions between authors and review editors, who include some of the world's best academicians. Research must be certified by peers before entering a stream of knowledge that may eventually reach the public - and shape society; therefore, Frontiers only applies the most rigorous and unbiased reviews. Frontiers revolutionizes research publishing by freely delivering the most outstanding research, evaluated with no bias from both the academic and social point of view. By applying the most advanced information technologies, Frontiers is catapulting scholarly publishing into a new generation.

What are Frontiers Research Topics?

Frontiers Research Topics are very popular trademarks of the *Frontiers journals series*: they are collections of at least ten articles, all centered on a particular subject. With their unique mix of varied contributions from Original Research to Review Articles, Frontiers Research Topics unify the most influential researchers, the latest key findings and historical advances in a hot research area.

Find out more on how to host your own Frontiers Research Topic or contribute to one as an author by contacting the Frontiers editorial office: frontiersin.org/about/contact

Images from red cells

Topic editors

Giampaolo Minetti — University of Pavia, Italy

Paola Bianchi — IRCCS Ca 'Granda Foundation Maggiore Policlinico Hospital, Italy

Lars Kaestner — Saarland University, Germany

Anna Bogdanova — University of Zurich, Switzerland

Citation

Minetti, G., Bianchi, P., Kaestner, L., Bogdanova, A., eds. (2023). *Images from red cells*. Lausanne: Frontiers Media SA. doi: 10.3389/978-2-83251-459-7

Table of contents

- 05 **Editorial: Images from red cell**
Paola Bianchi, Giampaolo Minetti, Anna Bogdanova and Lars Kaestner
- 08 **Rare Anemias: Are Their Names Just Smoke and Mirrors?**
Greta Simionato, Richard van Wijk, Stephan Quint, Christian Wagner, Paola Bianchi and Lars Kaestner
- 13 **Osmotic Vesicle Collapse of Sealed Inside–Out Membrane Vesicles From Red Blood Cells**
Teresa Tiffert and Virgilio L. Lew
- 17 **Redox Properties of Human Erythrocytes Are Adapted for Vitamin C Recycling**
Michael Eigenschink, Danylo Savran, Christoph P. Zitterer, Sebastian Granitzer, Magdalena Fritz, David M. Baron, Ernst W. Müllner and Ulrich Salzer
- 29 **Development of Mechanical Stability in Late-Stage Embryonic Erythroid Cells: Insights From Fluorescence Imaged Micro-Deformation Studies**
Luis F. Delgadillo, Yu Shan Huang, Sami Leon, James Palis and Richard E. Waugh
- 42 **Imaging Erythrocyte Sedimentation in Whole Blood**
Alexis Darras, Hans Georg Breunig, Thomas John, Renping Zhao, Johannes Koch, Carsten Kummerow, Karsten König, Christian Wagner and Lars Kaestner
- 52 **Transmission Electron Microscopy to Follow Ultrastructural Modifications of Erythroblasts Upon *ex vivo* Human Erythropoiesis**
Alice Dussouchaud, Julieta Jacob, Charles Secq, Jean-Marc Verbavatz, Martina Moras, Jérôme Larghero, Claudio M. Fader, Mariano A. Ostuni and Sophie D. Lefevre
- 67 **Storage-Induced Micro-Erythrocytes Can Be Quantified and Sorted by Flow Cytometry**
Mickaël Marin, Sandy Peltier, Youcef Hadjou, Sonia Georgeault, Michaël Dussiot, Camille Roussel, Olivier Hermine, Philippe Roingeard, Pierre A. Buffet and Pascal Amireault
- 77 **Reticulocyte Maturation and Variant Red Blood Cells**
Christian J. Stevens-Hernandez, Joanna F. Flatt, Sabine Kupzig and Lesley J. Bruce
- 86 **The Relation Between Extracellular Vesicles Released From Red Blood Cells, Their Cargo, and the Clearance by Macrophages**
Duc Bach Nguyen, Hanh Triet Tran, Lars Kaestner and Ingolf Bernhardt
- 99 **Membrane Localization of Piezo1 in the Context of Its Role in the Regulation of Red Blood Cell Volume**
Bojan Božič and Saša Svetina

- 107 **Light and Scanning Electron Microscopy of Red Blood Cells From Humans and Animal Species Providing Insights into Molecular Cell Biology**
Gheorghe Benga and Guy Cox
- 120 **The protective effect of the spleen in sickle cell patients. A comparative study between patients with asplenia/hyposplenism and hypersplenism**
Sari Peretz, Leonid Livshits, Ethersia Pretorius, Asya Makhro, Anna Bogdanova, Max Gassmann, Ariel Koren and Carina Levin



OPEN ACCESS

EDITED AND REVIEWED BY

Eitan Fibach,
Hadassah Medical Center, Israel

*CORRESPONDENCE

Paola Bianchi,
✉ paola.bianchi@policlinico.mi.it
Lars Kaestner,
✉ lars_kaestner@me.com

SPECIALTY SECTION

This article was submitted to Red Blood Cell Physiology, a section of the journal Frontiers in Physiology

RECEIVED 01 December 2022

ACCEPTED 13 December 2022

PUBLISHED 12 January 2023

CITATION

Bianchi P, Minetti G, Bogdanova A and Kaestner L (2023), Editorial: Images from red cell.
Front. Physiol. 13:1113951.
doi: 10.3389/fphys.2022.1113951

COPYRIGHT

© 2023 Bianchi, Minetti, Bogdanova and Kaestner. This is an open-access article distributed under the terms of the [Creative Commons Attribution License \(CC BY\)](https://creativecommons.org/licenses/by/4.0/). The use, distribution or reproduction in other forums is permitted, provided the original author(s) and the copyright owner(s) are credited and that the original publication in this journal is cited, in accordance with accepted academic practice. No use, distribution or reproduction is permitted which does not comply with these terms.

Editorial: Images from red cell

Paola Bianchi^{1*}, Giampaolo Minetti^{2,3}, Anna Bogdanova⁴ and Lars Kaestner^{5,6*}

¹Hematology Unit, Physiopathology of Anemias Unit, Fondazione IRCCS Ca' Granda Ospedale Maggiore Policlinico Milano, Milan, Italy, ²Red Blood Cell Research Group, Institute of Veterinary Physiology, and Center for Clinical Studies (ZKS), Vetsuisse Faculty, University of Zurich, Zurich, Switzerland, ³Zurich Center for Integrative Human Physiology (ZIHP), Zurich, Switzerland, ⁴Department of Biology and Biotechnology "L. Spallanzani", Laboratories of Biochemistry, University of Pavia, Pavia, Italy, ⁵Theoretical Medicine and Biosciences, Medical Faculty, Saarland University, Homburg, Germany, ⁶Dynamics of Fluids, Experimental Physics, Saarland University, Saarbruecken, Germany

KEYWORDS

red blood cell morphology, anemia, membrane-skeleton, ion channels, reticulocyte, membrane vesicles

Editorial on the Research Topic Images from Red Cells

Red blood cell (RBC) morphology is always a fascinating Research Topic. Being the most abundant cells in the organism that are easily collected, RBCs have been the object of research since the beginning of cellular morphological investigations (Bessis, 1974; Bain, 2005; Invernizzi et al., 2020). The many different shapes of RBCs reflect not only the cell integrity/abnormality but also its age and physical state. The different shapes of RBCs inspired morphologists, pathologists, and hematologists in naming different pathogenic conditions. Because of their “apparent” simplicity, resulting from the loss of all intracellular organelles that is associated to physiological deformability, fundamental for their squeezing through narrow capillaries of the microvasculature and splenic slits, RBCs have been considered for many years as mere hemoglobin-containing bags fit for oxygen delivery to and CO₂ removal from peripheral tissues.

However, new advancements in the research on cell ion balance, membrane transporters and cytoskeletal structure, and in studying RBC morphology, as well as novel insight into erythroid maturation, have shed new light on more detailed features of the physiology of these cells, reviving the interest in this cell that has served for decades as a model for studies of cell biology, membrane architecture and dynamics, pathophysiology, and drug delivery (Kaestner 2004; Kaestner and Minetti, 2017).

In the Research Topic—“*Images from Red cells*”, we provided a platform for exposing the main advancements in the ongoing RBC research. Twelve papers were published in the first volume. Inspired by this success, the second volume under the same title was initiated.

The opening article (Simionato et al.) focused on traditional and recent approaches to the study of RBC morphology. The new approaches, including 3D evaluation combined with artificial intelligence, ektacytometry and next-generation sequencing, suggest that not always the morphological-based nomenclature of some defects is sufficiently accurate and exhaustive in describing the pathogenic mechanisms involved. This is the case, for example, for band 3 protein defects that may result in spherocytosis, ovalocytosis or stomatocytosis, depending on the position of causative mutations (Bruce, 2006; Flatt and Bruce, 2018).

A very extensive overview of RBC morphology in different species is given by Benga and Cox, who evaluated RBCs by light- and scanning electron-microscopy. They focused on the water channel protein, aquaporin1, that ensures the exchange of water across the RBC membrane, as required in different species in relation to their physical activity, metabolic rate, and their mean blood flow rate.

Imaging RBCs is commonly performed on RBCs that are fixed and placed on a coverslip, thus precluding their dynamic imaging in action, e.g., *in vivo* (Kihm et al., 2021) or during measurements of their sedimentation rate *in vitro*. The latter is of particular interest since the model involving the sedimentation of RBC-aggregates was replaced by a percolating gel-based colloidal physics theory (Darras et al., 2022a). In their new contribution, Darras et al. present different imaging approaches, providing visual evidence for the breakdown of the percolating gel formed by RBCs as the mechanism underlying sedimentation during ESR measurements.

In recent years, ion channels represent an intriguing Research Topic of research associated with RBC morphology and cell volume regulation (von Lindern et al., 2022). Piezo1, for example, is a non-specific cation channel involved in RBC volume regulation; gain-of-function mutations in its gene are responsible for hereditary xerocytosis. Recent results based on high-resolution atomic force- and confocal-microscopy studies, indicate that this protein is distributed in the RBC membrane in a non-uniform manner (Dumitru et al., 2021). Božič and Svetina developed a mathematical model by minimizing the bending energy and the free energy of freely-moving membrane inclusions and used it to confirm the non-homogeneous distribution of Piezo1 molecules in the RBC membrane.

Aberrant maturation of RBCs from reticulocytes is involved in some RBC pathologies (Moura et al., 2020). The morphological changes during this process have been the object of different studies. During maturation, reticulocytes reduce their plasma membrane, removing or degrading residual internal organelles, proteins and membranes. By comparing the profile of pure cultured reticulocyte preparations and cells from different diseases, Stevens-Hernandez et al. showed that the size and composition of the different cells correlate with the different stages of reticulocyte maturation. A tight relationship between RBC volume, amount of intracellular unremoved proteins and immaturity has been observed in overhydrated hereditary stomatocytosis. Using transmission electron microscopy, Dussouchaud et al. followed ultrastructural changes of RBC precursors (erythroblasts) upon *ex vivo* human erythropoiesis. They showed that mitochondria are progressively cleared between the polychromatophilic erythroblast (Poly-E) to orthochromatophilic erythroblast (Ortho-E) stages. Furthermore, the intracellular vesicle trafficking depicts changes in endosomes and exosomes during the basophilic erythroblast to Poly-E transition; autophagosomes, in particular, are increased from pro-erythroblast to Ortho-E stages. The combined use of fluorescence labeling and micro-manipulation of RBCs has proven to be a powerful tool for studying the development of the bilayer-associated membrane skeleton in primary embryonic erythroid cells. Using this approach, Delgadillo et al., demonstrated that the localization of membrane-skeletal components of mammalian erythroid cells during their development is insufficient by itself to produce a mature membrane-skeleton, and that additional, subsequent, processes are required to strengthen intra-skeletal interactions.

Extracellular vesicles have been in the focus of other contributions in this Research Topic. They are cell-derived membrane particles including exosomes, ectosomes, microvesicles and microparticles. Some of them are formed during apoptosis. Vesicles are often involved in intercellular communication or in the transport of macromolecules between cells. Nguyen et al. tested the ability of RBC-derived vesicles to serve as potential drug carriers by loading them with DNA plasmids coding for the green fluorescent protein.

The modified vesicles were used to transfect THP-1-derived macrophages, which were then analyzed by fluorescence microscopy and flow cytometry. Although the treated vesicles were almost completely taken up by macrophages, the expression of the green fluorescent protein was only observed in a subpopulation of macrophages.

Usually, membrane vesicles are generated *in vitro* in media of extremely low tonicity. However, to maintain the concentration of substrates for various transporters and enzymes within the physiological range, vesicles should be suspended in media of higher tonicity. Tiffert and Lew investigated, by electron microscopy, the effects of these hypertonic changes on vesicle morphology. They demonstrated that hypertonic transitions cause an irreversible osmotic collapse of sealed membrane vesicles. Awareness of these phenomena is critical for the interpretation of experimental results.

Microenvironmental conditions associated with RBC storage, the presence or absence of the spleen, as well as the changes in the intraerythrocytic master regulators such as the redox balance and energy status (ATP concentration), have impact on RBC morphology. Cold storage of RBCs is associated with the accumulation of various morphological and functional alterations. Small “micro-erythrocytes” that accumulate during storage in variable amounts from donor to donor are cleared rapidly after transfusion and their proportion correlates with transfusion recovery. Investigating these changes is of utmost importance in transfusion medicine. Marin et al. studied and quantified micro-spherocyte formation by imaging flow cytometry. These strategies would further facilitate physiologically-relevant quality control of erythrocyte concentrates.

Sickle cell disease, caused by a point mutation in the beta-globin gene, got its name from a typical RBC morphology associated with the formation of aggregates of sickle hemoglobin. In a cooperative study, Peretz et al. investigated in these patients the association between the spleen status (hyper/hypo or asplenic) with clinical, laboratory and morphological parameters.

Finally, attention has been given to the redox properties of human RBCs, and in particular to their adaptation to vitamin C (ascorbic acid) recycling. In their study, Eigenschink et al. showed that the uptake of dehydroascorbate, the fully oxidized form of this vitamin, largely affects the redox metabolism of human RBCs by lowering cellular levels of reactive oxygen species and elevating the plasma membrane electron transport activity.

All the above-mentioned contributions to the second volume of “*Images from Red Cell*” provide evidence to the general notion that “seeing is believing”. We trust that this new article Research Topic will set a milestone and prove that the story continues.

Author contributions

All authors listed have made a substantial, direct, and intellectual contribution to the work and approved it for publication.

Conflict of interest

The authors declare that the research was conducted in the absence of any commercial or financial relationships that could be construed as a potential conflict of interest.

Publisher's note

All claims expressed in this article are solely those of the authors and do not necessarily represent those of their affiliated

organizations, or those of the publisher, the editors and the reviewers. Any product that may be evaluated in this article, or claim that may be made by its manufacturer, is not guaranteed or endorsed by the publisher.

References

- Bain, B. J. (2005). Diagnosis from the blood smear. *NEJM* 353 (5), 498–507. doi:10.1056/NEJMra043442
- Bessis, M. (1974). *Corpuscles: Atlas of red blood cell shapes*. Berlin and Heidelberg: Springer-Verlag.
- Bruce, L. (2006). Mutations in band 3 and cation leaky red cells. *Blood Cells Mol. Dis.* 36 (3), 331–336. doi:10.1016/j.bcmd.2006.01.008
- Darras, A., Dasanna, A. K., John, T., Gompfer, G., Kaestner, L., Fedosov, D. A., et al. (2022a). Erythrocyte sedimentation: Collapse of a high-volume-fraction soft-particle gel. *Phys. Rev. Lett.* 128 (8), 088101. doi:10.1103/PhysRevLett.128.088101
- Dumitru, A. C., Stommen, A., Koehler, M., Cloos, A. S., Yang, J., Leclercqz, A., et al. (2021). Probing PIEZO1 localization upon activation using high-resolution atomic force and confocal microscopy. *Nano Lett.* 21, 4950–4958. doi:10.1021/acs.nanolett.1c00599
- Flatt, J. F., and Bruce, L. J. (2018). The molecular basis for altered cation permeability in hereditary stomatocytic human red blood cells. *Front. Physiol.* 9, 367. doi:10.3389/fphys.2018.00367
- Invernizzi, R. (2020). “Chapter 26: Inherited hemolytic anemias,” in *Haematologica atlas of hematologic cytology*. Pavia, Italy: The Ferrata-Storti Foundation, 204–217.
- Kaestner, L., and Minetti, G. (2017). The potential of erythrocytes as cellular aging models. *Cell. Death Differ.* 24 (9), 1475–1477. doi:10.1038/cdd.2017.100
- Kaestner, L. (2004). Red blood cell ghosts and intact red blood cells as complementary models in photodynamic cell research. *Bioelectrochemistry* 62 (2), 123–126. doi:10.1016/j.bioelechem.2003.08.005
- Kihm, A., Quint, S., Laschke, M. W., Menger, M. D., John, T., Kaestner, L., et al. (2021). Lingering dynamics in microvascular blood flow. *Biophys. J.* 120 (3), 432–439. doi:10.1016/j.bpj.2020.12.012
- Moura, P. L., Hawley, B. R., Dobbe, I. G. G., Streekstra, G. J., Rab, M. A. E., Bianchi, P., et al. (2020). *PIEZO1* gain-of-function mutations delay reticulocyte maturation in hereditary xerocytosis. *Haematologica* 105 (6), e268–e271. doi:10.3324/haematol.2019.231159
- von Lindern, M., Egée, S., Bianchi, P., and Kaestner, L. (2022). The function of ion channels and membrane potential in red blood cells: Toward a systematic analysis of the erythroid channelome. *Front. Physiol.* 13, 824478. doi:10.3389/fphys.2022.824478



Rare Anemias: Are Their Names Just Smoke and Mirrors?

Greta Simionato^{1,2}, Richard van Wijk³, Stephan Quint^{2,4}, Christian Wagner^{2,5}, Paola Bianchi⁶ and Lars Kaestner^{2,7*}

¹ Institute for Clinical and Experimental Surgery, Campus University Hospital, Saarland University, Homburg, Germany,

² Experimental Physics, Dynamics of Fluids Group, Saarland University, Saarbrücken, Germany, ³ Central Diagnostic Laboratory - Research, University Medical Center Utrecht, Utrecht University, Utrecht, Netherlands, ⁴ Cysmic GmbH, Saarbrücken, Germany, ⁵ Physics and Materials Science Research Unit, University of Luxembourg, Luxembourg, Luxembourg, ⁶ Fondazione Istituto di Ricovero e Cura a Carattere Scientifico Ca' Granda Ospedale Maggiore Policlinico Milano, Unità Operativa Complessa Ematologia, Unità Operativa Semplice Fisiopatologia delle Anemie, Milan, Italy,

⁷ Theoretical Medicine and Biosciences, Campus University Hospital, Saarland University, Homburg, Germany

Keywords: rare anemias, red cell morphology, hereditary spherocytosis, dehydrated stomatocytosis, hereditary xerocytosis, Gárdos channelopathy

INTRODUCTION

Numerous anemias and even neurodegenerative diseases are named after the predominant red blood cell (RBC) shape observed by microscopy - within this paper we refer to this as RBC morphology. Examples are spherocytes in hereditary spherocytosis (Huisjes et al., 2019), stomatocytes in hereditary stomatocytosis (Andolfo et al., 2018), elliptocytes in hereditary elliptocytosis (Soderquist and Bagg, 2013), sickle shaped deoxygenated RBCs in sickle cell disease (Cisneros and Thein, 2020), or acanthocytes in neuroacanthocytosis syndromes (Peikert et al., 2017).

A good portion of these names are justified because a substantial portion of the patient RBCs show at least under particular conditions the corresponding morphology. At the same time we have to admit that sometimes the shape classification can be confusing when, for example, sphero-ovalocytes (Jarolim et al., 1995), ovalocytes (Mohandas et al., 1984), elliptocytes (Motulsky et al., 1954), or poikilocytes (Agre et al., 1981) can all be attributed to the same disease: elliptocytosis.

The clinical evaluation of the cell shapes depends widely on the use of peripheral blood smears, i.e., a drop of fresh blood is smeared on a glass slide, dried, fixed and stained, a procedure that partly deteriorates the original cell morphology (Wenk, 1976). Extensive work was performed to characterize RBC shapes at electron microscopic super-resolution in 3D. These partly artistic images culminated in the seminal work by Marcel Bessis in the last century (Bessis, 1973). In the meantime, optical imaging technology progressed, e.g., confocal microscopy became widely available (Pawley, 2006) and was explored for the 3D-visualization of RBCs both in stasis (Khairy et al., 2008) and in flow (Quint et al., 2017). Optical technologies have less stringent requirements for sample preparation compared to electron microscopy (Abay et al., 2019). Confocal microscopy combined with automated processes including machine learning-based algorithms seems to lead to a revival of RBC visualization in 3D and the subsequent shape evaluation (Kaestner and Bianchi, 2020), shedding new lights on RBC morphological complexity. It is worthwhile to mention that 3D renderings based on confocal microscopy allow, in contrast to electron microscopy and probe scanning techniques, an unlimited 360° view.

Furthermore, RBC in their physiological environment are in constant flow and at least in capillary flow take completely different cell shapes as in stasis, e.g., discocytes are transformed into “croissants” or “slippers” in a flow speed dependent manner (Kihm et al., 2018). For most pathophysiological conditions RBC morphology in (capillary) flow are not investigated, which is a so far missed diagnostic potential but at the same time is not in favor of naming anemias after RBC shapes in stasis.

OPEN ACCESS

Edited by:

Wassim El Nemer,
French Blood Establishment
(EFS), France

Reviewed by:

Roberta Russo,
University of Naples Federico II, Italy
Véronique Picard,
Assistance Publique Hôpitaux de
Paris, France

*Correspondence:

Lars Kaestner
lars_kaestner@me.com

Specialty section:

This article was submitted to
Red Blood Cell Physiology,
a section of the journal
Frontiers in Physiology

Received: 03 April 2021

Accepted: 17 May 2021

Published: 10 June 2021

Citation:

Simionato G, van Wijk R, Quint S,
Wagner C, Bianchi P and Kaestner L
(2021) Rare Anemias: Are Their
Names Just Smoke and Mirrors?
Front. Physiol. 12:690604.
doi: 10.3389/fphys.2021.690604

Here we like to discuss examples of rare anemias named after the RBC shapes found in blood smears that are not representative of the disease condition based on both new microscopy applications and functional tests.

SPHEROCYTE NUMBERS IN HEREDITARY SPHEROCYTOSIS - COMPARISON BETWEEN 2D AND 3D IMAGES

A recent study investigated the use of an artificial neural network to automatically recognize RBC shapes, proposing that the detailed 3D analysis may even identify the specific genetic defect causing a particular rare anemia (Simionato et al., 2021). As a side information, it was found that the spherocytes identified in peripheral blood smears from patients with hereditary spherocytosis are mostly just “pseudo spherocytes” (see **Figure 1**). The figure illustrates that information indeed gets lost in 2D images. Furthermore, the almost exclusive occurrence of “pseudo spherocytes” *per se* (not their number) seems to be independent of the particular mutation causing the hereditary spherocytosis.

This finding is actually not new, since Bessis already stated: “The cells it describes (spherocytes) are actually not spheres. They include a variety of cells which are etiologically and morphologically dissimilar. They have only one thing in common: an increase in their thickness” (Bessis, 1974). The scanning electron microscopy (SEM) allows a 3D surface scan (although not a 360° view), which allowed Bessis to make this statement and which is 100% confirmed by the 3D renderings based on confocal measurements (**Figure 1**).

DEHYDRATED STOMATOCYTOSIS IS A TERMINOLOGY CONTRADICTION IN ITSELF

When referring to RBC dehydration, currently we face two completely different approaches. The traditional one refers to the RBC shapes. If cells dehydrate, i.e., if they lose water, they shrink and this is associated with the formation of echinocytes. This holds true albeit there are also other isovolumetric mechanisms to transform discocytes into echinocytes (Fischer, 2003). The well-known but mechanistically elusive “glass effect” belongs to this kind of transformation. The way around, if RBC overhydrate, the uptake of water swells the discocytes toward a sphere through intermediate forms of stomatocytes (Lim et al., 2002). From that point of view, the terminology of “dehydrated stomatocytosis” is indeed a contradiction in itself. The alternative denomination for “dehydrated stomatocytosis” is “xerocytosis,” indicating the occurrence of another pathophysiological cell shape, the xerocytes. This partly addresses the aforementioned contradiction but the alternative use of both terms, “dehydrated stomatocytosis” and “xerocytosis” adds to the confusion.

However, there is the concept of testing osmotic resistance with the ektacytometry as an incarnation that allows widely automated testing under reproducible and interlaboratory

comparable conditions (Bianchi et al., 2015). This method became a kind of clinical standard and proved its usefulness in numerous hematological centers (Lazarova et al., 2017; Llaudet-Planas et al., 2018; Zaninoni et al., 2018; Vives-Corróns et al., 2021). In ektacytometry, a left shift of the osmotic fragility curve is compatible with a dehydration of the RBCs and due to differences in this curve, stomatocytosis was categorized into dehydrated and overhydrated stomatocytosis.

When comparing the two approaches, we favor the traditional cell shape-based concept because there is hardly any other option to explain the formation of stomatocytes, than overhydration. In contrast, a left shift of the curve in ektacytometry could have numerous explanations including the versatile composition of transmembrane transport proteins involved in volume regulation, such as the ion pumps Na^+/K^+ -ATPase (Petrushanko et al., 2017), the Ca^{2+} -ATPase (Dagher and Lew, 1988), ion channels such as TRPC6, Piezo1, the Gardos channel (Kaestner et al., 2020) or the recently described TRPV2 (Belkacemi et al., 2021), membrane transporters like band 3 protein (Bamberg and Passow, 1992) or the K^+/Cl^- -cotransporter (Adragna et al., 2006). Just to make it clear, we believe in the usefulness of ektacytometry as a diagnostic parameter for RBC-related diseases. It is only the strict terminological link to the hydration state that we like to discuss.

Although there is a deterministic relationship between hydration state and cell morphology in healthy RBCs as indicated by the SDE-scale (Lim et al., 2002), in the pathophysiological situations this relationship is widely distorted as the dehydration due to hemoglobinopathies indicate (Zaninoni et al., 2018; Krishnevskaia et al., 2021). Therefore, we believe the hydration state of the RBCs is an unsuitable parameter for disease classification.

DISCUSSION

The explanations above outline that a part of the nomenclature for rare anemias is not quite appropriate. The intention of this opinion paper is not to come up with a new terminology but to initiate the discussion about it. One possible and timely opportunity would be to orient the nomenclature of hereditary anemias on the mutation they are caused by, as it is done in other diseases, such as the “VSP13A disease,” which was proposed to replace “Chorea Acanthocytosis” (Walker and Danek, 2021). In hereditary dehydrated stomatocytosis/hereditary xerocytosis, we have partly experienced such a change. Mutations of the mechanosensitive ion channel Piezo1 were initially identified as the molecular cause for this disease (Zarychanski et al., 2012; Albuissou et al., 2013; Andolfo et al., 2013; Shmukler et al., 2014; Rotordam et al., 2018). Soon afterwards, a second molecular player was identified, namely the Gárdos channel (Andolfo et al., 2015; Glogowska et al., 2015; Rapetti-Mauss et al., 2015). However, it is increasingly recognized that the mutations of the Gárdos channel result in a distinct pathological phenotype compared to the mutations of Piezo1 and the former is now referred to as Gárdos channelopathy or *KCNN4* variants (Fermo et al., 2017, 2020). Ever since there is a kind of naming

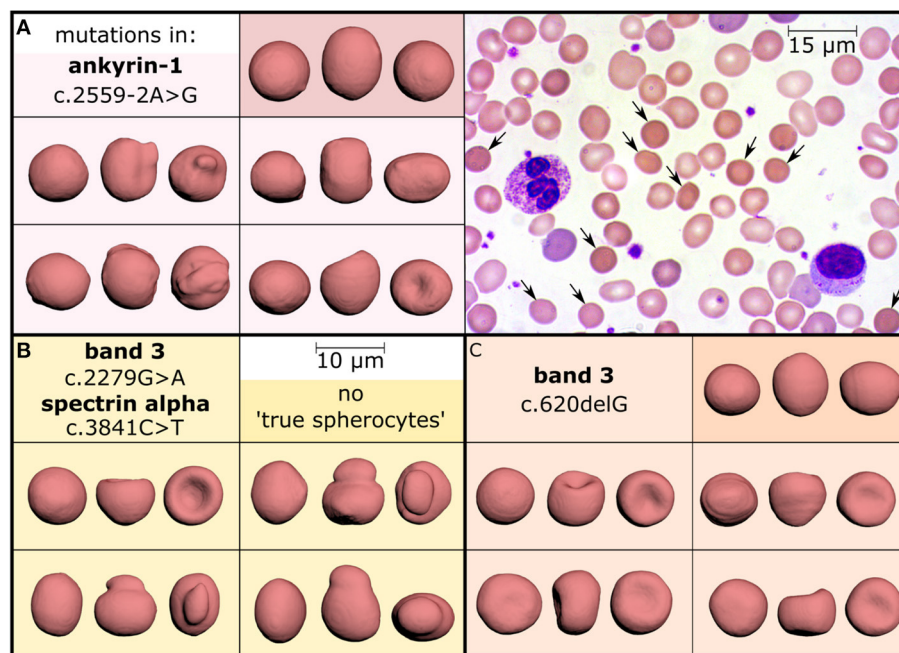


FIGURE 1 | Investigation of hereditary spherocytosis red blood cell shapes. Three patients diagnosed with hereditary spherocytosis caused by different mutations (panels **A–C**) showed a spherocyte count of 11% (**A**), 8% (**B**), and 10% (**C**) in their stained peripheral blood smears, as exemplified in panel **A** (arrows, objective-magnification 100x). Comparison with 3D-rendered confocal recordings (objective-magnification 60x) of glutaraldehyde fixed and CellMask stained cells, however, demonstrated a different percentage of “true spherocytes”: 2.5% (**A**), 0% (**B**), and 0.08% (**C**). They are visualized in the dark colored boxes, each showing one cell from three perpendicular directions and mostly reflecting the amount observed in healthy subjects (0–0.3%, examined in 15 donors). In contrast, many cells look like spherocytes from one direction (leftmost view in all boxes) but the other faces reveal different morphologies, such as mushroom-shaped cells, stomatocytes or other irregular-shaped cells (all light colored boxes) representing “pseudo spherocytes.” These observations could be confirmed in 10 hereditary spherocytosis patients after 3D-imaging of about 1,000 cells per subject. This Figure is a reprint of Simionato et al. (2021).

mess depending on the reporting authors, hereditary dehydrated stomatocytosis (hDSt) is differentiated into Piezo- or Gárdos-stomatocytosis, hDSt I and hDSt II or xerocytosis and Gárdos channelopathy, although this definition not always reflects the presence of stomatocytes or the dehydration state of the cell.

Also, in the case of hereditary spherocytosis we face two different problems: (i) sometimes spherocytes are not present and (ii) what we observe in blood films does not correspond to what we see in 3D (**Figure 1**). The 3D imaging approach helped us to realize that we need to think to a different nomenclature because morphology alone seems to be a limited diagnostic tool.

In any case, hereditary spherocytosis and hereditary stomatocytosis are presented here as examples to approach the problem. Hereditary spherocytosis because it is a well-known disease and among the rare anemias the most common one, with a clear diagnostic approach (Mohandas and Gallagher, 2008; Perrotta et al., 2008). However, in most centers of general medicine the first suspect of hereditary spherocytosis rises from the presence of spherocytes in the blood smear although it is known that the number of spherocytes may be low in most cases. On the contrary, the diagnosis of hereditary stomatocytosis was only based on morphological examination before the advent of the Next Generation Sequencing (NGS) technologies, and now we know that presence of stomatocytes may be associated to various different defects. Therefore, we

are convinced the name “stomatocytosis” is an example that the nomenclature is, based on the current knowledge, an insufficient naming.

We admit that the naming is much less confusing when it comes to the enzymopathies, pyruvate kinase deficiency (Bianchi and Fermo, 2020) or G6PD deficiency (Luzzatto and Arese, 2018) name the defect protein.

We propose here to tackle the nomenclature of membranopathies by a holistic concept considering the entity of hereditary anemias and the genetic variants they are caused by. This initiative is meant to make a transition for the nomenclature of rare anemias. Although just for a few of them applies that “their names are just smoke and mirrors” the transition is meant to follow “Nomen est omen” for all of them.

AUTHOR CONTRIBUTIONS

All authors listed have made a substantial, direct and intellectual contribution to the work, and approved it for publication.

FUNDING

This study was supported by the European Framework Horizon 2020 under grant agreement number 860436 (EVIDENCE).

Furthermore, we acknowledge support by the Deutsche Forschungsgemeinschaft (DFG, German Research Foundation)

and Saarland University within the funding programme Open Access Publishing.

REFERENCES

- Abay, A., Simionato, G., Chachanidze, R., Bogdanova, A., Hertz, L., Bianchi, P., et al. (2019). Glutaraldehyde – a subtle tool in the investigation of healthy and pathologic red blood cells. *Front. Physiol.* 10:514. doi: 10.3389/fphys.2019.00514
- Adragna, N. C., Ferrell, C. M., Zhang, J., Fulvio, M. D., Temprana, C. F., Sharma, A., et al. (2006). Signal transduction mechanisms of K⁺-Cl⁻-cotransport regulation and relationship to disease. *Acta Physiol.* 187, 125–139. doi: 10.1111/j.1748-1716.2006.01560.x
- Agre, P., Orringer, E. P., Chui, D. H., and Bennett, V. (1981). A molecular defect in two families with hemolytic poikilocytic anemia: reduction of high affinity membrane binding sites for ankyrin. *J. Clin. Invest.* 68, 1566–1576. doi: 10.1172/JCI110411
- Albuisson, J., Murthy, S. E., Bandell, M., Coste, B., Louis-dit-Picard, H., Mathur, J., et al. (2013). Dehydrated hereditary stomatocytosis linked to gain-of-function mutations in mechanically activated PIEZO1 ion channels. *Nat. Commun.* 4, 1–8. doi: 10.1038/ncomms3440
- Andolfo, I., Alper, S. L., Franceschi, L. D., Auriemma, C., Russo, R., Falco, L. D., et al. (2013). Multiple clinical forms of dehydrated hereditary stomatocytosis arise from mutations in PIEZO1. *Blood* 121, 3925–3935. doi: 10.1182/blood-2013-02-482489
- Andolfo, I., Russo, R., Gambale, A., and Iolascon, A. (2018). Hereditary stomatocytosis: an underdiagnosed condition. *Am. J. Hematol.* 93, 107–121. doi: 10.1002/ajh.24929
- Andolfo, I., Russo, R., Manna, F., Shmukler, B. E., Gambale, A., Vitiello, G., et al. (2015). Novel Gardos channel mutations linked to dehydrated hereditary stomatocytosis (xerocytosis). *Am. J. Hematol.* 90, 921–926. doi: 10.1002/ajh.24117
- Bamberg, E., and Passow, H. (1992) *The Band 3 Proteins: Anion Transporters, Binding Proteins and Senescent Antigens*. Amsterdam: Elsevier
- Belkacemi, A., Trost, C. F., Tinschert, R., Flormann, D., Malihpour, M., Wagner, C., et al. (2021). The TRPV2 channel mediates Ca²⁺ influx and the D9-THC-dependent decrease in osmotic fragility in red blood cells. *Haematologica* 106:274951. doi: 10.3324/haematol.2020.274951
- Bessis, M. (1973). *Living Blood Cells and Their Ultrastructure*. Berlin, Heidelberg: Springer-Verlag.
- Bessis, M. (1974). *Corpuscles, Atlas of Red Blood Cell Shapes*. Berlin, Heidelberg: Springer. doi: 10.1007/978-3-642-65657-6
- Bianchi, P., and Fermo, E. (2020). Molecular heterogeneity of pyruvate kinase deficiency. *Haematologica* 105:241141. doi: 10.3324/haematol.2019.241141
- Bianchi, P., Zaninoni, A., Fermo, E., Vercellati, C., Paola, M. A., Zanella, A., et al. (2015). Diagnostic power of laser assisted optical rotational cell analyzer (LoRRca MaxSis) evaluated in 118 patients affected by hereditary hemolytic anemias. *Blood* 126, 942–942. doi: 10.1182/blood.V126.23.942.942
- Cisneros, G. S., and Thein, S. L. (2020). Recent advances in the treatment of sickle cell disease. *Front. Physiol.* 11:435. doi: 10.3389/fphys.2020.00435
- Dagher, G., and Lew, V. L. (1988). Maximal calcium extrusion capacity and stoichiometry of the human red cell calcium pump. *J. Physiol.* 407, 569–586. doi: 10.1113/jphysiol.1988.sp017432
- Fermo, E., Bogdanova, A., Petkova-Kirova, P., Zaninoni, A., Marcello, A. P., Makhro, A., et al. (2017). “Gardos Channelopathy”: a variant of hereditary Stomatocytosis with complex molecular regulation. *Sci. Rep.* 7:1744. doi: 10.1038/s41598-017-01591-w
- Fermo, E., Monedero-Alonso, D., Petkova-Kirova, P., Makhro, A., Pérès, L., Bouyer, G., et al. (2020). Gardos channelopathy: functional analysis of a novel KCNN4 variant. *Blood Adv.* 4, 6336–6341. doi: 10.1182/bloodadvances.2020003285
- Fischer, T. M. (2003). “Human red cell shape and the mechanical characteristics of the membrane,” in *Red Cell Membrane Transport in Health and Disease*, eds I. Bernhardt and J. C. Ellory (Berlin, Heidelberg: Springer), 61–82. doi: 10.1007/978-3-662-05181-8_3
- Glogowska, E., Lezon-Geyda, K., Maksimova, Y., Schulz, V. P., and Gallagher, P. G. (2015). Mutations in the Gardos channel (KCNN4) are associated with hereditary xerocytosis. *Blood* 126, 1281–1284. doi: 10.1182/blood-2015-07-657957
- Huisjes, R., Makhro, A., Llaudet-Planas, E., Hertz, L., Petkova-Kirova, P., Verhagen, L. P., et al. (2019). Density, heterogeneity and deformability of red cells as markers of clinical severity in hereditary spherocytosis. *Haematologica* 105:188151. doi: 10.3324/haematol.2018.188151
- Jarolim, P., Wichterle, H., Hanspal, M., Murray, J., Robin, H. L., and Palek, J. (1995). β spectrinPRAGUE: a truncated β spectrin producing spectrin deficiency, defective spectrin heterodimer self-association and a phenotype of spherocytic elliptocytosis. *Brit. J. Haematol.* 91, 502–510. doi: 10.1111/j.1365-2141.1995.tb05330.x
- Kaestner, L., and Bianchi, P. (2020). Trends in the development of diagnostic tools for red blood cell-related diseases and anemias. *Front. Physiol.* 11:387. doi: 10.3389/fphys.2020.00387
- Kaestner, L., Bogdanova, A., and Egee, S. (2020). Calcium channels and calcium-regulated channels in human red blood cells. *Adv. Exp. Med. Biol.* 1131, 625–648. doi: 10.1007/978-3-030-12457-1_25
- Khairy, K., Foo, J., and Howard, J. (2008). Shapes of red blood cells: comparison of 3D confocal images with the bilayer-couple model. *Cell Mol. Bioeng.* 1:173. doi: 10.1007/s12195-008-0019-5
- Kihm, A., Kaestner, L., Wagner, C., and Quint, S. (2018). Classification of red blood cell shapes in flow using outlier tolerant machine learning. *PLoS Comput. Biol.* 14:e1006278. doi: 10.1371/journal.pcbi.1006278
- Krishnevskaya, E., Payán-Pernía, S., Hernández-Rodríguez, I., Sevilla, Á. F. R., Serra, Á. A., Morales-Indiano, C., et al. (2021). Distinguishing iron deficiency from beta-thalassemia trait by new generation ektacytometry. *Int. J. Lab Hematol.* 43, e58–e60. doi: 10.1111/ijlh.13362
- Lazarova, E., Gulbis, B., van Oirschot, B., and van Wijk, R. (2017). Next-generation osmotic gradient ektacytometry for the diagnosis of hereditary spherocytosis: interlaboratory method validation and experience. *Clin. Chem. Lab. Med.* 55, 394–402. doi: 10.1515/cclm-2016-0290
- Lim, G., Wortis, M., and Mukhopadhyay, R. (2002). Stomatocyte-discocyte-echinocyte sequence of the human red blood cell: evidence for the bilayer-couple hypothesis from membrane mechanics. *Proc. Natl. Acad. Sci. U. S. A.* 99, 16766–16769. doi: 10.1073/pnas.202617299
- Llaudet-Planas, E., Vives-Corrons, J. L., Rizzuto, V., Gómez-Ramírez, P., Navarro, J. S., Sibina, M. T. C., et al. (2018). Osmotic gradient ektacytometry: a valuable screening test for hereditary spherocytosis and other red blood cell membrane disorders. *Int. J. Lab. Hematol.* 40, 94–102. doi: 10.1111/ijlh.12746
- Luzzatto, L., and Arese, P. (2018). Favism and glucose-6-phosphate dehydrogenase deficiency. *New Engl. J. Med.* 378, 60–71. doi: 10.1056/NEJMr1708111
- Mohandas, N., and Gallagher, P. G. (2008). Red cell membrane: past, present, and future. *Blood* 112, 3939–3948. doi: 10.1182/blood-2008-07-161166
- Mohandas, N., Lie-Injo, L., Friedman, M., and Mak, J. (1984). Rigid membranes of Malayan ovalocytes: a likely genetic barrier against malaria. *Blood* 63, 1385–1392. doi: 10.1182/blood.V63.6.1385.1385
- Motulsky, A. G., Singer, K., Crosby, W. H., and Smith, V. (1954). The life span of the elliptocyte; hereditary elliptocytosis and its relationship to other familial hemolytic diseases. *Blood* 9, 57–72. doi: 10.1182/blood.V9.1.57.57
- Pawley, J. B. (2006). *Handbook of Biological Confocal Microscopy*. Boston, MA: Springer Verlag. doi: 10.1007/978-0-387-45524-2
- Peikert, K., Danek, A., and Hermann, A. (2017). Current state of knowledge in Chorea-Acanthocytosis as core Neuroacanthocytosis syndrome. *Eur. J. Med. Genet.* 61, 699–705. doi: 10.1016/j.ejmg.2017.12.007
- Perrotta, S., Gallagher, P. G., and Mohandas, N. (2008). Hereditary spherocytosis. *Lancet* 372, 1411–1426. doi: 10.1016/S0140-6736(08)61588-3
- Petrushanko, I., Yu., Mitkevich, V. A., Lakunina, V. A., Anashkina, A. A., Spirin, P. V., et al. (2017). Cysteine residues 244 and 458–459 within the catalytic subunit of Na,K-ATPase control the enzyme's hydrolytic and signaling function under hypoxic conditions. *Redox. Biol.* 13, 310–319. doi: 10.1016/j.redox.2017.05.021
- Quint, S., Christ, A. F., Guckenberger, A., Himbert, S., Kaestner, L., Gekle, S., et al. (2017). 3D tomography of cells in micro-channels. *Appl. Phys. Lett.* 111:103701. doi: 10.1063/1.4986392

- Rapetti-Mauss, R., Lacoste, C., Picard, V., Guitton, C., Lombard, E., Loosveld, M., et al. (2015). A mutation in the Gardos channel is associated with hereditary xerocytosis. *Blood* 126, 1273–1280. doi: 10.1182/blood-2015-04-642496
- Rotordam, G. M., Fermo, E., Becker, N., Barcellini, W., Brüggemann, A., Fertig, N., et al. (2018). A novel gain-of-function mutation of Piezo1 is functionally affirmed in red blood cells by high-throughput patch clamp. *Haematologica* 104:e179–83. doi: 10.3324/haematol.2018.201160
- Shmukler, B. E., Vidorpe, D. H., Rivera, A., Auerbach, M., Brugnara, C., and Alper, S. L. (2014). Dehydrated stomatocytic anemia due to the heterozygous mutation R2456H in the mechanosensitive cation channel PIEZO1: a case report. *Blood Cells Mol. Dis.* 52, 53–54. doi: 10.1016/j.bcmd.2013.07.015
- Simionato, G., Hinkelmann, K., Chachanidze, R., Bianchi, P., Fermo, E., Wijk, R., et al. (2021). Red blood cell phenotyping from 3D confocal images using artificial neural networks. *PLoS Comput. Biol.* 17:e1008934. doi: 10.1371/journal.pcbi.1008934
- Soderquist, C., and Bagg, A. (2013). Hereditary elliptocytosis. *Blood* 121, 3066–3066. doi: 10.1182/blood-2012-09-457788
- Vives-Corrons, J.-L., Krishnevskaya, E., Rodriguez, I. H., and Ancochea, A. (2021). Characterization of hereditary red blood cell membranopathies using combined targeted next-generation sequencing and osmotic gradient ektacytometry. *Int. J. Hematol.* 113, 163–174. doi: 10.1007/s12185-020-03010-9
- Walker, R. H., and Danek, A. (2021). “Neuroacanthocytosis” – overdue for a taxonomic update. *Tremor Other Hyperkinet. Mov.* 11:1. doi: 10.5334/tohm.583
- Wenk, R. E. (1976). Comparison of five methods for preparing blood smears. *Am. J. Med. Technol.* 42, 71–78.
- Zaninoni, A., Fermo, E., Vercellati, C., Consonni, D., Marcello, A. P., Zanella, A., et al. (2018). Use of laser assisted optical rotational cell analyzer (LoRRca MaxSis) in the diagnosis of rbc membrane disorders, enzyme defects, and congenital dyserythropoietic anemias: a monocentric study on 202 patients. *Front. Physiol.* 9:451. doi: 10.3389/fphys.2018.00451
- Zarychanski, R., Schulz, V. P., Houston, B. L., Maksimova, Y., Houston, D. S., Smith, B., et al. (2012). Mutations in the mechanotransduction protein PIEZO1 are associated with hereditary xerocytosis. *Blood* 120, 1908–1915. doi: 10.1182/blood-2012-04-422253

Conflict of Interest: The authors declare that the research was conducted in the absence of any commercial or financial relationships that could be construed as a potential conflict of interest.

Copyright © 2021 Simionato, van Wijk, Quint, Wagner, Bianchi and Kaestner. This is an open-access article distributed under the terms of the Creative Commons Attribution License (CC BY). The use, distribution or reproduction in other forums is permitted, provided the original author(s) and the copyright owner(s) are credited and that the original publication in this journal is cited, in accordance with accepted academic practice. No use, distribution or reproduction is permitted which does not comply with these terms.



Osmotic Vesicle Collapse of Sealed Inside–Out Membrane Vesicles From Red Blood Cells

Teresa Tiffert* and Virgilio L. Lew*

Physiological Laboratory, Department of Physiology, Development and Neuroscience, University of Cambridge, Cambridge, United Kingdom

OPEN ACCESS

Edited by:

Lars Kaestner,
Saarland University, Germany

Reviewed by:

Donatienne Tyteca,
Université catholique de
Louvain, Belgium
Mauro Magnani,
University of Urbino Carlo Bo, Italy

*Correspondence:

Teresa Tiffert
jtt1000@cam.ac.uk
Virgilio L. Lew
vll1@cam.ac.uk

Specialty section:

This article was submitted to
Red Blood Cell Physiology,
a section of the journal
Frontiers in Physiology

Received: 19 June 2021

Accepted: 23 July 2021

Published: 26 August 2021

Citation:

Tiffert T and Lew VL (2021)
Osmotic Vesicle Collapse of Sealed
Inside–Out Membrane Vesicles From
Red Blood Cells.
Front. Physiol. 12:727726.
doi: 10.3389/fphys.2021.727726

The preparation of plasma membrane vesicles from a large variety of cells has contributed a wealth of information on the identity and vectorial properties of membrane transporters and enzymes. Vesicles from red blood cell (RBC) membranes are generated in media of extremely low tonicity. For functional studies, it is required to suspend the vesicles in higher tonicity media in order to bring the concentrations of the substrates of transporters and enzymes under investigation within the physiological ranges. We investigated the effects of hypertonic transitions on the vesicle morphology using transmission electron microscopy. The results show that hypertonic transitions cause an irreversible osmotic collapse of sealed membrane vesicles. Awareness of the collapsed condition of vesicles during functional studies is critical for the proper interpretation of experimental results.

Keywords: red blood cells, inside–out membrane vesicles, electron microscopy of membrane vesicles, membrane transport, vesicle collapse

INTRODUCTION

The original method for generating inside–out vesicles (IOVs) from red blood cell (RBC) plasma membranes was developed by Steck et al. (1970) and Steck and Kant (1974). The initial step was to lyse the RBCs in large volumes of low-osmolarity, low-ionic strength media free of divalent cations, lightly buffered to pH 7.5–7.8. Further lengthy washes and incubations of the cell membranes in this medium at low temperature were shown to cause disassembly of their underlying cortical cytoskeleton, leaving naked membranes easily vesiculated by vigorous shearing forces.

In the IOVs generated by the Steck–Kant method, the activity of the Ca^{2+} -activated K^{+} channel (Gardos channel) was reported absent or inactivated (Sarkadi et al., 1980). Searching for the stage at which channel activity might have been lost, we discovered that incubating membranes from recently lysed cells at 37°C in the Steck–Kant lysis medium elicited rapid and *spontaneous* inside–out vesiculation during cytoskeletal disassembly (Lew et al., 1982; Lew et al., 1988; Tiffert and Lew, 2014). We labeled the vesicles generated by this rapid method as “one-step IOVs.” This discovery enabled us to follow the membrane changes during spontaneous vesiculation in organized samples, leading to the elucidation of the dynamic morphology of the process and the mechanism of vesiculation (Lew et al., 1988; Tiffert and Lew, 2014).

Vesicles generated by the “one-step” method show a remarkable heterogeneity of single, double, or triple concentric vesicles (Lew et al., 1988), as also shown in the electron micrograph of **Figure 1A**. Functional studies documented that the one-step vesicles retained the activity of the

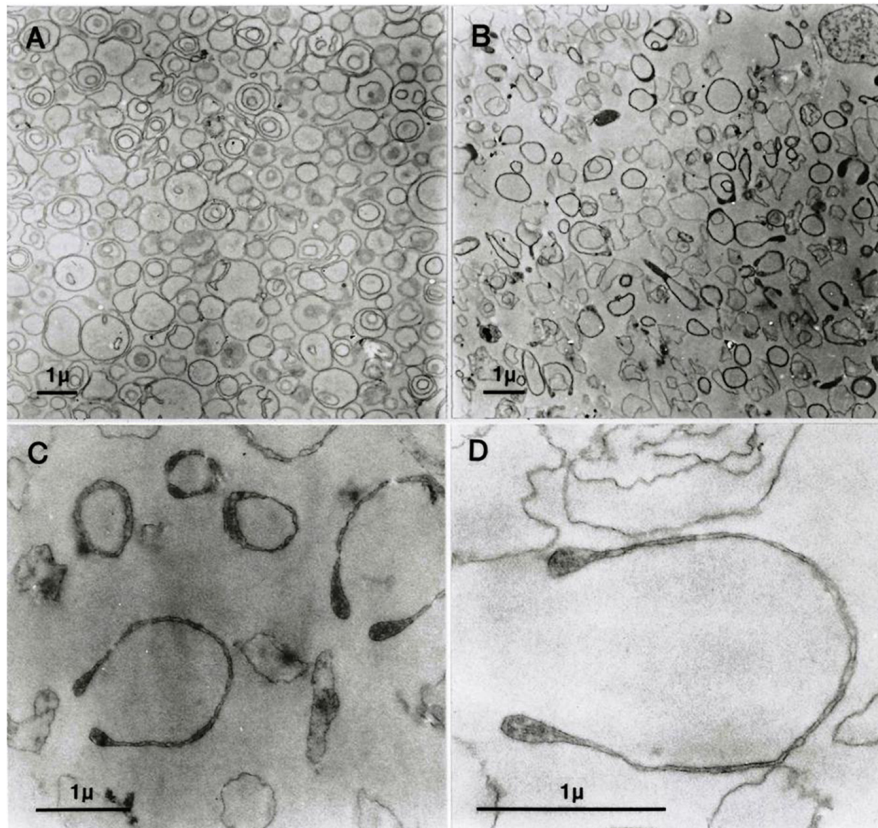


FIGURE 1 | Transmission electron micrographs (EMs) of predominantly inside-out vesicles obtained by the one-step method (Lew et al., 1982; Garcia-Sancho and Alvarez, 1989). **(A)** Aliquots of the vesicle suspension after incubation in lysis medium A at 37°C were treated and further processed for EM as outlined in Section “Materials and Methods”. **(B–D)** Vesicles in aliquots of the suspension described for panel A were spun, washed, and resuspended in medium B, processed for EM, and observed at increasing magnifications in **(C,D)**.

Na/K pump, plasma membrane calcium pump, Gardos channel, and anion exchanger, i.e., the main ion transporter of the RBC membrane (Garcia-Sancho et al., 1982; Lew et al., 1982; Alvarez and García-Sancho, 1987; Garcia-Sancho and Alvarez, 1989).

However, the effects of the hypertonic transitions required for functional studies on the morphology of the one-step IOVs have never been reported earlier. This is the subject of the current investigation.

MATERIALS AND METHODS

The protocol for the preparation of the one-step vesicles used in this study was comprehensively reported earlier (Garcia-Sancho et al., 1982; Lew et al., 1982; Garcia-Sancho and Alvarez, 1989) and was succinctly outlined in the study by Tiffert and Lew (2014; **Figure 1**). The composition of the hypotonic medium in which the RBCs were lysed and the vesicles were formed (medium A) was (in mM): HEPES-Na (pH 7.5) 2.5 and EGTA 0.1. The composition of the medium used for transport studies in the past (medium B) (Lew et al., 1982; Garcia-Sancho and Alvarez, 1989), which was applied here for resuspending the freshly prepared vesicles to investigate the morphological effects of the hypertonic

transition, was (in mM): NaCl, 50; KCl, 10; Na-HEPES (pH 7.5), 25; MgCl₂, 1.5; EGTA, 0.02.

Preparation of Samples for Electron Microscopy (EM)

Immediately after the incubation in lysis medium A at 37°C, aliquots of the vesicle suspension were transferred to 1.5-mL microfuge tubes and spun at 10,000 × *g* for 1 min. The loosely pelleted vesicles were postfixed in 1% OsO₄ and processed as reported earlier (Lew et al., 1985; Lew et al., 1988). For testing the hypertonicity effects, the vesicles in some of the aliquots were resuspended in medium B and incubated for 10–30 min at 37°C. After incubation, the vesicles were spun at 10,000 × *g* for 1 min in their original microfuge tubes, and the pellets were postfixed in 1% OsO₄ and processed similar to the samples in medium A.

RESULTS

Figure 1A shows freshly formed vesicles in hypotonic medium A with the mixture of single, double, and triple concentric vesicles typical of this preparation (Lew et al., 1988).

Figure 1B shows the change in appearance generated by suspending the freshly formed vesicles in medium B. Vesicle membranes are clearly divided into two distinct populations with thin or thick membrane outlines. Some of the thick membrane vesicles configure headphone shapes.

When vesicles suspended in medium B (**Figure 1B**) are washed and resuspended back in medium A, their appearance reverts as shown in **Figure 1A**. This was the only procedure found to be capable of reversing the effects of hypertonic exposure.

At higher magnifications, the thick membrane outlines in **Figure 1B** can be seen to result from double membranes in close apposition (**Figures 1C,D, 2, 3**). **Figure 1D** offers a direct comparison between thin and thick membrane outlines. The headphone configuration combined with the close double-membrane apposition evokes the shape of a fully deflated ball or double cup as seen in a longitudinal section. This exposes the three-dimensional (3D) cup-like shape of the double-membrane vesicles behind their headphone appearance in longitudinal sections. Transverse sections would be expected to render thick circular images as shown in **Figure 1C**. **Figures 2, 3** show how internalized membranes from original double and triple concentric vesicles become displaced toward the thick rim of the cups.

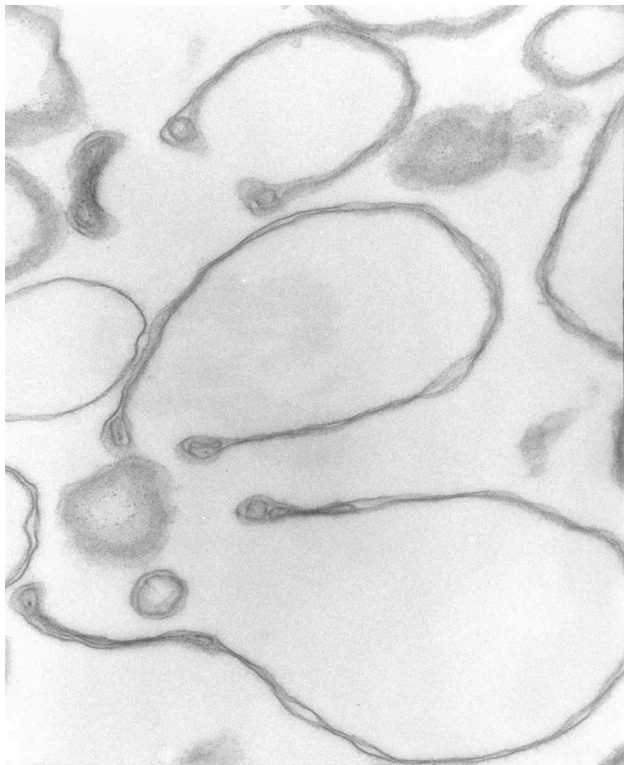


FIGURE 2 | Headphone shape samples. Transmission electron micrograph of selected collapsed vesicles showing the close apposition of the cytoskeleton-free membranes outlining the “headphone” shapes in longitudinal sections. Note the massive reduction in the intra-vesicular space, the outline of the 3D cup shape of the collapsed vesicles, and the displacement of contents toward the rim of the cup. 67,500x.

DISCUSSION

The results in **Figure 1** show that in heterogeneous populations of plasma membrane vesicles from human RBCs, a substantial fraction of the vesicles experiences a drastic volume collapse when transferred to media of increased osmolarity (**Figures 1B–D, 2**). Only sealed vesicles with retained water permeability and restricted solute permeability can experience such a collapse under osmotic gradients. Hence, the heterogeneous morphological response to hypertonic transitions segregates vesicles by their sealed condition.

Cytoskeleton-free RBC membranes were shown to behave like a two-dimensional liquid devoid of intrinsic shape control (Tiffert and Lew, 2014). The curvature along the rim of the cup-shaped collapsed vesicles, a sample of which is shown in more detail in **Figure 3**, is determined by a combination of the intrinsic bending modulus of the free membrane (Evans, 1983), membrane protein interactions on the membrane curvature (Reynwar et al., 2007), and the bulge created by internal vesicles displaced toward the rim during the volume collapse of the host vesicle. In retrospect, casual microscopic sightings of “sharper bordered” vesicles in medium B were noted during past functional studies (Lew et al., 1982), but not interpreted at time. This opens the possibility of estimating the proportion of collapsed vesicles from microscopic observations or light-scattering measurements.

Figures 1C,D, 2 reveal that the condition of sealed vesicle subpopulations during transport experiments is that of a greatly reduced intravesicular volume and a massive increase in



FIGURE 3 | Detail of cup rim and double membranes. Transmission electron micrograph showing details of membrane apposition proximities in collapsed vesicles and of a small internal vesicle with a collapsed double membrane displaced toward the rim of the larger host vesicle shaping the bulge of the rim at that point. 175,000x.

area/volume ratio relative to their original spherical condition. Rate constants used for estimates of membrane permeabilities in vesicles are heavily influenced by their area/volume ratio. It is therefore essential to be aware of the osmotic collapsed condition of the sealed vesicles exposed to the usual hyperosmotic transitions applied in functional studies for the correct interpretation of kinetic data (Lew et al., 1983; Alvarez et al., 1988).

DATA AVAILABILITY STATEMENT

The original contributions presented in the study are included in the article/supplementary material, further inquiries can be directed to the corresponding author/s.

REFERENCES

- Alvarez, J., and García-Sancho, J. (1987). An estimate of the number of Ca^{2+} -dependent K^+ channels in the human red cell. *Biochim. Biophys. Acta* 903, 543–546. doi: 10.1016/0005-2736(87)90062-9
- Alvarez, J., García-Sancho, J., and Herreros, B. (1988). All or none cell responses of Ca^{2+} -dependent K channels elicited by calcium or lead in human red cells can be explained by heterogeneity of agonist distribution. *J. Membr. Biol.* 104, 129–138. doi: 10.1007/bf01870925
- Evans, E. A. (1983). Bending elastic modulus of red blood cell membrane derived from buckling instability in micropipet aspiration tests. *Biophys. J.* 43, 27–30. doi: 10.1016/S0006-3495(83)84319-7
- García-Sancho, J., and Alvarez, J. (1989). Preparation and properties of one-step inside-out vesicles from red cell membranes. *Methods Enzymol.* 173, 368–377. doi: 10.1016/s0076-6879(89)73024-x
- García-Sancho, J., Sanchez, A., and Herreros, B. (1982). All-or-none response of the Ca^{2+} -dependent K^+ channel in inside-out vesicles. *Nature* 296, 744–746. doi: 10.1038/296744a0
- Lew, V. L., Hockaday, A., Freeman, C. J., and Bookchin, R. M. (1988). Mechanism of spontaneous inside-out vesiculation of red cell membranes. *J. Cell Biol.* 106, 1893–1901. doi: 10.1083/jcb.106.6.1893
- Lew, V. L., Hockaday, A., Sepulveda, M. I., Somlyo, A. P., Somlyo, A. V., Ortiz, O. E., et al. (1985). Compartmentalization of sickle cell calcium in endocytic inside-out vesicles. *Nature* 315, 586–589. doi: 10.1038/315586a0
- Lew, V. L., Muallem, S., and Seymour, C. A. (1982). Properties of the Ca^{2+} -activated K^+ channel in one-step inside-out vesicles from human red cell membranes. *Nature* 296, 742–744. doi: 10.1038/296742a0
- Lew, V. L., Muallem, S., and Seymour, C. A. (1983). The Ca^{2+} -activated K channel of human red cells: all or none behaviour of the Ca^{2+} -gating mechanism. *Cell Calcium* 4, 511–517. doi: 10.1016/0143-4160(83)90026-x
- Reynwar, B. J., Ilyia, G., Harmandaris, V. A., Muller, M. M., Kremer, K., and Deserno, M. (2007). Aggregation and vesiculation of membrane proteins by curvature-mediated interactions. *Nature* 447, 461–464. doi: 10.1038/nature05840
- Sarkadi, B., Szebeni, J., and Gardos, G. (1980). “Effects of calcium on cation transport processes in inside-out red cell membrane vesicles,” in *Membrane Transport in Erythrocytes. Relations Between Function and Structure. Alfred Benzon Symposium 14*, eds U. V. Lassen, H. H. Ussing, and J. O. Wieth (Copenhagen: Munksgaard).
- Steck, T. L., and Kant, J. A. (1974). Preparation of impermeable ghosts and inside-out vesicles from human erythrocyte membranes. *Methods Enzymol.* 31, 172–180. doi: 10.1016/0076-6879(74)31019-1
- Steck, T. L., Weinstein, R. S., Straus, J. H., and Wallach, D. F. H. (1970). Inside-out red cell membrane vesicles: preparation and purification. *Science* 168, 255–257. doi: 10.1126/science.168.3928.255
- Tiffert, T., and Lew, V. L. (2014). Dynamic morphology and cytoskeletal protein changes during spontaneous inside-out vesiculation of red blood cell membranes. *Pflugers Arch.* 466, 2279–2288. doi: 10.1007/s00424-014-1483-5

AUTHOR CONTRIBUTIONS

Both authors contributed equally to all aspects of this research.

FUNDING

This work was supported by The Wellcome Trust, United Kingdom (Ref.: 15543/1.5).

ACKNOWLEDGMENTS

We are grateful to Austin Hockaday for the excellent technical assistance with the EM images.

Conflict of Interest: The authors declare that the research was conducted in the absence of any commercial or financial relationships that could be construed as a potential conflict of interest.

Publisher's Note: All claims expressed in this article are solely those of the authors and do not necessarily represent those of their affiliated organizations, or those of the publisher, the editors and the reviewers. Any product that may be evaluated in this article, or claim that may be made by its manufacturer, is not guaranteed or endorsed by the publisher.

Copyright © 2021 Tiffert and Lew. This is an open-access article distributed under the terms of the Creative Commons Attribution License (CC BY). The use, distribution or reproduction in other forums is permitted, provided the original author(s) and the copyright owner(s) are credited and that the original publication in this journal is cited, in accordance with accepted academic practice. No use, distribution or reproduction is permitted which does not comply with these terms.



Redox Properties of Human Erythrocytes Are Adapted for Vitamin C Recycling

Michael Eigenschink¹, Danylo Savran¹, Christoph P. Zitterer¹, Sebastian Granitzer^{1,2}, Magdalena Fritz¹, David M. Baron³, Ernst W. Müllner¹ and Ulrich Salzer^{1*}

¹ Center for Medical Biochemistry, Max Perutz Labs Vienna, Medical University of Vienna, Vienna, Austria, ² Institute of Medical Genetics, Medical University of Vienna, Vienna, Austria, ³ Department of Anaesthesia, Intensive Care Medicine and Pain Medicine, Medical University of Vienna, Vienna, Austria

OPEN ACCESS

Edited by:

Giampaolo Minetti,
University of Pavia, Italy

Reviewed by:

Sakurako Neo,
Azabu University, Japan
Yeliz Cakir Sahilli,
Munzur University, Turkey

*Correspondence:

Ulrich Salzer
ulrich.salzer@meduniwien.ac.at

Specialty section:

This article was submitted to
Red Blood Cell Physiology,
a section of the journal
Frontiers in Physiology

Received: 30 August 2021

Accepted: 16 November 2021

Published: 06 December 2021

Citation:

Eigenschink M, Savran D,
Zitterer CP, Granitzer S, Fritz M,
Baron DM, Müllner EW and Salzer U
(2021) Redox Properties of Human
Erythrocytes Are Adapted for
Vitamin C Recycling.
Front. Physiol. 12:767439.
doi: 10.3389/fphys.2021.767439

Ascorbic acid (AA; or vitamin C) is an important physiological antioxidant and radical scavenger. Some mammalian species, including *homo sapiens*, have lost the ability to synthesize AA and depend on its nutritional uptake. Erythrocytes from AA-auxotroph mammals express high amounts of the glucose transporter GLUT1. This isoform enables rapid uptake of glucose as well as dehydroascorbate (DHA), the fully oxidized form of AA. Here, we explored the effects of DHA uptake on the redox metabolism of human erythrocytes. DHA uptake enhanced plasma membrane electron transport (PMET) activity. This process is mediated by DCytb, a membrane bound cytochrome catalyzing extracellular reduction of Fe³⁺ and ascorbate free radical (AFR), the first oxidized form of AA. DHA uptake also decreased cellular radical oxygen species (ROS) levels. Both effects were massively enhanced in the presence of physiological glucose concentrations. Reduction of DHA to AA largely depleted intracellular glutathione (GSH) and induced the efflux of its oxidized form, GSSG. GSSG efflux could be inhibited by MK-571 (IC₅₀ = 5 μM), indicating involvement of multidrug resistance associated protein (MRP1/4). DHA-dependent GSH depletion and GSSG efflux were completely rescued in the presence of 5 mM glucose and, partially, by 2-deoxy-glucose (2-DG), respectively. These findings indicate that human erythrocytes are physiologically adapted to recycle AA both intracellularly via GLUT1-mediated DHA uptake and reduction and extracellularly via DCytb-mediated AFR reduction. We discuss the possibility that this improved erythrocyte-mediated AA recycling was a prerequisite for the emergence of AA auxotrophy which independently occurred at least twice during mammalian evolution.

Keywords: ascorbic acid, dehydroascorbic acid, glutathione, MRP1, GLUT1, DCytb, vitamin C auxotrophy, evolution

INTRODUCTION

Ascorbic acid (AA), commonly known as vitamin C, is an antioxidant and radical scavenger. AA preferably engages in one-electron transfer-reactions resulting in the formation of ascorbate free radicals (AFR) but can also be further oxidized to dehydrascorbic acid (DHA) upon losing a second electron. Two molecules of AFR can disproportionate to DHA and AA. An additional characteristic

of AFR is its high reactivity with radicals and poor reactivity toward non-radical species (Tu et al., 2017). Due to these properties, AA and AFR are important physiological antioxidants for systemic radical scavenging. AA biosynthesis predominantly takes place in the liver of most mammalian species (Chatterjee et al., 1961). However, some species (fruit bats, guinea pigs, and higher primates including *homo sapiens*) depend on nutritional AA uptake since changes in the L-gulonolactone oxidase (GLO) gene inactivated the last step in AA biosynthesis (Chatterjee, 1973). Interestingly, rats with defects in AA biosynthesis require higher nutritional AA uptake than the “natural” AA auxotroph guinea pigs to prevent adverse systemic effects (Horio et al., 1985). This indicates that adaptations must have occurred during the evolution of AA auxotroph organisms to minimize systemic loss of vitamin C. Erythrocytes of all mammalian species that depend on dietary vitamin C supply express the glucose transporter isoform GLUT1 whereas species capable of AA biosynthesis express other GLUT isoforms in the plasma membrane of their erythrocytes (Montel-Hagen et al., 2008). In contrast to other isoforms, GLUT1 and 3 also efficiently facilitate the transport of DHA (Rumsey et al., 1997; Tu et al., 2015). The joint emergence of the loss of GLO activity and expression of GLUT1 in erythrocytes occurred independently at least twice during mammalian evolution (Drouin et al., 2011), suggesting that (i) this isoform switch is essential for vitamin C auxotroph species and (ii) erythrocytes play an important role in redox processes involving vitamin C. In contrast to AFR, DHA is unstable and quickly degraded to 2,3-diketo-1-gulonic acid in an irreversible reaction (Winkler, 1987). Hence, rapid recycling of DHA into the reduced AA state is crucial for vitamin C auxotrophs to minimize systemic loss of this vitamin. This is likely to be an essential evolutionary adaptation to reduce irreversible degradation of DHA resulting from oxidative processes within the blood stream.

Due to their function as oxygen carriers, erythrocytes contain several enzymes protecting against damage by radical oxygen species (ROS) as well as high concentrations of the antioxidant glutathione (GSH), ranging from 0.4 to 3.0 mM (van't Erve et al., 2013). Normally, the ratio between reduced GSH and its oxidized form, GSSG, is about 7:1. Erythrocytes are equipped with enzymes for GSH synthesis and have high-efficiency importers for its amino acid components (Raftos et al., 2010). GSH reacts with superoxides directly, is involved in degradation of hydrogen peroxide and lipid peroxides *via* glutathione peroxidases, and in covalent modifications of toxic xenobiotics by glutathione S-transferases (GSTs) (Ayala et al., 2014). By far the most abundant GST variant in human erythrocytes is GSTO-1 (Bryk and Wisniewski, 2017), the isoform 1 of the omega class of GSTs. It is an enzyme with specific DHA reductase activity (Zhou et al., 2012). Apart from a GSTO-1-mediated process, DHA can also be directly reduced by GSH, generating AA and GSSG (Winkler, 1992). Thus, with their high content of GLUT1, GSH and GSTO-1 human erythrocytes are well equipped for high-capacity uptake of DHA and its fast regeneration into the stable AA state.

Trans-membrane electron transport at the inner mitochondrial membrane is essential for oxygen-dependent transformation of nutrient-derived reduction equivalents into

ATP-stored chemical energy. *Trans*-plasma membrane electron transfer (PMET), in contrast, is more ambiguously defined as a process where reduction equivalents, either electrons or reductants, are exported to the extracellular environment. PMET is likely involved in a number of physiological processes (Lane and Lawen, 2008) and seems to play a crucial role in redox homeostasis of tumor cells (Sherman et al., 2019). In erythrocytes, various approaches have been undertaken to study *trans*-plasma membrane electron/reductant transport, and several mechanisms have been discussed (Kennett and Kuchel, 2003). These processes have therefore been differently referred to as plasma membrane electron transfer (PMET) (Kennett and Kuchel, 2003), plasma membrane redox system (PMRS) (Rizvi et al., 2006), or (extracellular) ascorbate recycling (Mendiratta et al., 1998). In most studies, transmembrane flow of electrons/reductants was assessed by incubating erythrocytes with the electron acceptor $[\text{Fe}(\text{CN})_6]^{3-}$ (ferricyanide) and the amount of $[\text{Fe}(\text{CN})_6]^{4-}$ (ferrocyanide) generated was quantified by colorimetric assays. Human erythrocytes express the duodenal isoform of cytochrome b561 (DCytb) (Su et al., 2006). DCytb is a transmembrane protein with two heme groups, known to be involved in duodenal iron absorption by reducing dietary Fe^{3+} prior to its uptake by enterocytes (McKie et al., 2001). DCytb has ascorbate binding sites, both at the cytoplasmic and the apical side, indicating that it not only reduces Fe^{3+} but also regenerates ascorbate from ascorbate free radicals (AFR) at the apical binding site, using electrons provided by ascorbate at the cytoplasmic binding site (Ganasen et al., 2018). Its presence at the erythrocyte plasma membrane indicates that the main function of DCytb in these cells is extracellular ascorbate recycling (VanDuijn et al., 2000). The AA-dependent export of electrons during extracellular ascorbate recycling (which can be regarded as PMET activity), however, requires an efficient mechanism of intracellular AFR reduction mediated by thioredoxin reductase, using NADPH as a reductant (May et al., 1998).

DHA uptake into erythrocytes, its recycling to AA within erythrocytes, and PMET activity are processes that consume intracellular reduction equivalents. This study investigates the effects of DHA uptake into human erythrocytes with respect to PMET activity and changes in intracellular ROS as well as GSH levels. Furthermore, we explore the consequences of DHA-dependent GSSG accumulation. In order to evaluate the physiological relevance of our findings, these effects were also studied in the absence and presence of increasing amounts of glucose and 2-deoxy-glucose (2-DG).

MATERIALS AND METHODS

Sample Collection and Study Population

This study was approved by the ethics commission of the Medical University of Vienna (EK Nr. 1752/2020). Blood was taken from 10 healthy volunteers between 18 and 30 years of age, with a BMI between 19 and 30 kg/m². Exclusion criteria were: pre-existing health conditions, regular smoking, substance abuse, regular usage of medications and/or vitamin supplements. Participants were specifically asked to remain abstinent from alcohol and

citrus fruits for 3 days, avoid excessive physical activity for at least 2 days, and fast for at least 8 h prior to blood sampling.

Blood was collected into 9 mL EDTA vacutainers (Greiner Bio-One, Kremsmünster, Austria) from an antecubital vein. Freshly drawn blood was aliquoted into 2 mL microcentrifuge tubes (Eppendorf, Hamburg, Germany), immediately centrifuged for 1 min at 8000 g (Eppendorf, 5415C), and plasma and buffy coat discarded. Subsequently, cells were resuspended in PBS, washed three times, and diluted to a suspension of 4×10^6 cells/ μ L.

Cell Counting

Aliquots of erythrocyte suspensions were diluted 10 or 40 times in PBS. For cell counting and quality control, samples were further diluted 1000 times in CASYton (Roche Applied Science, Penzberg, Germany) and their absolute number, diameter and volume determined using a CASYTM cell counter (Roche Applied Science) employing a 60 μ l capillary. Samples with aberrant peak shape or cell volume were excluded from further analyses. All measurements were performed in duplicates.

Plasma-Membrane Electron Transfer Assay

2×10^6 RBC/ μ L were incubated with 2 mM DHA (Sigma, 261556, Burlington, NJ, United States) or PBS in the absence or presence of 5 mM glucose (AppliChem, A3666, Darmstadt, Germany) for 15 min at room temperature (RT). Erythrocytes were then washed three times and resuspended in PBS. Afterward, cells were resuspended in 1 mM $[\text{Fe}(\text{CN})_6]^{3-}$ (AppliChem, A3883) with or without 5 mM glucose at a concentration of 5×10^5 cells/ μ L. At given time intervals, aliquots from samples were centrifuged for 1 min at 8000 g and supernatants recovered. Supernatants were then transferred into semi-micro cuvettes (Sarstedt, Nümbrecht, Germany) and diluted in PBS. Afterward, samples were incubated with a freshly prepared master mix consisting of bathophenanthroline-disulfonic acid (6 mM) (Sigma, 146617), sodium citrate (0.2 M) (Merck, 1.06432), sodium acetate (3 M, $\text{pH} = 6.5$) (AppliChem, 131632), and FeCl_3 (3 mM) (Merck, 236489) in the dark for 25 min as described by Avron and Shavit (1963). Subsequently, extinction was measured at 540 nm (U-2000 spectrophotometer, Hitachi, Tokyo, Japan). Ferrocyanide (Sigma, P3289) standard curves were determined and experimental data fitted to respective values.

Determination of Intracellular Radical Oxygen Species Levels by Flow Cytometry

RBCs were suspended to a final concentration of 1×10^4 cells/ μ L in PBS and incubated with 5 μ M 2',7'-dichlorodihydrofluorescein-diacetate ($\text{H}_2\text{DCF-DA}$) (Sigma, D6883) for 30 min. $\text{H}_2\text{DCF-DA}$ is a colorless reagent that becomes partially trapped in cells upon deacetylation and reacts with ROS to form the fluorescent DCF (Chen et al., 2010). Erythrocytes were then centrifuged for 4 min at 30 g and supernatants discarded. Resuspended cells were incubated at DHA concentrations from 0.1 to 2 mM in the presence or absence

of 5 mM glucose. After 15 min, samples were collected and ROS production measured by flow cytometry (LSRFortessaTM Cell Analyzer, BD Biosciences, Franklin Lakes, NJ, United States). All procedures were performed in the dark at RT.

Determination of Intracellular Thiol Content by Flow Cytometry

To assess the loss of intracellular glutathione (GSH) upon DHA uptake, erythrocytes at 2×10^6 cells/ μ L were incubated at DHA concentrations from 0.1 to 2 mM for 15 min at RT. Afterward, samples were washed three times in PBS and resuspended at 1×10^4 cells/ μ L. For GSH regeneration assays, 2×10^6 RBC/ μ L were incubated with 2 mM DHA in the presence of either glucose or 2-deoxy-glucose (2-DG) (Sigma, D8375) at concentrations between 5 μ M and 5 mM. After 15 min, samples were quickly diluted in PBS to a final concentration of 1×10^4 cells/ μ L. Incubations with 3 mM of 1-chloro-2,4-dinitrobenzene (CDNB) (Sigma, 138630) for 30 min at RT were used as negative controls for both types of experiments. CDNB is a substrate of GSH S-transferase ρ . Incubation of erythrocytes with 3 mM CDNB for 30 min has been shown to specifically deplete 96% of intracellular GSH by conversion to 2,4-dinitrophenyl-S-glutathione (Awasthi et al., 1981). Cells were then incubated with 50 μ M monobromobimane (MBB) (Sigma, B4380) for 10 min in the dark (Cossarizza et al., 2009). MBB spontaneously reacts with thiols in a biphasic reaction, preferring GSH over protein-sulfhydryls (Hedley and Chow, 1994). Suspensions were centrifuged at 4°C at 30 g for 4 min and the supernatant was discarded. Cells were resuspended in PBS and analyzed by flow cytometry (LSRFortessaTM Cell Analyzer, BD Biosciences).

Enzymatic Determination of Oxidized Glutathione (GSSG)

2×10^6 RBC/ μ L were incubated with PBS or 2 mM DHA in the presence or absence of 5 mM glucose or PBS with 100 μ M of the multidrug resistance protein (MRP) 1/4 inhibitor MK-571 (Sigma, M7571) for 15 min at RT. Erythrocytes were then washed three times with PBS or PBS containing 5 mM glucose, respectively, and resuspended in either PBS, PBS containing 5 mM glucose or PBS containing 100 μ M MK-571. Aliquots were collected at various time points, centrifuged at 8000 g for 1 min and supernatants recovered. To obtain DHA, glucose, and 2-DG dose-response curves, erythrocytes were incubated with the respective compounds as described in the section on flow cytometry of intracellular thiols. After 90 min, samples were centrifuged for 1 min at 8000 g and supernatants recovered. For MK-571 dose-response measurements, erythrocytes were incubated with 2 mM DHA and inhibitor concentrations from 0.1 to 100 μ M for 15 min at RT and processed as stated above. Based on protocols by Rahman et al. (2006) and Giustarini et al. (2013), a master mix containing 1.66 units/mL GSH reductase (Sigma, G3664) and 0.84 mM 5,5'-dithiobis-2-nitro benzoic acid (DTNB) (Sigma, D8130) was prepared freshly. Supernatants were diluted sevenfold in PB200 (0.16 mM Na_2HPO_4 , 0.038 mM KH_2PO_4 , $\text{pH} = 7.4$), and 120 μ l master mix was added. After 30 sec to allow for conversion of GSSG to GSH, NADPH (Roche

Diagnostics, 10107824001) was added to a final concentration of 54.54 μM and sample kinetics measured after 15 sec of equilibration continuously for 4 min at 412 nm (U-2000 spectrophotometer, Hitachi). In addition, GSSG standard-curves consisting of freshly prepared GSSG (Sigma, G4376) solutions (1.25, 2.5, 5, 10 μM) and a 10 μM GSSG frozen standard control were established with each experiment. To obtain reliable GSSG-efflux estimates, linear regression was applied to standard curves after correction for standard controls and sample data fitted to the respective regressions.

Statistical Analyses

All statistical analyses were performed in GraphPad Prism 9.1.1 (GraphPad Software Inc., San Diego, CA, United States). Dose-response curves were approximated by non-linear regression. Longitudinal data were analyzed in a mixed model. The Šidák correction was used as a rather conservative estimate to control for multiple comparisons (Liu et al., 2010). Where applicable, results of mixed models are presented as mean differences with confidence intervals. *P*-values are indicated as asterisks in bar charts, respectively. Data are shown as mean values with standard deviations. Flow cytometry data were exported as FCS 3.1 files and visualized as histograms with FlowJo™ Software Version 10 (Becton, Dickinson and Company, 2019). Time series were additionally analyzed by linear regression to retrieve respective equations.

RESULTS

To study dehydroascorbate (DHA)-dependent changes in erythrocyte redox properties we first investigated erythrocyte plasma membrane electron transport (PMET) activity by quantifying the amount of extracellular ferricyanide reduction over time. Upon pre-incubation with 2 mM DHA, ferrocyanide concentrations increased threefold [$153 \pm 16 \mu\text{mol}/10^{12}$ cells; mean difference (MD): 102 μmol , confidence interval (CI): (78–125 μmol)] within 10 min as compared to controls ($51 \pm 15 \mu\text{mol}/10^{12}$ cells) (Figure 1A). After this initial spike in electron export, however, PMET activity of DHA-loaded erythrocytes strongly decreased over time to a level even below that of controls. In the presence of 5 mM glucose, PMET increased both in DHA-loaded and control erythrocytes (Figure 1B). Remarkably, this increase in PMET activity was robust, persisting at a high level in DHA-loaded cells for up to 90 min ($1530 \pm 590 \mu\text{mol}/10^{12}$ cells). Thus, upon DHA uptake erythrocytes supplied with physiological glucose concentrations reveal their high and long-lasting capacity to export electrons/reduction equivalents to extracellular acceptors.

Since uptake of DHA and its reduction increases intracellular AA (May et al., 2001), we next asked whether this affects intracellular levels of reactive oxygen species (ROS) in erythrocytes. Therefore, cells were labeled with the cell-permeant reagent 2',7'-dichlorodihydrofluorescein-diacetate (H2DCF-DA), a widely used ROS indicator. Afterward samples were incubated with increasing amounts of DHA and analyzed by flow cytometry. Intracellular ROS levels

indeed decreased with increasing DHA concentrations during pre-incubation (Figure 2). Erythrocytes treated with 2 mM DHA had intracellular ROS levels of $68 \pm 10\%$ in comparison to controls. Physiological concentrations of glucose reduced intracellular ROS levels from 100% to $83 \pm 13\%$ in the absence and 83% to $57 \pm 8.0\%$ in the presence of 2 mM DHA, i.e., the effects of DHA and glucose on intracellular ROS levels were additive (Figure 2B).

Intracellular regeneration of AA upon DHA uptake requires 2 moles of reduction equivalents per mole of DHA. Since the major intracellular antioxidant GSH is highly abundant in erythrocytes and known to reduce DHA both directly and in an enzyme-mediated manner (Winkler, 1992; Zhou et al., 2012), we asked how DHA loading affects erythrocyte GSH levels. Assuming that GSH is the predominant low molecular weight thiol in erythrocytes, we used monobromobimane (MBB), a dye that becomes fluorescent upon reaction with such molecules, and flow cytometry to estimate changes in the GSH levels of erythrocytes upon DHA loading. There was an inverse correlation between DHA concentrations during pre-incubation and intracellular GSH content (Figure 3). At 2 mM DHA, intracellular GSH was reduced to $27 \pm 7\%$ as compared to that of cells pre-treated with PBS only (Figure 3C). Depletion of cellular GSH to 50% was achieved by pre-incubation with about 900 μM DHA. Since glutathione reductase, an enzyme highly abundant in erythrocytes, regenerates GSH in a NADPH-dependent process, we addressed the question whether glucose could rescue DHA-induced loss of GSH. In fact, erythrocytes loaded with 2 mM DHA in the presence of 5 mM glucose had GSH levels of $114 \pm 16\%$ as compared to cells pretreated with PBS only. The minimal glucose concentration for full recovery was 150 μM and half-maximal recovery occurred at 58 μM glucose [CI: (53–64 μM); EC_{50} , relative] (Figure 3D). Interestingly, 2-deoxyglucose (2-DG), a glucose derivative inhibiting glycolysis (Pajak et al., 2019), could also rescue DHA-dependent GSH depletion [$EC_{50} = 578 \mu\text{M}$, relative; CI: (386–1595 μM)], however, not to full extent even at 5 mM ($86 \pm 17\%$ GSH recovery) (Figure 3D).

It is known that human erythrocytes release GSSG in an ATP-dependent manner when exposed to hydrogen peroxide (Srivastava and Beutler, 1969). Thus, it was evaluated whether the DHA-dependent decrease in the GSH/GSSG ratio would also trigger GSSG efflux. We therefore incubated erythrocytes with 2 mM DHA for 15 min, removed it by washing, and continued the incubation for another 90 min in the presence or absence of glucose. Indeed, GSSG in the supernatant increased over time for DHA-loaded erythrocyte samples ($5.3 \pm 0.55 \mu\text{mol}/10^{12}$ cells after 90 min) (Figure 4A). In contrast, efflux was reduced to baseline levels upon incubation with 5 mM glucose. GSSG efflux correlated with the dose of DHA during pre-loading, was nearly saturated at about 1000 μM DHA ($96 \pm 26\%$) and half-maximal at 338 μM [CI: (309–368 μM); IC_{50} , absolute] (Figure 4B). Interestingly, maximal GSSG efflux rates from erythrocytes considerably varied between donors ($77 \pm 18 \text{ nmol}/10^{12}$ cells/min at 2 mM DHA) (Figure 4C), probably due to inherent variations in erythrocyte GSH levels (van't Erve et al., 2013). We further tested the sensitivity of the glucose-dependent inhibition of GSSG efflux and compared it to the effect of 2-DG.

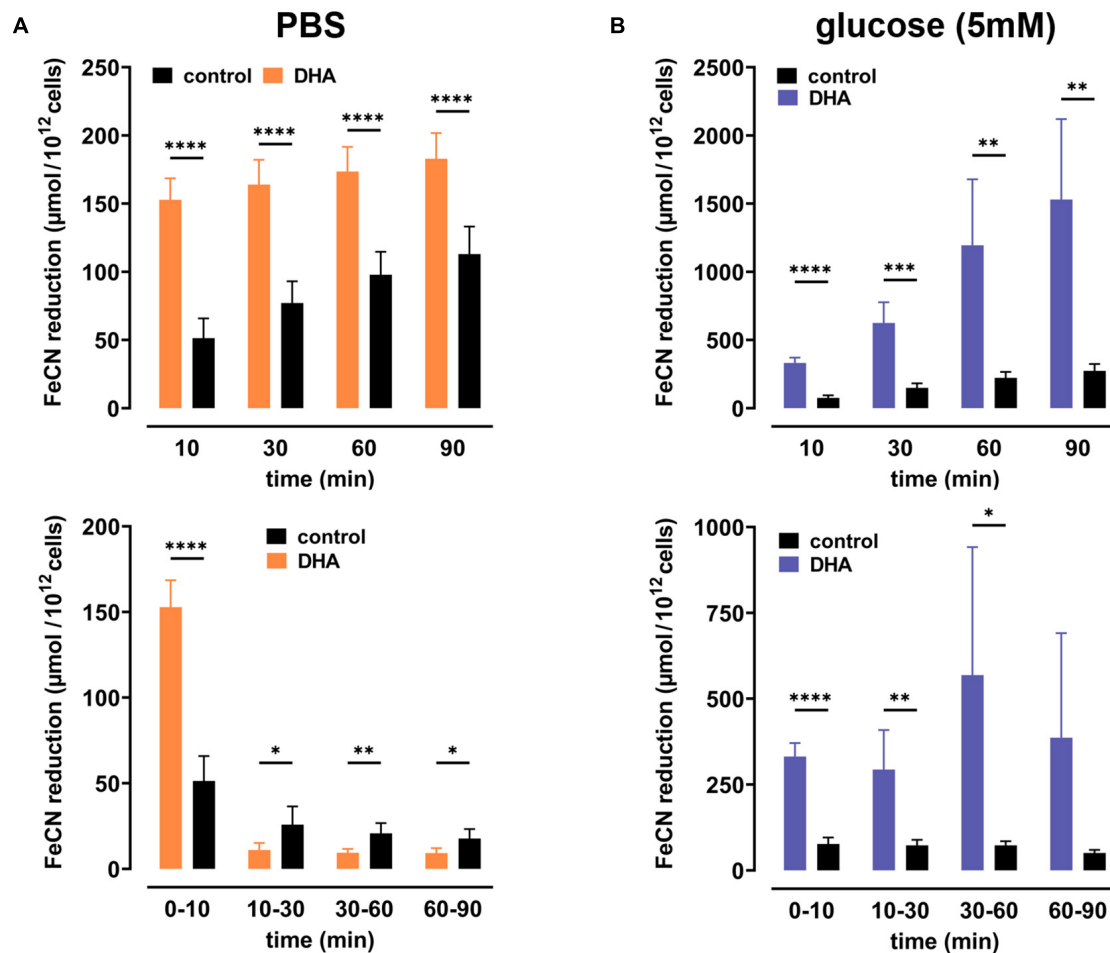


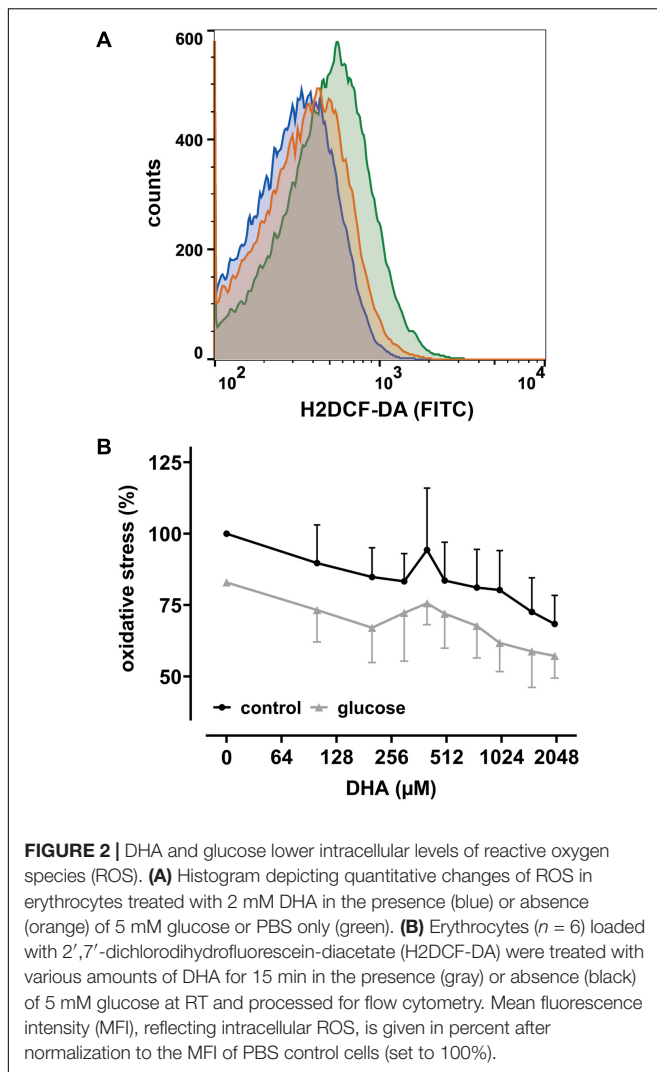
FIGURE 1 | Dehydroascorbic acid (DHA) uptake and glucose synergistically fuel erythrocyte plasma membrane electron transport. Erythrocytes ($n = 8$) were pre-incubated in 2 mM DHA or PBS (=control, black) in the presence (blue) or absence (orange) of glucose. After washing, cells were suspended in 1 mM ferricyanide in PBS (A) or PBS containing 5 mM glucose (B). Aliquots were removed at indicated time points and the amount of ferrocyanide in supernatants assessed as described in section “Materials and Methods.” Mean values of reduced ferrocyanide are given in $\mu\text{mol}/10^{12}$ cells and shown both as cumulative values (upper panels) and amount generated between time points (lower panels), respectively. Please mind the different scales of the y-axes in panels (A,B).

GSSG efflux was half-maximal at 95 μM [CI: (90–99 μM); IC_{50} , relative] glucose and maximal inhibition was achieved at about 175 μM glucose ($19 \pm 9 \mu\text{M}$) (Figure 4D). 2-DG also reduced GSSG efflux, but required higher concentrations as compared to glucose. A 50% inhibition of GSSG efflux was reached at 376 μM [CI: (309–477.3 μM); IC_{50} , relative] 2-DG, and 5 mM 2-DG reduced GSSG efflux to only $37 \pm 13\%$.

Release of GSSG/GSH from peroxide-treated or *Plasmodium falciparum*-infected erythrocytes can be inhibited by MK-571, indicating the involvement of the multidrug resistance associated protein 1 (MRP1) in GSSG efflux (Barrand et al., 2012; Ellison and Richie, 2012). We therefore tested whether DHA-induced GSSG efflux was also mediated by this transporter. Erythrocytes were treated with MK-571 during DHA loading and tested for release of GSSG. 100 μM MK-571 drastically reduced GSSG efflux from erythrocytes pre-loaded with 2 mM DHA to the level of control samples (Figure 5A). The IC_{50} (absolute) for MK-571 to inhibit DHA-dependent GSSG release was 5.5 μM [CI: (4.8–6.2 μM)]

(Figure 5B). Control PMET assays of MK-571-treated cells excluded the possibility that DHA-uptake was impaired in the presence of MK-571 (data not shown).

The GSH depletion data can be merged into a numerical estimation of intracellular GSSG levels based on the following approximations: (i) DHA-dependent loss of GSH can be coupled to the formation of GSSG at a ratio of 2:1; (ii) the DHA-dependent loss of cellular GSH was estimated by normalizing to cells incubated in PBS only (set to 100%) and cells treated with 1-chloro-2,4-dinitrobenzene (CDNB) set to 0%, assuming total depletion of free GSH under these conditions (Figure 3C); (iii) mean GSH and GSSG content in human erythrocytes should be 1.4 mM and 0.214 mM, respectively, based on published data (van 't Erve et al., 2013). Half-maximal GSSG efflux was obtained in erythrocytes upon preloading with about 350 μM DHA (Figure 4B). This DHA concentration induced a GSH depletion of about 20% (Figure 3C) which translates into a change of intracellular GSH to 1.12 mM and GSSG to 0.35 mM,



respectively (0.21 mM basal plus 0.14 mM DHA-induced GSSG). The corresponding correlation curve between cellular GSSG content and GSSG efflux based on these considerations is shown in **Figure 6A** for each concentration of DHA. Another correlation can be plotted for the metabolic rescue of DHA-dependent GSH depletion by increasing concentrations of glucose and 2-DG (**Figure 6B**). In the presence of glucose, near maximal GSSG efflux was already reached at about 350 μM GSSG, whereas GSSG levels had to exceed 600 μM to achieve maximal efflux when cells were supplemented with 2-DG. Interestingly, the correlation curves of 2-DG and DHA almost overlap, suggesting comparable metabolic conditions in these two experimental settings (**Figure 6C**).

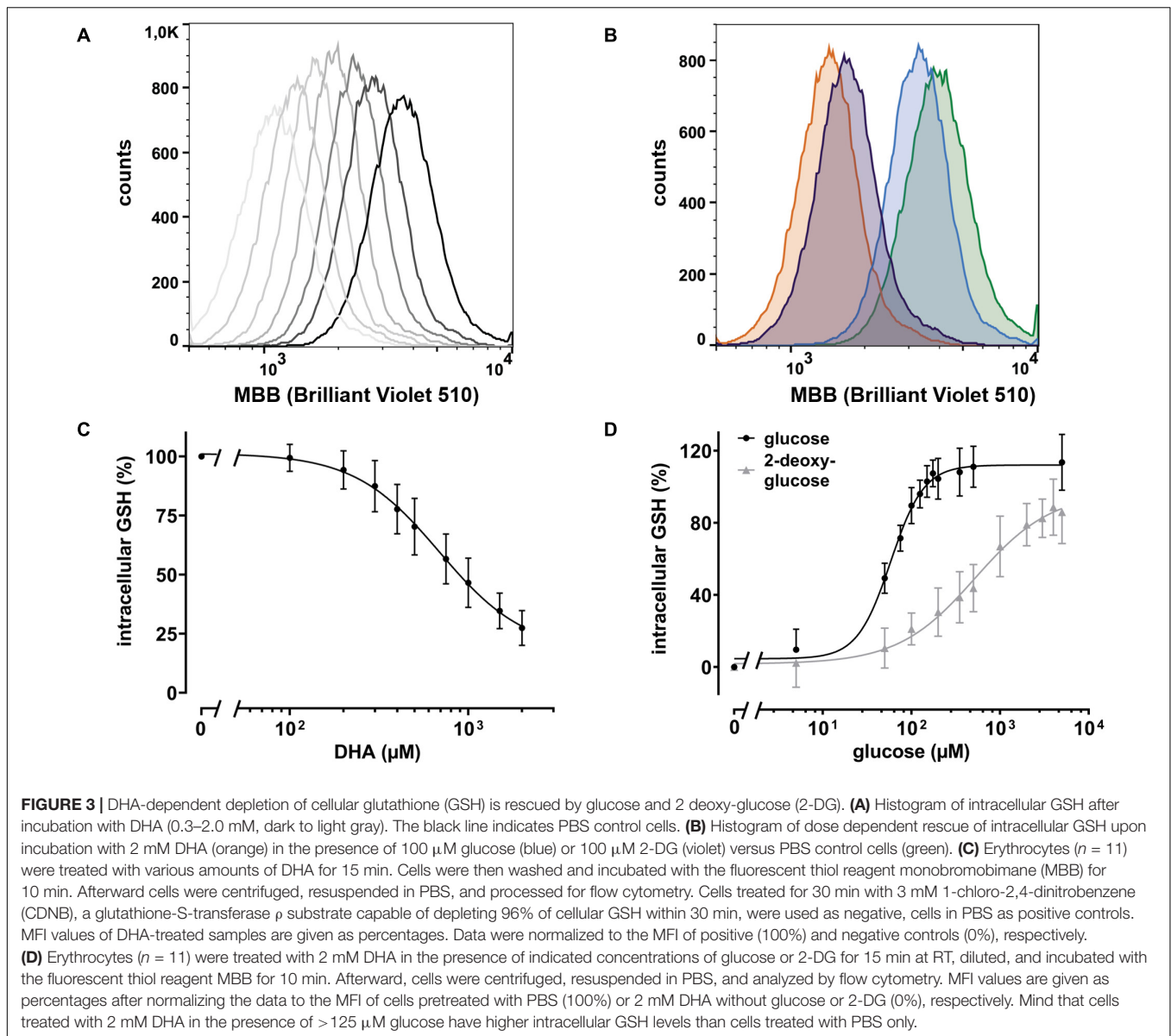
DISCUSSION

In this study we show that uptake of DHA largely affects the redox metabolism of human erythrocytes. DHA reduction and the concomitant increase in intracellular AA lowers cellular ROS

levels and elevates PMET activity of the cells. On the other hand, DHA reduction is associated with depletion of intracellular GSH and export of GSSG *via* the ATP binding cassette transporter MRP1/4. Importantly, in the presence of physiological glucose concentrations, PMET activity is further increased whereas intracellular GSH depletion and GSSG export are blunted. In the light of pertinent phylogenetic findings, these results suggest that erythrocytes of the vitamin C auxotroph species *homo sapiens* are evolutionary adapted to maximize dietary uptake of vitamin C and minimize its loss in the blood stream.

In the absence of glucose, DHA loading resulted in an MK-571-inhibitable efflux of GSSG from erythrocytes (**Figure 5**). MRP1-mediated GSSG efflux was previously reported to be triggered by exposure to oxidative stress and upon infection with *Plasmodium falciparum* (Barrand et al., 2012; Ellison and Richie, 2012). The presence of MRP1 in erythrocytes, its activity, substrate specificity, and inhibition have already been described before (Dekkers et al., 1998; Mrowczynska et al., 2005; Wu et al., 2005). Recent proteomic analyses revealed that three isoforms of the MRP type of ATP binding cassette (ABC) transporters, MRP1, MRP4, and MRP5, are present at the erythrocyte membrane (Bryk and Wisniewski, 2017). MK-571 inhibits MRP1 and MRP4 with IC_{50} values of 1.1 and 0.41 μM , respectively, as assessed on human erythrocyte inside-out vesicles (Wu et al., 2005). The IC_{50} of MK-571 for MRP5 is 40 μM , as determined in a different cellular system (Reid et al., 2003). We found the half-maximal inhibitory concentration of MK-571 for DHA-induced GSSG efflux to be about 5 μM (**Figure 5B**). This intermediary value could indicate the involvement of all three isoforms in this process. Alternatively, higher inhibitory concentrations could be necessary in the normal right side-out as compared to the artificial inside-out situation. Therefore, exclusive involvement of MRP1 and/or MRP4 in DHA-induced GSSG efflux cannot be excluded and has yet to be addressed in detail. It can be roughly approximated that GSSG efflux from DHA loaded cells is half-maximal at intracellular GSSG concentrations of 315 μM (**Figure 6A**). For MRP1 expressed in membrane vesicles from HeLa T5 cells, the K_m value for ATP-dependent transport of GSSG was $93 \pm 26 \mu\text{M}$ (Leier et al., 1996). Considering that our efflux data were obtained in the absence of glucose, diminished ATP levels could reduce the activity of the ATP-dependent GSSG transporter, thus accounting for the higher concentration of 315 μM GSSG required for half-maximal efflux. In fact, increasing glucose concentrations not only gradually diminished intracellular GSSG levels upon pre-treatment with 2 mM DHA but concomitantly decreased intracellular concentration of GSSG required for half-maximal efflux to 245 μM (**Figure 6B**). Thus, glucose not only provides reduction equivalents (NADPH) for GSH regeneration but also ATP for earlier onset of maximal GSSG efflux by MRP isoforms.

Metabolic rescue of DHA-dependent GSH depletion by glucose and 2-DG revealed interesting differences. 5 mM glucose increased intracellular GSH levels of DHA treated cells to 114% as compared to non-treated cells in the absence of glucose (**Figure 3D**). This indicates that reduction equivalents derived from active glucose catabolism more than fully compensate



the oxidation equivalents generated during DHA uptake and subsequent AA regeneration. In contrast, 5 mM 2-DG is not fully capable to counter the loss of reduction equivalents upon DHA treatment (85%). Further, compared to glucose, about ten- and four-times higher concentrations of 2-DG are required for half-maximal maintenance of GSH levels during incubation with 2 mM DHA (**Figure 3D**) and half-maximal inhibition of GSSG efflux (**Figure 4D**), respectively. Moreover, at about 400 μ M intracellular GSSG, efflux rates were nearly maximal in cells supplemented with 75 μ M glucose but only half maximal in the presence of 1 mM 2-DG (**Figure 6B**). In this context, it is interesting to note that 2-DG was described as a substrate for regeneration of GSH from GSSG in human erythrocytes, presumably by producing NADPH in the glucose-6-phosphate dehydrogenase-mediated first step of the pentose phosphate pathway (Suzuki et al., 1983). This is in line with our

findings, as 2-DG partially rescued DHA-induced GSH depletion (**Figure 3D**). However, DHA depleted cells supplemented with 2-DG likely could not produce ATP since 2-DG blocks glycolysis, the only energy producing pathway available to erythrocytes (Pajak et al., 2019). Since MRP1/4 activity is ATP-dependent, ATP would become rate limiting in 2-DG treated cells, thus accounting for the higher cellular GSSG concentrations needed to reach half-maximal GSSG efflux rates (**Figure 6B**).

GLUT1-mediated DHA uptake increases the intracellular concentration of AA in erythrocytes. The elevation of cytoplasmic AA was highlighted in this study, albeit indirectly, by the reduction of intracellular ROS levels (**Figure 2**) and increase in PMET activity (**Figure 1**). The experiments were designed to best explore the capacity of DHA uptake, AA recycling and PMET activity using up to 2 mM DHA, concentrations likely not reached *in vivo*. We show that GSH depletion and GSSG

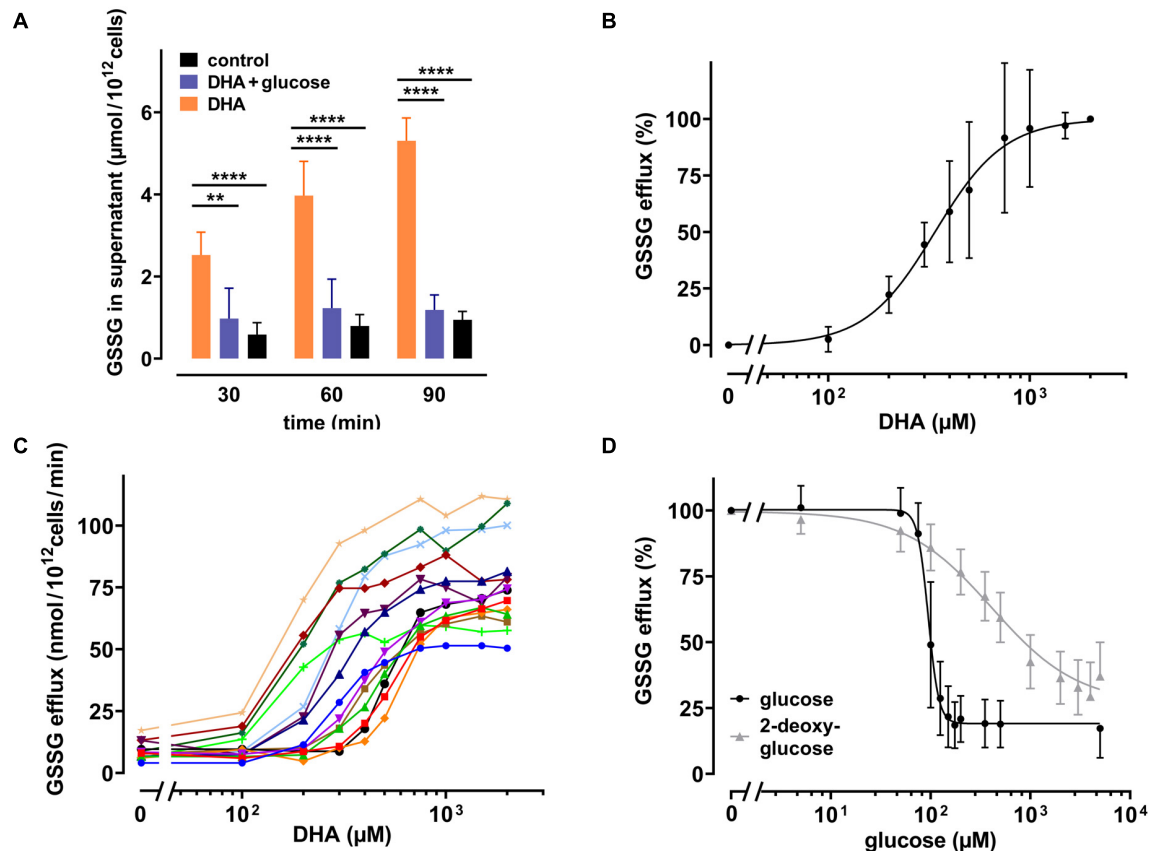
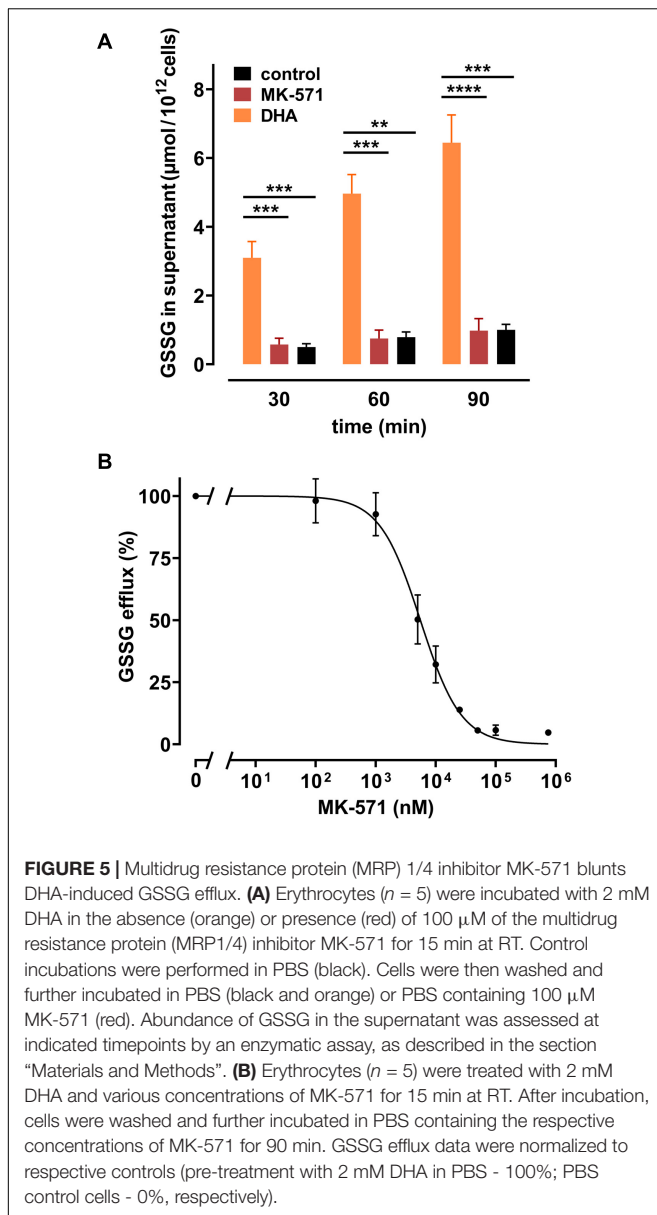


FIGURE 4 | DHA-dependent GSSG efflux from erythrocytes is rescued by glucose as well as 2-DG. **(A)** Erythrocytes ($n = 7$) were incubated with 2 mM DHA in the absence (orange) or presence (blue) of 5 mM glucose for 15 min at RT. Control incubations were carried out in PBS (black). Afterward, cells were washed and resuspended in PBS (black and orange) or PBS containing 5 mM glucose (blue). Aliquots were taken at indicated time points and GSSG concentrations in the supernatant enzymatically assessed as described in the section “Materials and Methods”. **(B,C)** Erythrocytes ($n = 14$) were treated with various amounts of DHA for 15 min at RT, washed and resuspended in PBS for 90 min. GSSG content in the supernatants was assessed and the efflux rates calculated. Data are given as mean values in percent after normalizing to control conditions (pre-treatment with 2 mM DHA in PBS - 100%; PBS control cells - 0%, respectively) **(B)**, or in absolute values for individual experiments **(C)**. **(D)** Erythrocytes ($n = 14$) were treated with 2 mM DHA in the presence of glucose (black) or 2-DG (gray) for 90 min at RT and the GSSG content in the supernatant assessed. GSSG efflux rates are given in percent after normalization to control conditions (pre-treatment with 2 mM DHA in PBS without glucose or 2-DG - 100%; PBS control cells - 0%, respectively).

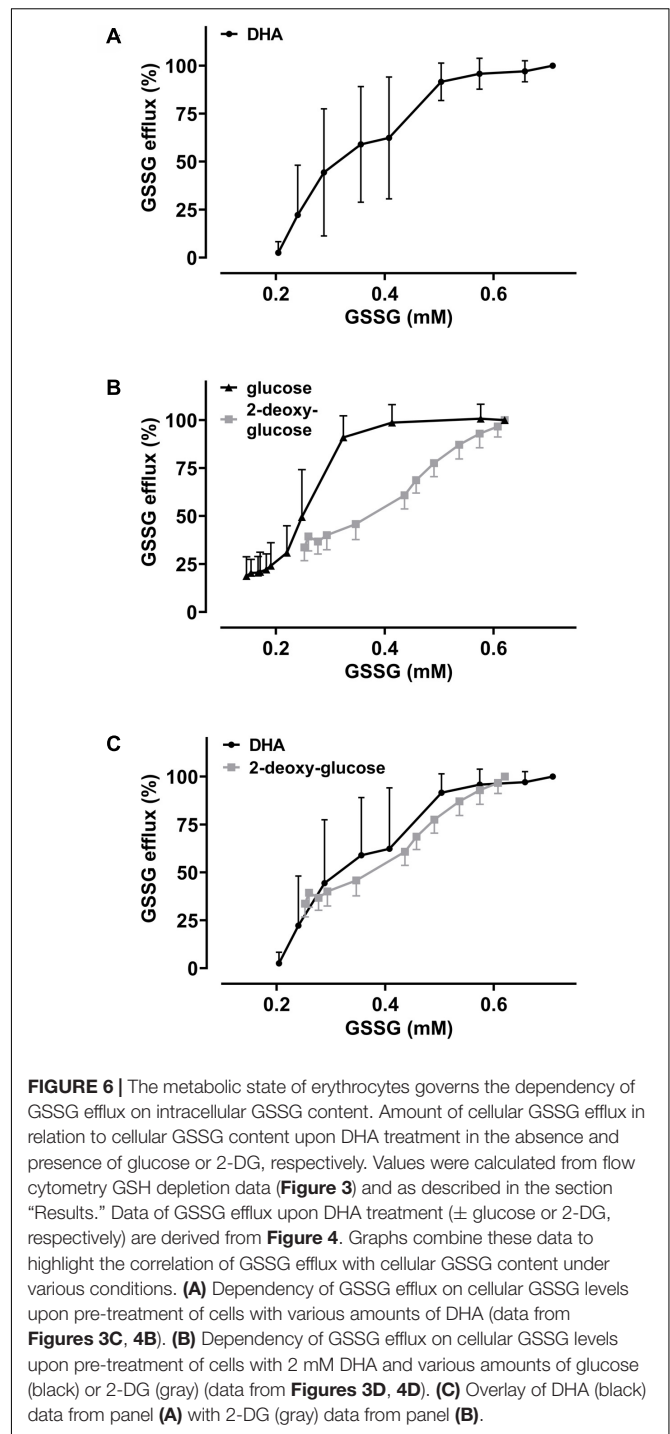
efflux upon maximal DHA uptake is completely rescued even by low glucose levels, thereby indicating that erythrocytes are metabolically adapted for efficient intracellular AA recycling (Figures 3, 4). In order to put our findings in a physiological context, we will now envisage situations where GLUT1-mediated DHA uptake and increase in PMET activity may be of relevance *in vivo*. These considerations suggest that erythrocytes play an important role in systemic vitamin C metabolism.

The normal concentrations of AA in erythrocytes and blood plasma are similar and considerably low (50–80 μM) (Rumsey and Levine, 1998; Lindblad et al., 2013). However, upon oral uptake, peak AA plasma levels can rise up to 200 μM (Padayatty et al., 2004). Moreover, plasma AA levels are mostly assessed in blood sampled from antecubital veins but likely fluctuate depending on the localization within the circulatory system. Conceivably, higher AA/DHA plasma levels are encountered in vessels along the peritubular capillaries of the kidney, where AA/DHA reabsorption takes place, and along the intestinal

epithelium upon food consumption (Rumsey and Levine, 1998). Epithelial cells in the intestine express GLUT1 both at the apical and basolateral membrane (Lindblad et al., 2013) thereby (i) allowing the uptake of DHA (oxidized from dietary AA by digestive processes) and (ii) partly bypassing it *via* facilitated diffusion to the blood stream, thus, promoting uptake and intracellular recycling by erythrocytes. As erythrocytes lack sodium-dependent vitamin C transporters (Nualart et al., 2014) DHA uptake does not result in persistently elevated intracellular AA levels - as known e.g., for neutrophils which have intracellular AA levels in the millimolar range (Wang et al., 1997; Bozonet and Carr, 2019). Rather, AA concentrations tend to equilibrate between erythrocytes and blood plasma either by anionic exchange of ascorbate ions or by passive diffusion of the uncharged weak acid AA (Przybyło and Langner, 2020). Thus, erythrocytes are capable of elevating AA levels in the plasma by intracellular reduction of DHA upon dietary uptake and tubular reabsorption.



Temporarily elevated AA/DHA levels are further expected in the adrenal veins, since stimulation of the adrenal glands by adrenocorticotrophic hormone (ACTH) triggers the release of AA from the adrenal cortex (Padayatty et al., 2007). AA is a cofactor for the conversion of dopamine to noradrenalin (norepinephrine) by dopamine- β -hydroxylase (D β H) which takes place in chromaffin cells of the adrenal medulla. Interestingly, this process is located in the lumen of chromaffin vesicles and driven by DCytb which reduces the generated DHA to AA (Levine, 1986; van den Berg et al., 2018; Shibao et al., 2020). Intraluminal recycling of AA is dependent on cytoplasmic AA, thereby strongly resembling the PMET mechanism of and extracellular AA recycling by erythrocytes. Since adrenal catecholamines are released into the blood stream together with soluble D β H, it is tempting to speculate that erythrocytes also



contribute to the process of noradrenaline generation in the adrenal veins upon activation by ACTH.

DHA uptake and PMET activity of erythrocytes may further play an important role in oxidative stress response. Oxidative stressors and ROS in the blood plasma are efficiently detoxified by AA (Frei et al., 1989) at the cost of AFR and DHA generation. DHA is efficiently absorbed by erythrocytes and immediately reduced to AA, a process enabled by high intracellular GSH

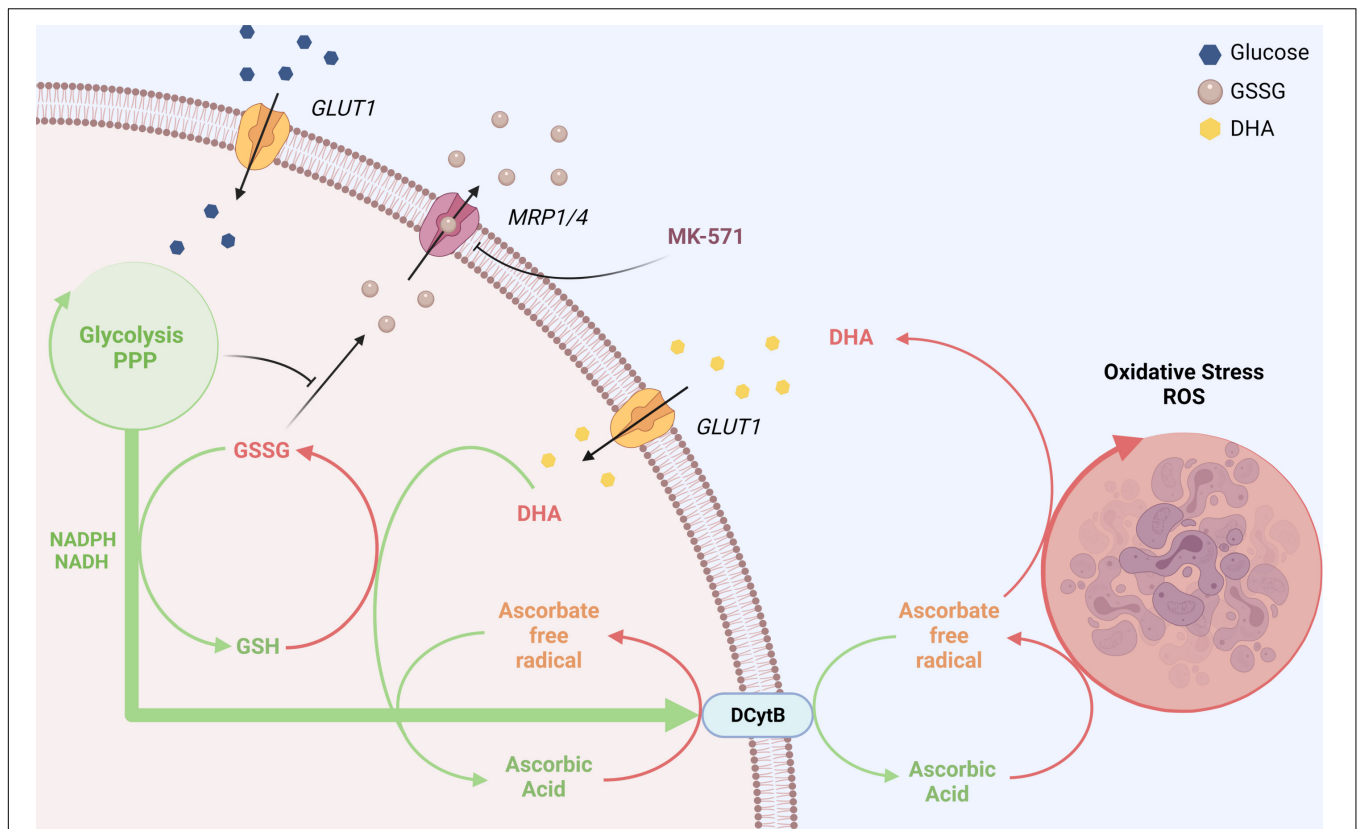


FIGURE 7 | GLUT1 and DCytb-mediated vitamin C recycling as a common feature of erythrocytes from vitamin C auxotroph mammals? The plasma membrane of human erythrocytes contains high amounts of GLUT1 and DCytb. The GLUT1 glucose transporter not only facilitates the uptake of glucose but also that of DHA, the oxidized form of vitamin C. Fast intracellular reduction of DHA to AA is ensured by high cellular GSH concentrations and the high abundance of the DHA reductase GSTO-1. Thus, spontaneous decomposition and irreversible loss of the labile DHA is prevented. DHA-dependent generation of GSSG and its export via MRP1/4 is prevented in the presence of physiological glucose concentrations. Furthermore, increased intracellular AA levels reduce intracellular ROS levels (not depicted here) and fuel DCytb-mediated plasma membrane electron transport (PMET). While in duodenal enterocytes DCytb mediates Fe^{3+} reduction for dietary iron absorption, the main extracellular substrate of DCytb in the erythrocyte membrane appears to be ascorbate free radical (AFR), which is consequently reduced to AA. Both processes, (i) uptake of DHA and its intracellular reduction, and (ii) DCytb-mediated PMET activity which recycles extracellular AA from AFR (generated upon reduction of ROS in the plasma), can be considered a “vitamin C recycling mechanism.” This underestimated physiological function of human erythrocytes likely contributes to (i) oxidative stress defense in blood and (ii) sustainability of systemic AA supply, considering the fluctuating dietary uptake. The importance of this system is underlined by the finding that, in contrast to most other mammalian species, erythrocytes of vitamin C auxotroph mammals harbor GLUT1 and possibly also DCytb (see section “Discussion”). “Created with BioRender.com”.

levels. The transient accumulation of AA in erythrocytes in turn strongly enhances PMET activity which largely potentiates extracellular AA regeneration by AFR reduction *via* DCytb (Figure 1A). Physiological blood glucose levels (i) are sufficient to continuously restore the full reductive capacity of erythrocytes by regenerating intracellular GSH and concomitantly preventing GSSG accumulation as well as efflux (Figures 3–6) and (ii) drive high capacity, long lasting PMET activity for extracellular ROS defense (Figures 1B, 7).

In short, erythrocytes prevent loss of dietary AA by rapid uptake of DHA and extracellular reduction of AFR - processes mediated by GLUT-1 and DCytb, respectively. While high level expression of GLUT-1 has already been recognized as an (most likely) essential adaptation in vitamin C auxotroph mammals (Montel-Hagen et al., 2008; Hornung and Biesalski, 2019) a similar impact of DCytb has not been considered yet. Indeed, DCytb is abundant in erythrocytes of *homo sapiens* and guinea pigs but absent in erythrocytes of mice and rats,

two rodent species capable of AA-biosynthesis (Su et al., 2006). This raises the thrilling question whether expression of DCytb at the erythrocyte membrane is a second necessary adaptation to compensate for the loss of AA biosynthesis. Corresponding analyses of erythrocytes of higher apes and fruit bats will tell and may contribute to our understanding of molecular mechanisms at work during evolution to select for and adapt to novel traits. From a systemic perspective, “outsourcing” AA production can even be viewed as beneficial, since AA biosynthesis produces the oxidant H_2O_2 as a by-product in the final GLO-mediated step of synthesis. Obviously, this outsourcing requires a permanent AA supply which must be sufficient to reduce the selection pressure for AA biosynthesis (Drouin et al., 2011). However, in view of the amazing coincidence of GLUT1 (and possibly also DCytb) expression in erythrocytes and vitamin C auxotrophy (in the respective species), it is tempting to assume that these changes in erythrocyte redox properties were a prerequisite for the loss of GLO activity without causing an evolutionary disadvantage.

Conceivably, erythrocyte-mediated vitamin C recycling, both intracellular *via* GLUT1-mediated DHA uptake and reduction as well as extracellular *via* DCytb-mediated AFR reduction, contributes to a “sustainable” usage of this antioxidant by minimizing its loss in the blood stream and boosting its efficacy *via* PMET activity. Improvement in sustainable vitamin C usage by shifting to erythrocytes expressing high levels of GLUT1 and DCytb may indeed have been prerequisite steps ahead of the emergence of vitamin C auxotrophy. Only after that had been established, selection pressure on maintenance of endogenous AA biosynthesis was gone and inactivation of the GLO gene could take place. Interestingly, this evolutionary selection process would have independently occurred at least twice in the phylogeny of mammals (Drouin et al., 2011).

DATA AVAILABILITY STATEMENT

The raw data supporting the conclusions of this article will be made available by the authors, without undue reservation.

ETHICS STATEMENT

The studies involving human participants were reviewed and approved by Ethics Commission of the Medical University of

Vienna (EK Nr. 1752/2020). The patients/participants provided their written informed consent to participate in this study.

AUTHOR CONTRIBUTIONS

ME and US designed the study and drafted the manuscript. ME, DS, CZ, and SG acquired the data. ME, DS, CZ, SG, MF, DB, EM, and US analyzed and contributed to the interpretation of the data. EM and DB revised the manuscript critically. All authors approved the final version.

FUNDING

This study was supported by grants from the Herzfeldersche Familienstiftung (to US and EM) and by EM (private donation).

ACKNOWLEDGMENTS

The authors thank Thomas Sauer for excellent technical assistance.

REFERENCES

- Avron, M., and Shavit, N. (1963). A sensitive and simple method for determination of Ferrocyanide. *Anal. Biochem.* 6, 549–554. doi: 10.1016/0003-2697(63)90149-0
- Awasthi, Y. C., Garg, H. S., Dao, D. D., Partridge, C. A., and Srivastava, S. K. (1981). Enzymatic conjugation of erythrocyte glutathione with 1-chloro-2, 4-dinitrobenzene: the fate of glutathione conjugate in erythrocytes and the effect of glutathione depletion on hemoglobin. *Blood* 58, 733–738. doi: 10.1182/blood.v58.4.733.bloodjournal584733
- Ayala, A., Muñoz, M. F., and Argüelles, S. (2014). Lipid peroxidation: production, metabolism, and signaling mechanisms of malondialdehyde and 4-hydroxy-2-nonenal. *Oxid. Med. Cell. Longev.* 2014:360438. doi: 10.1155/2014/360438
- Barrand, M. A., Winterberg, M., Ng, F., Nguyen, M., Kirk, K., and Hladky, S. B. (2012). Glutathione export from human erythrocytes and *Plasmodium falciparum* malaria parasites. *Biochem. J.* 448, 389–400. doi: 10.1042/BJ20121050
- Becton, Dickinson and Company (2019). *FlowJo™ Software (for Windows) Version 10*. Ashland, OR: Becton, Dickinson and Company.
- Bozonet, S. M., and Carr, A. C. (2019). The role of physiological vitamin C concentrations on key functions of neutrophils isolated from healthy individuals. *Nutrients* 11:1363. doi: 10.3390/nu11061363
- Bryk, A. H., and Wisniewski, J. R. (2017). Quantitative analysis of human red blood cell proteome. *J. Proteome Res.* 16, 2752–2761. doi: 10.1021/acs.jproteome.7b00025
- Chatterjee, I. B. (1973). Evolution and the biosynthesis of ascorbic acid. *Science* 182, 1271–1272. doi: 10.1126/science.182.4118.1271
- Chatterjee, I. B., Kar, N. C., Ghosh, N. C., and Guha, B. C. (1961). Biosynthesis of L-ascorbic acid: missing steps in animals incapable of synthesizing the vitamin. *Nature* 192, 163–164. doi: 10.1038/192163a0
- Chen, X., Zhong, Z., Xu, Z., Chen, L., and Wang, Y. (2010). 2', 7'-Dichlorodihydrofluorescein as a fluorescent probe for reactive oxygen species measurement: forty years of application and controversy. *Free Radic. Res.* 44, 587–604. doi: 10.3109/10715761003709802
- Cossarizza, A., Ferraresi, R., Troiano, L., Roat, E., Gibellini, L., Bertoncelli, L., et al. (2009). Simultaneous analysis of reactive oxygen species and reduced glutathione content in living cells by polychromatic flow cytometry. *Nat. Protoc.* 4, 1790–1797. doi: 10.1038/nprot.2009.189
- Dekkers, D. W., Comfurius, P., Schroit, A. J., Bevers, E. M., and Zwaal, R. F. (1998). Transbilayer movement of NBD-labeled phospholipids in red blood cell membranes: outward-directed transport by the multidrug resistance protein 1 (MRP1). *Biochemistry* 37, 14833–14837. doi: 10.1021/bi981011w
- Drouin, G., Godin, J.-R., and Pagé, B. J. (2011). The genetics of vitamin C loss in vertebrates. *Curr. Genomics* 12, 371–378. doi: 10.2174/138920211796429736
- Ellison, I., and Richie, J. P. Jr. (2012). Mechanisms of glutathione disulfide efflux from erythrocytes. *Biochem. Pharmacol.* 83, 164–169. doi: 10.1016/j.bcp.2011.09.016
- Frei, B., England, L., and Ames, B. N. (1989). Ascorbate is an outstanding antioxidant in human blood plasma. *Proc. Natl. Acad. Sci. U.S.A.* 86, 6377–6381. doi: 10.1073/pnas.86.16.6377
- Ganasen, M., Togashi, H., Takeda, H., Asakura, H., Tosha, T., Yamashita, K., et al. (2018). Structural basis for promotion of duodenal iron absorption by enteric ferric reductase with ascorbate. *Commun. Biol.* 1:120. doi: 10.1038/s42003-018-0121-8
- Giustarini, D., Dalle-Donne, I., Milzani, A., Fanti, P., and Rossi, R. (2013). Analysis of GSH and GSSG after derivatization with N-ethylmaleimide. *Nat. Protoc.* 8, 1660–1669. doi: 10.1038/nprot.2013.095
- Hedley, D. W., and Chow, S. (1994). Evaluation of methods for measuring cellular glutathione content using flow cytometry. *Cytometry* 15, 349–358. doi: 10.1002/cyto.990150411
- Horio, F., Ozaki, K., Yoshida, A., Makino, S., and Hayashi, Y. (1985). Requirement for ascorbic acid in a rat mutant unable to synthesize ascorbic acid. *J. Nutr.* 115, 1630–1640.
- Hornung, T. C., and Biesalski, H. K. (2019). Glut-1 explains the evolutionary advantage of the loss of endogenous vitamin C-synthesis: the electron transfer hypothesis. *Evol. Med. Public Health* 2019, 221–231. doi: 10.1093/emph/eoz024
- Kennett, E. C., and Kuchel, P. W. (2003). Redox reactions and electron transfer across the red cell membrane. *IUBMB Life* 55, 375–385. doi: 10.1080/15216540310001592843
- Lane, D. J., and Lawen, A. (2008). Transplasma membrane electron transport comes in two flavors. *BioFactors* 34, 191–200. doi: 10.3233/BIO-2009-1072
- Leier, I., Jedlitschky, G., Buchholz, U., Center, M., Cole, S. P., Deeley, R. G., et al. (1996). ATP-dependent glutathione disulphide transport mediated by the

- MRP gene-encoded conjugate export pump. *Biochem. J.* 314(Pt. 2), 433–437. doi: 10.1042/bj3140433
- Levine, M. (1986). Ascorbic acid specifically enhances dopamine beta-monooxygenase activity in resting and stimulated chromaffin cells. *J. Biol. Chem.* 261, 7347–7356. doi: 10.1016/s0021-9258(17)38398-9
- Lindblad, M., Tveden-Nyborg, P., and Lykkesfeldt, J. (2013). Regulation of vitamin C homeostasis during deficiency. *Nutrients* 5, 2860–2879. doi: 10.3390/nu5082860
- Liu, C., Cripe, T. P., and Kim, M.-O. (2010). Statistical issues in longitudinal data analysis for treatment efficacy studies in the biomedical sciences. *Mol. Ther.* 18, 1724–1730. doi: 10.1038/mt.2010.127
- May, J. M., Cobb, C. E., Mendiratta, S., Hill, K. E., and Burk, R. F. (1998). Reduction of the ascorbyl free radical to ascorbate by thioredoxin reductase. *J. Biol. Chem.* 273, 23039–23045. doi: 10.1074/jbc.273.36.23039
- May, J. M., Qu, Z., and Morrow, J. D. (2001). Mechanisms of ascorbic acid recycling in human erythrocytes. *Biochim. Biophys. Acta* 1528, 159–166. doi: 10.1016/s0304-4165(01)00188-x
- McKie, A. T., Barrow, D., Latunde-Dada, G. O., Rolfs, A., Sager, G., Mudaly, E., et al. (2001). An iron-regulated ferric reductase associated with the absorption of dietary iron. *Science* 291, 1755–1759. doi: 10.1126/science.1057206
- Mendiratta, S., Qu, Z. C., and May, J. M. (1998). Erythrocyte ascorbate recycling: antioxidant effects in blood. *Free Radic. Biol. Med.* 24, 789–797. doi: 10.1016/s0891-5849(97)00351-1
- Montel-Hagen, A., Kinet, S., Manel, N., Mongellaz, C., Prohaska, R., Battini, J. L., et al. (2008). Erythrocyte Glut1 triggers dehydroascorbic acid uptake in mammals unable to synthesize vitamin C. *Cell* 132, 1039–1048. doi: 10.1016/j.cell.2008.01.042
- Mrowczynska, L., Bobrowska-Hagerstrand, M., Wrobel, A., Soderstrom, T., and Hagerstrand, H. (2005). Inhibition of MRP1-mediated efflux in human erythrocytes by mono-anionic bile salts. *Anticancer Res.* 25, 3173–3178.
- Nualart, F., Mack, L., Garcia, A., Cisternas, P., Bongarzone, E. R., Heitzer, M., et al. (2014). Vitamin C transporters, recycling and the bystander effect in the nervous system: SVCT2 versus glut1. *J. Stem Cell Res. Ther.* 4:209. doi: 10.4172/2157-7633.1000209
- Padayatty, S. J., Doppman, J. L., Chang, R., Wang, Y., Gill, J., Papanicolaou, D. A., et al. (2007). Human adrenal glands secrete vitamin C in response to adrenocorticotrophic hormone. *Am. J. Clin. Nutr.* 86, 145–149. doi: 10.1093/ajcn/86.1.145
- Padayatty, S. J., Sun, H., Wang, Y., Riordan, H. D., Hewitt, S. M., Katz, A., et al. (2004). Vitamin C pharmacokinetics: implications for oral and intravenous use. *Ann. Intern. Med.* 140, 533–537. doi: 10.7326/0003-4819-140-7-200404060-00010
- Pajak, B., Siwiak, E., Soltyka, M., Priebe, A., Zielinski, R., Fokt, I., et al. (2019). 2-Deoxy-d-glucose and its analogs: from diagnostic to therapeutic agents. *Int. J. Mol. Sci.* 21:234. doi: 10.3390/ijms21010234
- Przybylo, M., and Langner, M. (2020). On the physiological and cellular homeostasis of ascorbate. *Cell. Mol. Biol. Lett.* 25:32. doi: 10.1186/s11658-020-00223-y
- Raftos, J. E., Whillier, S., and Kuchel, P. W. (2010). Glutathione synthesis and turnover in the human erythrocyte: alignment of a model based on detailed enzyme kinetics with experimental data. *J. Biol. Chem.* 285, 23557–23567. doi: 10.1074/jbc.M109.067017
- Rahman, I., Kode, A., and Biswas, S. K. (2006). Assay for quantitative determination of glutathione and glutathione disulfide levels using enzymatic recycling method. *Nat. Protoc.* 1, 3159–3165. doi: 10.1038/nprot.2006.378
- Reid, G., Wielinga, P., Zelcer, N., De Haas, M., Van Deemter, L., Wijnholds, J., et al. (2003). Characterization of the transport of nucleoside analog drugs by the human multidrug resistance proteins MRP4 and MRP5. *Mol. Pharmacol.* 63, 1094–1103. doi: 10.1124/mol.63.5.1094
- Rizvi, S. I., Jha, R., and Maurya, P. K. (2006). Erythrocyte plasma membrane redox system in human aging. *Rejuvenation Res.* 9, 470–474. doi: 10.1089/rej.2006.9.470
- Rumsey, S. C., and Levine, M. (1998). Absorption, transport, and disposition of ascorbic acid in humans. *J. Nutr. Biochem.* 9, 116–130. doi: 10.1016/s0955-2863(98)00002-3
- Rumsey, S. C., Kwon, O., Xu, G. W., Burant, C. F., Simpson, I., and Levine, M. (1997). Glucose transporter isoforms GLUT1 and GLUT3 transport dehydroascorbic acid. *J. Biol. Chem.* 272, 18982–18989. doi: 10.1074/jbc.272.30.18982
- Sherman, H. G., Jovanovic, C., Abuawad, A., Kim, D. H., Collins, H., Dixon, J. E., et al. (2019). Mechanistic insight into heterogeneity of trans-plasma membrane electron transport in cancer cell types. *Biochim. Biophys. Acta Bioenerg.* 1860, 628–639. doi: 10.1016/j.bbabi.2019.06.012
- Shibao, C. A., Garland, E. M., Black, B. K., Mathias, C. J., Grant, M. B., Root, A. W., et al. (2020). Congenital absence of norepinephrine due to CYB561 mutations. *Neurology* 94, e200–e204. doi: 10.1212/WNL.0000000000008734
- Srivastava, S. K., and Beutler, E. (1969). The transport of oxidized glutathione from human erythrocytes. *J. Biol. Chem.* 244, 9–16.
- Su, D., May, J. M., Koury, M. J., and Asard, H. (2006). Human erythrocyte membranes contain a cytochrome b561 that may be involved in extracellular ascorbate recycling. *J. Biol. Chem.* 281, 39852–39859. doi: 10.1074/jbc.M606543200
- Suzuki, M., O'Dea, J. D., Suzuki, T., and Agar, N. S. (1983). 2-Deoxyglucose as a substrate for glutathione regeneration in human and ruminant red blood cells. *Comp. Biochem. Physiol. B* 75, 195–197. doi: 10.1016/0305-0491(83)90312-7
- Tu, H., Li, H., Wang, Y., Niyati, M., Wang, Y., Leshin, J., et al. (2015). Low red blood cell vitamin C concentrations induce red blood cell fragility: a link to diabetes via glucose, glucose transporters, and Dehydroascorbic acid. *EBioMedicine* 2, 1735–1750. doi: 10.1016/j.ebiom.2015.09.049
- Tu, Y. J., Njus, D., and Schlegel, H. B. (2017). A theoretical study of ascorbic acid oxidation and HOO/O2 (-) radical scavenging. *Org. Biomol. Chem.* 15, 4417–4431. doi: 10.1039/c7ob00791d
- van den Berg, M. P., Almomani, R., Biaggioni, I., van Faassen, M., van der Harst, P., Sillje, H. H. W., et al. (2018). Mutations in CYB561 causing a novel orthostatic hypotension syndrome. *Circ. Res.* 122, 846–854. doi: 10.1161/CIRCRESAHA.117.31949
- van Erve, T. J., Wagner, B. A., Ryckman, K. K., Raife, T. J., and Buettner, G. R. (2013). The concentration of glutathione in human erythrocytes is a heritable trait. *Free Radic. Biol. Med.* 65, 742–749. doi: 10.1016/j.freeradbiomed.2013.08.002
- VanDuijn, M. M., Tijssen, K., VanSteveninck, J., Van den Broek, P. J., and Van der Zee, J. (2000). Erythrocytes reduce extracellular ascorbate free radicals using intracellular ascorbate as an electron donor. *J. Biol. Chem.* 275, 27720–27725. doi: 10.1074/jbc.M910281199
- Wang, Y., Russo, T. A., Kwon, O., Chanock, S., Rumsey, S. C., and Levine, M. (1997). Ascorbate recycling in human neutrophils: induction by bacteria. *Proc. Natl. Acad. Sci. U.S.A.* 94, 13816–13819. doi: 10.1073/pnas.94.25.13816
- Winkler, B. S. (1987). In vitro oxidation of ascorbic acid and its prevention by GSH. *Biochim. Biophys. Acta* 925, 258–264. doi: 10.1016/0304-4165(87)90190-5
- Winkler, B. S. (1992). Unequivocal evidence in support of the nonenzymatic redox coupling between glutathione/glutathione disulfide and ascorbic acid/dehydroascorbic acid. *Biochim. Biophys. Acta* 1117, 287–290. doi: 10.1016/0304-4165(92)90026-q
- Wu, C. P., Klokouzas, A., Hladky, S. B., Ambudkar, S. V., and Barrand, M. A. (2005). Interactions of mefloquine with ABC proteins, MRP1 (ABCC1) and MRP4 (ABCC4) that are present in human red cell membranes. *Biochem. Pharmacol.* 70, 500–510. doi: 10.1016/j.bcp.2005.05.022
- Zhou, H., Brock, J., Liu, D., Board, P. G., and Oakley, A. J. (2012). Structural insights into the dehydroascorbate reductase activity of human omega-class glutathione transferases. *J. Mol. Biol.* 420, 190–203. doi: 10.1016/j.jmb.2012.04.014

Conflict of Interest: The authors declare that the research was conducted in the absence of any commercial or financial relationships that could be construed as a potential conflict of interest.

Publisher's Note: All claims expressed in this article are solely those of the authors and do not necessarily represent those of their affiliated organizations, or those of the publisher, the editors and the reviewers. Any product that may be evaluated in this article, or claim that may be made by its manufacturer, is not guaranteed or endorsed by the publisher.

Copyright © 2021 Eigenschink, Savran, Zitterer, Granitzer, Fritz, Baron, Müllner and Salzer. This is an open-access article distributed under the terms of the Creative Commons Attribution License (CC BY). The use, distribution or reproduction in other forums is permitted, provided the original author(s) and the copyright owner(s) are credited and that the original publication in this journal is cited, in accordance with accepted academic practice. No use, distribution or reproduction is permitted which does not comply with these terms.



Development of Mechanical Stability in Late-Stage Embryonic Erythroid Cells: Insights From Fluorescence Imaged Micro-Deformation Studies

Luis F. Delgadillo¹, Yu Shan Huang², Sami Leon³, James Palis² and Richard E. Waugh^{1*}

¹ Department of Biomedical Engineering, University of Rochester, Rochester, NY, United States, ² Department of Pediatrics, School of Medicine and Dentistry, University of Rochester, Rochester, NY, United States, ³ Department of Biostatistics and Computational Biology, School of Medicine and Dentistry, University of Rochester, Rochester, NY, United States

OPEN ACCESS

Edited by:

Giampaolo Minetti,
University of Pavia, Italy

Reviewed by:

Theodosia A. Kalfa,
Cincinnati Children's Hospital Medical
Center, United States
Sophie D. Lefevre,
Université Paris Diderot, France

*Correspondence:

Richard E. Waugh
richard.waugh@rochester.edu

Specialty section:

This article was submitted to
Red Blood Cell Physiology,
a section of the journal
Frontiers in Physiology

Received: 20 August 2021

Accepted: 02 November 2021

Published: 10 January 2022

Citation:

Delgadillo LF, Huang YS, Leon S,
Palis J and Waugh RE (2022)
Development of Mechanical Stability
in Late-Stage Embryonic Erythroid
Cells: Insights From Fluorescence
Imaged Micro-Deformation Studies.
Front. Physiol. 12:761936.
doi: 10.3389/fphys.2021.761936

The combined use of fluorescence labeling and micro-manipulation of red blood cells has proven to be a powerful tool for understanding and characterizing fundamental mechanisms underlying the mechanical behavior of cells. Here we used this approach to study the development of the membrane-associated cytoskeleton (MAS) in primary embryonic erythroid cells. Erythropoiesis comes in two forms in the mammalian embryo, primitive and definitive, characterized by intra- and extra-vascular maturation, respectively. Primitive erythroid precursors in the murine embryo first begin to circulate at embryonic day (E) 8.25 and mature as a semi-synchronous cohort before enucleating between E12.5 and E16.5. Previously, we determined that the major components of the MAS become localized to the membrane between E10.5 and E12.5, and that this localization is associated with an increase in membrane mechanical stability over this same period. The change in mechanical stability was reflected in the creation of MAS-free regions of the membrane at the tips of the projections formed when cells were aspirated into micropipettes. The tendency to form MAS-free regions decreases as primitive erythroid cells continue to mature through E14.5, at least 2 days after all detectable cytoskeletal components are localized to the membrane, indicating continued strengthening of membrane cohesion after membrane localization of cytoskeletal components. Here we demonstrate that the formation of MAS-free regions is the result of a mechanical failure within the MAS, and not the detachment of membrane bilayer from the MAS. Once a “hole” is formed in the MAS, the skeletal network contracts laterally along the aspirated projection to form the MAS-free region. In protein 4.1-null primitive erythroid cells, the tendency to form MAS-free regions is markedly enhanced. Of note, similar MAS-free regions were observed in maturing erythroid cells from human marrow, indicating that similar processes occur in definitive erythroid cells. We conclude that localization of cytoskeletal components to the cell membrane of mammalian erythroid cells during maturation is insufficient by itself to produce a mature MAS, but that subsequent processes are additionally required to strengthen intraskeletal interactions.

Keywords: erythrocyte, membrane, cytoskeleton, FIMD, mechanics, stability, maturation, embryonic

INTRODUCTION

The red blood cell is perhaps the simplest cell in the human body. It has no nucleus, its interior consists largely of a concentrated solution of hemoglobin, and its mechanical stability resides entirely in its plasma membrane and a thin, membrane-associated cytoskeleton (MAS). Despite its simplicity, many mysteries remain about its function and structure, its maturation from erythroid precursors, and how abnormalities in its proteins and maturation process lead to hemolytic disease (Lux, 2016). The mechanical properties and physical stability of the red blood cell are paramount because of its role as a circulating corpuscle. The simplicity of the cell structure and its ready availability have contributed to a plethora of theoretical and experimental studies of the structures that account for its mechanical behavior (Skalak et al., 1973; Chien et al., 1978; Evans and Skalak, 1979; Waugh and Evans, 1979; Discher et al., 1994; Li et al., 2005; Svetina et al., 2016). Key to understanding the relationship between the structure of the MAS and cellular properties is the ability to manipulate the cell mechanically and image the resulting deformation and structural reorganizations that accompany cell deformation. The most advanced studies have combined fluorescence labeling of membrane components and controlled mechanical deformation of the cell (fluorescence imaged microdeformation, FIMD) to gain insights into how specific membrane components are re-distributed during deformation (Lee et al., 1999; Picart et al., 2000; Dahl et al., 2003; Huang et al., 2017). Here, we applied this approach to document and quantify the changes in the mechanical stability of the MAS in primary mammalian erythroid cells at different stages of maturation.

The organization of the MAS in erythrocytes has been extensively studied. It consists primarily of a network of spectrin α - β dimers that self-associate at one end to form tetramers and higher oligomers, and associate at the opposite end with junctional complexes that are organized around short filaments of actin. The spectrin network is attached to the membrane bilayer at multiple points, the most prominent being associations with band-3, an integral membrane protein that serves both as an anion transporter and the principal attachment site for the MAS and other enzymes and proteins of the cell interior (Zhang et al., 2000; Anong et al., 2009). Auxiliary proteins of the MAS and its attachment sites to the membrane have been thoroughly reviewed by others (Mohandas and An, 2006; Gautier et al., 2018). Notably, abnormalities in these proteins frequently lead to a weakening of the mechanical stability of the membrane composite and are known to result in chronic hemolytic anemias, such as hereditary spherocytosis and hereditary elliptocytosis, that can be life-threatening (Palek and Sahr, 1992). Thus, the proper assembly of a mechanically stable yet deformable MAS in red blood cells is essential for human health.

The model system we use to study progressive erythroid maturation are primary primitive erythroid cells isolated from progressive stages of mouse embryogenesis. Primitive erythroblasts initiate the onset of blood cell circulation in the mammalian embryo (McGrath et al., 2003). These cells are larger than definitive erythroid cells, which ultimately become

the predominant and then exclusive cell type in the late-stage embryo and postnatal organism, respectively. Primitive erythroid cells begin circulating as immature erythroblasts that progressively mature as a semi-synchronous cohort reaching the orthochromatic stage of differentiation at E12.5 in the murine embryo (Kingsley et al., 2004). We previously determined that protein components of the MAS become localized to the membrane between E10.5–E12.5 (Huang et al., 2017). Interestingly, the mechanical stability of primitive erythroid cells continues to increase independently of enucleation status even after localization of the MAS components to the membrane (Waugh et al., 2013; Huang et al., 2017).

Here we demonstrate that the creation of MAS-free regions by mechanical deformation is the result of an isotropic rupture of the MAS, creating a hole in the MAS that propagates away from the tip of the cell projection in the micropipette, forming the MAS into an open-ended cylinder within the lumen of the pipette and a MAS-free region at the tip of the projection. We further document that the likelihood of MAS rupture increases with increasing deformation and decreases with erythroid cell maturation. Finally, we show that deficiencies in the cytoskeletal protein 4.1 also lead to increased susceptibility of the membrane to rupture compared to wild-type cells at the same stage of maturation.

MATERIALS AND METHODS

Cell Collection

All animal procedures were approved by the University Committee on Animal Resources at the University of Rochester. ICR mice were obtained from Taconic (Germantown, NY, United States). Protein 4.1R (*Epb41*) heterozygous mice, a generous gift from John Conboy (UC Berkeley), were on a C57Bl/6 background (Shi et al., 1999). Mice were mated overnight and vaginal plugs were examined the following morning. At 10.5–14.5 days of gestation, mice were killed by CO₂ inhalation, followed by cervical dislocation and embryos removed from decidual tissues in PB2 {[Dulbecco PBS (GibcoBRL, Gaithersburg, MD, United States), 0.3% BSA (Gemini Bio-Products, Sacramento, CA, United States), 0.68 mmol/L CaCl₂ (Sigma-Aldrich, St Louis, MO, United States), 0.1% glucose]}. Individual embryos were transferred into 35 mm dishes with PB2 plus 12.5 μ g/mL heparin, and circulating fetal blood cells were collected as previously described (Huang et al., 2017). *Epb41* embryos were genotyped using the AccuStart II Mouse Genotyping Kit (Quanta Biosciences) using primer pairs for *Neo* and *Epb41* exon 4 (Shi et al., 1999). Littermate control cells were protein 4.1R(+/-).

Human bone marrow cells were aspirated from the iliac crest of healthy donors after informed consent according to the University of Rochester's Research Subjects Review Board. The total marrow cells were diluted 1:1 with McCoy's 5A medium (Gibco, Grand Island, NY, United States) and layered onto Ficoll-Paque (1.077 g/mL; Pharmacia, Piscataway, NJ, United States). Mononuclear cells (MNCs) from the interface band were collected after centrifugation at 300 \times g for 30 min at

room temperature. The MNCs were washed twice in McCoy's 5A medium and then resuspended at a cell density of 1×10^6 cells/ml in filter-sterilized PBS (Gibco) supplemented with 5% v/v FBS (Gibco), 4.5 g/L D-Glucose (Sigma, St. Louis, MO, United States), 0.2 mM L-glutamine (Gibco), 50 U/ml penicillin (Gibco), and 50 μ g/ml streptomycin (Gibco). Cells were labeled by incubation for 30 min at 4°C in the dark with R-phycoerythrin (PE)-conjugated antibody to glycophorin A (DAKO/Agilent, Santa Clara, CA, United States).

Fluorescence Imaged Microdeformation

Embryonic blood cells in PB2 buffer at 300 mOsmols at room temperature were labeled with Ter-119-Alexa 488 antibody (0.5 mg/ml) for 30 min in the dark at room temperature. The cell concentration for antibody labeling was kept constant for all gestation days. After antibody labeling, the cells were suspended at high dilution in a chamber on the stage of an inverted fluorescence microscope (Nikon TE2000-E, Roper Quantem512SC digital camera, and Elements software, Nikon Instruments). Individual cells were aspirated into a micropipette at a pressure of approximately 1.47 kPa (15 cm H₂O). This pressure was sufficient to minimize the appearance of folds in the membrane projection in the micropipette and to form the portion of the cell outside the pipette into a spherical shape. Brightfield and fluorescence images were then captured and saved for later analysis to assess cytoskeletal distribution. Formation of a membrane skeleton-free region of the lipid bilayer was observed as differences in the extension lengths of fluorescently-labeled membrane skeleton and the full cell projection observed in brightfield microscopy. Bright field images were taken using a 40 \times objective lens at an exposure of 60 ms with a 120 multiplier and fluorescence images were obtained with the same objective lens at an exposure of 500 ms with a 500 multiplier. After an image was taken, the cell was released, the pressure brought back to the original starting point, and a different cell was selected. The process was repeated 5–10 times using the same micropipette.

Ghost Protocol

Transient exposure to low ionic strength buffer causes red blood cells to swell and burst, releasing cell contents and allowing large molecules outside the cell to enter (Nash and Meiselman, 1983). The resulting red cell ghosts have lost hemoglobin content and their color. Mouse primitive cells were spun down at $1,000 \times g$ for 5 min. The supernatant was removed, and the cells were washed 3 \times at room temperature with PBS (Gibco, pH 7.4, osmolality adjusted using distilled water to 292 mOsm). Meanwhile, 300 U of Alexa 488 phalloidin (Invitrogen) were dissolved in 1.5 mL of ethanol, and 12 μ L of this solution was dried onto the bottom of an amber vial. A 50% suspension of cells (20 μ L) was added to the vial and chilled to 0.0°C. 80 μ L of chilled lysis buffer (7.5 mM Na₂HPO₄ and 7.5 mM NaH₂PO₄ mixed to obtain a pH of 6.0, plus a protease inhibitor (0.1 mM phenyl-methyl-sulfonyl fluoride) and incubated for 5 min at 0.0°C pH 6.0. We note that it is critical to maintain constant temperature and pH throughout the lysing and resealing steps. Buffers and cells were pre-cooled prior to mixing. 12 μ L of resealing buffer [2M KCL, 21 mM MgCl₂, 10 mM ATP, 25 mM tris (hydroxymethyl)aminomethane], 0.1 mM dithioerythritol

was added and the suspension was stirred for 10 min at 0.0°C, followed by 45 min incubation at 37°C. Cells were pelleted at $1,000 \times g$ for 4 min, and after supernatant removal, cells were washed three times with PBS (292 mOsm) and two times with PBS (210 mOsm) with 5% fetal bovine serum (FBS). After washing, the cells were suspended in PBS (210 mOsm) with 5% FBS for measurement.

Statistics

Analysis of the FIMD images was carried out using measurements of the brightfield and fluorescence images. The percentages of cells that showed skeleton-free regions for a given gestation day and extension ratio, were compared. Statistical significance was assessed using a logistic regression that models the probability of MAS failure given the covariates cell extension (L_e/R_p) and gestation day. Statistical differences were assessed for different days compared against the data for cells from E14.5 ($p < 0.05$). Logistic regression was also performed comparing results for protein 4.1R-null cells with littermate controls that were homozygous for 4.1R expression (WT).

RESULTS

Observations of the Formation of Membrane-Associated Cytoskeleton-Free Membrane Regions

The Ter-119 antibody associates with glycophorin A and increases its association with the MAS, making it a reliable indicator of MAS localization (Lee et al., 2004). Inspection of FIMD images of aspirated primitive erythroid cells revealed that in a significant fraction of aspirated cells, the fluorescence distribution did not fully extend to the tip of the micropipette where the bright field image shows the cell to be present (**Figure 1**). These differences in the extension lengths of fluorescently labeled MAS and the full cell projection observed in brightfield demonstrate the formation of MAS-free regions of the membrane. Measurements of fluorescence distribution using FIMD have enabled us to determine the frequency with which such regions form and how this frequency changes with both the magnitude of the deformation and the maturity of the cells.

Membrane-associated cytoskeleton-free regions in micropipette-aspirated cells appeared at all stages of maturation tested (**Figure 2A**). The frequency with which these regions formed decreased with increasing maturation and increased with the magnitude of deformation. Cell maturation was gauged by the gestation day at which the cells were harvested, (E10.5 through E14.5), since primitive erythroid cells differentiate as a semi-synchronous cohort, reaching the basophilic erythroblast stage at E10.5 and the orthochromatic erythroblast stage by E12.5–E13.5 (Kingsley et al., 2004, 2013). The magnitude of deformation was gauged by measuring the ratio of the length of the extended projection of the cell inside the micropipette L_e to the radius of the pipette R_p . This ratio, L_e/R_p , provides an indication of the maximum mechanical extensions of the cell membrane (Evans and Skalak, 1979). At E10.5, nearly all the cells tested exhibited the formation of MAS-free regions,

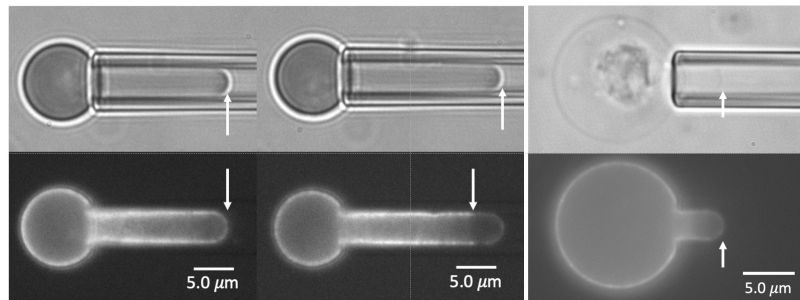


FIGURE 1 | Images of E13.5 primitive erythroid cells aspirated into a micropipette. Two pairs of images for each of three cells are shown, brightfield at the top, fluorescence at the bottom. In the left and center panels, the fluorescent label is TER-119. In the right panels, the label is Alexa-488 phalloidin. The cell at the left shows bright edge-labeling around the entire projection of the cell in the micropipette, including the tip, indicating an intact MAS. The cell in the center shows fluorescent labeling that stops approximately 3.0 μm from the tip, indicating rupture of the MAS and formation of a MAS-free region at the tip of the projection. The rightmost cell is a ghost cell with an intact MAS from an E14.5 embryo. Scale bars as shown.

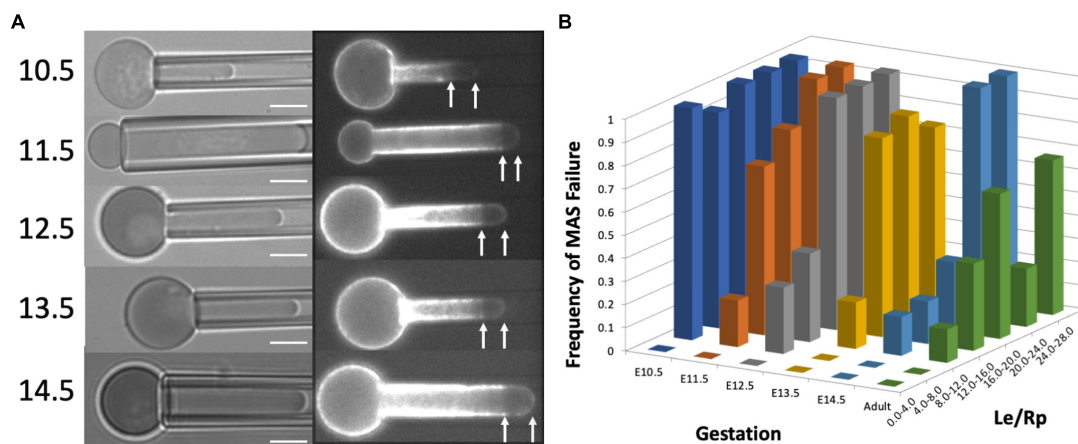


FIGURE 2 | (A) Images of cells from each gestation day showing failure of the MAS. Scale bar = 5.0 μm . **(B)** The dependence of the frequency of MAS failure on projection length (L_e/R_p) and cell maturation (gestation day). Each column represents the fraction of cells observed to have MAS-free regions for the range of L_e/R_p ratios shown on the right-hand axis. Approximately 50 cells were measured for each different gestation day (except E13.5, for which there were 28 cells measured). The number of cells represented by each column depended on the distribution of projection lengths for the cell population and ranged from 1 to 27. Based on logistic regression to the entire data set (without binning), all days were significantly different from E14.5, except for the adult definitive cells, which were not significantly different from primitive cells on E14.5.

regardless of the magnitude of deformation. As the cells matured (at later days of gestation), larger and larger deformations were required in order to observe MAS-free regions. To characterize this dependence, 40–50 cells were tested from multiple embryos at each day of gestation. The data were binned according to the measured ratio L_e/R_p , and the fraction of cells exhibiting MAS-free regions was calculated for each group (**Figure 2B**). Based on logistic regression, the likelihood of failure at a given extension was significantly higher for all days relative to E14.5, except the adult definitive cells, which did not show a statistical difference in failure rate compared to E14.5.

Similar phenomena were observed in immature erythroid cells harvested from adult human marrow (**Figure 3**). Maturing erythroblasts obtained directly from marrow can be identified by their high contrast in blue illumination (reflecting hemoglobin content), but cells at all stages of maturation are represented. Therefore, we must rely on morphology to estimate the level of

cell maturity. Two examples of human marrow erythroid cells subjected to FIMD are shown in **Figure 3**. One cell appears to be similar to erythroid cells found in mouse embryos at E10.5 or before, and the other appears to be a multi-lobulated marrow reticulocyte, probably similar to primitive erythroid cells found in mouse embryos at E14.5. In both of these example cells, MAS-free regions are observed, demonstrating that this phenomenon also occurs in cells maturing in adult human marrow.

Deficiencies in the Cytoskeletal Protein 4.1 Enhance the Formation of Membrane-Associated Cytoskeleton-Free Regions

The erythroid-specific isoform of protein 4.1 (protein 4.1R) stabilizes the interaction between spectrin and junctional complexes within the MAS (Ungewickell et al., 1979). To explore

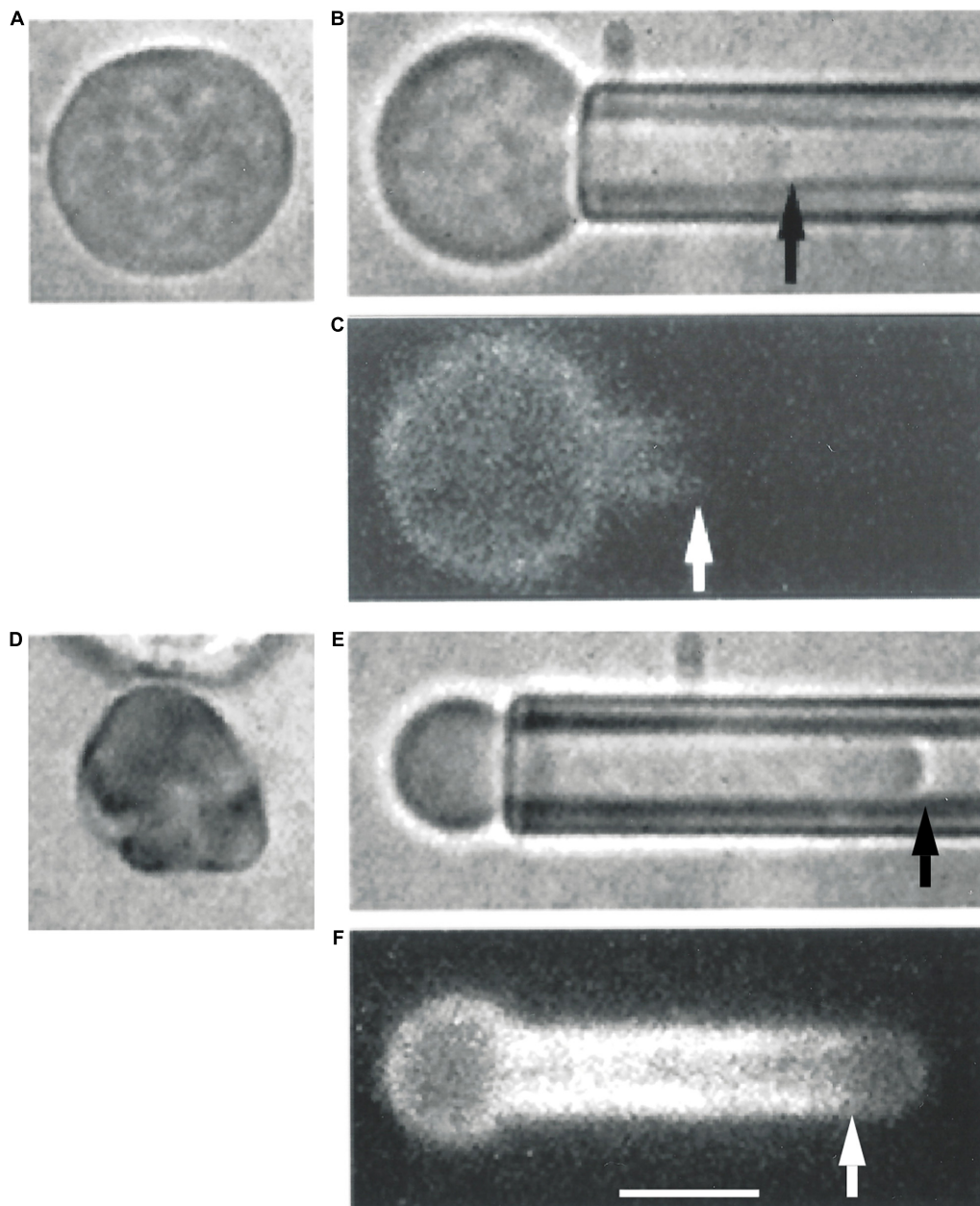


FIGURE 3 | Erythroid cells from adult human marrow also exhibit the formation of MAS-free regions. Two cells prior to aspiration are depicted in panels (A,D). Panel (A) shows an erythroid precursor identified by a darker color in blue illumination due to the presence of Hb in the cell. The cell in panel (D) appears to be a marrow reticulocyte, based on its lobular appearance and lack of a nucleus. When the cell in panel (A) was aspirated into a micropipette, the distribution of fluorescence resembled that of primitive mouse cells from E10.5 [panels (B,C)]. When the cell in panel (D) was aspirated, the fluorescence distribution resembled that of primitive erythroid cells obtained at E14.5 [panels (E,F)]. Scale bar is 5.0 μm for all images.

the consequences of protein 4.1 deficiency during erythroid maturation, we examined primitive erythroblasts from protein 4.1R knockout mice. Previously we have reported that the recruitment of MAS proteins to the cell membrane between E10.5 and E12.5 appears to occur normally in these mice, but that the membranes of the 4.1R-null primitive erythroid cells at E12.5 were mechanically less stable (Huang et al., 2017). Here we further document the mechanical instability of these cells

and the spherocytic phenotype of the adult red blood cells in these mice. Protein 4.1R-null cells showed a greater tendency to form MAS-free regions than wild type cells when deformed into micropipettes. This is illustrated in **Figure 4**, where we plot the fraction of E12.5 primitive erythroid cells exhibiting MAS-free regions for different ranges of deformation (L_e/R_p). Note that for the littermate controls (resulting from the mating of mice that are heterozygous for the missing protein 4.1R gene) the

increase in the fraction of cells exhibiting MAS-free regions is shifted toward higher values of L_e/R_p . Based on logistic regression analysis, this difference is statistically significant, indicating that less deformation is required to produce MAS-free regions in the 4.1R-null cells, consistent with a less-stable MAS. The L_e/R_p ratio needed to generate a 50% failure rate was approximately 8.0 for the protein 4.1R-null cells and approximately 12.0 for the littermate controls. There was no significant difference in stability measures between the normal protein 4.1R littermate control cells (on a C57Bl/6 background) compared to wild type E12.5 erythroblasts (ICR mice). Cells at E10.5 do not express the erythroid-specific splice variant of protein 4.1 (4.1R) and lack many of the key components of the erythroid-specific MAS (e.g., band-3, protein 4.2, β -actin) at the cell membrane (Huang et al., 2017). At this stage, 4.1R-null and 4.1R-positive cells behaved similarly, all cells showing Ter-119-free regions for even small deformations.

Membrane instability was also evident in the cell morphology (Figures 4B,C). Protein 4.1R-null cells exhibited blebbing behavior, and spherical cell fragments could be observed in the cell suspension. The membrane instability resulted in a more spherical phenotype for the protein 4.1R-null cells even at E12.5. This was quantified by calculating the area A and volume V of the pipette-aspirated cells using measurements of the radius of the spherical portion of the cell outside the pipette R_s , the length of the projection inside the pipette L_e , and the pipette radius R_p :

$$A = 2\pi R_s \left[R_s + \sqrt{R_s^2 - R_p^2} \right] + 2\pi R_p L_e$$

$$V = \frac{2\pi}{3} \left[R_s^3 + \left(R_s^2 + \frac{R_p^2}{2} \right) \sqrt{R_s^2 - R_p^2} + R_p^3 \right] + \pi R_p^2 (L_e - R_p)$$

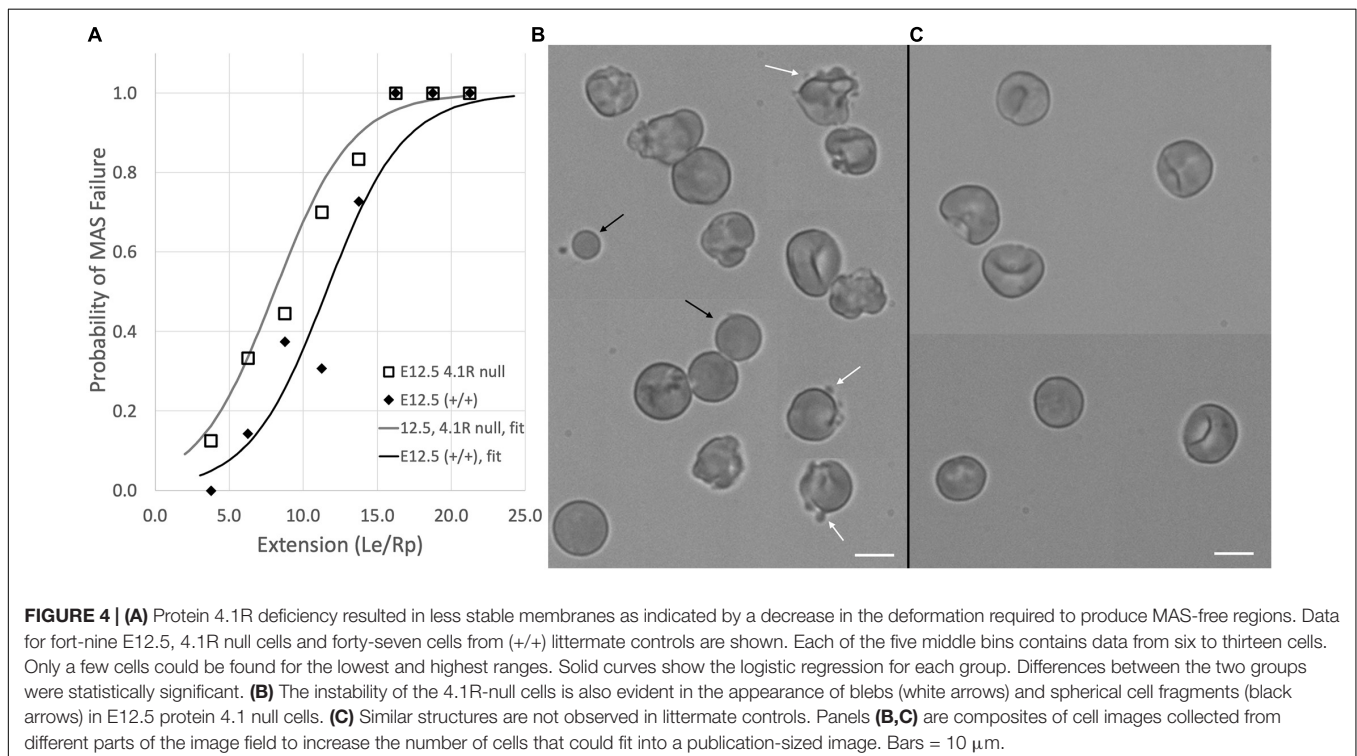
How spherical a cell is can be expressed in terms of the “sphericity,” a dimensionless ratio of the volume to the 2/3 power divided by the cell area:

$$S = \left(\frac{4\pi}{(4\pi/3)^{2/3}} \right) \frac{V^{2/3}}{A}$$

A perfect sphere has a sphericity of 1.0. The sphericity for E12.5 4.1R null cells (mean \pm standard deviation) was 0.86 ± 0.06 , $n = 49$, and the sphericity for the WT cells of the littermate controls was 0.78 ± 0.09 , $n = 37$, a statistically significant difference (Student's t -test). The sphericity of the 4.1R null cells remained high throughout maturation, making it difficult to make meaningful comparisons between the null cells and their littermate controls beyond E12.5 because the magnitude of the deformation was so different between the two cell types. By the time the null cells reached maturity, hardly any membrane projection into the pipette could be achieved (Figure 5).

Mechanism of Failure: Detachment From Bilayer or Lateral Dissociation?

There are two basic ways in which MAS-free regions of the plasma membrane can be formed. One is by the “vertical” detachment of the MAS from the membrane bilayer, and the other is by a lateral dissociation of proteins forming MAS network, creating a “hole” that propagates laterally



along the length of the cell projection. Interpretation of the separation experiments depends critically on which of these two mechanisms is occurring. A cartoon representation of the two different mechanisms is shown in **Figure 6** along with the consequent organization of the MAS and the bilayer membrane after failure. Note that for a “vertical” failure, the MAS network remains intact, forming a flat septum of networked proteins across the lumen of the cell projection. In the case of lateral (“horizontal”) failure, the lumen of the cell projection remains open as the MAS contracts along the cylindrical portion of the membrane projection. Labeling extracellular proteins on the surface of the membrane, such as TER-119 labeling, does not permit us to distinguish between these two mechanisms, but intracellular labeling of the MAS itself does.

To label the MAS intracellularly, red cell “ghosts” were made from primitive erythroid cells, enabling the incorporation of Alexa-488 phalloidin into the interior of the cell to label the actin portion of the MAS. Examples of cells with fluorescently labeled actin are shown in **Figure 7**. One intact MAS example and three ruptured MAS examples are shown. Note the absence of “edge-bright” fluorescence in the lumen of the pipette, except at the tip of the intact example. These images provide clear evidence that the failure mechanism we are observing represents a lateral tearing (rupture) of the MAS and the formation of an open-ended cylindrical sleeve of MAS inside the cell projection into the micropipette. This further reveals that our approach assesses the strength of lateral attachments within the MAS and how this strength increases with maturation.

Dimple Formation Reveals a Contractile Tension at the Edge of the Torn Membrane-Associated Cytoskeleton

When a red blood cell is fully aspirated into a micropipette, a pressure is generated inside the cell that is greater than both the aspiration pressure in the micropipette and the pressure in

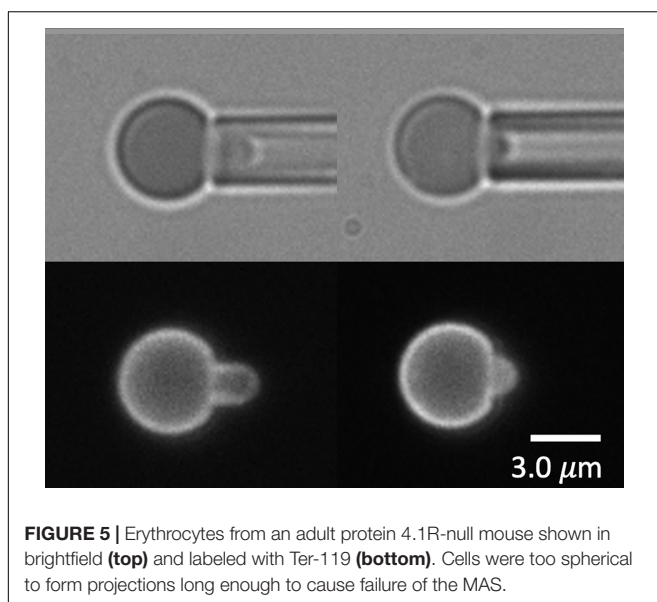
the suspending medium outside the cell. This pressure acts to press the membrane against the inner wall of the pipette lumen and maintain its cylindrical geometry. In cases where the MAS has been torn and forms a truncated cylinder inside the cell projection, an indentation can form at the edge of the torn skeleton when the aspiration pressure, and the corresponding pressure inside the cell, are reduced. This phenomenon is illustrated in **Figure 8**. Images showing the dimple formation in brightfield microscopy and the corresponding distribution of fluorescence in FIMD are shown in **Figure 8A**. This phenomenon indicates that despite having ruptured, the MAS retains some elastic cohesion at its edge that would contribute to cell fragmentation leading to the loss of MAS-free regions of the cell membrane. In **Figure 8B** we show an example of a projection that is “necking” down at the edge of the MAS, a step prior to cell fragmentation. An example showing complete fragmentation of a maturing primitive erythroid cell is shown in **Figure 8C**. Note that TER-119 labeling of the MAS is absent from the separated fragment indicating that cell fragments formed in this way lack MAS components. Formation of MAS-free fragments are also observed in primary erythroid cells from human marrow (See **Figure 9**).

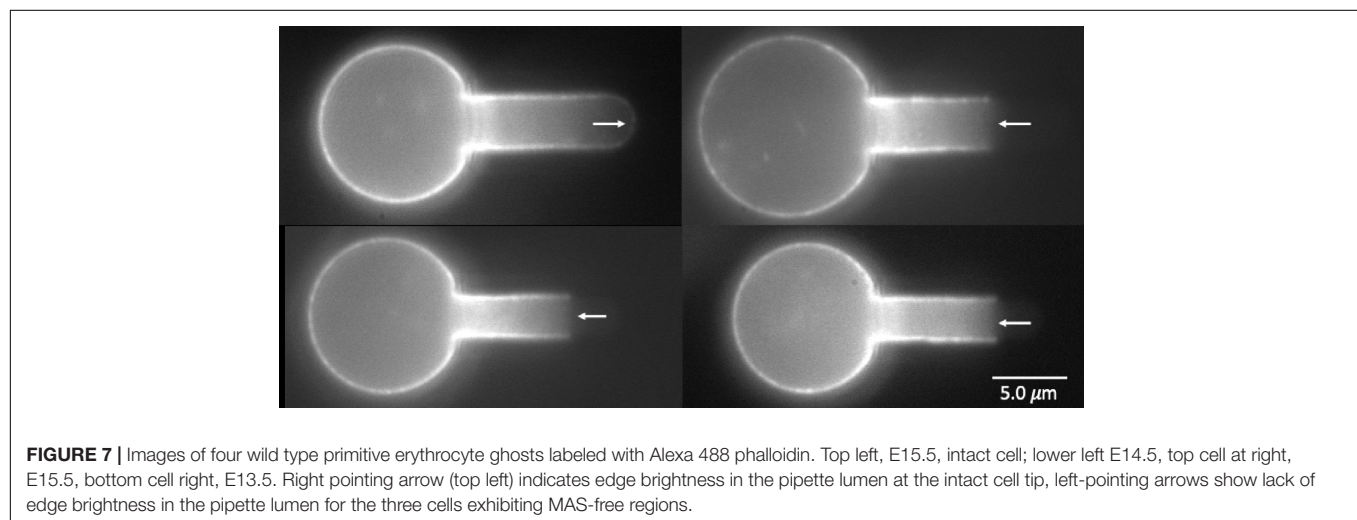
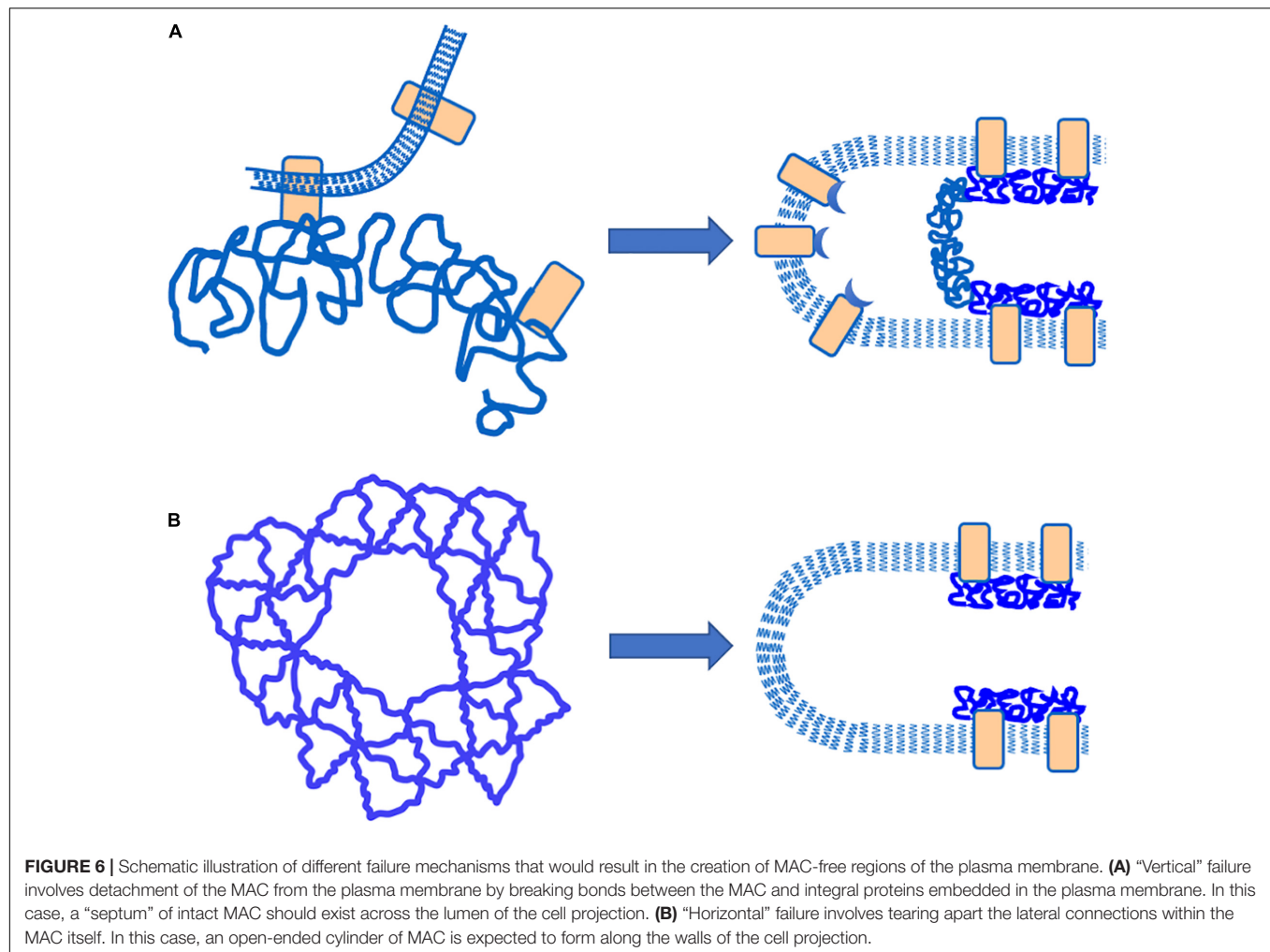
DISCUSSION

The Power of Fluorescence Imaged Microdeformation

The combination of fluorescence labeling of cell structural components and applied micro-deformation is a powerful approach for understanding the structural mechanisms leading to cell behavior in response to applied forces. The application of this experimental approach to adult human red blood cells revealed that the local density of the MAS changes when cells are deformed (Discher et al., 1994). This was significant because many theoretical treatments of red blood cell mechanical behavior had previously made the assumption that the density of the MAS was uniform in deformation (Evans and Skalak, 1979). The FIMD observations supported the development of more complex theoretical descriptions that account for changes in local MAS density (Dao et al., 2006; Peng et al., 2010; Svetina et al., 2016; Feng et al., 2020). In this report, we document an important mechanism of MAS failure in primary primitive erythroid cells from mice, namely the lateral separation of MAS components to form a hole in the MAS. As was observed for the energy cost of tether formation in prior studies (Vaughn et al., 2001, 2013), the tendency of the MAS to undergo lateral failure decreases as the cells mature in the embryo, even days after the MAS protein components become localized to the membrane. These observations lead to the conclusion that localization of the MAS components to the membrane is not in itself sufficient to allow full MAS assembly, but that additional events are required after localization to further strengthen the inter-protein connections with the MAS.

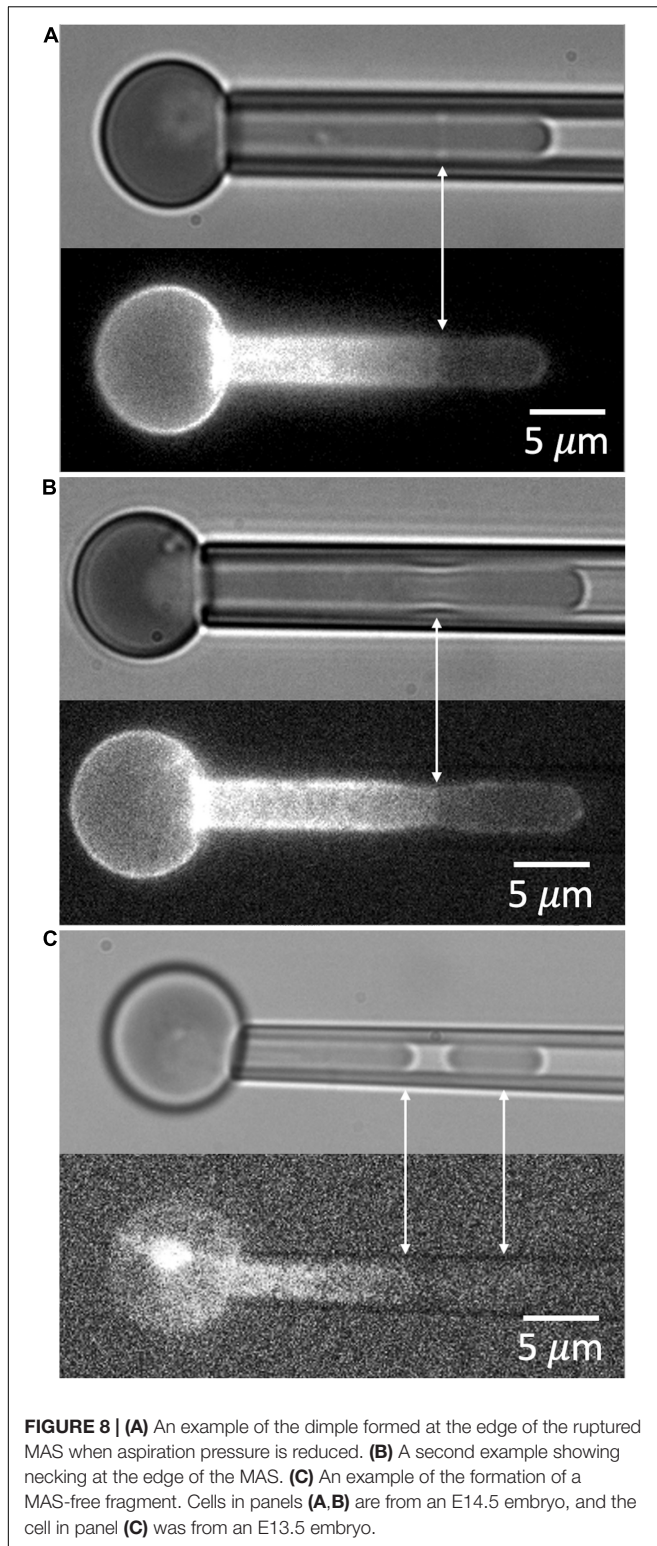
Whenever cell labels are used one should consider the possibility that the label itself could have effects on cell behavior. This is relevant in the current context. Lee et al. (2004) have



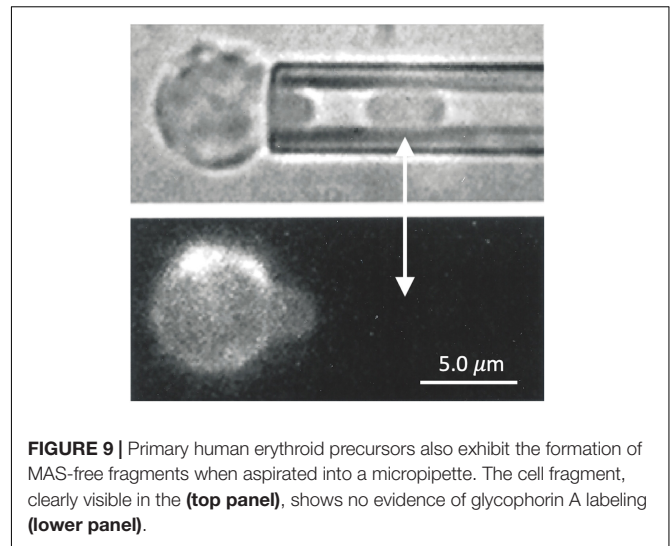


shown that labeling mouse erythrocytes with TER119 increases their mechanical stiffness (Lee et al., 2004), consistent with the observation that antibodies against human glycophorin A increase the stiffness of human red blood cells (Knowles et al.,

1994). It is also conceivable that the use of phalloidin as a label for the actin junctional complexes could also affect the stability of junctional complexes if the label competes for binding with native proteins in the MAS, although this has never been documented,



to our knowledge. It is worth noting, however, that in the limited number of phalloidin labeled ghosts of E14.5 embryos that we tested, a high fraction of cells exhibited MAS-free regions for L_e/R_p ratios > 8.0 , whereas in intact cells labeled with TER119,



the extension at which 50% of cells form MAS-free regions was approximately 18.7. This discrepancy could be the result of alterations to the MAS during the ghost preparation process, an effect of the phalloidin, or an effect of the TER119. The fact that both labeling approaches show consistent trends lends confidence that our general conclusions are valid, and that the behavior of unlabeled, intact cells likely falls in the range between the two labeling approaches.

Membrane-Associated Cytoskeleton Development During Erythroid Maturation

The development of a functional MAS during erythroid maturation is fundamentally important for health. Much of the research in this area has focused on the expression and localization of the principal proteins of the MAS (Minetti et al., 2018). The challenge in most of these studies is the ability to define specific stages of maturation so that the proper sequence of events can be ascertained. Early studies relied on non-mammalian models, or erythroleukemia cells in order to observe the sequencing of protein synthesis (Cox et al., 1987; An et al., 2014). With the advent of flow cytometric methods to assist with lineage definition and cellular staging (Hu et al., 2013), and approaches to detect both messenger RNA and proteins in small quantities (An et al., 2014; Gautier et al., 2018), more recent studies have been able to refine our understanding of the synthesis of MAS components and their assembly in primary erythroid cells at progressive stages of maturation, both mouse and human. The principal MAS proteins, with the exception of actin, progressively increase as a percentage of total protein during maturation from proerythroblasts through the orthochromatic erythroblast stages (Hu et al., 2013). Our model system using primitive erythroid cells that mature as a semi-synchronous cohort in mouse embryos provides an alternate approach for evaluating MAS synthesis and assembly in a primary mammalian system. Using this approach, we have previously demonstrated that the principal

protein components of the MAS are significantly synthesized as early as the proerythroblast stage (E10.5) and that their presence as a percentage of total protein continues to increase through the orthochromatic stage (E12.5) (Huang et al., 2017). The localization of MAS components at the membrane only occurs after the proerythroblast stage, timing that coincides with the beginning of the erythroid-specific splicing of protein 4.1 mRNA in a narrow time interval between E10.5 and E11.5 (Huang et al., 2017).

These approaches have added considerably to our understanding of protein and gene expression during terminal erythroid differentiation, but studies documenting the functional development of the MAS during maturation, particularly those that focus in the critically important development of mechanical stability during maturation, have remained a challenge. In a previous report, we documented the changes in surface area and volume, resistance to deformation, and the strength of the bilayer-skeletal association in maturing primitive erythroid cells from E12.5 through E16.5 (Waugh et al., 2013). While the resistance to membrane deformation did not change over this period, the surface-to-volume ratio of the cell increased, thereby increasing cellular deformability, and the strength of association between the MAS and the membrane bilayer also increased. This latter finding points to a continued increase in mechanical stability of cells in the late stages of erythropoiesis long after the principal protein components are localized to the membrane, a conclusion that is further supported in the current study.

It is interesting to speculate about what additional changes in the MAS proteins at the red cell surface might contribute to the continued strengthening of the MAS after E12.5. On plausible mechanism might be changes in the phosphorylation state of key MAS proteins. It has long been known that many MAS proteins can be phosphorylated and de-phosphorylated (Boivin, 1988). Of relevance to the current topic, increased phosphorylation of both protein 4.1R and β -spectrin lead to decreases in the strength of protein-protein interactions (Eder et al., 1986; Subrahmanyam et al., 1991; Gauthier et al., 2011) as well as the mechanical stability of the intact MAS *in situ* (Manno et al., 1995, 2005). Thus, one likely mechanism for the increased mechanical stability we have observed is the progressive dephosphorylation of one or both of these key MAS proteins.

Mechanisms of Membrane-Associated Cytoskeleton Mechanical Failure and the Formation of Cell Fragments

The membrane composite (bilayer plus MAS) can fail mechanically in multiple ways. Protein-protein interactions within the red cell membrane have been classified as being “vertical” (between the MAS and the bilayer) or “horizontal” (within the MAS) (Tse and Lux, 1999). Failure of horizontal associations typically leads to fragmentation of the cell, while failure of vertical associations typically leads to bilayer detachment. As is evident from the current results, the process can be more complex than this simple picture. The lack of edge fluorescence in aspirated cells (Figure 7) shows that the measurements here involve a “horizontal” failure of the MAS, but

this failure is also associated with the detachment of MAS-free bilayer from the cell (Figures 8, 9).

Given that the mechanisms underlying membrane stability are diverse, it follows that assessment of the mechanical stability of the membrane should involve multiple approaches, and that different testing methods may reveal different underlying mechanisms by which cells maintain (or lose) cohesion. In previous work, we used membrane tether formation to evaluate the strength of the association between the MAS and the membrane bilayer (Waugh et al., 2013). Tethers are thin, cylindrical strands of membrane bilayer pulled from red blood cell surfaces. They do not contain MAS (Butler et al., 2008), and therefore, the force required to form a tether provides a direct measure of the energy cost of creating an MAS-free region of membrane. This energy is manifested in the present study by the fact that after lateral rupture, the MAS cylinder inside the cell projection does not collapse to zero length, but is maintained at finite length by the energy cost of creating additional MAS-free area. Based on tether formation measurements, this energy is approximately $78 \mu\text{J}/\text{m}^2$ for mature human red blood cells, which is substantially higher than for human marrow reticulocytes ($19 \mu\text{J}/\text{m}^2$) (Waugh et al., 2001). Similar increases were observed for maturing primitive mouse erythroid cells, the energy of association increasing from $30 \mu\text{J}/\text{m}^2$ at E12.5 to $53 \mu\text{J}/\text{m}^2$ at E16.5 (Waugh et al., 2013). The physical basis for this energy has yet to be ascertained. Tether formation does not require the breakage of protein-protein interactions between the MAS and the bilayer because the fluid-like membrane can simply flow between the integral membrane “posts” that are attached to the intact MAS. One plausible mechanism for this energy cost is the concept of an “osmotic tension” generated by the different mole fractions of lipid in the membrane region that is associated with the membrane bilayer and in the region that is not (Waugh and Bauserman, 1995).

Caution should be exercised in extending the present findings to interpret membrane fragmentation events and extracellular vesicle (EV) formation from red cells in general. The fact that the MAS-free regions produced in our experiments can be pulled away to form fragments does not mean that all cell fragments are likely to be free of MAS components. On this point, it is relevant that labeling GPA with TER119 increases GPA association with the MAS (Lee et al., 2004), and this will likely artificially prevent the appearance of GPA in the detached vesicles in our experiments. Indeed, a proteomic study of erythrocyte-derived microvesicles from human red cells used GPA to identify RBC-derived microvesicles from plasma. Interestingly, and in contrast to some early reports (Lutz et al., 1977), vesicles isolated in this way do contain some cytoskeletal proteins (Bosman et al., 2012), although at lower proportions than in intact cells. Vorselen et al. (2018) have also found evidence of MAS proteins in EVs both from normal donors and patients with hereditary spherocytosis. It should be kept in mind that EVs can arise from a variety of mechanisms, and that these will likely lead to significant heterogeneity in composition and properties. It is also the case that methods used to isolate and identify EVs will likely lead to the preparation of different populations of EVs reflecting

contributions from different types of EVs and different levels of contamination (Hebbel and Key, 2016; Lapping-Carr et al., 2020).

Consequences of Protein 4.1R Deficiency

Our observation that protein 4.1 deficiency leads to an increased tendency to form MAS-free regions is expected given the long-standing understanding that protein 4.1 serves to strengthen the association between spectrin and actin (Ungewickell et al., 1979), and is a key component of the junctional complexes within the MAS. While it is tempting to argue based on the absence of membrane strengthening we see in the absence of protein 4.1 that protein 4.1 may play a role in the strengthening of the MAS during maturation. However, a network is only as strong as its weakest link, and it is at least as likely that in the presence of protein 4.1, other associations (such as spectrin-spectrin interactions) are the first to fail, and that it is the strengthening of these associations that leads to a more stable MAS overall. Indeed, there is evidence in the literature about the lability of spectrin-spectrin associations in response to surface deformation (An et al., 2002), and it is known that deficiencies in this association can lead to hemolytic anemia in the form of hereditary elliptocytosis (Nicolas et al., 1998). In human patients, abnormalities in protein 4.1 (as is the case for abnormalities affecting spectrin self-association) typically lead to elliptocytosis (Palek and Sahr, 1992). Complete 4.1 deficiencies in human patients are rare, but in the few cases that have been identified, the phenotypic presentation includes characteristics of elliptocytosis and spherocytosis (Feo et al., 1980; Baklouti et al., 2011). A new insight provided by the present study is that the spherocytic phenotype is detectable as early as E12.5 in primitive erythroid cells, a stage equivalent to orthochromatic erythroblasts. It is unknown whether protein 4.1 deficient cells in the marrows of human patients exhibit similar characteristics. The precise nature of the lateral associations within the MAS that are being broken and the associated biochemical changes that serve to increase the strength of those associations during maturation will be the subject of future studies.

DATA AVAILABILITY STATEMENT

The raw data supporting the conclusions of this article will be made available by the authors, without undue reservation.

REFERENCES

- An, X., Lecomte, M. C., Chasis, J. A., Mohandas, N., and Gratzer, W. (2002). Shear-response of the spectrin dimer-tetramer equilibrium in the red blood cell membrane. *J. Biol. Chem.* 277, 31796–31800. doi: 10.1074/jbc.M204567200
- An, X., Schulz, V. P., Li, J., Wu, K., Liu, J., Xue, F., et al. (2014). Global transcriptome analyses of human and murine terminal erythroid differentiation. *Blood* 123, 3466–3477. doi: 10.1182/blood-2014-01-548305

ETHICS STATEMENT

The studies involving human participants were reviewed and approved by Institutional Review Board, Office of Human Subjects Protection, University of Rochester. The patients/participants provided their written informed consent to participate in this study. The animal study was reviewed and approved by University Committee on Animal Resources, University of Rochester.

AUTHOR CONTRIBUTIONS

LD performed all of the experiments involving FIMD on primitive erythroid cells except for the actin-labeled ghost experiments and portions of the materials and methods section and the results section were adapted from his Master's Thesis at the University of Rochester. YH provided most of the primitive erythroid cells used in these studies and performed genotyping of the Epb41 mouse embryos. SL provided statistics expertise and performed statistical analysis of the failure data for **Figures 2B, 4A**. JP provided oversight to YH as her doctoral advisor and helped co-write the manuscript with RW. RW wrote the main draft of the manuscript and oversaw all FIMD experiments on both embryonic mouse and adult human erythroid cells. All authors contributed to the article and approved the submitted version.

FUNDING

Support for this research came from the United States Public Health Service, National Institutes of Health grant numbers HL18208 (RW) and HL116364 (JP). Additional resources were provided by the University of Rochester *via* an internal funding mechanism.

ACKNOWLEDGMENTS

Athanasios Mantalaris isolated and labeled the human marrow cells. Richard Bauserman performed FIMD experiments on human marrow cells and on actin-labeled mouse primitive erythroid ghost cells. Margaret Youngman made actin-labeled ghosts of mouse primitive erythroid cells. Anne Koniski and Paul Kingsley provided primitive erythroid cells from mice for some experiments.

- Anong, W. A., Franco, T., Chu, H., Weis, T. L., Devlin, E. E., Bodine, D. M., et al. (2009). Adducin forms a bridge between the erythrocyte membrane and its cytoskeleton and regulates membrane cohesion. *Blood* 114, 1904–1912. doi: 10.1182/blood-2009-02-203216
- Baklouti, F., Morinière, M., Haj-Khéil, A., Fénéant-Thibault, M., Gruffat, H., Couté, Y., et al. (2011). Homozygous deletion of EPB41 genuine AUG-containing exons results in mRNA splicing defects, NMD activation and protein 4.1R complete deficiency in hereditary elliptocytosis. *Blood Cells Mol. Dis.* 47, 158–165. doi: 10.1016/j.bcmd.2011.07.001

- Boivin, P. (1988). Role of the phosphorylation of red blood cell membrane proteins. *Biochem. J.* 256, 689–695. doi: 10.1042/bj2560689
- Bosman, G. J., Lasonder, E., Groenen-Döpp, Y. A., Willekens, F. L., and Werre, J. M. (2012). The proteome of erythrocyte-derived microparticles from plasma: new clues for erythrocyte aging and vesiculation. *J. Proteomics* 76, 203–210. doi: 10.1016/j.jprot.2012.05.031
- Butler, J., Mohandas, N., and Waugh, R. E. (2008). Integral protein linkage and the bilayer-skeletal separation energy in red blood cells. *Biophys. J.* 95, 1826–1836. doi: 10.1529/biophysj.108.129163
- Chien, S., Sung, K. L., Skalak, R., Usami, S., and Tözeren, A. (1978). Theoretical and experimental studies on viscoelastic properties of erythrocyte membrane. *Biophys. J.* 24, 463–487. doi: 10.1016/s0006-3495(78)85395-8
- Cox, J. V., Stack, J. H., and Lazarides, E. (1987). Erythroid anion transporter assembly is mediated by a developmentally regulated recruitment onto a preassembled membrane cytoskeleton. *J. Cell Biol.* 105, 1405–1416. doi: 10.1083/jcb.105.3.1405
- Dahl, K. N., Westhoff, C. M., and Discher, D. E. (2003). Fractional attachment of CD47 (IAP) to the erythrocyte cytoskeleton and visual colocalization with Rh protein complexes. *Blood* 101, 1194–1199. doi: 10.1182/blood-2002-04-1187
- Dao, M., Li, J., and Suresh, S. (2006). Molecularly based analysis of deformation of spectrin network and human erythrocyte. *Mater. Sci. Eng. C* 26, 1232–1244. doi: 10.1016/j.msec.2005.08.020
- Discher, D. E., Mohandas, N., and Evans, E. A. (1994). Molecular maps of red cell deformation: hidden elasticity and in situ connectivity. *Science* 266, 1032–1035. doi: 10.1126/science.7973655
- Eder, P. S., Soong, C. J., and Tao, M. (1986). Phosphorylation reduces the affinity of protein 4.1 for spectrin. *Biochemistry* 25, 1764–1770. doi: 10.1021/bi00355a047
- Evans, E. A., and Skalak, R. (1979). Mechanics and thermodynamics of biomembranes. *CRC Crit. Rev. Biomed. Eng.* 3, 181–330.
- Feng, Z., Waugh, R. E., and Peng, Z. (2020). Constitutive model of erythrocyte membranes with distributions of spectrin orientations and lengths. *Biophys. J.* 119, 2190–2204. doi: 10.1016/j.bpj.2020.10.025
- Feo, C. J., Fischer, S., Piau, J. P., Grange, M. J., and Tchernia, G. (1980). [1st instance of the absence of an erythrocyte membrane protein (band 4(1)) in a case of familial elliptocytic anemia]. *Nouv. Rev. Fr. Hematol.* 22, 315–325.
- Gauthier, E., Guo, X., Mohandas, N., and An, X. (2011). Phosphorylation-dependent perturbations of the 4.1R-associated multiprotein complex of the erythrocyte membrane. *Biochemistry* 50, 4561–4567. doi: 10.1021/bi200154g
- Gautier, E. F., Leduc, M., Cochet, S., Bailly, K., Lacombe, C., Mohandas, N., et al. (2018). Absolute proteome quantification of highly purified populations of circulating reticulocytes and mature erythrocytes. *Blood Adv.* 2, 2646–2657. doi: 10.1182/bloodadvances.2018023515
- Hebbel, R. P., and Key, N. S. (2016). Microparticles in sickle cell anaemia: promise and pitfalls. *Br. J. Haematol.* 174, 16–29. doi: 10.1111/bjh.14112
- Hu, J., Liu, J., Xue, F., Halverson, G., Reid, M., Guo, A., et al. (2013). Isolation and functional characterization of human erythroblasts at distinct stages: implications for understanding of normal and disordered erythropoiesis in vivo. *Blood* 121, 3246–3253. doi: 10.1182/blood-2013-01-476390
- Huang, Y. S., Delgadillo, L. F., Cyr, K. H., Kingsley, P. D., An, X., McGrath, K. E., et al. (2017). Circulating primitive erythroblasts establish a functional, protein 4.1R-dependent cytoskeletal network prior to enucleating. *Sci. Rep.* 7:5164. doi: 10.1038/s41598-017-05498-4
- Kingsley, P. D., Greenfest-Allen, E., Frame, J. M., Bushnell, T. P., Malik, J., McGrath, K. E., et al. (2013). Ontogeny of erythroid gene expression. *Blood* 121, e5–e13. doi: 10.1182/blood-2012-04-422394
- Kingsley, P. D., Malik, J., Fantauzzo, K. A., and Palis, J. (2004). Yolk sac-derived primitive erythroblasts enucleate during mammalian embryogenesis. *Blood* 104, 19–25. doi: 10.1182/blood-2003-12-4162
- Knowles, D. W., Chasis, J. A., Evans, E. A., and Mohandas, N. (1994). Cooperative action between band 3 and glycophorin A in human erythrocytes: immobilization of band 3 induced by antibodies to glycophorin A. *Biophys. J.* 66, 1726–1732. doi: 10.1016/S0006-3495(94)80965-8
- Lapping-Carr, G., Gemel, J., Mao, Y., and Beyer, E. C. (2020). Circulating extracellular vesicles and endothelial damage in sickle cell disease. *Front. Physiol.* 11:1063. doi: 10.3389/fphys.2020.01063
- Lee, J. C., Gimm, J. A., Lo, A. J., Koury, M. J., Krauss, S. W., Mohandas, N., et al. (2004). Mechanism of protein sorting during erythroblast enucleation: role of cytoskeletal connectivity. *Blood* 103, 1912–1919. doi: 10.1182/blood-2003-03-0928
- Lee, J. C., Wong, D. T., and Discher, D. E. (1999). Direct measures of large, anisotropic strains in deformation of the erythrocyte cytoskeleton. *Biophys. J.* 77, 853–864. doi: 10.1016/S0006-3495(99)76937-7
- Li, J., Dao, M., Lim, C. T., and Suresh, S. (2005). Spectrin-level modeling of the cytoskeleton and optical tweezers stretching of the erythrocyte. *Biophys. J.* 88, 3707–3719. doi: 10.1529/biophysj.104.047332
- Lutz, H. U., Liu, S. C., and Palek, J. (1977). Release of spectrin-free vesicles from human erythrocytes during ATP depletion. I. Characterization of spectrin-free vesicles. *J. Cell Biol.* 73, 548–560. doi: 10.1083/jcb.73.3.548
- Lux, S. E. (2016). Anatomy of the red cell membrane skeleton: unanswered questions. *Blood* 127, 187–199. doi: 10.1182/blood-2014-12-512772
- Manno, S., Takakuwa, Y., and Mohandas, N. (2005). Modulation of erythrocyte membrane mechanical function by protein 4.1 phosphorylation. *J. Biol. Chem.* 280, 7581–7587. doi: 10.1074/jbc.M410650200
- Manno, S., Takakuwa, Y., Nagao, K., and Mohandas, N. (1995). Modulation of erythrocyte membrane mechanical function by beta-spectrin phosphorylation and dephosphorylation. *J. Biol. Chem.* 270, 5659–5665. doi: 10.1074/jbc.270.10.5659
- McGrath, K. E., Koniski, A. D., Malik, J., and Palis, J. (2003). Circulation is established in a stepwise pattern in the mammalian embryo. *Blood* 101, 1669–1676. doi: 10.1182/blood-2002-08-2531
- Minetti, G., Achilli, C., Perotti, C., and Ciana, A. (2018). Continuous change in membrane and membrane-skeleton organization during development from proerythroblast to senescent red blood cell. *Front. Physiol.* 9:286. doi: 10.3389/fphys.2018.00286
- Mohandas, N., and An, X. (2006). New insights into function of red cell membrane proteins and their interaction with spectrin-based membrane skeleton. *Transfus. Clin. Biol.* 13, 29–30. doi: 10.1016/j.tracbi.2006.02.017
- Nash, G. B., and Meiselman, H. J. (1983). Red cell and ghost viscoelasticity. Effects of hemoglobin concentration and in vivo aging. *Biophys. J.* 43, 63–73. doi: 10.1016/S0006-3495(83)84324-0
- Nicolas, G., Pedroni, S., Fournier, C., Gautero, H., Craescu, C., Dhermy, D., et al. (1998). Spectrin self-association site: characterization and study of beta-spectrin mutations associated with hereditary elliptocytosis. *Biochem. J.* 332(Pt 1), 81–89. doi: 10.1042/bj3320081
- Palek, J., and Sahr, K. E. (1992). Mutations of the red blood cell membrane proteins: from clinical evaluation to detection of the underlying genetic defect. *Blood* 80, 308–330.
- Peng, Z., Asaro, R. J., and Zhu, Q. (2010). Multiscale simulation of erythrocyte membranes. *Phys. Rev. E Stat. Nonlin. Soft Matter Phys.* 81(3 Pt 1):031904. doi: 10.1103/PhysRevE.81.031904
- Picart, C., Dalhaimer, P., and Discher, D. E. (2000). Actin protofilament orientation in deformation of the erythrocyte membrane skeleton. *Biophys. J.* 79, 2987–3000. doi: 10.1016/S0006-3495(00)76535-0
- Shi, Z. T., Afzal, V., Coller, B., Patel, D., Chasis, J. A., Parra, M., et al. (1999). Protein 4.1R-deficient mice are viable but have erythroid membrane skeleton abnormalities. *J. Clin. Invest.* 103, 331–340. doi: 10.1172/JCI3858
- Skalak, R., Tozeren, A., Zarda, R. P., and Chien, S. (1973). Strain energy function of red blood cell membranes. *Biophys. J.* 13, 245–264. doi: 10.1016/S0006-3495(73)85983-1
- Subrahmanyam, G., Bertics, P. J., and Anderson, R. A. (1991). Phosphorylation of protein 4.1 on tyrosine-418 modulates its function in vitro. *Proc. Natl. Acad. Sci. U.S.A.* 88, 5222–5226. doi: 10.1073/pnas.88.12.5222
- Svetina, S., Kokot, G., Kebe, T. Š, Žekš, B., and Waugh, R. E. (2016). A novel strain energy relationship for red blood cell membrane skeleton based on spectrin stiffness and its application to micropipette deformation. *Biomech. Model. Mechanobiol.* 15, 745–758. doi: 10.1007/s10237-015-0721-x
- Tse, W. T., and Lux, S. E. (1999). Red blood cell membrane disorders. *Br. J. Haematol.* 104, 2–13. doi: 10.1111/j.1365-2141.1999.01130.x

- Ungewickell, E., Bennett, P. M., Calvert, R., Ohanian, V., and Gratzner, W. B. (1979). In vitro formation of a complex between cytoskeletal proteins of the human erythrocyte. *Nature* 280, 811–814. doi: 10.1038/280811a0
- Vorselen, D., van Dommelen, S. M., Sorkin, R., Piontek, M. C., Schiller, J., Döpp, S. T., et al. (2018). The fluid membrane determines mechanics of erythrocyte extracellular vesicles and is softened in hereditary spherocytosis. *Nat. Commun.* 9:4960. doi: 10.1038/s41467-018-07445-x
- Waugh, R., and Evans, E. A. (1979). Thermoelasticity of red blood cell membrane. *Biophys. J.* 26, 115–132. doi: 10.1016/S0006-3495(79)85239-X
- Waugh, R. E., and Bauserman, R. G. (1995). Physical measurements of bilayer-skeletal separation forces. *Ann. Biomed. Eng.* 23, 308–321. doi: 10.1007/BF02584431
- Waugh, R. E., Huang, Y. S., Arif, B. J., Bauserman, R., and Palis, J. (2013). Development of membrane mechanical function during terminal stages of primitive erythropoiesis in mice. *Exp. Hematol.* 41, 398–408.e2. doi: 10.1016/j.exphem.2012.11.007
- Waugh, R. E., Mantalaris, A., Bauserman, R. G., Hwang, W. C., and Wu, J. H. (2001). Membrane instability in late-stage erythropoiesis. *Blood* 97, 1869–1875. doi: 10.1182/blood.v97.6.1869
- Zhang, D., Kiyatkin, A., Bolin, J. T., and Low, P. S. (2000). Crystallographic structure and functional interpretation of the cytoplasmic domain of erythrocyte membrane band 3. *Blood* 96, 2925–2933.

Conflict of Interest: The authors declare that the research was conducted in the absence of any commercial or financial relationships that could be construed as a potential conflict of interest.

Publisher's Note: All claims expressed in this article are solely those of the authors and do not necessarily represent those of their affiliated organizations, or those of the publisher, the editors and the reviewers. Any product that may be evaluated in this article, or claim that may be made by its manufacturer, is not guaranteed or endorsed by the publisher.

Copyright © 2022 Delgadillo, Huang, Leon, Palis and Waugh. This is an open-access article distributed under the terms of the Creative Commons Attribution License (CC BY). The use, distribution or reproduction in other forums is permitted, provided the original author(s) and the copyright owner(s) are credited and that the original publication in this journal is cited, in accordance with accepted academic practice. No use, distribution or reproduction is permitted which does not comply with these terms.



Imaging Erythrocyte Sedimentation in Whole Blood

Alexis Darras^{1*}, Hans Georg Breunig², Thomas John¹, Renping Zhao³, Johannes Koch³, Carsten Kummerow³, Karsten König^{2,4}, Christian Wagner^{1,5} and Lars Kaestner^{1,6*}

¹ Experimental Physics, Saarland University, Saarbrücken, Germany, ² Biophotonics and Laser Technology, Saarland University, Saarbrücken, Germany, ³ Department of Biophysics, Center for Integrative Physiology and Molecular Medicine, School of Medicine, Saarland University, Homburg, Germany, ⁴ JenLab GmbH, Berlin, Germany, ⁵ Department of Physics and Materials Science, University of Luxembourg, Luxembourg City, Luxembourg, ⁶ Theoretical Medicine and Biosciences, Saarland University, Homburg, Germany

OPEN ACCESS

Edited by:

Lesley Jean Bruce,
NHS Blood and Transplant,
United Kingdom

Reviewed by:

Yang Jun Kang,
Chosun University, South Korea
Eon Soo Lee,
New Jersey Institute of Technology,
United States
Guy Cloutier,
Université de Montréal, Canada

*Correspondence:

Alexis Darras
alexis.darras@uni-saarland.de
Lars Kaestner
lars_kaestner@me.com

Specialty section:

This article was submitted to
Red Blood Cell Physiology,
a section of the journal
Frontiers in Physiology

Received: 22 June 2021

Accepted: 23 November 2021

Published: 28 January 2022

Citation:

Darras A, Breunig HG, John T,
Zhao R, Koch J, Kummerow C,
König K, Wagner C and Kaestner L
(2022) Imaging Erythrocyte
Sedimentation in Whole Blood.
Front. Physiol. 12:729191.
doi: 10.3389/fphys.2021.729191

The erythrocyte sedimentation rate (ESR) is one of the oldest medical diagnostic tools. However, currently there is some debate on the structure formed by the cells during the sedimentation process. While the conventional view is that erythrocytes sediment as separate aggregates, others have suggested that they form a percolating gel, similar to other colloidal suspensions. However, visualization of aggregated erythrocytes, which would settle the question, has always been challenging. Direct methods usually study erythrocytes in 2D situations or low hematocrit (~1%). Indirect methods, such as scattering or electric measurements, provide insight on the suspension evolution, but cannot directly discriminate between open or percolating structures. Here, we achieved a direct probing of the structures formed by erythrocytes in blood at stasis. We focused on blood samples at rest with controlled hematocrit of 45%, from healthy donors, and report observations from three different optical imaging techniques: direct light transmission through thin samples, two-photon microscopy and light-sheet microscopy. The three techniques, used in geometries with thickness from 150 μm to 3 mm, highlight that erythrocytes form a continuous network with characteristic cracks, i.e., a colloidal gel. The characteristic distance between the main cracks is of the order of ~100 μm . A complete description of the structure then requires a field of view of the order of ~1 mm, in order to obtain a statistically relevant number of structural elements. A quantitative analysis of the erythrocyte related processes and interactions during the sedimentation need a further refinement of the experimental set-ups.

Keywords: red cells, erythrocyte sedimentation rate (ESR), mesoscopic microscopy, two-photon microscopy, light-sheet microscopy, particle gel

INTRODUCTION

The erythrocyte sedimentation rate (ESR) is one of the oldest diagnostic methods. Already in ancient times it was known that the sedimentation of the red part of the blood can be very different (Kushner, 1988). In fact, it was known even before the thermometer was invented that many diseases cause a higher ESR (Bernhardt and Hianik, 2000), which as we know today is also related to increased body temperature.

At the end of the 19th century, the ESR was developed into a diagnostic tool very close to how it is used nowadays (Biernacki, 1894; Westergreen, 1921). It was recognized as a non-specific measure of inflammation with all the advantages and disadvantages of an unspecific test.

The primary explanation of the process goes back to the seminal work of Robin Fåhræus (Fåhræus, 1929) and is based on the effect that erythrocytes form aggregates phenomenologically described as the formation of “stack of coins,” also known as “rouleaux.” There has been a long dispute whether this is caused by depletion or specific binding and probably both mechanisms contribute to the effect (Baskurt et al., 2012; Flormann et al., 2017). Medically, there are two effects involving the erythrocytes: (i) the increase of plasma proteins associated with inflammation. This is the case for fibrinogen. Although also C-reactive protein (CRP) is increased in inflammation, it does not contribute to increased ESR (Flormann et al., 2015). In contrast, (ii) also the erythrocyte shape and rigidity contributes to the ESR. Irregular shaped or rigidified cells, like sickle cells (Jan et al., 1981; Lawrence and Fabry, 1986) or acanthocytes (Salt et al., 1960) decrease the ESR. Although there is no lower limit established as a pathological limit, a low ESR was proposed as a biomarker for diseases belonging to the neuroacanthocytosis syndrome (NAS) (Darras et al., 2021a; Rabe et al., 2021). Moreover, the viscosity of the plasma also have an influence on the ESR (Késmárky et al., 2008).

The conventional view of erythrocytes sedimentation is that erythrocytes sediment as separate aggregates (Baskurt et al., 2012). This assumption suits the observation of a higher sedimentation rate for higher blood plasma protein concentrations, inducing a higher aggregation force between the cells. Indeed, in such a situation, the bigger the aggregates are, the faster they sediment. However, it is at odds with the existence of a sharp phase transition between plasma and erythrocyte suspension that is clearly visible in all phases of the sedimentation process (Pribush et al., 2010). This could be explained by the fact that erythrocytes aggregate into a percolating gel that collapses during the sedimentation process (Darras et al., 2021a,b), as it is the case for other colloidal suspensions. Regarding blood, the position of the sharp transition interface can oscillate in time (Tuchin et al., 2002). The evolution of the suspension's electrical conductivity over time also supports the idea that the structure evolves into a gel containing some plasma channels (Pribush et al., 2010). However, classical colloidal gels tend to sediment slower when the attraction between the suspended particles increases (Gopalakrishnan et al., 2006), then supporting the conventional view, although recent results show that erythrocyte shapes and flexibility might change this behavior (Darras et al., 2021b; Dasanna et al., 2021). To settle these discrepancies and better understand the fundamental mechanisms of erythrocyte sedimentation, it is necessary to have a closer mesoscopic or microscopic view on the sedimentation process.

Previously, visualization and characterization of aggregated erythrocytes has always been challenging. The direct optical transmission methods usually study erythrocytes in 2D situations (Kaliviotis and Yianneskis, 2007), or at very low hematocrit (~1%) (Shiga et al., 1983). Indirect methods, such as ultrasound

or light scattering (Yeom and Lee, 2015; Gyawali et al., 2018) or electric properties (Pribush et al., 2010) provide useful insight on the changes of the suspensions. However, they could only be directly associated to aggregation states when the previous direct techniques are applicable (Kaliviotis et al., 2010), while further extrapolations are based on extensive theoretical assumptions (Pribush and Meyerstein, 2007). In particular, those techniques don't allow to discriminate between percolating or disparate aggregates.

Here, we present an attempt to perform such direct microscopic observation of the sedimentation process. Due to the high optical density of erythrocytes in whole blood, this microscopic task is a challenge. Furthermore, we have to match the need to image perpendicularly to the gravitational force, which excludes classical upright and inverted microscopes. Therefore, we compared three different approaches: (i) mesoscopic transmission microscopy with a microscope put on its side, (ii) two-photon microscopy with a special device with an objective mounted on a hinged bracket designed for *in vivo* investigations of human skin (König, 2018), and (iii) light-sheet microscopy, which intrinsically has the right geometry.

We show that, for every geometry we probed, erythrocytes form a continuous network with characteristic cracks, i.e., a colloidal gel. These imaging techniques then support the most recent models for erythrocytes sedimentation (Darras et al., 2021b; Dasanna et al., 2021) and supports mechanistic explanation of how deformed erythrocytes influence the ESR (Darras et al., 2021a; Rabe et al., 2021). Furthermore, they open the way for a quantitative analysis of the erythrocyte related processes and interactions during the sedimentation, even though such analysis requires a further refinement of the experimental set-ups.

MATERIALS AND METHODS

We attempted to highlight the structure adopted by erythrocytes during sedimentation with three different imaging techniques. The first one is a simple transmission of blue light through a thin sample. The two others are advanced but well-established techniques, namely two-photon microscopy and light-sheet microscopy. This section details the sample preparations and the basic principles of each technique.

Blood samples were collected as previously described (Abay et al., 2019). Blood was exclusively used from healthy volunteers with an informed consent, according to the declaration of Helsinki and the approval by the ethics committee “Ärztchamber des Saarlandes,” ethics votum 51/18. Nine mL of blood were collected in EDTA-containing tubes (Sarstedt, Nümbrecht, Germany). If indicated, a fluorescent dye was added and then the blood directly transferred into the measurement containers. All measurements were performed within 6 h after withdrawal.

Since the container's geometry is known to have an influence on the ESR (Patton et al., 1989; Brigden and Page, 1993), we performed experiments to assess variations between our three setups. We performed classic ESR measurements with the same healthy sample with a controlled hematocrit of 45%. The

height of cell-free plasma layer on top of erythrocytes after 1 h are, respectively, 9.3 ± 0.3 , 7.5 ± 0.3 , and 9.9 ± 0.3 mm for the transmission, two-photon and light-sheet microscopy. Average sedimentation velocity of the erythrocytes in the various containers then have the same order of magnitude (respectively, 9.3 ± 0.3 , 7.5 ± 0.3 , and 9.9 ± 0.3 mm/h).

Mesoscopic Blue-Light Transmission Imaging

We first tried to image the structure of erythrocytes during sedimentation in a thin container via direct blue-light transmission. We chose blue light because this provides the highest contrast due to the Soret band in the absorption spectrum of hemoglobin (Kaestner et al., 2006).

We prepared containers with two microscope glass slides (1 mm thickness, VWR, Radnor, PA, United States), separated by two bands of paraffin, 150 ± 50 μm thick (see **Figure 1A** for the set-up, **Figure 1B** for a scheme and **Figure 1C** for a picture of the container). To ensure homogenous wetting, both plates were first washed with isopropanol and distilled water, then dried with clean compressed air. The paraffin layer was made by cutting a few Parafilm® M (Carl Roth GmbH, Karlsruhe, Germany) bands, placing them on one of the glass slides and then heating the system briefly to 70°C on a heating plate (RCT basic, IKA-Werke GmbH, Staufen, Germany). Once the paraffin became malleable, the second glass plate was placed on top and the whole system was gently pressed together by hand.

The blood sample was completely drawn into the space between the plates by capillary forces. The bottom and top openings were then sealed with petroleum jelly (KORASILON-Paste, Kurt Obermeier GmbH, Bad Berleburg, Germany).

For high-resolution pictures of the observed cell-free areas, we illuminated the samples with blue light (High-power LED SOLIS-415C, Thorlabs, Newton, NJ, United States). Transmission images were then obtained with a microscope whose observation axis was horizontal. **Figure 1B** shows the scheme of the set-up and **Figure 1A** the corresponding set-up of the Stereomicroscope (Zeiss, Jena, Germany) with an $8\times$ zoom objective. A frame rate of 0.2 Hz was chosen, since it seems sufficient to capture the mesoscopic changes observed at this scale.

Two-Photon Microscopy

Two-photon microscopy is a technique which is applied whenever a high penetration depth into tissue is required, e.g., when imaging skin layers *in vivo* (König and Riemann, 2003; Breunig et al., 2012; König et al., 2015; König, 2018), brain structures (Denk et al., 1995; Cartarozzi et al., 2018) or cardiac tissue (Kaestner and Lipp, 2007; Hammer et al., 2014). Here, we used the MTPflex CARS tomograph (JenLab GmbH, Berlin, Germany) with a flexible arm, originally designed to assess skin lesions by *in vivo* imaging (Weinigel et al., 2015).

A 30 mM stock suspension of free-acid fluorescein (Sigma-Aldrich, St. Louis, MO, United States) in phosphate buffered saline (PBS, Gibco, New York, NY, United States) was prepared. For the observations, erythrocytes and plasma were first separated by centrifugation. Subsequently, 10 μL of the

fluorescein 30 mM stock suspension were added to 1 mL of plasma, thereby creating a 300 μM concentration of fluorescein. The dyed plasma was then mixed again with packed erythrocytes to reach a final hematocrit of 45%. When macroscopically compared with erythrocytes resuspended in pure plasma, the dyed suspension did not present any significant modification of the ESR.

We used spectroscopy cuvettes with a square cross-section of 3 mm \times 3 mm and 20 mm high (Art. No. 101-015-40, Hellma Analytics, Müllheim, Germany). The cuvettes were filled with 180 μL suspension by the means of a micropipette. They were then sealed by a cover glass slide, on which a thin layer of petroleum jelly had been spread, and the cuvette was eventually turned upside-down for a better reproducibility of the top surface. For imaging, femtosecond laser pulses were focused into the sample and the focal position scanned across the region of interest. Fluorescence signals were pixel wise collected in reflection geometry to generate the two photon images. The mean laser power was approximately 38 mW, the laser wavelength was set to 800 nm. A low NA objective (Fluar $5\times/0.25\text{NA}$, Zeiss, Germany) was employed to enable a large field-of-view. The achievable resolutions for this objective were estimated to be 2 μm and 20 μm lateral and axially, respectively, while providing a maximum image region of approximately 2 mm \times 2 mm. The corresponding focal volume is then of 125 μm^3 . **Figures 2A,B** show the tomograph and the sample setup, respectively. A frame rate of 0.25 Hz was achieved. This value was the limit set by the scanning speed of the sample.

Light-Sheet Microscopy

Light sheet microscopy is based on separate light paths for sample excitation and image acquisition (Huisken et al., 2004). It has in common with the two-photon microscopy that fluorophores are excited only in the layers where image generation occurs. This is in contrast to confocal microscopy and other sectioning microscopy methods (Lipp and Kaestner, 2006) and has the advantage to avoid unnecessary photobleaching of the samples.

Finally, we prepared a 10 mM stock solution of Atto 647 carboxyl (Atto-Tec, Siegen, Germany) in PBS. For the observations, erythrocytes and plasma were first separated by centrifugation. Subsequently, 1 μL of the dye solution was added to 1 mL of plasma, thereby creating a 10 μM concentration of Atto647. The stained plasma was then mixed again with packed erythrocytes to reach a final hematocrit of 45%.

To prepare the sample, 60 μL of the stained erythrocyte suspension was then placed in a fluorinated ethylene propylene (FEP)-tube (KAP 101.653, Techlab, Braunschweig, Germany) with inner diameter of 1.6 mm. The bottom of the tube was sealed with petroleum jelly. The sample was then placed inside the light-sheet microscope chamber (Z1, Zeiss, Jena, Germany) and illuminated with a laser sheet, as illustrated schematically in **Figure 3A** and in the actual device **Figures 3B,C**.

A z-stack, recorded with a $20\times$ objective and a $0.4\times$ post reduction, was performed by modifying the position of the sample relative to the light sheet in steps of 5 μm , with a total of 74 slices, in approximately 8s. The resulting frame rate of the eventual recordings is then of 0.13 Hz. Given the high-volume

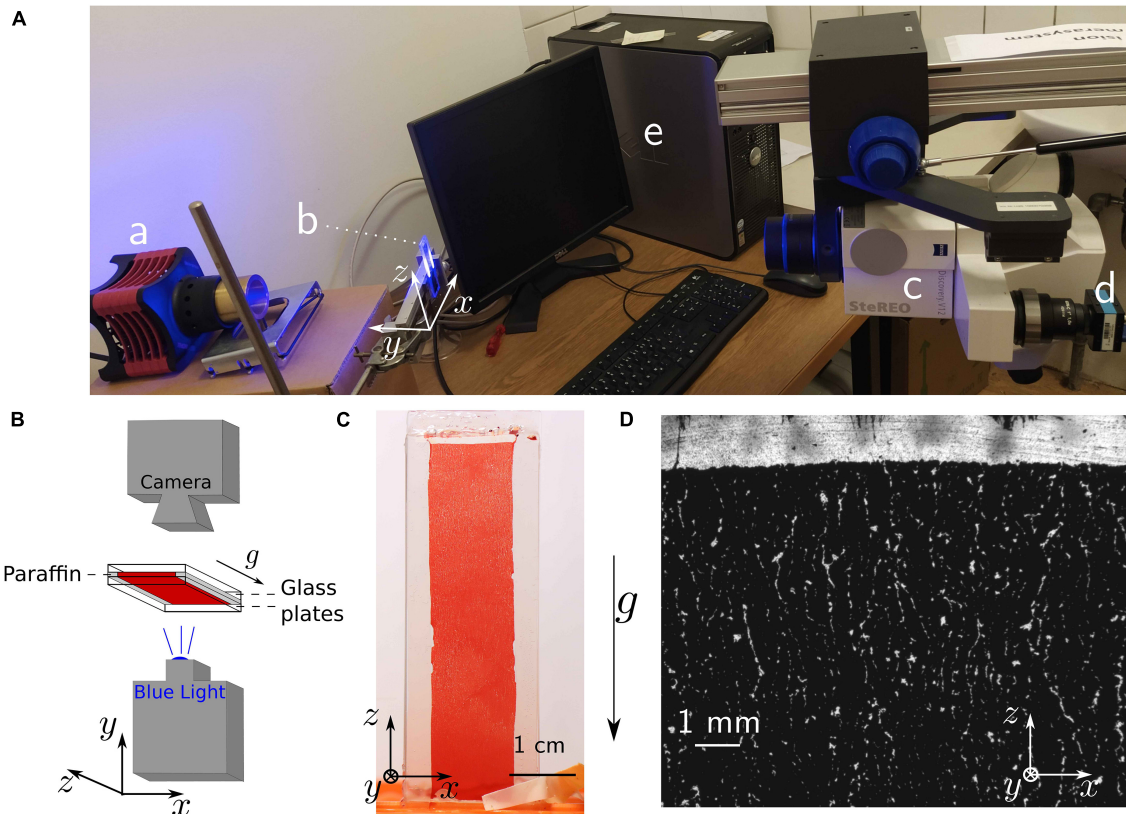


FIGURE 1 | Mesoscopic blue-light transmission observation. **(A)** Picture of the whole set-up with **(a)** the blue light source, **(b)** the sample, **(c)** the microscope connected to **(d)** the camera and **(e)** the computer. **(B)** Scheme of the microscopy set-up and the sample structure. **(C)** Picture of the whole sample, as obtained from a regular camera with macroscopic objective. The picture has been obtained after 90 min sedimentation time. **(D)** Microscopic picture obtained with blue light transmission after 30 min sedimentation time (wide view). Bright areas are the ones where no cells are observed along the y axis, since erythrocytes absorb the transmitted blue light.

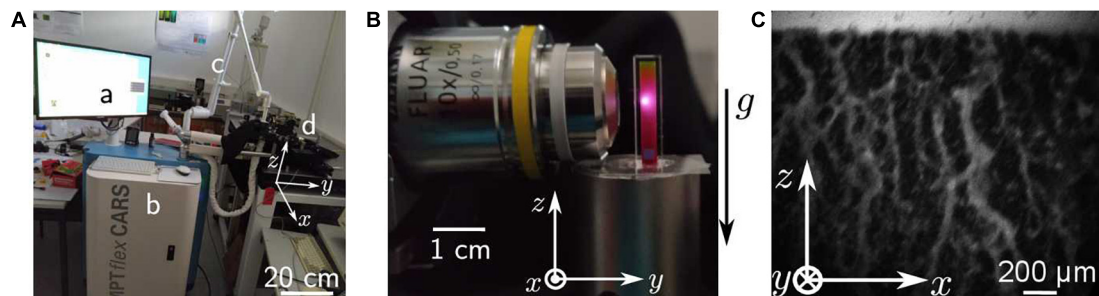
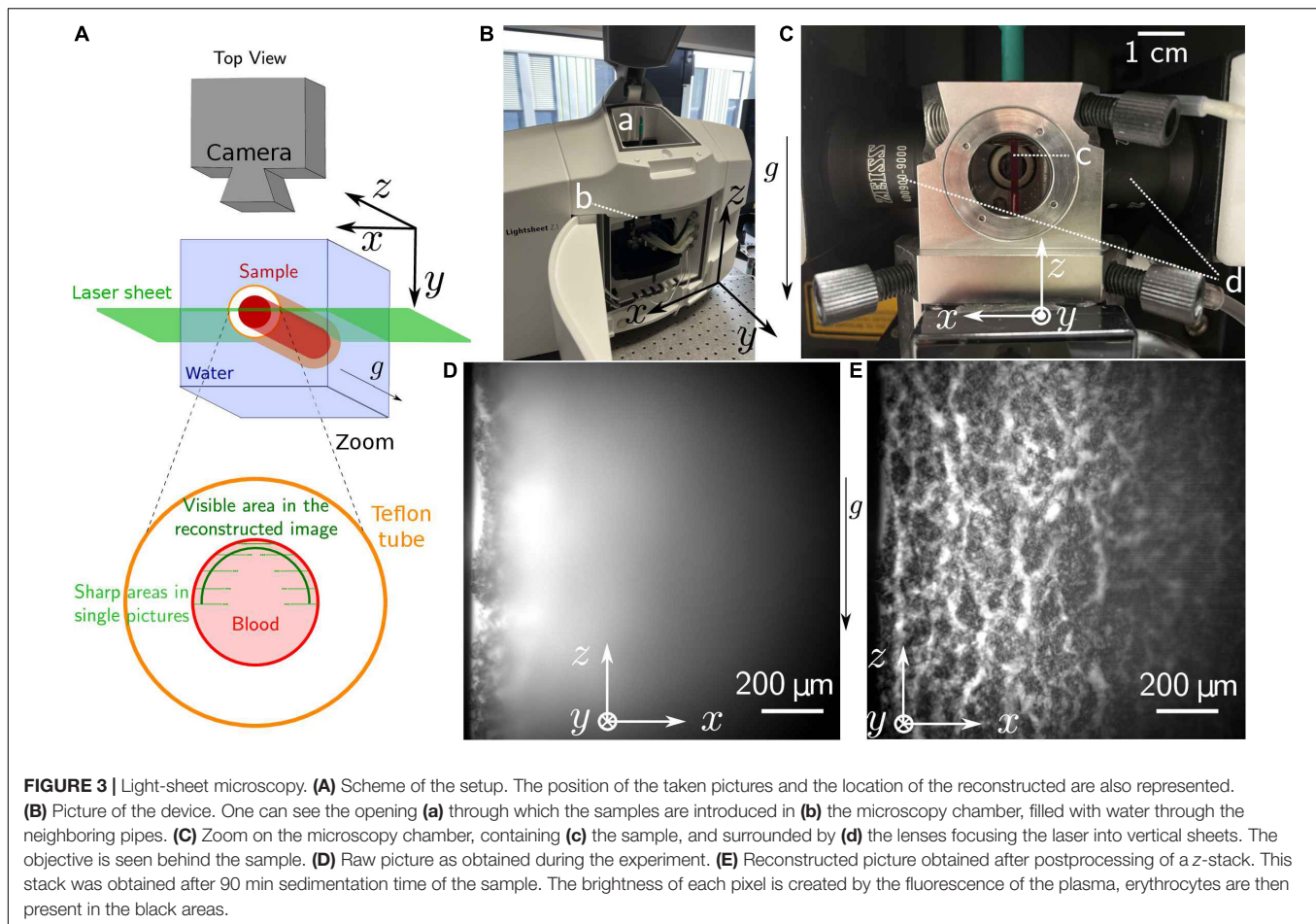


FIGURE 2 | Two-photon microscopy. **(A)** Photograph of the whole MTP flex CARS tomograph, used for two-photon imaging. The visible parts are **(a)** the control station, **(b)** the core of the device containing the laser and the control computer unit, **(c)** the light-guiding tube, and **(d)** the objective with the samples. **(B)** Zoomed picture of a sample and the objective. Picture taken for illustration purpose, the laser isn't focused at the observation plane, which is the surface of the sample. **(C)** Picture obtained of the erythrocytes configuration after 30 min of sedimentation. The brightness of each pixel is created by the fluorescence of the plasma, erythrocytes are then present in the black areas.

fraction of the erythrocytes, the region suitable for imaging is actually limited to approximately $100\ \mu\text{m}$ from the sample border. However, one can then reconstruct a complete picture by averaging the areas in which structures appear sharp from the different pictures of the z -stack.

For the picture reconstruction, a dedicated Matlab (MathWorks, Natick, MA, United States) routine was implemented. An inhomogeneous background level was identified for each picture through morphological opening using a circle with a radius of $60\ \mu\text{m}$ as a structuring element. The



background levels were then removed from the initial images and the resulting filtered images were averaged.

RESULTS

Mesoscopic Blue-Light Transmission Imaging

Figures 1C,D show the setup with the blood sample in between the two coverslips separated by a distance of approximately $150\ \mu\text{m}$ and a representative image obtained with the stereo microscope ($8\times$ zoom), respectively. Additionally, we present a movie of the sedimentation process in the **Supplementary Movie 1**. The suspension is initially homogeneous, but mesoscopic channels appear in the container within 15 min. The observation of some winding cell-free channels is already possible in daylight by eye or with a macroscopic objective and a regular camera. However, the characteristic width of such channels is typically a few tens of micrometers. Since the thickness of the container itself was already approximately $150\ \mu\text{m}$, it is clear that only parts of the biggest cell-free channels were actually observable with this technique.

The images highlight the appearance of cell-free crack-like structures and indicate the potential for easily reproducible mesoscopic observations. It then qualitatively supports the hypothesis that erythrocytes organize into a percolating colloidal gel, and already leads to the observation of a characteristic distance of the order of a few hundreds of micrometers between two of the visible cracks. These first observations then imply that further observation techniques should cover an area of approximately 1 mm wide to capture a statistically relevant part of the sample organization. However, these pictures cannot resolve the actual size and properties of the channels, nor the detailed cell organization. Furthermore, the width of the samples is only reproducible with an accuracy of 33%, due to its handcrafting. This creates almost a ratio of two between the thickness of the thinnest (thickness of $102 \pm 20\ \mu\text{m}$) and the thickest containers (average thickness of $170 \pm 20\ \mu\text{m}$), as measured on microscopic images of the container sides. We then turned toward more sophisticated microscopy techniques, in order to improve the quality of the information obtained.

Sample Staining Concepts

While the transmission imaging works marker free with unstained samples, the following microscopy approaches

require fluorescence staining. In an initial attempt we aimed to stain the erythrocytes. To be outside the main absorption of the hemoglobin (Kaestner et al., 2006) we looked for dyes that could be excited with a 640 nm laser or appropriate two-photon excitation wavelengths. Furthermore, we wanted the dye to be cytosolic in order to avoid any changes in the membrane structure and hence putative erythrocyte interaction properties. Therefore, we chose Cell Tracer deep red and Cell Tracker far red. Both dyes gave in principle nice erythrocyte staining as exemplified in **Supplementary Figure 1A**. However, the erythrocyte staining required the separation of the erythrocytes from the plasma (otherwise all dye is bound to albumin in the plasma) and a resuspension of cells after passing the staining procedure. We did not investigate the mechanism, but this staining procedure significantly altered the ESR (**Supplementary Figure 1B** and **Supplementary Movie 2**) and was therefore rejected. Instead, we aimed for a staining of the plasma and performed it with Atto 647 carboxyl and fluorescein as detailed above. When macroscopically compared with erythrocytes resuspended in pure plasma, the dyed suspension did not present any significant modification of the ESR as outlined in **Supplementary Figure 2**.

Two-Photon Microscopy

The two-photon microscopy is normally performed with high-NA objectives since the non-linear intensity dependence of the excitation requires very high intensity thereby providing intrinsic high-resolution sectioning capability with limited field of view. However, in order to maximize the imaging region a low NA objective was employed here. **Figure 2C** shows a picture of blood in a cuvette obtained by two-photon microscopy.

The two-photon microscopy offers a real-time transverse view of the erythrocyte organization. Indeed, as estimated from classic ESR measurements, instantaneous sedimentation speeds are up to approximately 8 μm per seconds. The two-photon microscopy allows us to take one image in approximately 4 s, meaning that the cells can then move up to ~ 30 μm within one frame recording. Since we image a gel with a characteristic width of a few millimeter, this maximal displacement is around 1% of the total structure size, and is therefore negligible when compared to the characteristic size of the image and the observed structures.

This is also highlighted in the corresponding movie of the sedimentation process in the **Supplementary Movie 3**. The images nicely resolve channels appearing in a continuous structure. However, with the low NA objective, the erythrocytes cannot be clearly resolved in the bulk, and the initial state of the gel is not resolved at all. Moreover, due to the high absorption of the emitted light by the sample, the focal position had to be set close to the lateral face of the gel. Its exact position is actually the position of the only plane where we can obtain a sharp image at physiological volume fractions. We then assume that it is at the lateral face, within a range equal to the focal depth (20 μm). Eventually, the illumination profile follows a Gaussian intensity profile, making it difficult to analyze quantitatively a large area.

Subsuming the two-photon imaging approach, this technique offers a real time direct observation of the channels at the lateral face of the colloidal gel. However, the field of view and resolution of the imaging in our setting is limited, and the individual cells cannot be resolved.

Light-Sheet Microscopy

The light-sheet microscopy has a default configuration that fits the measurement geometry required for the erythrocyte sedimentation (cp. **Figure 3A**). However, the samples are usually embedded in a matrix (gel), which is then suspended in a physiological solution. This works well for individual cells (Backes et al., 2018; Schoppmeyer et al., 2018), embryos (Huisken et al., 2004) or even isolated sinoatrial nodes (Flügel et al., 2018). However, this kind of sample preparation would completely alter the erythrocyte sedimentation process, therefore we had to go new routes. We looked for a transparent material with an optical refraction index similar to water, and we identified fluorinated ethylene propylene tubes as a suitable cylindrical geometry that is compatible with both the erythrocyte sedimentation in blood and the light-sheet microscope from sample holder to optical arrangements (**Figure 3A**). Refractive index of fluorinated ethylene propylene (1.344) is actually between and close to the refractive index of water (1.33) and the one of healthy plasma (1.351) (Reddy et al., 2012), then ensuring no significant light refraction.

As depicted in **Figure 3D**, the penetration depth of the light sheet is limited, but based on a z stack of such images, we managed to reconstruct an image representing a curved plane as outlined in **Figure 3A**. An example of such a reconstructed average picture is shown in **Figure 3E**. A movie, based on such reconstructed images, is provided in the **Supplementary Movie 4**.

The raw pictures obtained from the light sheet microscopy do not provide a complete overview of the structure adopted by aggregated erythrocytes during their sedimentation, since the penetration depth was limited to approximately 100 μm by absorption and scattering (**Figure 3D**). A live observation of the entire sample is therefore not possible. However, combining these pictures afterward, allows to obtain a good estimation of the real-time process with a curved interface structure and a time resolution limited to the acquisition time required for one z -stack. For the **Supplementary Movie 4**, one scan of the sample was performed every 7.9s, with a step of 5 μm between each of the 74 steps. The last picture of the scan lies at the front interface of the tube. Each slice is taken in 105 ms.

Even though the obtained pictures do not represent an actual cross-section of the 3D structure adopted by the erythrocytes during their sedimentation, the resulting pictures have a higher resolution compared to the other techniques tested. Some single cells are even resolved in the final processed picture. Overall, this imaging technique clearly shows that erythrocytes aggregate into a percolating structure, i.e., a colloidal gel, containing dynamic plasma channels allowing this liquid to flow up to the gel surface. The required post-processing prevents a live observation of the whole structure, which might be a limitation for more complex experimental protocols.

DISCUSSION

Table 1 shows a comparison of the various advantages and drawbacks of each imaging technique. The following subsections also sum up the main original observations obtained with each technique.

Mesoscopic Blue Light Transmission Imaging

The unique feature of the transmission imaging concept compared to the other methods is the marker free character, i.e., the sedimentation process is completely undisturbed. However, this holds only true for the composition of the blood, whereas the container has probably the biggest influence of the three methods tested: the distance of the coverslips of approximately 150 μm results in 'wall effects' (Starrs et al., 2002) most probably in the entire volume. Nevertheless, we are able to demonstrate the channel formation and its dynamics and such support the concept of the erythrocyte sedimentation of whole blood as a process which can be described as a percolating gel.

Two-Photon Microscopy

Two-photon microscopy is the technique that theoretically should be ideally suited to image blood sedimentation. A sub-micrometer optical resolution and a tissue penetration depth of up to 1 mm (Denk et al., 1995) should allow imaging of erythrocytes in a cuvette, with a cellular resolution and at sufficient distance from the cuvette wall to prevent wall effects. However, this applies to ideal conditions using high magnification objectives with a high numerical aperture. Due to the nature of the process, we want to image a field of view

with a width of the order of a millimeter, which made us choose a 5 \times objective (with a numerical aperture of 0.25). Such an objective is far away from the ideal conditions sketched above. Although the laser scanning process results in a temporal delay of the points/pixels of the image, the sedimentation process is slow enough to regard the two-photon image acquisition as quasi live recording.

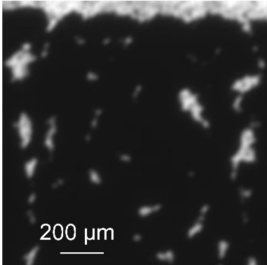
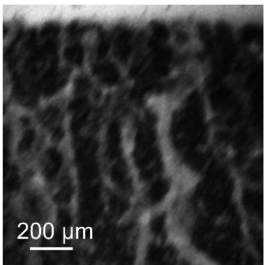
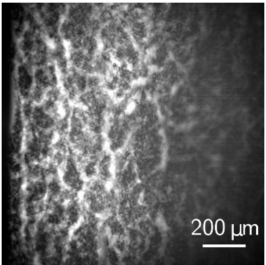
Furthermore, the dye / laser wavelength combination (fluorescein / 800 nm) was selected for highest signals, which is perfectly fine considering the excitation process, because the 800 nm is outside the hemoglobin absorption peaks and the two-photon excitation (corresponding to approximately 400 nm) needs to happen outside the erythrocytes in the plasma. However, the emitted light around 520 nm is still absorbed to a considerable degree by the hemoglobin and this loss in signal could be minimized with a dye emitting around 700 nm, which in turn would also require a laser excitation wavelength around or above 1200 nm, which is not a standard in most two-photon microscopes. Additionally, the light scatter induced by the lipids of the erythrocytes is a parameter that should be considered in further approaches.

In spite of all these limitations, the resolution we get is highly improved compared to the mesoscopic approach described above and although individual cells could not be resolved, we get a more detailed impression of the hydrodynamic processes occurring during the gel percolation.

Light Sheet Microscopy

Also, for the light sheet microscopy we faced hardware limitations. The 20 \times objective was the one with the lowest magnification available on site and a 0.4 \times post

TABLE 1 | Comparison of the imaging techniques.

	Blue light mesoscopic transmission imaging	Two-photon microscopy	Light sheet microscopy
Sample reproducibility	Variable thickness of the sample due to hardly reproducible sample preparation	Sampling in standardized optical cuvettes	Medium, the tube has a roughly constant diameter but sample is prone to slight tube bending
Live observation	Yes, acquisition speed only limited frame rate of camera	Yes, acquisition speed limited by the scanning process	No, a single plane image requires the recording of an entire stack; image generation needs stack processing
Simultaneous resolution of erythrocytes and plasma channels	No, mesoscopic imaging, just the high contrast plasma channels are visible	Limited resolution within a relevant field of view; potential for improvements	Best resolution among the systems tested
Actual cross-section of the sample	Limited, as we image a projection of the entire thickness of the sample	Well defined cross section of a plane in the sample	Calculated image along the inner surface of the circular tube, sectioning occurs in principle but hard to specify
Same scale comparison pictures (zoom and crop from Figures 1D, 2C, 3E leading to the same scale view)			

reduction was required to achieve a field of view with a width of 1.2 mm. Nevertheless, the light sheet microscopy is very promising to extract a quantitative description of the percolating gel, if one can establish a reproducible observation protocol which does not require a live feedback to the observer. In our opinion, this technique then offers the best resolution possible, but does not show an actual linear cross-section of the structure. Nonetheless, the images obtained from the reconstruction of the z-stack shows a realistic structure when compared with the two-photon microscopic images. The description of the surface geometry can then be acceptably described by the provided pictures. However, this does not offer any guarantee that the structure in the bulk of the structure is similar, which is a possibly problematic outcome when investigating the detailed colloidal physics process. However, the surface properties of fluorinated ethylene propylene (teflon) might have advantageous properties compared to the glass surface of cuvettes. Certainly, the good match of refractive indices of FEP and water and the higher aperture of the water immersion lens (NA 1.0) yielded a good resolution of the sedimentation process.

Observed Structures of Erythrocytes

From the structural point of view, on both transmission and two-photons images (**Figures 1D, 2C**), we can observe a sharp phase transition between plasma and erythrocyte suspension, as expected from previous studies (Pribush et al., 2010). Observation of this interface was unfortunately not possible with the light-sheet microscope, due to the lack of instantaneous feedback to identify the interface. In the erythrocyte suspension, one observes a continuous network, containing some cracks channeling the plasma upward (see **Figures 1D, 2C, 3D** and **Supplementary Movies 1, 3, 4**). Those characteristics (continuous network and channeling cracks) define a colloidal gel (Senis et al., 2001; Derec et al., 2003), and definitely excludes that disparate aggregates could dominate the sedimentation process (Allain et al., 1995; Whitmer and Luijten, 2011; Harich et al., 2016).

CONCLUSION

All imaging methods tested undoubtedly proved that erythrocyte sedimentation occurs as the dynamic compaction of a colloidal gel with plasma channels. Namely, all pictures showed a cohesive and percolating structure of erythrocytes containing plasma channels. Such structure is what defines a colloidal gel. Moreover, the **Supplementary Movies 1–4** clearly show that the only sudden velocity variations are in the plasma channels, where the liquid is flowing upward and can rip off and drag up some small erythrocyte aggregates from the cohesive structure. Thus, all methods were able to allow insights into the process of the percolating gel during erythrocyte sedimentation of whole blood, however, the channel formation dynamics needs to be investigated in more detail in further studies. All methods have their advantages and disadvantages as outlined in **Table 1**,

and therefore we cannot select one method as being best suited. A limitation of all methods is the limited penetration depth into the blood and therefore the imaged processes might be influenced by erythrocyte interactions with the respective container walls. In that respect, multi-photon imaging has the highest optimization potential for improvements by, e.g., the application of bathochromic shifted laser wavelength or use of adaptive optics.

DATA AVAILABILITY STATEMENT

The original contributions presented in the study are included in the article/**Supplementary Material**, further inquiries can be directed to the corresponding authors.

ETHICS STATEMENT

The studies involving human participants were reviewed and approved by Ärztekammer des Saarlandes, Saarbrücken, Germany. The patients/participants provided their written informed consent to participate in this study.

AUTHOR CONTRIBUTIONS

AD and LK: conceptualization, data curation, writing—original draft preparation, and visualization. AD, HB, TJ, RZ, JK, CK, and LK: methodology. AD: software. AD, HB, RZ, and JK: investigation. KK and CW: resources. CK, KK, and CW: supervision. LK: project administration. CW and LK: funding acquisition. All authors contributed to writing—review and editing, and read and agreed to the published version of the manuscript.

FUNDING

This work was supported by the Deutsche Forschungsgemeinschaft (DFG) in the framework of the research unit FOR 2688 “Instabilities, Bifurcations, and Migration in Pulsatile Flows,” European Union Horizon 2020 Research and Innovation Program under the Marie Skłodowska-Curie grant agreement No. 860436 – EVIDENCE, and French German University (DFH/UFA). We acknowledge support by the Deutsche Forschungsgemeinschaft (DFG, German Research Foundation) for funding of the light-sheet microscope (INST 256/423-1 FUGG). We also acknowledge the support of the project by Markus Hoth (Biophysics, Saarland University).

SUPPLEMENTARY MATERIAL

The Supplementary Material for this article can be found online at: <https://www.frontiersin.org/articles/10.3389/fphys.2021.729191/full#supplementary-material>

REFERENCES

- Abay, A., Simionato, G., Chachanidze, R., Bogdanova, A., Hertz, L., Bianchi, P., et al. (2019). Glutaraldehyde – a subtle tool in the investigation of healthy and pathologic red blood cells. *Front. Physiol.* 10:514. doi: 10.3389/fphys.2019.00514
- Allain, C., Cloitre, M., and Wafra, M. (1995). Aggregation and sedimentation in colloidal suspensions. *Phys. Rev. Lett.* 74:1478. doi: 10.1103/PhysRevLett.74.1478
- Backes, C. S., Friedmann, K. S., Mang, S., Knörck, A., Hoth, M., and Kummerow, C. (2018). Natural killer cells induce distinct modes of cancer cell death: discrimination, quantification, and modulation of apoptosis, necrosis, and mixed forms. *J. Biol. Chem.* 293, 16348–16363. doi: 10.1074/jbc.RA118.004549
- Baskurt, O., Neu, B., and Meiselman, H. J. (2012). *Red Blood Cell Aggregation*. Boca Raton, FL: CRC Press.
- Bernhardt, I., and Hianik, T. (2000). Editorial. *Bioelectrochemistry* 52:115. doi: 10.1016/S0302-4598(00)00113-6
- Biernacki, E. (1894). Blutkörperchen und plasma in ihren gegenseitigen Beziehungen. *Wien. Med. Wochenschr.* 44, 36–37.
- Breunig, H. G., Bückle, R., Kellner-Höfer, M., Weinigel, M., Lademann, J., Sterry, W., et al. (2012). Combined in vivo multiphoton and CARS imaging of healthy and disease-affected human skin. *Microsc. Res. Tech.* 75, 492–498. doi: 10.1002/jemt.21082
- Brigden, M. L., and Page, N. E. (1993). Three closed-tube methods for determining erythrocyte sedimentation rate. *Lab. Med.* 24, 97–102.
- Cartarozzi, L. P., Rieder, P., Bai, X., Scheller, A., de Oliveira, A. L. R., and Kirchhoff, F. (2018). In vivo two-photon imaging of motoneurons and adjacent glia in the ventral spinal cord. *J. Neurosci. Methods* 299, 8–15. doi: 10.1016/j.jneumeth.2018.01.005
- Darras, A., Peikert, K., Rabe, A., Yaya, F., Simionato, G., John, T., et al. (2021a). Acanthocyte sedimentation rate as a diagnostic biomarker for neuroacanthocytosis syndromes: experimental evidence and physical justification. *Cells* 10:788.
- Darras, A., Dasanna, A. K., John, T., Gompper, G., Kaestner, L., Fedosov, D. A., et al. (2021b). Erythrocyte sedimentation: fracture and collapse of a high-volume-fraction soft-colloid gel. *arXiv [Preprint]*. arXiv:2108.13841.
- Dasanna, A. K., Darras, A., John, T., Gompper, G., Kaestner, L., Wagner, C., et al. (2021). Erythrocyte sedimentation: effect of aggregation energy on gel structure during collapse. *arXiv [Preprint]*. arXiv:2108.13848.
- Denk, W., Piston, D. W., and Webb, W. W. (1995). “Two-photon molecular excitation in laser-scanning microscopy,” in *Handbook of Biological Confocal Microscopy*, ed. J. B. Pawley (Boston, MA: Springer), 445–458.
- Derec, C., Senis, D., Talini, L., and Allain, C. (2003). Rapid settling of a colloidal gel. *Phys. Rev. E* 67:062401. doi: 10.1103/PhysRevE.67.062401
- Fahraeus, R. (1929). The suspension stability of the blood. *Phys. Rev.* 9, 241–274. doi: 10.1152/physrev.1929.9.241
- Flormann, D., Aouane, O., Kaestner, L., Ruloff, C., Misbah, C., Podgorski, T., et al. (2017). The buckling instability of aggregating red blood cells. *Sci. Rep.* 7:7928. doi: 10.1038/s41598-017-07634-6
- Flormann, D., Kuder, E., Lipp, P., Wagner, C., and Kaestner, L. (2015). Is there a role of C-reactive protein in red blood cell aggregation? *Int. J. Lab. Hematol.* 37, 474–482. doi: 10.1111/ijlh.12313
- Flügel, K., Tian, Q., and Kaestner, L. (2018). “Optical sectioning microscopy at ‘temporal super-resolution,’” in *Microscopy of the Heart*, eds L. Kaestner and P. Lipp (Cham: Springer Nature), 21–35.
- Gopalakrishnan, V., Schweizer, K. S., and Zukoski, C. F. (2006). Linking single particle rearrangements to delayed collapse times in transient depletion gels. *J. Phys. Condens. Matter* 18:11531. doi: 10.1088/0953-8984/18/50/009
- Gyawali, P., Ziegler, D., Cailhier, J. F., Denault, A., and Cloutier, G. (2018). Quantitative measurement of erythrocyte aggregation as a systemic inflammatory marker by ultrasound imaging: a systematic review. *Ultrasound Med. Biol.* 44, 1303–1317.
- Hammer, K., Lipp, P., and Kaestner, L. (2014). Multi-beam two-photon imaging of fast Ca²⁺ signals in the langendorff mouse heart. *Cold Spring Harb. Protoc.* 2014:rot077016. doi: 10.1101/pdb.prot077016
- Harich, R., Blythe, T. W., Hermes, M., Zaccarelli, E., Sederman, A. J., Gladden, L. F., et al. (2016). Gravitational collapse of depletion-induced colloidal gels. *Soft Matter* 12, 4300–4308. doi: 10.1039/C5SM02651B
- Huisken, J., Swoger, J., Bene, F. D., Wittbrodt, J., and Stelzer, E. H. K. (2004). Optical sectioning deep inside live embryos by selective plane illumination microscopy. *Science* 305, 1007–1009. doi: 10.1126/science.1100035
- Jan, K., Usami, S., and Smith, J. A. (1981). Influence of oxygen tension and hematocrit reading on ESRs of sickle cells. Role of RBC aggregation. *Arch. Intern. Med.* 141, 1815–1818. doi: 10.1001/archinte.141.13.1815
- Kaestner, L., and Lipp, P. (2007). Non-linear and ultra high-speed imaging for explorations of the murine and human heart. *Prog. Biomed. Opt. Imaging* 8, 66330K–1–66330K–10.
- Kaestner, L., Tabellion, W., Weiss, E., Bernhardt, I., and Lipp, P. (2006). Calcium imaging of individual erythrocytes: problems and approaches. *Cell Calcium* 39, 13–19. doi: 10.1016/j.ceca.2005.09.004
- Kaliviotis, E., Ivanov, I., Antonova, N., and Yianneskis, M. (2010). Erythrocyte aggregation at non-steady flow conditions: a comparison of characteristics measured with electrorheology and image analysis. *Clin. Hemorheol. Microcirc.* 44, 43–54. doi: 10.3233/CH-2009-1251
- Kaliviotis, E., and Yianneskis, M. (2007). On the effect of dynamic flow conditions on blood microstructure investigated with optical shearing microscopy and rheometry. *Proc. Inst. Mech. Eng. H* 221, 887–897. doi: 10.1243/09544119JIM243
- Késmárky, G., Kenyeres, P., Rábai, M., and Tóth, K. (2008). Plasma viscosity: a forgotten variable. *Clin. Hemorheol. Microcirc.* 39, 243–246.
- König, K. (2018). “Multiphoton tomography,” in *Multiphoton Microscopy and Fluorescence Lifetime Imaging*, ed. K. König (Berlin: De Gruyter), 247–267.
- König, K., Andersen, P., Le, T., and Breunig, H. G. (2015). Multiphoton imaging with a novel compact diode-pumped Ti:sapphire oscillator. *Microsc. Res. Tech.* 78, 1154–1158. doi: 10.1002/jemt.22599
- König, K., and Riemann, I. (2003). High-resolution multiphoton tomography of human skin with subcellular spatial resolution and picosecond time resolution. *J. Biomed. Opt.* 8, 432–439. doi: 10.1117/1.1577349
- Kushner, I. (1988). The acute phase response: an overview. *Methods Enzymol.* 163, 373–383. doi: 10.1016/0076-6879(88)63037-0
- Lawrence, C., and Fabry, M. E. (1986). Erythrocyte sedimentation rate during steady state and painful crisis in sickle cell anemia. *Am. J. Med.* 81, 801–808. doi: 10.1016/0002-9343(86)90349-9
- Lipp, P., and Kaestner, L. (2006). “Image-based high-content Screening – a view from basic science,” in *High Throughput-Screening in Drug Discovery*, ed. J. Hüser (Weinheim: Wiley-VCH), 129–149.
- Patton, W. N., Meyer, P. J., and Stuart, J. (1989). Evaluation of sealed vacuum extraction method (Seditainer) for measurement of erythrocyte sedimentation rate. *J. Clin. Pathol.* 42, 313–317.
- Pribush, A., Meyerstein, D., and Meyerstein, N. (2010). The mechanism of erythrocyte sedimentation. Part 1: channeling in sedimenting blood. *Colloids Surf. B Biointerfaces* 75, 214–223. doi: 10.1016/j.colsurfb.2009.08.036
- Pribush, A., and Meyerstein, N. (2007). Methodological aspects of erythrocyte aggregation. *Recent Pat. Anticancer Drug Discov.* 2, 240–245. doi: 10.2174/157489207782497226
- Rabe, A., Kihm, A., Darras, A., Peikert, K., Simionato, G., Dasanna, A. K., et al. (2021). The erythrocyte sedimentation rate and its relation to cell shape and rigidity of red blood cells from chorea-acanthocytosis patients in an off-label treatment with dasatinib. *Biomolecules* 11:727. doi: 10.3390/biom11050727
- Reddy, N. M., Kothandan, D., Lingam, S. C., and Ahmad, A. (2012). A study on refractive index of plasma of blood of patients suffering from tuberculosis. *Int. J. Technol. Eng.* 8, 23–25.
- Salt, H. B., Wolff, O. H., Lloyd, J. K., Fosbrooke, A. S., Cameron, A. H., and Hubble, D. V. (1960). On having no beta-lipoprotein a syndrome comprising a-beta-lipoproteaemia, acanthocytosis, and steatorrhea. *Lancet* 276, 325–329. doi: 10.1016/S0140-6736(60)91478-1
- Schoppmeyer, R., Zhao, R., Hoth, M., and Qu, B. (2018). Light-sheet microscopy for three-dimensional visualization of human immune cells. *J. Vis. Exp.* 2018:57651. doi: 10.3791/57651
- Senis, D., Gorre-Talini, L., and Allain, C. (2001). Systematic study of the settling kinetics in an aggregating colloidal suspension. *Eur. Phys. J. E* 4, 59–68. doi: 10.1007/PL00013683
- Shiga, T., Imaizumi, K., Harada, N., and Sekiya, M. (1983). Kinetics of rouleaux formation using TV image analyzer. I. Human erythrocytes. *Am. J. Physiol. Heart Circ. Physiol.* 245, H252–H258. doi: 10.1152/ajpheart.1983.245.2.H252

- Starrs, L., Poon, W. C. K., Hibberd, D. J., and Robins, M. M. (2002). Collapse of transient gels in colloid-polymer mixtures. *J. Phys. Condens. Matter*. 14:2485. doi: 10.1088/0953-8984/14/10/302
- Tuchin, V. V., Xu, X., and Wang, R. K. (2002). Dynamic optical coherence tomography in studies of optical clearing, sedimentation, and aggregation of immersed blood. *Appl. Opt.* 41:258. doi: 10.1364/ao.41.000258
- Weinigel, M., Breunig, H. G., Uchugonova, A., and König, K. (2015). Multipurpose nonlinear optical imaging system for in vivo and ex vivo multimodal histology. *J. Med. Imaging* 2:016003. doi: 10.1117/1.jmi.2.1.016003
- Westergreen, A. V. A. (1921). Studies of the suspension stability of the blood in pulmonary tuberculosis. *Acta Med. Scand.* 54, 247–282.
- Whitmer, J. K., and Luijten, E. (2011). Sedimentation of aggregating colloids. *J. Chem. Phys.* 134:034510. doi: 10.1063/1.3525923
- Yeom, E., and Lee, S. J. (2015). Microfluidic-based speckle analysis for sensitive measurement of erythrocyte aggregation: a comparison of four methods for detection of elevated erythrocyte aggregation in diabetic rat blood. *Biomicrofluidics* 9:024110. doi: 10.1063/1.4917023

Conflict of Interest: KK is CEO of JenLab GmbH, the manufacturer of the two-photon tomograph used within this study.

The remaining authors declare that the research was conducted in the absence of any commercial or financial relationships that could be construed as a potential conflict of interest.

Publisher's Note: All claims expressed in this article are solely those of the authors and do not necessarily represent those of their affiliated organizations, or those of the publisher, the editors and the reviewers. Any product that may be evaluated in this article, or claim that may be made by its manufacturer, is not guaranteed or endorsed by the publisher.

Copyright © 2022 Darras, Breunig, John, Zhao, Koch, Kummerow, König, Wagner and Kaestner. This is an open-access article distributed under the terms of the Creative Commons Attribution License (CC BY). The use, distribution or reproduction in other forums is permitted, provided the original author(s) and the copyright owner(s) are credited and that the original publication in this journal is cited, in accordance with accepted academic practice. No use, distribution or reproduction is permitted which does not comply with these terms.



Transmission Electron Microscopy to Follow Ultrastructural Modifications of Erythroblasts Upon *ex vivo* Human Erythropoiesis

Alice Dussouchaud^{1†}, Julieta Jacob^{2†}, Charles Secq¹, Jean-Marc Verbavatz³, Martina Moras¹, Jérôme Larghero⁴, Claudio M. Fader², Mariano A. Ostuni¹ and Sophie D. Lefevre^{1*}

¹ Université de Paris and Université des Antilles, INSERM, BGR, Paris, France, ² Laboratorio de Biología Celular y Molecular, Instituto de Histología y Embriología, CONICET, Universidad Nacional de Cuyo, Mendoza, Argentina, ³ Facultad de Odontología, Universidad Nacional de Cuyo, Mendoza, Argentina, ⁴ CNRS, UMR 7592, Institut Jacques Monod, Université de Paris, Paris, France

OPEN ACCESS

Edited by:

Giampaolo Minetti,
University of Pavia, Italy

Reviewed by:

Konstantinos Palikaras,
National and Kapodistrian University
of Athens, Greece
Erik L. Jensen,
FRC550 Institut de Biologie
Physico-Chimique (IBPC), France

*Correspondence:

Sophie D. Lefevre
sophie.lefevre@inserm.fr

[†]These authors have contributed
equally to this work

Specialty section:

This article was submitted to
Red Blood Cell Physiology,
a section of the journal
Frontiers in Physiology

Received: 08 October 2021

Accepted: 23 December 2021

Published: 09 February 2022

Citation:

Dussouchaud A, Jacob J,
Secq C, Verbavatz J-M, Moras M,
Larghero J, Fader CM, Ostuni MA
and Lefevre SD (2022) Transmission
Electron Microscopy to Follow
Ultrastructural Modifications
of Erythroblasts Upon *ex vivo* Human
Erythropoiesis.
Front. Physiol. 12:791691.
doi: 10.3389/fphys.2021.791691

Throughout mammal erythroid differentiation, erythroblasts undergo enucleation and organelle clearance becoming mature red blood cell. Organelles are cleared by autophagic pathways non-specifically targeting organelles and cytosolic content or by specific mitophagy targeting mitochondria. Mitochondrial functions are essential to coordinate metabolism reprogramming, cell death, and differentiation balance, and also synthesis of heme, the prosthetic group needed in hemoglobin assembly. In mammals, mitochondria subcellular localization and mitochondria interaction with other structures as endoplasmic reticulum and nucleus might be of importance for the removal of the nucleus, that is, the enucleation. Here, we aim to characterize by electron microscopy the changes in ultrastructure of cells over successive stages of human erythroblast differentiation. We focus on mitochondria to gain insights into intracellular localization, ultrastructure, and contact with other organelles. We found that mitochondria are progressively cleared with a significant switch between PolyE and OrthoE stages, acquiring a rounded shape and losing contact sites with both ER (MAM) and nucleus (NAM). We studied intracellular vesicle trafficking and found that endosomes and MVBs, known to be involved in iron traffic and heme synthesis, are increased during BasoE to PolyE transition; autophagic structures such as autophagosomes increase from ProE to OrthoE stages. Finally, consistent with metabolic switch, glycogen accumulation was observed in OrthoE stage.

Keywords: erythropoiesis, electron microscopy, mitochondria, autophagy, vesicles

INTRODUCTION

Erythropoiesis is a finely regulated process producing two million erythrocytes every second in healthy human adults (Palis, 2014). During the late phase of erythropoiesis, called terminal erythropoiesis, proerythroblast (ProE) undergoes several cellular divisions to give rise to basophilic (BasoE), polychromatic (PolyE), and orthochromatic (OrthoE) erythroblasts, successively.

Through these divisions, morphological changes, such as cell size reduction and chromatin condensation, will occur (Wickramasinghe et al., 2011). The nomenclature of these stages is given by morphological description after May-Grünwald-Giemsa coloration (Wickramasinghe et al., 2011). Indeed, the ProE has a large nucleus and the cytoplasm contain free ribosomes giving it a basophilic (purple) appearance. The BasoE is smaller, which has a more basophilic cytoplasm due to increased numbers of ribosomes and chromatin condenses. The PolyE appears grayer due to the increased acidophilic staining caused by the presence of hemoglobin. Cell division stops at this stage. At the end, the OrthoE has more acidophilic (pink) appearance. At this stage, the transcription stops and the nucleus becomes pyknotic, as the chromatin condenses, and polarizes to prepare for enucleation (Wickramasinghe et al., 1968, 2011). At the end of human terminal erythropoiesis, OrthoE gave rise to reticulocyte, a cell devoid of nucleus, which migrates toward the blood stream and matures into red blood cell.

During this last phase of erythropoiesis, some specific proteins, such as hemoglobin or the membrane protein Band 3, will be expressed under the control of specific transcription factors to allow the cell to become highly specialized (Peters et al., 1992; Liu et al., 2011; Fan et al., 2015). Large amount of iron will be imported in the first stages of terminal erythropoiesis to fulfill the cell requirement for heme synthesis (Fontenay et al., 2006; Dailey and Meissner, 2013). In parallel, some other proteins will be specifically removed (Blanc et al., 2005; Gautier et al., 2016). In addition, organelles including the Golgi apparatus, endoplasmic reticulum (ER), ribosomes, and mitochondria are eliminated (Moras et al., 2017). Organelles can be eliminated by the general process of macroautophagy, which starts by the formation of a double membrane structure called phagophore, engulfing cytoplasmic material to form the autophagosome which fuses with a lysosome for degradation (Klionsky, 2005). All these processes including membrane remodeling, changes in metabolic pathways, and organelle clearance involved high intracellular vesicle trafficking such as the generation and dynamic of endosomes, multivesicular bodies, or autophagosomes.

Mitochondria can specifically be removed by mitophagy (Sandoval et al., 2008; Moras et al., 2020, 2022). A prerequisite for mitochondrial clearance is mitochondria fragmentation, as impaired fragmentation results in the inhibition hemoglobin biosynthesis and erythropoiesis (Gonzalez-Ibanez et al., 2020). Mitochondria are also known to form contact sites with other organelles such as ER, lipid droplets, endosomes, lysosomes, plasma membranes, and nucleus (Lackner, 2019). These membrane-to-membrane contact sites are essential to exchange metabolites and to regulate several pathways allowing cellular adaptation to metabolic changes and cellular stress (Giamogante et al., 2020). Even so the mitochondria contact sites are not well studied throughout erythropoiesis, a recent elegant article demonstrated that a perinuclear mitochondria localization is necessary to achieve the enucleation of orthochromatic erythroblasts in mice (Liang et al., 2021). Furthermore, we have recently described a reduction of mitochondria to ER contact site number in a context of impaired terminal erythroid maturation (Moras et al., 2022).

Only a few very interesting papers have partially described ultrastructural changes during erythropoiesis in mammals (Betin et al., 2013; Gonzalez-Ibanez et al., 2020; Moras et al., 2022). The more exhaustive characterization of the progressive changes in endomembrane compartments during human erythroid differentiation was reported by Betin et al. (2013) who described the appearance of different autophagic compartments and the reduction in the number of mitochondria.

Mitochondrial retention was previously associated with deficient mitophagy following mitophagy receptors knockdown in mice (Sandoval et al., 2008) and humans (Moras et al., 2022). During the last 5 years, growing evidences were reported correlating autophagy deficiencies and particularly mitophagy defaults with different pathologies as sickle cell disease (SCD) or systemic lupus erythematosus (SLE; Jagadeeswaran et al., 2017; Caielli et al., 2021; Martino et al., 2021). Moreover, a novel atypical anemia was associated with the presence of miscellaneous membranous structure on patients' reticulocytes and mature red blood (Ru et al., 2018). Then, the whole characterization of ultrastructural changes during erythroid terminal differentiation is a necessary tool helping to analyze and understand pathological anomalies specially found in dyserythropoiesis.

Herein, we performed human *ex vivo* erythropoiesis and sorted different erythroblasts stages during terminal erythropoiesis to identify and quantify by electron microscopy the ultrastructural features appearing throughout differentiation steps. We characterized cell shape, nucleus localization, chromatin condensation, mitochondrial distribution and shape, and also the presence of mitochondrial-ER and mitochondrial nucleus contact site. We also quantified endomembrane vesicles such as multivesicular bodies, endosomes, and autophagosomes through differentiation stages. Finally, we identified the appearance of glycogen stores at the late stages of differentiation, as a signal of metabolic switch.

MATERIALS AND METHODS

Human CD34-Positive Cell Purification and Differentiation

Cord bloods from healthy donors from Saint-Louis Hospital Cord Blood Bank registered to the French Ministry of Research under number AC-2016-2756 and to the French Normalization Agency under number 201/51848.1 were used in this study. This study was approved and conducted according to Institutional Ethical Guidelines of the National Institute of Blood Transfusion (N°2019-1, INTS, Paris, France). All procedures were carried out in accordance with the Declaration of Helsinki. Written informed consent was given by the donors. Mononuclear cells were separated from blood using Ficoll-Paque (GE Healthcare), and CD34⁺ cells were enriched using magnetic cell sorting beads (Miltenyi Biotec, Paris, France) according to the manufacturer's instruction.

CD34⁺ cells were cultured in Iscove's Modified Dulbecco's Medium (IMDM) GlutaMAXTM (Thermo Fischer Scientific, Courtaboeuf, France), 2% human peripheral blood plasma

(STEMCELL Technologies, Saint-Égrève, France), 3% human AB serum (Merck KGaA, Darmstadt, Germany), 15% BIT 9500 serum substitute (STEMCELL Technologies), and 3 IU/mL heparin (Merck KGaA). During expansion phase (day −4 to day 0), cells were seeded at a concentration of 10^5 cells/mL in culture medium supplemented with 25 ng/mL stem cell factor (hSCF), 10 ng/mL IL-3, 10 ng/mL IL-6 from Miltenyi Biotec. From day 0 to day 4, medium was supplemented with 10 μ g/mL insulin (Merck, KGaA), 200 μ g/mL human holo-transferrin (Merck KGaA), 10% penicillin/streptomycin, 10 ng/mL SCF, 1 ng/mL IL-3, and 3 IU/mL erythropoietin (EPO), whereas IL-6 and BIT were removed from the medium. From day 7, IL-3 was omitted from culture media and from day 10, and hSCF was removed. Holo-transferrin concentration was increased up to 1,000 μ g/mL. Cell concentration was maintained between 10^5 and 10^6 at 37°C with the presence of 5% CO₂. **Figure 1A** presents the culture protocol.

Flow Cytometry-Based Erythroid Differentiation Analysis and Erythroblast Sorting

ProE, BasoE, and PolyE, and OrthoE were sorted at day 6, 12, and 15, respectively, based on the expression of surface markers expression as described by Hu et al. (2013). Briefly, 20 million cells were incubated with PBS 0.5% BSA supplemented with 10% AB serum for 10 min at 4°C for blocking. BV510-coupled antiglycophorin A (GPA) antibody (1/25e), APC-Cy7-coupled anti- α 4-integrin antibody (1/8e), and PE-coupled anti-band 3 antibody (1/16e) were added to the cells. After 20 min of incubation at 4°C, cells were washed with PBS 0.5% BSA, and 7-amino-actinomycin-D (7-AAD, BD Biosciences) (1/200e) was added just before reading to exclude dead cells. For orthochromatic erythroblast sorting, 1 μ g/mL Hoechst 34580 (BD Biosciences) was added to the culture and incubated 30 min at 37°C prior to antibodies labeling. Cells were sorted using the cell sorter SONY MA900.

May-Grünwald Giemsa-Based Identification of Erythroblasts

Morphological quantifications were performed on 10^5 cells, before and after sorting, cytopspin on a glass slide for 3 min at 300 G using the Thermo Fisher Shandon 4 Cytospin. After drying, slides were stained with 5 min in May-Grünwald (MG) solution (Merck KGaA), transferred in 1/2-diluted MG solution for 5 min, washed in potassium phosphate buffer 8.5 mM pH 7.2 for 3 min, incubated in 1/20-diluted Giemsa solution (Merck KGaA) for 15 min, and washed in phosphate buffer 8.5 mM pH 7.2 for 3 min before drying. Cells were then imaged using Leica DMI4000 microscope 100x/0.6 objective. A number of 30–35 cells per sample were analyzed.

Cell Preparation for Electron Microscopy and Image Acquisition

After sorting, 3–5 million cells were immediately fixed with 1% glutaraldehyde/2.5% paraformaldehyde for at least 2 h. After washing, cells were postfixed with 1% osmium tetroxide reduced with 1.5% potassium ferrocyanide in PBS (pH 7.4),

progressively dehydrated in ethanol, and embedded in low-viscosity epoxy resin. However, 70-nm-thin sections were cut, mounted on copper grids, and stained with uranyl acetate and lead citrate. Sections were examined with a 120 kV TEM (Tecnai 12, Thermo Fischer Scientific) equipped with a 4K CDD camera (OneView, Gatan). At least 20 images per replicates were analyzed using 3DMOD and IMOD or FIJI software depending on the application.

Statistical Tests

Erythroid differentiation was repeated in triplicates, with a satisfactory correlation between the results of individual experiments. Statistical analyses were performed using Prism 8 (GraphPad Software). Data were evaluated using Mann–Whitney or Kruskal–Wallis tests, and all comparisons with a *p*-value less than 0.05 were considered statistically significant.

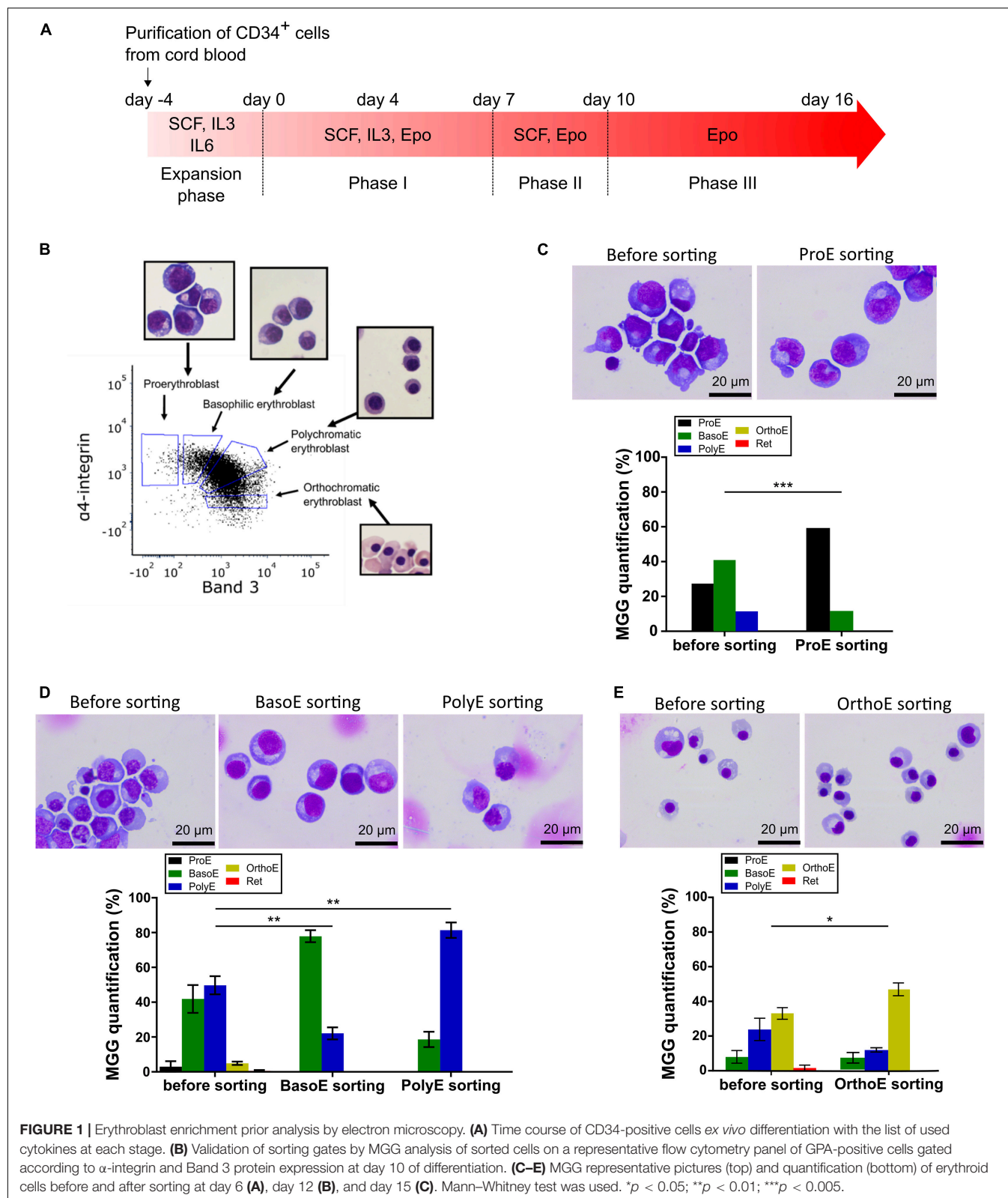
RESULTS

Electron Microscopy to Identify Erythroblasts

Relatively recent works characterized membrane protein expression in erythroblast stages, which generate a standardized protocol for human erythroblast identification and sorting by flow cytometry (Chen et al., 2009; Hu et al., 2013). To generate from ProE to OrthoE, differentiation of cord blood purified CD34-positive cells was started by adding EPO (day 0). The expression of α 4-integrin and Band 3 on glycophorin (GPA)-positive cells was analyzed by flow cytometry to quantify the proportion of ProE, BasoE, PolyE, and OrthoE. Cells were sorted accordingly, May-Grünwald Giemsa (MGG) staining was used to validate the gating on a standard experiment, and gates were not changed afterward (**Figure 1B**).

As differentiation progresses, various days after EPO addition were selected to sort different erythroblast stages (**Figure 1A**). With 27.37% of ProE prior sorting, day 6 after EPO addition was used to sort this stage; BasoE and PolyE were the most frequent stages at day 12 after EPO addition, and $35 \pm 5.7\%$ of cells were OrthoE at day 15 after EPO addition. The enrichment of sorted fractions was evaluated based on MGG staining by calculating the ratio expressed in percent of the representativity of each stage after related to before sorting. For ProE fractions, the enrichment was 310% for each replicate (**Figure 1C**). For BasoE and PolyE, it was 202, 146, and 224% and 143, 196, and 156%, respectively (**Figure 1D**). For OrthoE fractions, the enrichment ratio is of 176, 129, and 132% for the three replicates (**Figure 1E**). For all stages, the enrichment was statistically significant (**Figure 1**).

Electron micrographs of each stage of the terminal differentiation from ProE (**Supplementary Figure 1**), to BasoE (**Supplementary Figure 2**), to PolyE (**Supplementary Figure 3**), and OrthoE (**Supplementary Figure 4**) were analyzed. Over differentiation, erythroblast size decreases. We can follow and quantify this change by measuring the 2D area of electron microscopy sections (**Figure 2A**). The quantification of the average cellular area per stage shows a decrease through stages (**Figure 2B**). The cellular area represents $80 \pm 11\%$ for a BasoE,



77 ± 4% for a PolyE, and 61 ± 2% for a OrthoE of the cellular area of a ProE. Using the eccentricity value from the IMOD software, we can monitor the cellular roundness. Values vary

from 0 (round) to 1 (elongated shape). ProE and BasoE are relatively round cells with an eccentricity value of 0.604 ± 0.007 and 0.608 ± 0.016, respectively (**Figure 2C**). Eccentricity value

for PolyE and OrthoE is slightly higher (0.628 ± 0.029 and 0.629 ± 0.028 , respectively), sign of an elongation throughout the differentiation (**Figure 2C**).

Nucleus size, chromatin localization, and condensation reflect the transcriptional status of the cell (Koury et al., 1988). Histological analysis describes ProE as characterized by high nuclear to cytoplasmic ratio, loose chromatin, 1 or 2 nucleoli and basophilic cytoplasm (Wickramasinghe et al., 1968, 2011). BasoE are described to have high nuclear to cytoplasmic ratio and basophilic cytoplasm but condensed chromatin and no nucleoli, whereas PolyE have round nucleus, condensed chromatin, no nucleoli, and less basophilic cytoplasm due to hemoglobin synthesis. This is the last stage to divide. OrthoE have dense pyknotic nucleus with acidophilic cytoplasm (Wickramasinghe et al., 1968, 2011). Here, we showed a decrease in nucleus size over stage (**Figure 2D**). Nucleus area decreases from $82 \pm 10\%$ for BasoE, $78 \pm 9\%$ for PolyE, to $42 \pm 3\%$ for OrthoE compared to ProE. We observed an increase in nucleus sphericity in OrthoE (0.63 ± 0.18 in OrthoE compared to 0.76 ± 0.12 in ProE, 0.77 ± 0.11 in BasoE, 0.74 ± 0.14 in PolyE, **Figure 2E**). The nucleus to cytoplasm ratio is also statistically reduced of $78 \pm 8\%$ in OrthoE compared to earlier stages (**Figure 2F**). Loose vs. condensed chromatin and pyknotic nucleus with high electron dense chromatin are also observed in erythroblasts (**Figure 2G**).

Mitochondria Characterization Over Erythroid Differentiation

By flow cytometry and biochemical approaches, we have previously showed progressive clearance of mitochondria starting from the transition between BasoE and PolyE (Moras et al., 2020, 2022). Here, we followed mitochondria quantity per cell. We observed a decreased in mitochondria number starting from BasoE (17.98 ± 0.810 mitochondria sections per cell) to PolyE (13.30 ± 0.631 mitochondria sections per cell) transition, with a subsequent decrease observed in OrthoE (4.28 ± 0.429 mitochondria sections per cell) (**Figure 3A**). This phenomenon is also detected when analyzing the total area of mitochondria sections per cell between erythroblast stages (**Figure 3B**).

Changes in mitochondrial metabolism, oxidative stress, or regulation of mitochondria abundance within cells can be accompanied by changes in mitochondrial morphology. Mitochondrial functions are tightly regulated over erythroid differentiation (Oburoglu et al., 2014, 2016; Gonzalez-Menendez et al., 2021; Rossmann et al., 2021). Mitochondria fragmentation is an essential step for maturation (Gonzalez-Ibanez et al., 2020). Rounded and elongated mitochondria can be observed in all differentiation stages (**Supplementary Figure 5**). Here, we analyzed mitochondrial morphology first manually (**Figure 3C**) and second using the eccentricity quantification (**Figure 3D**). We observed a progressive change in mitochondria shape from elongated to more rounded shape within the differentiation stages (**Figure 3C**). Looking at the distribution of mitochondria eccentricity values, OrthoE exhibit a left shift toward more rounded forms (OrthoE vs. PolyE, $p = 0.0026$) (**Figure 3D**). In OrthoE interestingly, the mitochondrial morphology is not homogeneous, and some of the most elongated

mitochondria were observed, always in close proximity to the nucleus (**Figure 3E**).

Mitochondria can form contact sites with virtually all organelles in the cell (Lackner, 2019). These structures are involved in protein and lipid transport, calcium homeostasis, vesicular trafficking, mitochondrial dynamic, apoptosis, and autophagy (Ellenrieder et al., 2017; Giamogante et al., 2020). Regardless of organelle and cristae morphology, mitochondrial functionality can be studied through the quantification of interorganelle contact sites, as for example mitochondria-associated membranes (MAMs) adapt to glucose availability to regulate mitochondrial dynamics and bioenergetics (Theurey et al., 2016). Such contact sites can be observed in human erythroblasts (**Figure 4A**). Membrane-membrane contact of several organelles is determined by specific protein complex and has an intermembrane distance of approximately 5–8 nm (Zanetti and Mayorga, 2009). This is the maximal distance measured between both membranes, which we have considered as a positive membrane-membrane contact site. The number of MAM, which bring together mitochondria and endoplasmic reticulum membranes, is relatively constant from ProE to PolyE (6.15 ± 3.22 in ProE, 6.40 ± 3.38 in BasoE, 5.12 ± 2.29 in PolyE, **Figure 4B**). Concomitant with the decrease in mitochondria abundance in this stage, the number of MAMs decreases significantly in OrthoE (1.35 ± 1.97 , **Figure 4B**). On mitochondria-containing erythroblasts, we analyzed the percentage of mitochondria forming MAMs in different erythroblast stages. Despite the decrease in mitochondria number, we observe $34.73 \pm 20.32\%$ in ProE, $34.27 \pm 15.02\%$ in BasoE, $44.10 \pm 23.10\%$ in PolyE, and only $8.687 \pm 14.49\%$ in OrthoE of mitochondria forming MAMs (**Figure 4C**).

Mitochondria are also known to make contact with the nuclear membrane, forming nucleus-associated mitochondria (NAM; Desai et al., 2020; Eisenberg-Bord et al., 2021). As a part of the retrograde signaling response that links mitochondria homeostasis to the activation of adaptative response from transcriptional control within the nucleus, NAM participate in the regulation of many cellular processes such as cell proliferation, stress adaptation, metabolic switch, autophagy, and mitochondrial biogenesis (Strobbe et al., 2021). We quantified NAM in erythroblasts based on the same criteria of distance as previously described for MAMs (Zanetti and Mayorga, 2009). Whereas this structure appears to be relatively rare with a mean of 1.50 ± 0.22 in ProE and 1.92 ± 0.19 in BasoE, they are statistically decreased in Poly (0.72 ± 0.09) and OrthoE (0.39 ± 0.07) (**Figure 4D**). The percentage of mitochondria forming NAM remain unchanged between differentiation stages (**Figure 4E**). This might suggest a specific removal of a subset of mitochondrial population, maintaining those in proximity to the nucleus despite the total reduced number of this structure (**Figure 3E**).

Cellular Trafficking and Autophagy

Endosomes and multivesicular bodies (**Figure 5A**) are both structures involved in iron uptake, and also transferrin and transferrin receptor recycling, the first steps in the heme biosynthesis pathway (Killisch et al., 1992). BasoE and PolyE presented higher number of these structures with a mean of

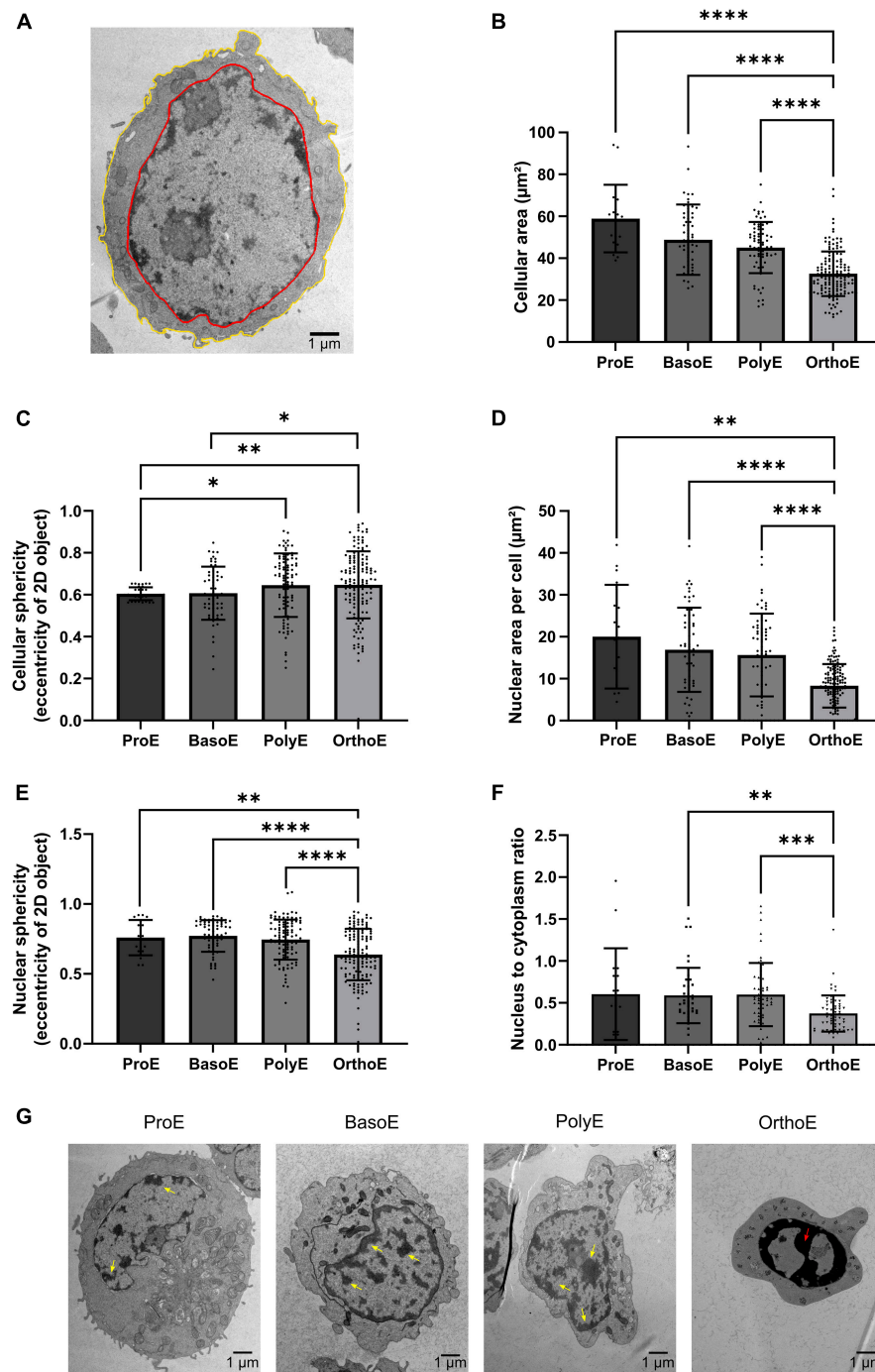


FIGURE 2 | Cellular and nuclear characteristics of erythroblasts. **(A)** 3DMOD-based drawing of cellular (yellow) and nucleus (red) rims on a ProE permitting area quantification from 2D section. **(B,C)** Quantification of cellular area **(B)** and eccentricity **(C)** of erythroblasts. **(D–F)** Quantification of area **(D)**, eccentricity **(E)** of nucleus, and ratio of nucleus to cytoplasm area **(F)** in each of the differentiation stage. **(G)** Representative images of chromatin condensation from ProE to OrthoE. Yellow arrow: condensed chromatin; red arrow: pyknotic nucleus. Kruskal–Wallis analysis on at least 20 images for the three replicates. * $p < 0.05$; ** $p < 0.01$; *** $p < 0.005$, **** $p < 0.001$.

5.96 ± 3.72 endosomes per BasoE and 7.7 ± 3.36 endosomes per PolyE (**Figures 5B,C**). On the contrary, the mean number of endosomes in OrthoE drastically drops to 1.7 ± 1.4 (**Figure 5B**). The pattern of MVB abundance is similar with one of the

endosomes as with MVBs that are more represented in BasoE and PolyE (mean of 5.09 ± 3.7 structures per cell in BasoE and 4.26 ± 2.69 in PolyE), whereas OrthoE contain only 1.04 ± 0.98 MVBs per cell (**Figure 5C**).

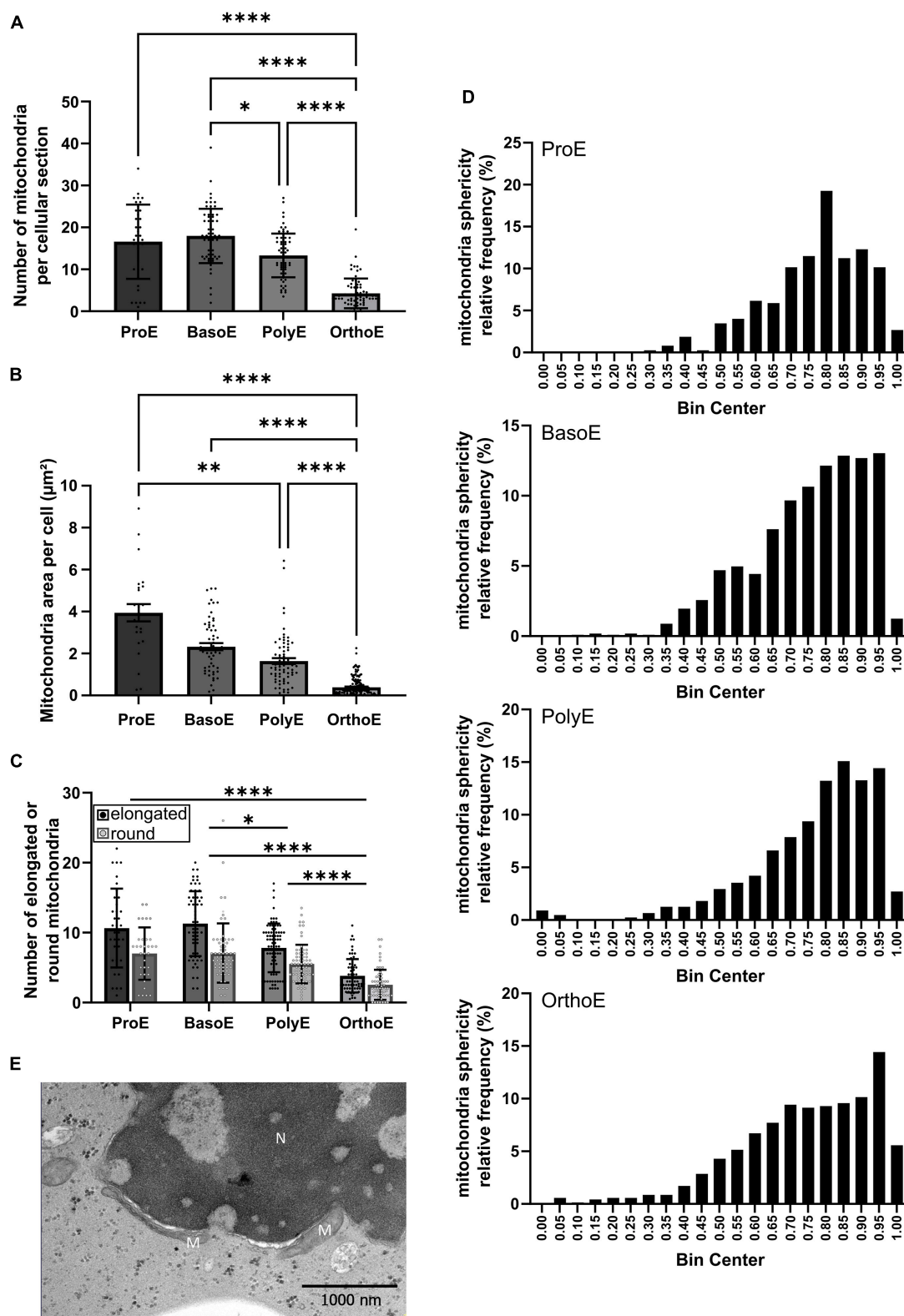


FIGURE 3 | Mitochondria characterization during erythroid differentiation. **(A,B)** The number **(A)** and the total area **(B)** of mitochondria per cell were quantified in the different erythroid differentiation stages. **(C,D)** Mitochondrial morphology (elongated or rounded shape) was measured manually **(C)** or using the eccentricity quantification **(D)**. **(E)** Elongated mitochondria close to the nucleus of an OrthoE. M, mitochondria; N, nucleus. Kruskal–Wallis analysis on at least 20 images for the three replicates. * $p < 0.05$; ** $p < 0.01$; **** $p < 0.001$.

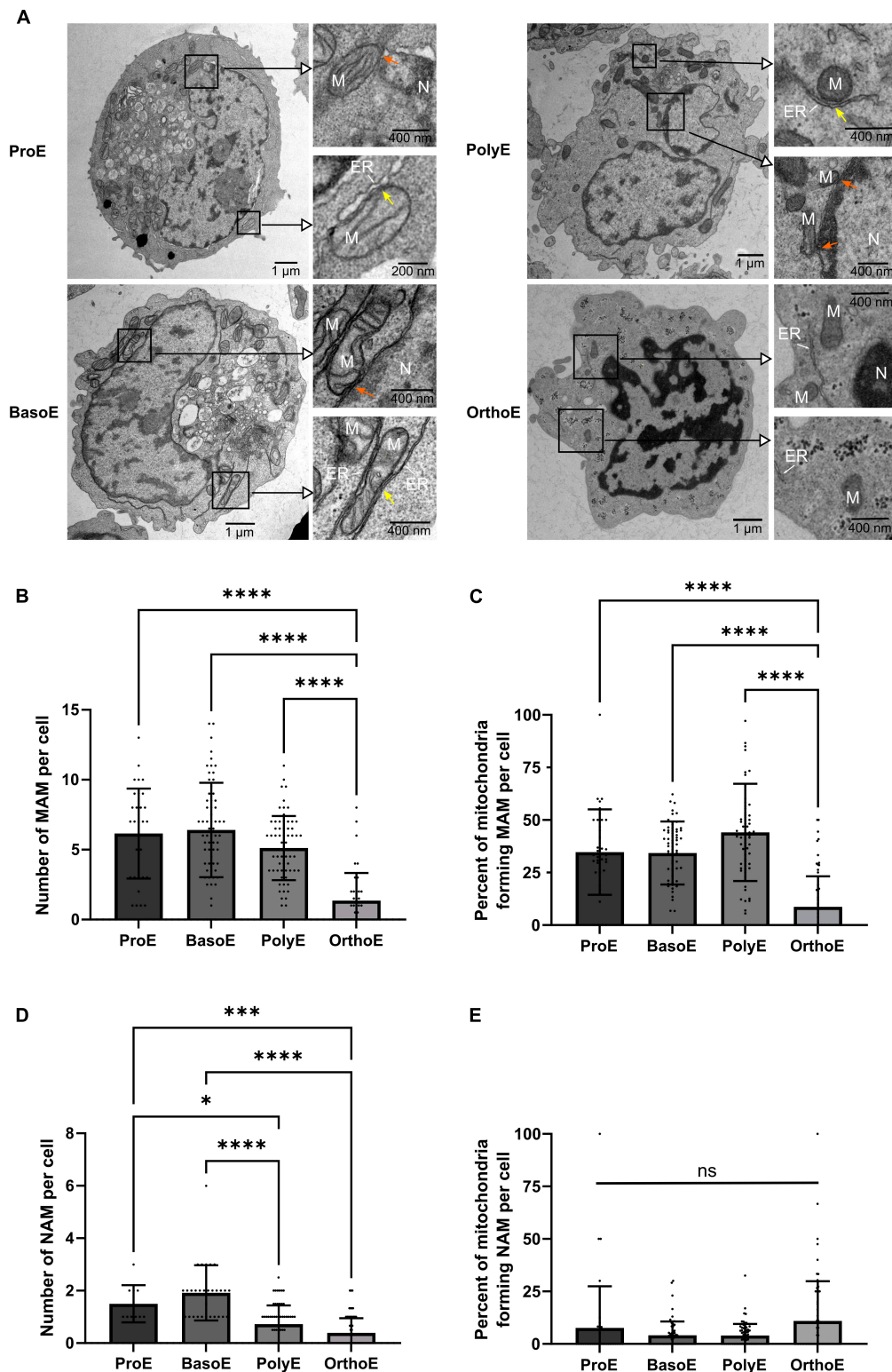


FIGURE 4 | Quantification of mitochondria-organelle contact sites. **(A)** Representative images of erythroblasts at various stages with insets on mitochondria. Orange arrow: mitochondria-ER contact site, yellow arrow: mitochondria-nucleus contact site. M, mitochondria; N, nucleus; ER, endoplasmic reticulum. **(B)** Quantification of mitochondria-endoplasmic reticulum (MAM) per cell at each stage. **(C)** Percentage of mitochondria forming MAM contact site per cell. **(D)** Quantification of nucleus-mitochondria (NAM) per cell at each stage. **(E)** Percentage of mitochondria forming NAM contact site per cell. Kruskal-Wallis analysis on at least 20 images for the three replicates. * $p < 0.05$; **** $p < 0.001$.

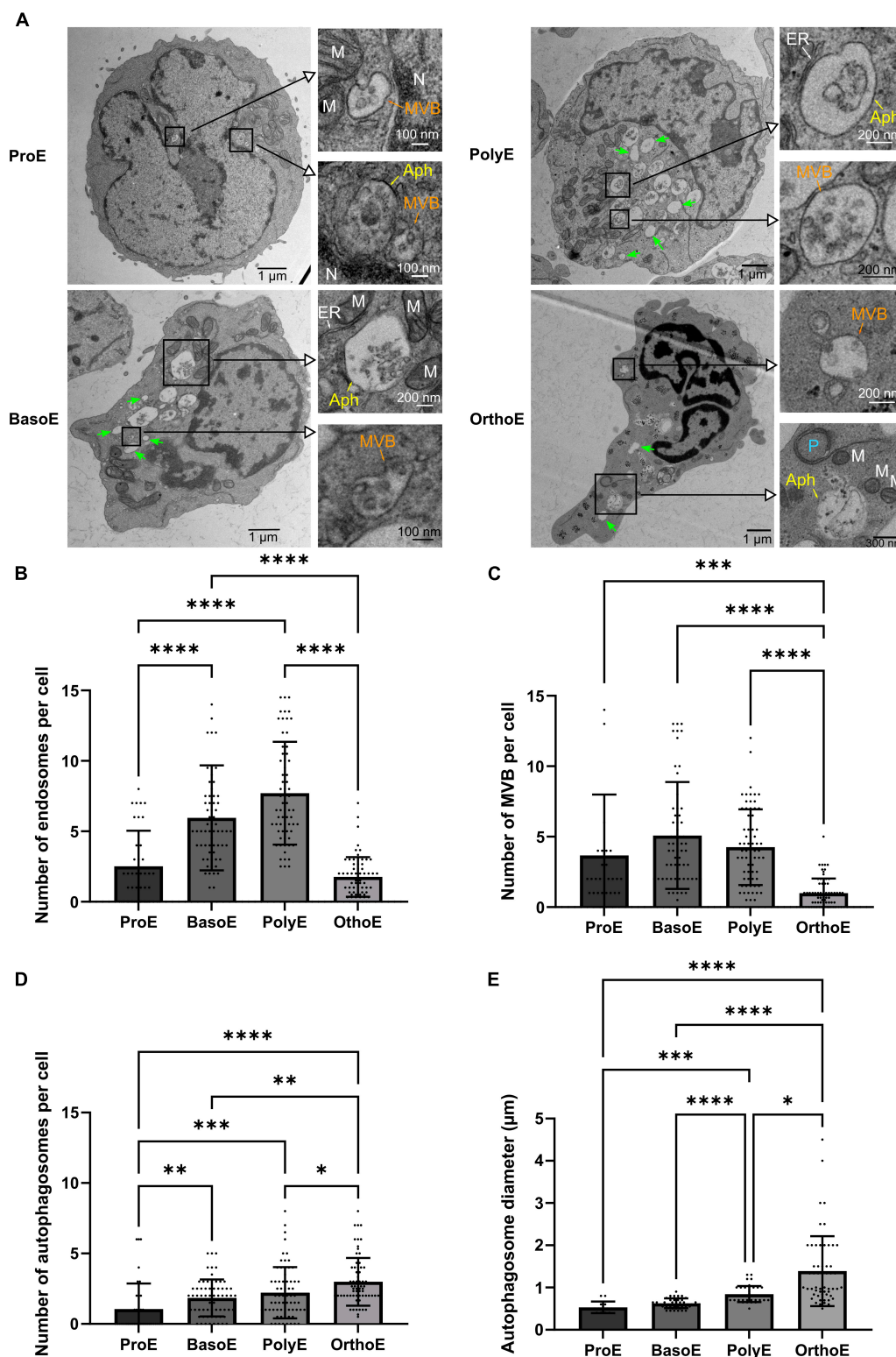


FIGURE 5 | Characterization of the endosomal and autophagic pathway during erythroid differentiation. **(A)** Representative images of erythroblasts at various stages with insets on intracellular vesicles. Green arrow: endosomes, MVB, multivesicular body; Aph, autophagosome; P, phagophore; M, mitochondria; N, nucleus; ER, endoplasmic reticulum. **(B–D)** Quantification of endosomes **(B)**, multivesicular bodies **(C)**, and autophagic vesicles **(D)** in each differentiation stage. **(E)** Measure of the diameter of the autophagic structures over the different erythroid differentiation stages. Kruskal–Wallis analysis on at least 20 images for the three replicates. * $p < 0.05$; ** $p < 0.01$; *** $p < 0.005$; **** $p < 0.001$.

Through terminal erythropoiesis, cell size decreases and organelles are progressively removed. Several evidences point out the role of general autophagy and/or specific mitophagy in terminal mitochondrial clearance (Schweers et al., 2007; Kundu et al., 2008; Zhang et al., 2009; Betin et al., 2013; Honda et al., 2014; Moras et al., 2022). Here, we showed a progressive increase in autophagosome number with a mean of 1.05 in ProE, 1.84 in BasoE, 2.21 in PolyE, and 2.99 autophagosomes per cell in OrthoE (**Figure 5D**). Concomitantly, the diameter of autophagosomes that reflect the size of the structure in a 2S section is also progressively increasing through the differentiation (0.53 μm in ProE, 0.63 μm in BasoE, 0.84 μm in PolyE, and 1.39 μm in OrthoE, **Figure 5E**). This is the sign of an intense activation of autophagic pathways in late stages of erythropoiesis.

Glycogen Accumulation

In early expansion of erythropoiesis – from hematopoietic stem cell (HSC) to colony-forming unit-erythroid (CFU-E) – cell metabolism switches from glycolytic and proliferative to oxidative and differentiating metabolism (Oburoglu et al., 2014; Bonora et al., 2015; Schell and Rutter, 2017). In late stages, we could observe dark granules that we identified as glycogen granules, according to the literature (Revel et al., 1960; Castejon et al., 2002; Ørtenblad et al., 2013; Vezzoli et al., 2020; **Figure 6A**). Except in one PolyE cell out of 106 images, glycogen granules were found only in OrthoE (**Figure 6A**). We quantified up to 65 vesicles per cell (**Figure 6B**) that represent around 1% of the cell surface (**Figure 6C**) in OrthoE, the stage when most of mitochondria were lost (**Figure 6B**).

DISCUSSION

Well-admitted morphological changes regarding cell and nucleus morphology observed throughout human erythroid are detectable on electron microscopy pictures. From 2D cellular sections, we quantified the reduction in cell and nucleus size and roundness (eccentricity). In histology books, proerythroblast size is 14–19 μm , basophilic erythroblast size is 12–17 μm , polychromatophilic erythroblast size is 12–15 μm , and orthochromatic erythroblast size is 8–12 μm . According to these data, the reduction in size from ProE to OrthoE is 60%. Only differences with OrthoE are significant in our analyses of TEM 2D sections but the decrease percentage of each stage is reproduced. Finally, we were also able to observe the progressive chromatin condensation (**Figure 2**).

Focusing on mitochondria, we showed its progressive clearance along the terminal maturation with a significant switch between PolyE and OrthoE (**Figure 3**). We also observed a shift toward more rounded shape along the differentiation (**Figure 3**). Mitochondria are highly dynamic organelles; therefore, the number of mitochondria reflects the overall aspect of the mitochondrial network. Gonzalez-Ibanez described recently the importance of FIS1 and MFN1 in the control of mitochondria shape during erythropoiesis, showing that mitochondria fragmentation is a prerequisite for proper progression through differentiation (Gonzalez-Ibanez et al., 2020). In relation to its

dynamic, mitochondria are important organelles reflecting the energetic status of the cell (Benard et al., 2007). Under conditions of high energetic demand, mitochondria are abundant, fused, and provide the cells with high levels of ATP. Erythroblasts were described to undergo metabolic switch to synthesize specialized proteins allowing the mature red blood cell to be fully functional (Oburoglu et al., 2016). This is in agreement with the elongated shape of mitochondria that we observed at ProE stage and the progressively more rounded morphology we described throughout terminal erythropoiesis.

Functions of mitochondria are tightly linked to communication among organelles (Theurey et al., 2016; Desai et al., 2020; Gao et al., 2020; Kohler et al., 2020; Yang et al., 2020; Strobbe et al., 2021). The quantification of MAMs shows no difference from ProE to PolyE. At the transition from PolyE to OrthoE, the total of MAM structures per cell decreases together with the percentage of mitochondria forming MAMs (**Figure 4**). MAMs are well-known structures involved in regulation of calcium homeostasis, lipid synthesis and transfer, mitochondria movement and dynamics, ER stress regulation, inflammation, and autophagy (Gao et al., 2020; Kohler et al., 2020; Yang et al., 2020). OrthoE stage also corresponds to a stage with drastic changes in cellular functions, where the cell needs to shut down several functions and to prepare for enucleation. On the one hand, lacking contact points between organelles could simply result from the decrease in organelles abundance. Nevertheless, our observations suggest that there is a specific decrease of MAM structures not related to the overall mitochondria clearance that can be related to the loss of relevance of MAM-associated structures over differentiation. This speculation is supported by our recent findings which demonstrate that mitochondrial clearance and enucleation were strongly diminished when VDAC1 and TSPO1 were downregulated (Moras et al., 2020, 2022). Indeed, these proteins are mitochondrial outer membrane proteins known to be involved in outer MAM contact sites and also heme and cholesterol traffic.

Regarding mitochondria or nucleus communication, we showed that the percentage of mitochondria forming NAM is not different among stages, whereas the total amount of NAM decreases in PolyE and OrthoE compared to ProE and BasoE. This might suggest a specific removal of a subset of mitochondrial population, maintaining those in proximity to the nucleus despite the total reduced number of these structures. NAM were first described 50 years ago (McCully and Robinow, 1971; Franke et al., 1973) and they were speculated to participate in several functions as yeast fission and heme and phospholipid traffic in yeast (McCully and Robinow, 1971; Franke et al., 1973; Martinez-Guzman et al., 2020; Eisenberg-Bord et al., 2021). They are described to regulate the localization of transcription factors and consequently controls cellular adaptation to stress by retro-communicating with the nucleus (Jazwinski, 2014; Desai et al., 2020; Strobbe et al., 2021). Precise regulation of mitochondrial activity is essential to complete an efficient enucleation (Gonzalez-Menendez et al., 2021; Liang et al., 2021). In fact, perinuclear localization of functional mitochondria is required for mice enucleation (Liang et al., 2021). Here, we showed that whereas some mitochondria appear small

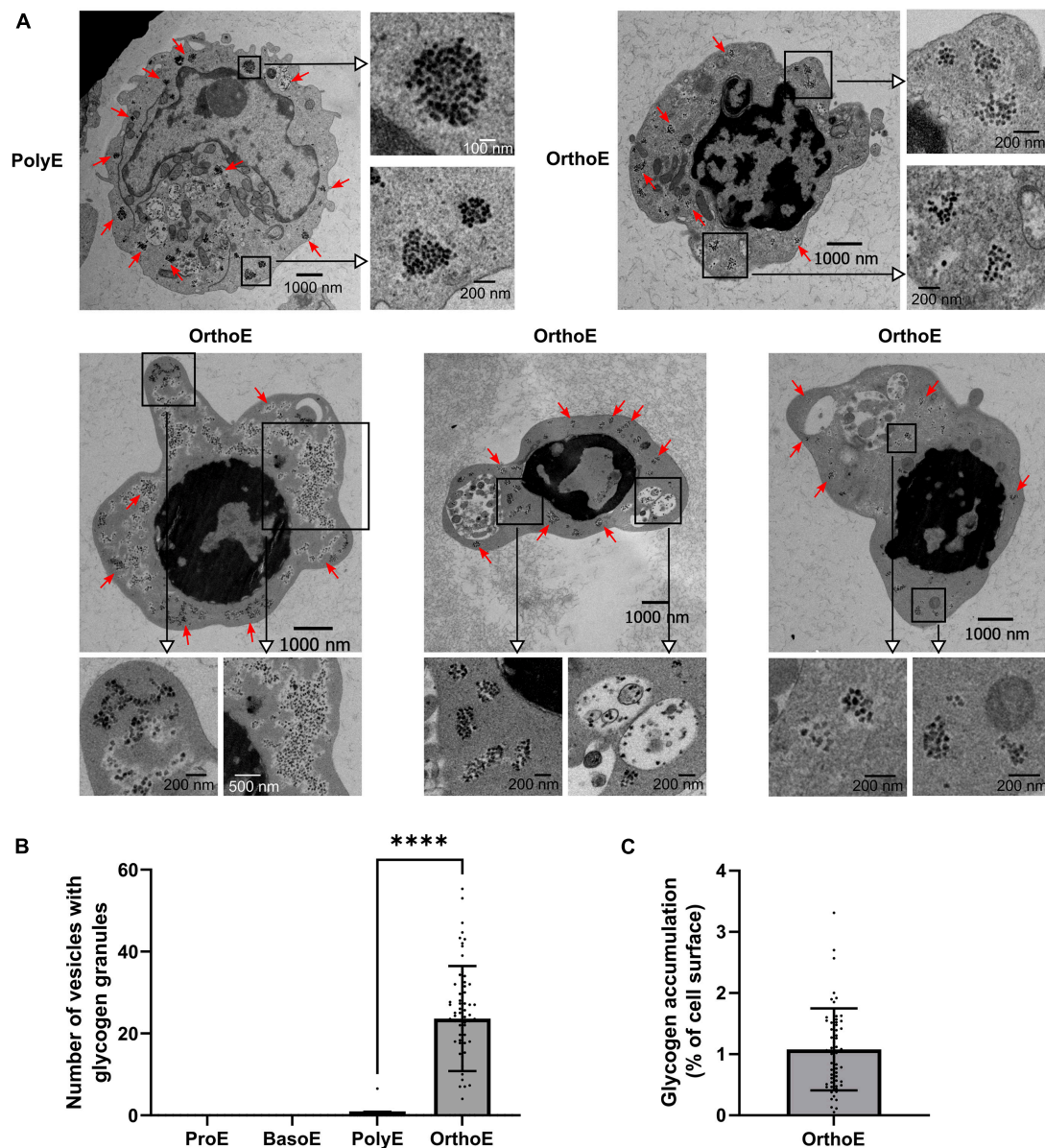


FIGURE 6 | Glycogen accumulation in OrthoE. **(A)** Representative images of the only ProE exhibiting glycogen granules and several OrthoE with inset on glycogen granules (red arrows). **(B)** Quantification of vesicles containing glycogen granules and **(C)** percentage of cell surface occupied by glycogen granules (surface of glycogen granules relative to cell surface $\times 100$) in OrthoE. Kruskal–Wallis analysis on at least 20 images for the three replicates. **** $p < 0.001$.

and rounded in OrthoE, some were elongated and in close proximity to the nucleus (Figure 3E). This might suggest that not all mitochondria in OrthoE are committed to the same function. Subcellular repartition of mitochondria with different morphologies and specialized functions has been identified in muscles (Willingham et al., 2021). The same might be true for OrthoE and should be taking into account while functionality studies might be accounted for different subpopulations of mitochondria within the cell.

Another role of mitochondria is to synthesize heme, a crucial component of hemoproteins as hemoglobin

(Dailey and Meissner, 2013; Hamdi et al., 2016). In erythroid cells, hemoglobin synthesis starts from BasoE to PolyE transition and is accompanied by a strong intracellular trafficking (Rio et al., 2019). We highlighted in Figure 5 an increase in endosomes number from ProE to PolyE. This can be the reflection of the stimulation of the intracellular trafficking to import iron and heme, as expected for differentiation stages presenting the higher rate of hemoglobin synthesis. PolyE is also the pivotal stage where erythroid membrane proteins are translated and addressed to the plasma membrane (Blanc et al., 2005; Gautier et al., 2016). This process involved trafficking from the ER to

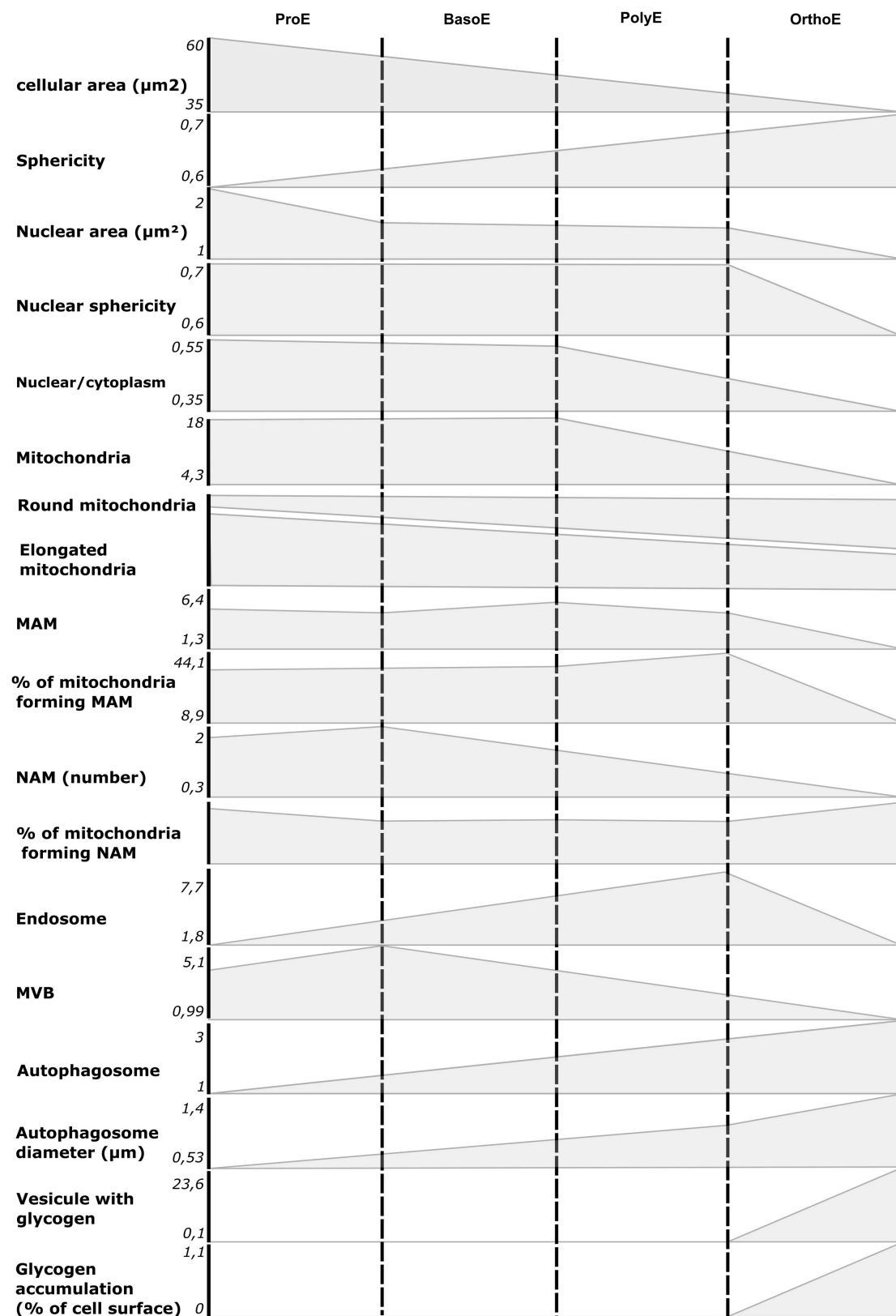


FIGURE 7 | Summary of morphological and ultrastructural quantifications from our analysis. The mean value for ProE to OrthoE stages was reported on ordinate for each quantified item presented in this article.

the plasma membrane and would participate to the high level of intracellular trafficking that is observed at this maturation stage. PolyE are also the latest stage to divide. In OrthoE, transcription is highly reduced and also protein synthesis (Ludwig et al., 2019). This is consistent with the lower activity of the endocytosis or recycling pathway we observed (Figures 5B,C). MVBs, also known as exosomes, are reduced at OrthoE stage. Whereas it is known that MVBs are involved in exocytosis in an erythroid context (Fader and Colombo, 2006), this pathway seems not to be the major way of unneeded cellular components clearance.

Mammals' terminal erythropoiesis requires the clearance of organelles and the enucleation to achieve final mature erythrocyte. These processes occur at OrthoE and reticulocyte stages, where the activation of general autophagy and/or specific mitophagy occurs (Schweers et al., 2007; Kundu et al., 2008; Zhang et al., 2009; Betin et al., 2013; Honda et al., 2014; Moras et al., 2022). Supporting these reports, we observed here an increase in autophagosome abundance and size in OrthoE (Figure 5) that might reflect an increase in autophagic activity within the cell. Defect in proper mitochondria degradation leads to the maintenance of mitochondria in mature circulating red blood cells, as recently described for SCD or for SLE (Jagadeeswaran et al., 2017; Caielli et al., 2021; Martino et al., 2021). While not completely elucidated, this defective mitochondrial clearance might participate in the pathophysiology of the diseases.

Adaptative changes in OrthoE metabolism could also be highlighted by the presence of glycogen granules (Figure 6). Energy requirement is low in OrthoE (Gonzalez-Menendez et al., 2021). Within the cell, allosteric regulation of glycolytic enzymes prevents glucose to be processed by glycolysis and divert the flux toward storage forms. Without knowing whether this accumulation is a side effect of *ex vivo* differentiation, accumulation of glycogen can be indicating of a preparatory mechanism to provide enucleated red cells with glycolysis substrates. In mature red blood cells devoid of functional mitochondria, the energetic metabolism relies on glycolysis. Moreover, glucose also fueled the pentose phosphate pathway, leading to the production of NADPH, the major coenzyme required to replenish glutathione-based antioxidative defenses. To better understand this phenomenon, further experiments will be required to confirm the glycogen granules accumulation *in vivo* and to study the molecular players involved in this pathway.

In summary, we showed that TEM is a valuable tool to study morphological and ultrastructural changes within erythroblasts (Figure 7). We showed the decrease in size of the cell and the nucleus and also the chromatin condensation, hallmark of the transcription arrest throughout terminal erythropoiesis. Insights into organelles morphology and cellular metabolism can also come from micrographs. In this regard, we could monitor the progressive decrease in mitochondria abundance, the mitochondrial fragmentation, the decrease in interorganelle communication by the reduction in MAM and NAM count, the elevated intracellular trafficking from the endosomal pathway, and the induction of autophagy. All of these processes are essential for proper erythropoiesis, and we believe that

characterization of ultrastructural changes in erythroblasts would be of a great interest to further investigate the origin of dyserythropoietic diseases.

DATA AVAILABILITY STATEMENT

The original contributions presented in the study are included in the article/**Supplementary Material**, further inquiries can be directed to the corresponding author.

ETHICS STATEMENT

This study was approved and conducted according to the Institutional Ethical Guidelines of the National Institute of Blood Transfusion (N°2019-1, INTS, Paris, France). The patients/participants provided their written informed consent to participate in this study.

AUTHOR CONTRIBUTIONS

MO and SL conceived the project and obtained funding. SL designed the experiments. AD, MM, and SL performed the experiments. JL evaluated protocols and supervised blood samples purchasing. AD, JJ, CS, J-MV, CF, and SL analyzed the data. MO, CF, J-MV, and SL critically evaluated the experiments. AD, CF, MO, and SL wrote the manuscript. MO, CF, and SL provided supervision. All authors read and commented on the manuscript and approved the final version.

FUNDING

This study was supported by the IdEx Université de Paris, ANR-18-IDEX-0001. AD's internship was founded by the "Club du Globule Rouge et du Fer." JJ is the recipient of a Ph.D. fellowship from CONICET.

ACKNOWLEDGMENTS

We thank Jean-Philippe Semblat and Laetitia Claer from the UMRS_1134 cytometry platform (Paris, France) for their precious help in cell sorting, Catherine Durieu and Rémi Le Borgne from the ImagoSeine facility (Institute Jacques Monod, Paris, France), and the France Bioimaging Infrastructure supported by the French National Research Agency (ANR-10-INSB-04, « Investments fit the future ») for precious help in sample preparations and image acquisitions, and Sorine Brisseau and Rafael Ferreira-Veloso for their participation in MGG staining and counting during their Master Sc internship. We also thank the Guests Researcher program from the University of Paris, Abdellah Nait and Corentine Chrysostome for their technical and administrative assistance, respectively, and the VOUSH group for fruitful discussions.

SUPPLEMENTARY MATERIAL

The Supplementary Material for this article can be found online at: <https://www.frontiersin.org/articles/10.3389/fphys.2021.791691/full#supplementary-material>

Supplementary Figure 1 | Electron micrographs of ProE.

Supplementary Figure 2 | Electron micrographs of BasoE.

Supplementary Figure 3 | Electron micrographs of PolyE.

Supplementary Figure 4 | Electron micrographs of OrthoE.

Supplementary Figure 5 | Mitochondrial morphology in erythroblasts.

Representative images of rounded and elongated mitochondria in erythroblasts with inserts of rounded (R) or elongated mitochondria (E).

REFERENCES

- Benard, G., Bellance, N., James, D., Parrone, P., Fernandez, H., Letellier, T., et al. (2007). Mitochondrial bioenergetics and structural network organization. *J. Cell Sci.* 120, 838–848. doi: 10.1242/jcs.03381
- Bein, V. M., Singleton, B. K., Parsons, S. F., Anstee, D. J., and Lane, J. D. (2013). Autophagy facilitates organelle clearance during differentiation of human erythroblasts: evidence for a role for ATG4 paralogs during autophagosome maturation. *Autophagy* 9, 881–893. doi: 10.4161/auto.24172
- Blanc, L., De Gassart, A., Geminard, C., Bette-Bobillo, P., and Vidal, M. (2005). Exosome release by reticulocytes—an integral part of the red blood cell differentiation system. *Blood Cells Mol. Dis.* 35, 21–26. doi: 10.1016/j.bcmd.2005.04.008
- Bonora, M., Pinton, P., and Ito, K. (2015). Mitochondrial control of hematopoietic stem cell balance and hematopoiesis. *Front. Biol.* 10:117–124. doi: 10.1007/s11515-015-1356-0
- Caielli, S., Cardenas, J., de Jesus, A. A., Baisch, J., Walters, L., Blanck, J. P., et al. (2021). Erythroid mitochondrial retention triggers myeloid-dependent type I interferon in human SLE. *Cell* 184, 4464–4479 e4419. doi: 10.1016/j.cell.2021.07.021
- Castejon, O. J., Diaz, M., Castejon, H. V., and Castellano, A. (2002). Glycogen-rich and glycogen-depleted astrocytes in the oedematous human cerebral cortex associated with brain trauma, tumours and congenital malformations: an electron microscopy study. *Brain Inj.* 16, 109–132. doi: 10.1080/02699050110088218
- Chen, K., Liu, J., Heck, S., Chasis, J. A., An, X., and Mohandas, N. (2009). Resolving the distinct stages in erythroid differentiation based on dynamic changes in membrane protein expression during erythropoiesis. *Proc. Natl. Acad. Sci. U.S.A.* 106, 17413–17418. doi: 10.1073/pnas.0909296106
- Dailey, H. A., and Meissner, P. N. (2013). Erythroid heme biosynthesis and its disorders. *Cold Spring Harb. Perspect. Med.* 3:a011676. doi: 10.1101/cshperspect.a011676
- Desai, R., East, D. A., Hardy, L., Faccenda, D., Rigon, M., Crosby, J., et al. (2020). Mitochondria form contact sites with the nucleus to couple prosurvival retrograde response. *Sci. Adv.* 6:eabc9955. doi: 10.1126/sciadv.abc9955
- Eisenberg-Bord, M., Zung, N., Collado, J., Drwesh, L., Fenech, E. J., Fadel, A., et al. (2021). Cnm1 mediates nucleus-mitochondria contact site formation in response to phospholipid levels. *J. Cell Biol.* 220:e202104100. doi: 10.1083/jcb.202104100
- Ellenrieder, L., Rampelt, H., and Becker, T. (2017). Connection of protein transport and organelle contact sites in mitochondria. *J. Mol. Biol.* 429, 2148–2160. doi: 10.1016/j.jmb.2017.05.023
- Fader, C. M., and Colombo, M. I. (2006). Multivesicular bodies and autophagy in erythrocyte maturation. *Autophagy* 2, 122–125. doi: 10.4161/auto.2.2.2350
- Fan, A. X., Hossain, M. A., Stees, J., Gavrilova, E., and Bungert, J. (2015). “Chapter 11—Regulation of erythroid cell differentiation by transcription factors, chromatin structure alterations, and noncoding RNA,” in *Epigenetic Gene Expression and Regulation*, eds S. Huang, M. D. Litt, and C. A. Blakey (Oxford: Academic Press), 237–264. doi: 10.1016/b978-0-12-799958-6.00011-1
- Fontenay, M., Cathelin, S., Amiot, M., Gyan, E., and Solary, E. (2006). Mitochondria in hematopoiesis and hematological diseases. *Oncogene* 25, 4757–4767. doi: 10.1038/sj.onc.1209606
- Franke, W. W., Deumling, B., Zentgraf, H., Falk, H., and Rae, P. M. (1973). Nuclear membranes from mammalian liver. IV. Characterization of membrane-attached DNA. *Exp. Cell Res.* 81, 365–392. doi: 10.1016/0014-4827(73)90527-2
- Gao, P., Yang, W., and Sun, L. (2020). Mitochondria-associated endoplasmic reticulum membranes (MAMs) and their prospective roles in kidney disease. *Oxid. Med. Cell Longev.* 2020:3120539. doi: 10.1155/2020/3120539
- Gautier, E.-F., Ducamp, S., Leduc, M., Salnot, V., Guillonnet, F., Dussiot, M., et al. (2016). Comprehensive proteomic analysis of human erythropoiesis. *Cell Rep.* 16, 1470–1484. doi: 10.1016/j.celrep.2016.06.085
- Giamogante, F., Barazzuol, L., Brini, M., and Cali, T. (2020). ER-mitochondria contact sites reporters: strengths and weaknesses of the available approaches. *Int. J. Mol. Sci.* 21:8157. doi: 10.3390/ijms21218157
- Gonzalez-Ibanez, A. M., Ruiz, L. M., Jensen, E., Echeverria, C. A., Romero, V., Stiles, L., et al. (2020). Erythroid differentiation and heme biosynthesis are dependent on a shift in the balance of mitochondrial fusion and fission dynamics. *Front. Cell Dev. Biol.* 8:592035. doi: 10.3389/fcell.2020.592035
- Gonzalez-Menendez, P., Romano, M., Yan, H., Deshmukh, R., Papoin, J., Oburoglu, L., et al. (2021). An IDH1-vitamin C crosstalk drives human erythroid development by inhibiting pro-oxidant mitochondrial metabolism. *Cell Rep.* 34:108723. doi: 10.1016/j.celrep.2021.108723
- Hamdi, A., Roshan, T. M., Kahawita, T. M., Mason, A. B., Sheftel, A. D., and Ponka, P. (2016). Erythroid cell mitochondria receive endosomal iron by a “kiss-and-run” mechanism. *Biochim. Biophys. Acta* 1863, 2859–2867. doi: 10.1016/j.bbamcr.2016.09.008
- Honda, S., Arakawa, S., Nishida, Y., Yamaguchi, H., Ishii, E., and Shimizu, S. (2014). Ulk1-mediated Atg5-independent macroautophagy mediates elimination of mitochondria from embryonic reticulocytes. *Nat. Commun.* 5:4004. doi: 10.1038/ncomms5004
- Hu, J., Liu, J., Xue, F., Halverson, G., Reid, M., Guo, A., et al. (2013). Isolation and functional characterization of human erythroblasts at distinct stages: implications for understanding of normal and disordered erythropoiesis in vivo. *Blood* 121, 3246–3253. doi: 10.1182/blood-2013-01-476390
- Jagadeeswaran, R., Vazquez, B. A., Thirupathi, M., Ganesh, B. B., Ibanez, V., Cui, S., et al. (2017). Pharmacological inhibition of LSD1 and mTOR reduces mitochondrial retention and associated ROS levels in the red blood cells of sickle cell disease. *Exp. Hematol.* 50, 46–52. doi: 10.1016/j.exphem.2017.02.003
- Jazwinski, S. M. (2014). The retrograde response: a conserved compensatory reaction to damage from within and from without. *Prog. Mol. Biol. Transl. Sci.* 127, 133–154. doi: 10.1016/B978-0-12-394625-6.00005-2
- Killisch, I., Steinlein, P., Romisch, K., Hollinshead, R., Beug, H., and Griffiths, G. (1992). Characterization of early and late endocytic compartments of the transferrin cycle. Transferrin receptor antibody blocks erythroid differentiation by trapping the receptor in the early endosome. *J. Cell Sci.* 103 (Pt 1), 211–232. doi: 10.1242/jcs.103.1.211
- Klionsky, D. J. (2005). The molecular machinery of autophagy: unanswered questions. *J. Cell Sci.* 118, 7–18. doi: 10.1242/jcs.01620
- Kohler, V., Aufschnaiter, A., and Buttner, S. (2020). Closing the gap: membrane contact sites in the regulation of autophagy. *Cells* 9:1184. doi: 10.3390/cells9051184
- Koury, S. T., Koury, M. J., and Bondurant, M. C. (1988). Morphological changes in erythroblasts during erythropoietin-induced terminal differentiation in vitro. *Exp. Hematol.* 16, 758–763.
- Kundu, M., Lindsten, T., Yang, C. Y., Wu, J., Zhao, F., Zhang, J., et al. (2008). Ulk1 plays a critical role in the autophagic clearance of mitochondria and ribosomes during reticulocyte maturation. *Blood* 112, 1493–1502. doi: 10.1182/blood-2008-02-137398
- Lackner, L. L. (2019). The Expanding and unexpected functions of mitochondria contact sites. *Trends Cell Biol.* 29, 580–590. doi: 10.1016/j.tcb.2019.02.009
- Liang, R., Menon, V., Qiu, J., Arif, T., Renuse, S., Lin, M., et al. (2021). Mitochondrial localization and moderated activity are key to murine erythroid enucleation. *Blood Adv.* 5, 2490–2504. doi: 10.1182/bloodadvances.2021004259

- Liu, J., Mohandas, N., and An, X. (2011). Membrane assembly during erythropoiesis. *Curr. Opin. Hematol.* 18, 133–138. doi: 10.1097/MOH.0b013e32834521f3
- Ludwig, L. S., Lareau, C. A., Bao, E. L., Nandakumar, S. K., Muus, C., Ulirsch, J. C., et al. (2019). Transcriptional States and chromatin accessibility underlying human erythropoiesis. *Cell Rep* 27, 3228–3240.e3227. doi: 10.1016/j.celrep.2019.05.046
- Martinez-Guzman, O., Willoughby, M. M., Saini, A., Dietz, J. V., Bohovych, I., Medlock, A. E., et al. (2020). Mitochondrial-nuclear heme trafficking in budding yeast is regulated by GTPases that control mitochondrial dynamics and ER contact sites. *J. Cell Sci.* 133:jcs.237917. doi: 10.1242/jcs.237917
- Martino, S., Arlet, J. B., Odievre, M. H., Jullien, V., Moras, M., Hattab, C., et al. (2021). Deficient mitophagy pathways in sickle cell disease. *Br. J. Haematol.* 5, 988–993. doi: 10.1111/bjh.17416
- McCully, E. K., and Robinow, C. F. (1971). Mitosis in the fission yeast *Schizosaccharomyces pombe*: a comparative study with light and electron microscopy. *J. Cell Sci.* 9, 475–507. doi: 10.1242/jcs.9.2.475
- Moras, M., Hattab, C., Gonzalez-Menendez, P., Fader, C. M., Dussiot, M., Larghero, J., et al. (2022). Human erythroid differentiation requires VDAC1-mediated mitochondrial clearance. *Haematologica* 107, 167–177. doi: 10.3324/haematol.2020.257121
- Moras, M., Hattab, C., Gonzalez-Menendez, P., Martino, S., Larghero, J., Le Van Kim, C., et al. (2020). Downregulation of mitochondrial TSPO inhibits mitophagy and reduces enucleation during human terminal erythropoiesis. *Int. J. Mol. Sci.* 21:9066. doi: 10.3390/ijms21239066
- Moras, M., Lefevre, S. D., and Ostuni, M. A. (2017). From erythroblasts to mature red blood cells: organelle clearance in mammals. *Front. Physiol.* 8:1076. doi: 10.3389/fphys.2017.01076
- Oburoglu, L., Romano, M., Taylor, N., and Kinet, S. (2016). Metabolic regulation of hematopoietic stem cell commitment and erythroid differentiation. *Curr. Opin. Hematol.* 23, 198–205. doi: 10.1097/MOH.0000000000000234
- Oburoglu, L., Tardito, S., Fritz, V., Merida, P., Craveiro, M., Mamede, J., et al. (2014). Glucose and glutamine metabolism regulate human hematopoietic stem cell lineage specification. *Cell Stem Cell* 15, 169–184. doi: 10.1016/j.stem.2014.06.002
- Örtenblad, N., Westerblad, H., and Nielsen, J. (2013). Muscle glycogen stores and fatigue. *J. Physiol.* 591, 4405–4413. doi: 10.1113/jphysiol.2013.251629
- Palis, J. (2014). Primitive and definitive erythropoiesis in mammals. *Front. Physiol.* 5:3. doi: 10.3389/fphys.2014.00003
- Peters, L. L., White, R. A., Birkenmeier, C. S., Bloom, M. L., Lux, S. E., and Barker, J. E. (1992). Changing patterns in cytoskeletal mRNA expression and protein synthesis during murine erythropoiesis in vivo. *Proc. Natl. Acad. Sci. U.S.A.* 89, 5749–5753. doi: 10.1073/pnas.89.13.5749
- Revel, J. P., Napolitano, L., and Fawcett, D. W. (1960). Identification of glycogen in electron micrographs of thin tissue sections. *J. Biophys. Biochem. Cytol.* 8, 575–589. doi: 10.1083/jcb.8.3.575
- Rio, S., Gastou, M., Karboul, N., Derman, R., Suriyun, T., Manceau, H., et al. (2019). Regulation of globin-heme balance in Diamond-Blackfan anemia by HSP70/GATA1. *Blood* 133, 1358–1370. doi: 10.1182/blood-2018-09-875674
- Rossmann, M. P., Hoi, K., Chan, V., Abraham, B. J., Yang, S., Mullahoo, J., et al. (2021). Cell-specific transcriptional control of mitochondrial metabolism by TIF1gamma drives erythropoiesis. *Science* 372, 716–721. doi: 10.1126/science.aaz2740
- Ru, Y. X., Dong, S. X., Li, Y., Zhao, S. X., Liang, H. Y., Zhu, X. F., et al. (2018). A novel anemia associated with membranous cytoplasm degeneration in 16 patients: an ultrastructural study. *Ultrastruct. Pathol.* 42, 350–357. doi: 10.1080/01913123.2018.1485807
- Sandoval, H., Thiagarajan, P., Dasgupta, S. K., Schumacher, A., Prchal, J. T., Chen, M., et al. (2008). Essential role for Nix in autophagic maturation of erythroid cells. *Nature* 454, 232–235. doi: 10.1038/nature07006
- Schell, J. C., and Rutter, J. (2017). Mitochondria link metabolism and epigenetics in haematopoiesis. *Nat. Cell Biol.* 19, 589–591. doi: 10.1038/ncb3540
- Schweers, R. L., Zhang, J., Randall, M. S., Loyd, M. R., Li, W., Dorsey, F. C., et al. (2007). NIX is required for programmed mitochondrial clearance during reticulocyte maturation. *Proc. Natl. Acad. Sci. U.S.A.* 104, 19500–19505. doi: 10.1073/pnas.0708818104
- Strobbe, D., Sharma, S., and Campanella, M. (2021). Links between mitochondrial retrograde response and mitophagy in pathogenic cell signalling. *Cell Mol. Life Sci.* 78, 3767–3775. doi: 10.1007/s00018-021-03770-5
- Theurey, P., Tubbs, E., Vial, G., Jacquemetton, J., Bendridi, N., Chauvin, M. A., et al. (2016). Mitochondria-associated endoplasmic reticulum membranes allow adaptation of mitochondrial metabolism to glucose availability in the liver. *J. Mol. Cell Biol.* 8, 129–143. doi: 10.1093/jmcb/mjw004
- Vezzoli, E., Cali, C., De Roo, M., Ponzoni, L., Sogne, E., Gagnon, N., et al. (2020). Ultrastructural evidence for a role of astrocytes and glycogen-derived lactate in learning-dependent synaptic stabilization. *Cereb. Cortex* 30, 2114–2127. doi: 10.1093/cercor/bhz226
- Wickramasinghe, S. N., Cooper, E. H., and Chalmers, D. G. (1968). A study of erythropoiesis by combined morphologic, quantitative cytochemical and autoradiographic methods. Normal human bone marrow, vitamin B12 deficiency and iron deficiency anemia. *Blood* 31, 304–313. doi: 10.1182/blood.v31.3.304.304
- Wickramasinghe, S. N., Porwit, A., and Erber, W. N. (2011). “Normal bone marrow cells. development and cytology,” in *Blood and Bone Marrow Pathology*, eds A. Porwit, J. McCullough, and W. N. Erber (Amsterdam: Elsevier).
- Willingham, T. B., Ajayi, P. T., and Glancy, B. (2021). Subcellular specialization of mitochondrial form and function in skeletal muscle cells. *Front. Cell Dev. Biol.* 9:757305. doi: 10.3389/fcell.2021.757305
- Yang, M., Li, C., Yang, S., Xiao, Y., Xiong, X., Chen, W., et al. (2020). Mitochondria-associated ER membranes—the origin site of autophagy. *Front. Cell Dev. Biol.* 8:595. doi: 10.3389/fcell.2020.00595
- Zanetti, N., and Mayorga, L. S. (2009). Acrosomal swelling and membrane docking are required for hybrid vesicle formation during the human sperm acrosome reaction. *Biol. Reprod.* 81, 396–405. doi: 10.1095/biolreprod.109.07.6166
- Zhang, J., Randall, M. S., Loyd, M. R., Dorsey, F. C., Kundu, M., Cleveland, J. L., et al. (2009). Mitochondrial clearance is regulated by Atg7-dependent and -independent mechanisms during reticulocyte maturation. *Blood* 114, 157–164.

Conflict of Interest: The authors declare that the research was conducted in the absence of any commercial or financial relationships that could be construed as a potential conflict of interest.

Publisher's Note: All claims expressed in this article are solely those of the authors and do not necessarily represent those of their affiliated organizations, or those of the publisher, the editors and the reviewers. Any product that may be evaluated in this article, or claim that may be made by its manufacturer, is not guaranteed or endorsed by the publisher.

Copyright © 2022 Dussouchaud, Jacob, Secq, Verbavatz, Moras, Larghero, Fader, Ostuni and Lefevre. This is an open-access article distributed under the terms of the Creative Commons Attribution License (CC BY). The use, distribution or reproduction in other forums is permitted, provided the original author(s) and the copyright owner(s) are credited and that the original publication in this journal is cited, in accordance with accepted academic practice. No use, distribution or reproduction is permitted which does not comply with these terms.



Storage-Induced Micro-Erythrocytes Can Be Quantified and Sorted by Flow Cytometry

Mickaël Marin^{1,2,3}, Sandy Peltier^{1,2,3}, Youcef Hadjou^{1,2,3}, Sonia Georgeault⁴, Michaël Dussiot^{3,5}, Camille Roussel^{1,2,3,6}, Olivier Hermine^{3,5,7}, Philippe Roingeard^{4,8}, Pierre A. Buffet^{1,2,3,9} and Pascal Amireault^{1,2,3,5*}

¹ INSERM, BIGR, Université de Paris and Université des Antilles, Paris, France, ² Institut National de la Transfusion Sanguine, Paris, France, ³ Laboratoire d'Excellence GR-Ex, Paris, France, ⁴ Plateforme des Microscopies, Infrastructures de Recherche en Biologie Santé et Agronomie, Programme Pluriformation Analyse des Systèmes Biologiques, Tours, France, ⁵ U1163, Laboratory of Cellular and Molecular Mechanisms of Hematological Disorders and Therapeutic Implications, INSERM, Université de Paris, Paris, France, ⁶ AP-HP, Laboratoire d'Hématologie, Hôpital Necker-Enfants Malades, Paris, France, ⁷ Département d'Hématologie, Hôpital Necker-Enfants Malades, Assistance Publique-Hôpitaux de Paris, Paris, France, ⁸ U1259, Centre Hospitalier Régional Universitaire de Tours, Morphogenèse et Antigénicité du VIH et des Virus des Hépatites, INSERM, Université de Tours, Tours, France, ⁹ AP-HP, Paris, France

OPEN ACCESS

Edited by:

Lars Kaestner,
Saarland University, Germany

Reviewed by:

Gregory Barshtein,
Hebrew University of Jerusalem, Israel
Greta Simionato,
Saarland University, Germany

*Correspondence:

Pascal Amireault
pascal.amireault@inserm.fr

Specialty section:

This article was submitted to
Red Blood Cell Physiology,
a section of the journal
Frontiers in Physiology

Received: 17 December 2021

Accepted: 31 January 2022

Published: 23 February 2022

Citation:

Marin M, Peltier S, Hadjou Y,
Georgeault S, Dussiot M, Roussel C,
Hermine O, Roingeard P, Buffet PA
and Amireault P (2022)
Storage-Induced Micro-Erythrocytes
Can Be Quantified and Sorted by
Flow Cytometry.
Front. Physiol. 13:838138.
doi: 10.3389/fphys.2022.838138

Refrigerated storage of red cell concentrates before transfusion is associated with progressive alterations of red blood cells (RBC). Small RBC (type III echinocytes, spherocytes, and spherocytes) defined as storage-induced micro-erythrocytes (SME) appear during pretransfusion storage. SME accumulate with variable intensity from donor to donor, are cleared rapidly after transfusion, and their proportion correlates with transfusion recovery. They can be rapidly and objectively quantified using imaging flow cytometry (IFC). Quantifying SME using flow cytometry would further facilitate a physiologically relevant quality control of red cell concentrates. RBC stored in blood bank conditions were stained with a carboxyfluorescein succinimidyl ester (CFSE) dye and incubated at 37°C. CFSE intensity was assessed by flow cytometry and RBC morphology evaluated by IFC. We observed the accumulation of a CFSE^{high} RBC subpopulation by flow cytometry that accounted for 3.3 and 47.2% at day 3 and 42 of storage, respectively. IFC brightfield images showed that this CFSE^{high} subpopulation mostly contains SME while the CFSE^{low} subpopulation mostly contains type I and II echinocytes and discocytes. Similar numbers of SME were quantified by IFC (based on projected surface area) and by flow cytometry (based on CFSE intensity). IFC and scanning electron microscopy showed that $\geq 95\%$ pure subpopulations of CFSE^{high} and CFSE^{low} RBC were obtained by flow cytometry-based sorting. SME can now be quantified using a common fluorescent dye and a standard flow cytometer. The staining protocol enables specific sorting of SME, a useful tool to further characterize this RBC subpopulation targeted for premature clearance after transfusion.

Keywords: red blood cell (RBC), RBC storage, RBC morphology, flow cytometry, imaging flow cytometry (IFC), RBC storage lesion

INTRODUCTION

During hypothermic pre-transfusion storage, part of the RBC metabolism shifts from glycolysis to the pentose phosphate pathway after 10–14 days of storage, leading to a progressive decrease of the intracellular ATP level (D'Alessandro et al., 2015; Bordbar et al., 2016). The fragilized RBC is thus less capable of coping with the oxidative stress generated by storage, further affecting RBC integrity (Reisz et al., 2016). These metabolic and oxidative stresses contribute to the progressive modifications of RBC properties (Yoshida et al., 2019). Among those, RBC morphology is a well-documented and key RBC property altered during storage.

A number of techniques are used to explore RBC morphology. The pioneer work of Bessis (1972, 1974) using scanning electron microscopy defined RBC morphological categories. This technique is still used to assess RBC morphology during storage (Berezina et al., 2002; Zehnder et al., 2008; Antonelou et al., 2012; Blasi et al., 2012; D'Alessandro et al., 2012; Roussel et al., 2021).

Digital holographic microscopy was recently used to explore RBC morphology along storage (Bardyn et al., 2017). Light microscopy can also be used to observe fixed (Högman et al., 1985; Tchir et al., 2013; Reinhart et al., 2015) or unfixed cells in a physiological medium (Roussel et al., 2017; Lu and Shevkoplyas, 2020). RBC morphology is indeed sensitive to RBC intrinsic properties and to the suspension medium (Bessis, 1972). Imaging flow cytometry (IFC) rapidly acquires tens of thousands of images of unfixed cells in a physiological medium and identifies a well-demarcated subpopulation of morphologically altered and smaller RBC, comprising type III echinocytes, spherocytocytes, and spherocytes (Roussel et al., 2017). These small RBC, defined as storage-induced micro-erythrocytes (SME), accumulate during storage, reaching a mean proportion of 24% of the entire RBC population at day 42 and their proportion negatively correlates with post-transfusion recovery in healthy volunteers (Roussel et al., 2021). Furthermore, the capacity of IFC to discriminate fluorescently stained RBC allowed to observe their clearance from circulation upon *ex vivo* perfusion in human spleens and *in vivo* transfusion in mice (Roussel et al., 2021). The proportion of SME is thus a relevant storage quality marker that identifies the erythrocyte subpopulation targeted for rapid post-transfusion clearance. This study aimed to develop an alternative method of SME quantification and sorting using standard flow cytometry. Obtaining pure subpopulations of SME or morphologically normal erythrocytes would indeed greatly facilitate the exploration of the intrinsic alterations of RBC inducing their clearance.

MATERIALS AND METHODS

Red Blood Cells Concentrate Collection and Storage

Eight leukoreduced RBC concentrates provided by the Etablissement Français du Sang (French blood banking system) from healthy donors were stored in

saline-adenine-glucose-mannitol (SAGM) solution at 2–6°C for 42 days. Samples were aseptically collected and analyzed at defined time-points (days 3, 21, 28, 35, and 42).

Carboxyfluorescein Diacetate Succinimidyl Ester Staining

Red blood cells were washed once in phosphate buffer saline (PBS) and stained with CFDA-SE (5.5 millions RBC/mL, 0.05 μ M CFSE in PBS) for 20 min at 37°C. Non-fluorescent CFDA-SE diffuses passively into cells and is rapidly processed by cellular esterases resulting in high fluorescent carboxyfluorescein succinimidyl esters (CFSE) that bind cellular components. RBC were then centrifuged, washed once in RPMIc (RPMI 1640 supplemented with 10% FBS, 1% Antibiotic/Antimycotic solution) to remove excess of CFDA-SE and incubated overnight in RPMIc at 22 millions RBC/mL. Following incubation, RBC were centrifuged, resuspended in a fresh RPMIc solution and stored at 4°C until analysis.

Flow Cytometry Analysis

Carboxyfluorescein succinimidyl ester stained RBC were analyzed using FACSCanto II (BD Biosciences) by recording 50,000 events. First, single cells were selected using morphological parameters (FSC-H vs. FSC-A). CFSE^{low} and CFSE^{high} subpopulations were gated according to their size (FSC-W) and their CFSE intensity (collected in FITC channel).

Imaging Flow Cytometry Analysis

Imaging flow cytometry was performed by ImageStream X Mark II (Amnis® Flow Cytometry, Luminex, Seattle, WA, United States) to determine RBC dimensions and morphology as described (Roussel et al., 2017). RBC were suspended at 1% hematocrit (Hct) just before acquisition in a Krebs-albumin solution (Krebs-Henseleit buffer, Sigma-Aldrich) modified with 2 g of glucose, 2.1 g of sodium bicarbonate, 0.175 g of calcium chloride dehydrate, and 5 g of lipid-rich bovine serum albumin (AlbuMAX II, Thermo Fisher Scientific) for 1 L of sterile water (pH 7.4). Images (x60 magnification) were recorded (INSPIRE software, AMNIS) by the brightfield and FITC channels to be then processed by a dedicated computer software [IDEAS (version 6.2); Amnis]. Focused cells and single cells were, respectively, selected using the features gradient RMS_M01_Ch01 and Aspect ratio_M01_Ch01 versus Area_M01_Ch01. Front views were selected using the feature Circularity_Object (M01, Ch01, Tight) and projected surface area was determined using the feature Area_Object (M01, Ch01, Tight). At least 6,000 front views of focused single RBC/condition were analyzed. SME proportion and CFSE intensity were determined independently for each donor, using the nadir of the bimodal frequency histograms as the gating boundary.

Cell Sorting

Sorting of CFSE^{low} and CFSE^{high} cells was performed using MA900 Cell Sorter (Sony) with a 100 μ m sorting-chip at the

maximum speed of 10,000 events per second in semi-purity mode. Unsorted RBC were selected using BSC-A vs. FSC-A then CFSE^{low} and CFSE^{high} subpopulations were gated according to their size (FSC-W) and their CFSE intensity (collected in FITC channel). Cell doublets were excluded by using FSC-H vs. FSC-A and target cells were collected in tubes containing 1 mL of RPMIc, then centrifuged and resuspended in RPMIc to be stored at 4°C until analysis.

Scanning Electron Microscopy

Samples were fixed by incubation (minimum 24 h) in a mix of 4% paraformaldehyde and 1% glutaraldehyde diluted in 0.1 M of phosphate buffer (pH, 7.3) at 4°C, then washed in phosphate buffer, and postfixed by 1-h incubation with 2% osmium tetroxide. Samples were then fully dehydrated in a graded series of ethanol solutions and dried by hexamethyldisilazane. Finally, samples were coated with 4 nm of carbon using a GATAN PECS 682 apparatus before observation under a Zeiss Ultra plus field emission-scanning electron microscope (ZEISS).

Statistical Analysis

Data were analyzed using GraphPad Prism version 9.2.0 for Windows (GraphPad Software, San Diego, CA, United States). To compare two groups of subpopulations (CFSE^{low} vs. CFSE^{high} intensities or SME vs. normal erythrocytes), Wilcoxon tests, for non-parametric and paired data, were applied. To compare means of morphologically altered RBC over time, two-way ANOVA with the Geisser-Greenhouse correction was performed with Sidak's multiple comparison test. Simple linear regression and a correlation test of Spearman were used to assess correlation between the two quantification techniques of morphologically altered RBC. A *P*-value < 0.05 was considered statistically significant.

RESULTS

Incubation-Related Bimodality in Carboxyfluorescein Diacetate Succinimidyl Ester Staining Intensity of Red Blood Cells Stored in Blood Bank Conditions

Red blood cells, sampled from long-stored RBC concentrates, were stained using CFDA-SE and then incubated at 37°C in RPMIc medium. Immediately after CFDA-SE staining, CFSE fluorescence intensity exhibited a unimodal distribution (0 h, gray histogram, **Figure 1**). Incubation of the stained RBC at 37°C led to a progressive decline of fluorescence intensity until 8 h of incubation (black curves, **Figure 1**). Following an overnight incubation, the CFSE intensity showed a clear bimodality separating two RBC subpopulations (Panel 24 h, **Figure 1**). The bimodality in CFSE staining was not visible when fresh RBC were observed or when RBC were incubated at 4°C after staining (data not shown). These results show that

the CFDA-SE staining protocol with an overnight incubation identifies a discrete RBC subpopulation present in long-stored RBC.

CFSE^{high} Erythrocytes Correspond to a Morphologically Altered Subpopulation That Accumulates During Pretransfusion Storage

We next used imaging flow cytometry, that enables simultaneous analysis of fluorescence and morphological parameters, on eight RBC concentrates stored for 42 days. A bimodal distribution of CFDA-SE staining was detected (purple curve, **Figure 2A**) and visible in 8/8 RBC concentrates. Segregating CFSE^{low} RBC (pink line, **Figure 2A**) from CFSE^{high} RBC (light green line, **Figure 2A**) was performed independently for each donor, using the nadir of the bimodal frequency histograms as the gating boundary. The mean fluorescence intensity of CFSE^{high} RBC (154729 a.u. ± 34931) was statistically higher than that of the CFSE^{low} subpopulation (39055 a.u. ± 6980; *p* = 0.0078; **Figure 2B**).

We next determined the projected surface area of each subpopulation along storage to discriminate morphologically altered RBC, named storage-induced micro-erythrocytes (SME), from morphologically normal erythrocytes (Roussel et al., 2017, 2021). Comparison of the distribution of projected surface area between the two subpopulations showed that CFSE^{high} RBC have a lower projected surface area than RBC from the CFSE^{low} subpopulation (**Figure 2C**). CFSE^{high} RBC were significantly smaller than CFSE^{low} RBC (projected surface area of 50.1 μm² ± 2.2 versus 73.7 μm² ± 1.7; *p* = 0.0078; **Figure 2D**). Morphologic analysis of IFC brightfield images showed that the CFSE^{high} RBC were predominantly echinocytes III, spherocytocytes and spherocytes (**Figure 2E**) while the CFSE^{low} subpopulation was composed mostly of discocytes and echinocytes I and II (**Figure 2F**). Reciprocally, selection of SME and morphologically normal erythrocytes (by their projected surface area) confirmed that most SME are CFSE^{high} and that morphologically normal erythrocytes are CFSE^{low} (**Supplementary Figure 1**). The gating strategy to segregate CFSE^{low} and CFSE^{high} subpopulations could be improved using a size parameter, in addition to CFSE intensity (**Supplementary Figure 2**).

Carboxyfluorescein Diacetate Succinimidyl Ester Staining Enables the Flow Cytometry-Based Quantification of Storage-Induced Micro-Erythrocytes Along Storage

We next evaluated the evolution of RBC morphology during storage by flow cytometry using the CFDA-SE staining protocol and compared these observations to the proportion of SME detected by IFC on unstained RBC (Roussel et al., 2017, 2021). A CFSE^{high} subpopulation (now gated using FSC-W and CFSE intensity) accumulated along storage (**Figure 3A**) in the eight

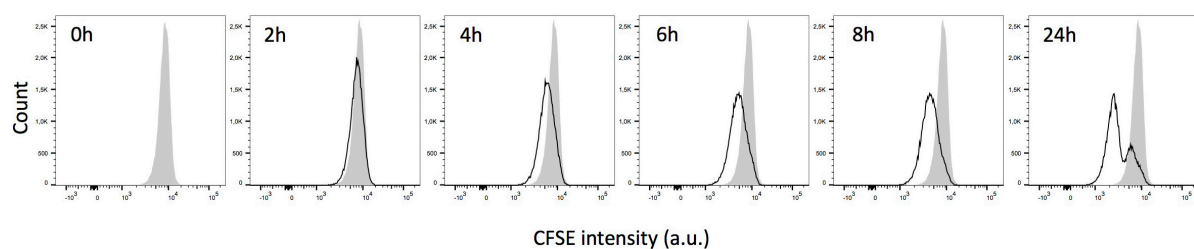


FIGURE 1 | Bimodality in carboxyfluorescein diacetate succinimidyl ester (CFDA-SE) staining intensity of RBC stored in blood bank conditions. Representative frequency plots of CFSE fluorescence intensity for RBC stored for 42 days in SAGM either immediately after CFDA-SE staining (gray histogram) and during the 24 first hours of incubation at 37°C (black line).

RBC concentrates studied (green line, **Figure 3C**). A SME subpopulation (using the nadir of the projected surface area bimodality) also accumulated along storage (**Figure 3B**) in the eight RBC concentrates studied (black line, **Figure 3C**). For all donors, the CFSE^{high} subpopulation accumulated upon storage from $3.3 \pm 1.4\%$ on day 3 to $47.2 \pm 18.8\%$ on day 42 (green line, **Figure 3C**), with marked inter-donor variability. Similarly, the SME subpopulation accumulated upon storage from $1.3 \pm 0.8\%$ on day 3 to $38.7 \pm 22.9\%$ on day 42 (black line, **Figure 3C**). The proportion of morphologically altered RBC followed a similar evolution along storage with both techniques, increasing more rapidly after day 21. The proportion of CFSE^{high} RBC was slightly higher than the proportion of SME at each time point, reaching statistical significance on day 3 and 35 of storage. There was a very strong correlation between the proportion of CFSE^{high} RBC determined using flow cytometry and the proportion of SME determined by IFC ($p < 0.0001$; Spearman $r = 0.93$; $r^2 = 0.88$; **Figure 3D**).

Pure Subpopulations of Morphologically Normal Erythrocytes or Storage-Induced Micro-Erythrocytes Can Be Obtained by Flow Cytometry-Based Sorting

A flow cytometry gating strategy was next used to sort CFSE^{low} and CFSE^{high} RBC subpopulations (**Figure 4A**). IFC was used to evaluate the content of each preparation, using fluorescence intensity and projected surface area. In **Figure 4B**, representative density plots of unsorted (middle panel), sorted CFSE^{low} (left panel), and CFSE^{high} (right panel) subpopulations illustrate the average purity obtained. From five separate experiments conducted on RBC stored 42 days, preparations of CFSE^{low} and CFSE^{high} contained, respectively, a mean proportion of RBC of interest of $96.4 \pm 1.4\%$ and $97.9 \pm 2.0\%$. Scanning electron microscopy images confirmed that a majority of morphologically normal erythrocytes (as discocytes and echinocytes I) were found in CFSE^{low} subpopulations (**Figure 4C**, left panel) while a majority of SME (echinocytes III, spherocytes and spherocytes) were present in CFSE^{high} subpopulation (right panel) with a mix of these morphologies in the unsorted fraction (middle panel).

DISCUSSION

We describe here a simple staining flow cytometry-based protocol to quantify SME that accumulate during pretransfusion storage. In addition, pure subpopulations of SME and long-stored morphologically normal erythrocytes can now be obtained using flow cytometry-based sorting.

We observed that CFDA-SE stained long-stored RBC show a bimodality in fluorescence intensity after an incubation at 37°C. This bimodality was not observed immediately after staining nor after a 24 h incubation at 4°C suggesting that it could be due to an enzymatic process. Non-fluorescent CFDA-SE diffuses passively into cells and is rapidly processed by cellular esterases resulting in high fluorescent CFSE. The resulting molecule is less permeant to cell membrane and highly reactive to free cellular amines, which leads to its spontaneous covalent binding to cellular components, mostly intracellular proteins (Banks et al., 2013). Thus, the persistence of CFSE labeling in cells is expected to depend predominantly on protein turn-over and its natural fluorescence decay, making it a useful and widely used cell division tracker (Lyons et al., 2013).

In our study, the decrease in CFSE fluorescence intensity was not evenly distributed across all long-stored RBC, revealing instead two well-demarcated RBC subpopulations. IFC images showed that RBC with stable and thus higher CFSE fluorescence display marked morphological alterations comprising mostly SME, while RBC with decreased CFSE fluorescence are morphologically normal. This suggests that an enzymatic and/or metabolic process is lost in SME and preserved in morphologically normal erythrocytes. Even though the nature of the enzymatic and/or metabolic process remains to be identified, CFDA-SE reactivity can now be considered a new marker of the storage lesion. The segregation of this defect in the morphologically altered RBC strongly suggests that only a subpopulation of RBC is severely altered during storage, possibly corresponding to the older RBC present in the concentrate at the beginning of storage, as previously suggested by others (Tuo et al., 2014; Mykhailova et al., 2020).

A classic approach to study the accumulation of storage lesions is to compare groups of different storage durations (Paglia et al., 2016). Another possible approach is by using

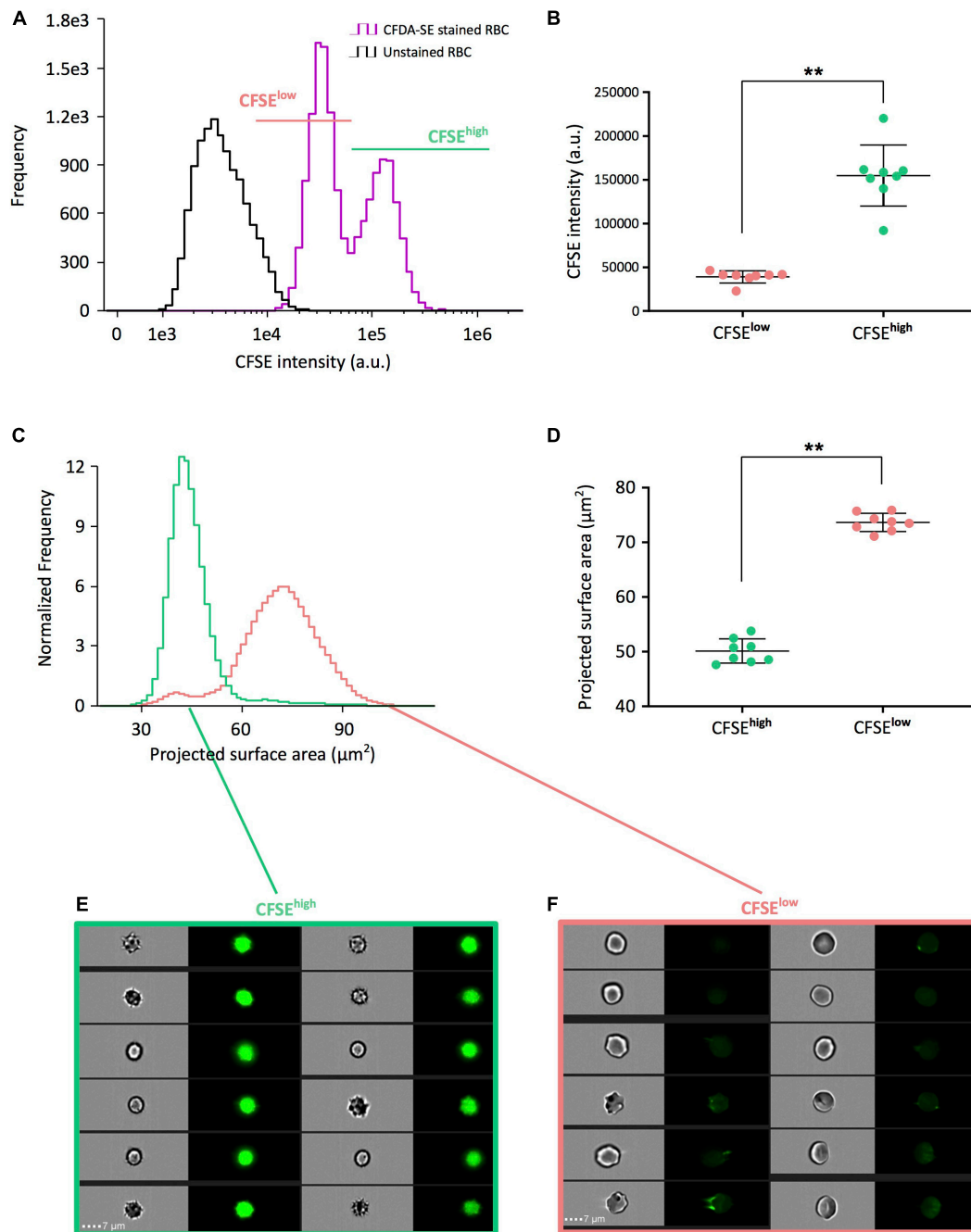


FIGURE 2 | CFSE^{high} RBC correspond to a morphologically altered subpopulation that accumulates during pretransfusion storage. **(A)** Representative CFSE intensity frequency plots of unstained (black line) and CFDA-SE stained (purple line) long-stored RBC allowing to select CFSE^{low} (pink) and CFSE^{high} (light green) subpopulations by the nadir point of the bimodality of frequency plots using imaging flow cytometry (IFC). **(B)** Comparison of the mean CFSE fluorescence intensities of each subpopulation obtained from eight red cell concentrates (RCC) stored 42 days and determined by IFC. **(C)** Representative projected surface area frequency plots of the CFSE^{low} and CFSE^{high} subpopulations previously selected in **(A)**. **(D)** Comparison of the mean projected surface area from the CFSE subpopulations previously selected in **(B)** from the eight long-stored RCC. Representative brightfield and fluorescence images from CFSE^{high} **(E)** showing mostly echinocytes III, spherocytes and spherocytes, and CFSE^{low} subpopulations **(F)** showing discocytes, echinocytes I and echinocytes II. Scale bars represent 7 μm. Results are presented as mean ± SD in **(B,D)** and tests of Wilcoxon for non-parametric and paired data were applied for group comparisons (***p* = 0.0078).

a property that evolves during storage and that allows the implementation of an enrichment strategy. Cell density is known to increase during storage (Diaz et al., 1996) and permits to study

the evolution of cellular properties in each cell fraction along storage (Owusu et al., 2013; Ciana et al., 2017) or even to first separate different subpopulations and to evaluate the evolution of

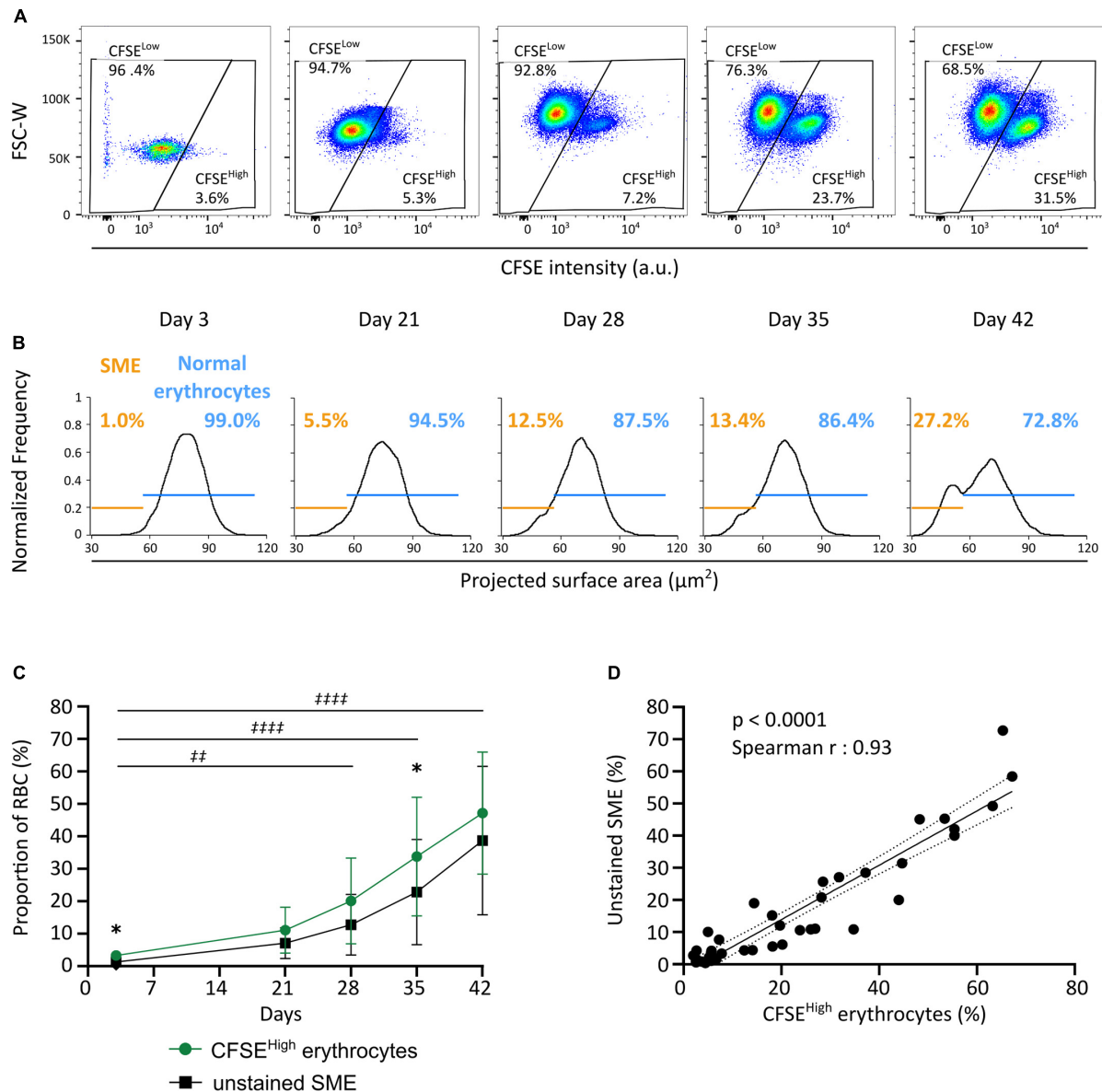


FIGURE 3 | CFDA-SE staining allows the quantification of SME by flow cytometry. **(A)** Representative density plots allowing the quantification of CFSE^{Low} and CFSE^{High} subpopulations along storage by flow cytometry. **(B)** Representative projected surface area frequency plots for unstained RBC allowing quantification of morphologically normal erythrocytes (blue) and SME (orange) along storage using imaging flow cytometry (IFC). **(C)** Evolution of the proportion of CFSE^{High} (green line) and unstained SME subpopulations (black line) during red cell concentrates storage ($n = 8$). **(D)** Correlation between results obtained across storage with either of the two quantification techniques: i.e., CFSE^{High} erythrocytes and SME that accumulate along storage [Spearman $r = 0.93$, $p < 0.0001$; best-fit line is presented (black solid line) with its 95% confidence interval (black dotted lines)]. Results in **(C)** are represented as mean \pm SD (vertical bars) and a two-way ANOVA, with the Geisser–Greenhouse correction followed by a Sidak’s multiple comparison, compared both techniques at each time point ($*p < 0.05$) or the accumulation of CFSE^{High} subpopulation along storage vs. day 3 ($\#p = 0.0011$; $###p < 0.0001$).

storage lesion markers in each fraction (Mykhailova et al., 2020). Microfluidics can also be used to enrich in RBC based on their margination capacity in circulation (Chen et al., 2018).

Imaging flow cytometry and scanning electron microscopy show that the CFDA-SE staining protocol presented here offers the possibility to obtain $>95\%$ pure subpopulations of SME (CFSE^{High}) by flow cytometry-based sorting. Pure subpopulations of SME or morphologically normal erythrocytes would greatly

facilitate the exploration of the intrinsic alterations of RBC inducing their clearance.

In our study, CFSE^{High} erythrocytes were slightly more numerous than SME. This difference may stem from the presence of a few additional altered erythrocytes appearing upon incubation for staining, not detected when experiments are performed on RBC sampled directly from refrigerated blood bag. These erythrocytes, unable to maintain their cellular

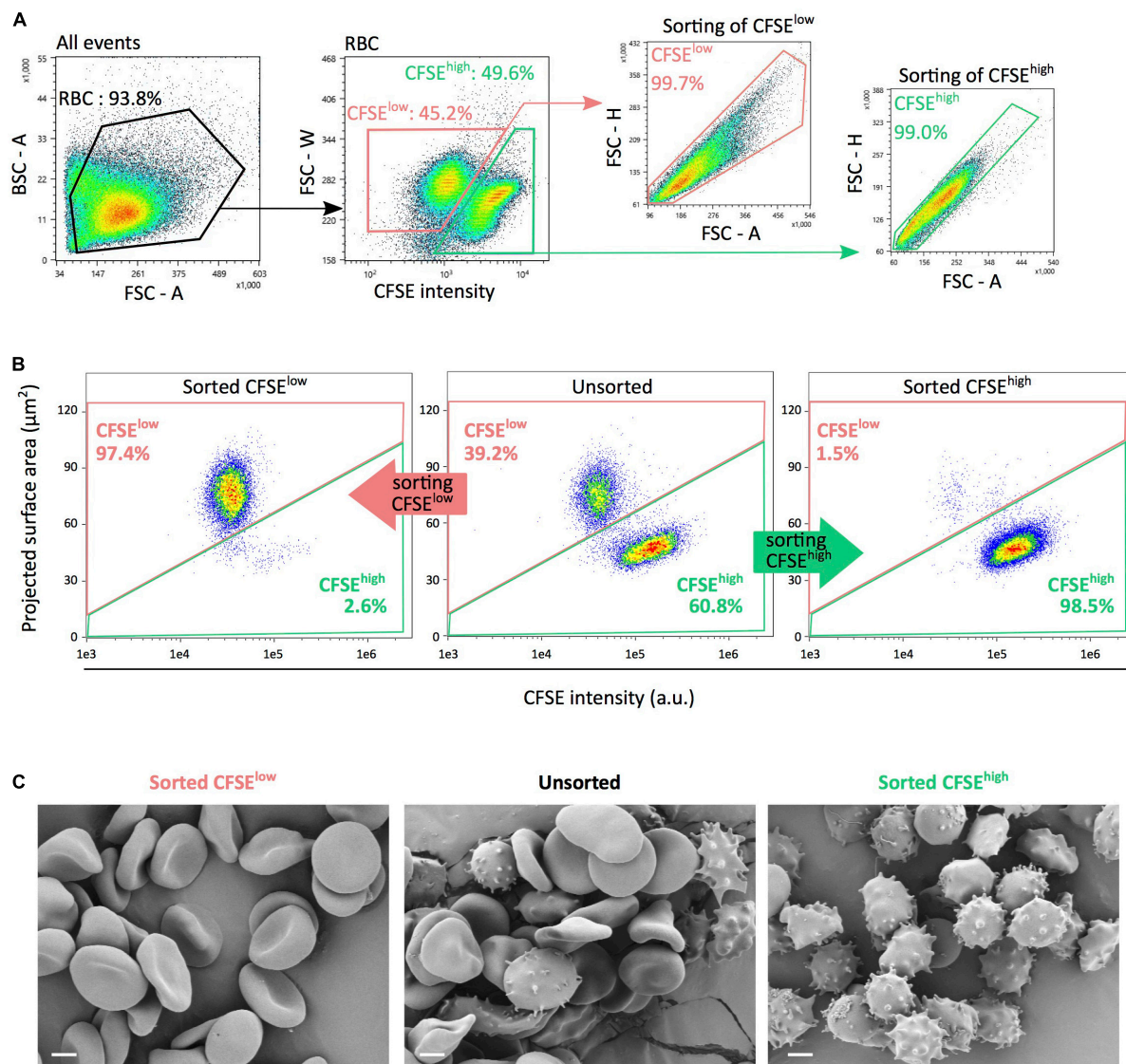


FIGURE 4 | FACS-based sorting generates pure subpopulations of either morphologically normal erythrocytes or SME. **(A)** Flow cytometry sorting gating strategy for sorting, using fluorescence intensity and morphological parameters to select CFSE^{low} (pink) and CFSE^{high} (light green) RBC subpopulations. Morphological criteria comprised the forward scatter (FSC) or back scatter (BSC) signals and their respective parameter of area (A), height (H), and width (W). **(B)** Representative imaging flow cytometry density plots of unsorted (middle panel), sorted CFSE^{low} (left panel), and CFSE^{high} (right panel) subpopulations illustrating each preparation purity. **(C)** Scanning electron microscopy images showing typical morphological patterns (discocytes, echinocytes and spherocytes, or balanced distribution) of RBC in each unsorted or sorted subpopulations. CFSE^{low} and CFSE^{high} subpopulations are presented in pink and light green, respectively. Scale bars represent 2 μm.

homeostasis at 37°C, would become SME and remain highly fluorescent due to their enzymatic and/or metabolic lesions. Indeed, an overnight incubation step at 37°C was shown to expose some RBC lesions induced by hypothermic storage (Burger et al., 2013).

Roussel et al. (2021) recently showed that SME accumulate during storage, reaching a mean proportion of 24% of the entire RBC population at day 42 of storage. The proportion of SME in circulation decreased rapidly when perfusing long-stored red cell concentrates in an *ex vivo* model of human spleen. Similarly, a mouse model showed decreased transfusion

recovery of SME when compared to morphologically normal long-stored RBC. Furthermore, the proportion of SME in red cell concentrates negatively correlated with transfusion recovery in healthy volunteers using ⁵¹Chr-labeling procedure, confirming that SME quantification is a physiologically relevant marker of RBC storage quality, predictive of transfusion recovery.

Even though transfusing short-stored, as compared with standard-issue, red cell concentrates does not reduce mortality (Lelubre and Vincent, 2013; McQuilten et al., 2018, 2020), storage duration is associated with decreased transfusion recovery (Luten et al., 2008; Rapido et al., 2018). Suboptimal transfusion recovery

is expected to increase the number of red blood cell concentrates needed to restore hemoglobin concentration. Along this line, transfusion-induced hemoglobin increments are significantly decreased when red cell concentrates are stored for longer durations (Hunsicker et al., 2018; Roubinian et al., 2019; Rydén et al., 2019) and may be associated with donor genetic factors (Roubinian et al., 2022). Pretransfusion control of SME, and elimination of lower-quality products, would be particularly beneficial to chronically transfused patients with sickle cell disease, thalassemia or myelodysplastic syndromes. Transfusion-related iron overload is indeed a major cause of morbidity and mortality in these patients and the need to provide more transfusions could have significant adverse consequences.

Quantification of SME using IFC is a label-free, operator-independent, quantitative, reproducible and simple method that can be achieved in a short time. Classical microscopy techniques are effective and reliable to quantify the evolution of RBC morphology but often require long experiments and analysis by qualified technicians. Automatic morphology classification approaches by machine-learning is an active field of research that can be used, for example, to analyze images acquired with a confocal microscope or IFC (Doan et al., 2020; Simionato et al., 2021). The use of IFC and/or artificial-intelligence driven analysis promises a rapid evolution of accurate and fast methods of morphological characterization in the research field. They, however, necessitate specialized equipment, which are not yet present in a majority of clinical hematology laboratories.

Quantification of CFSE^{high} RBC is also operator-independent and reproducible. It does not directly provide information regarding RBC morphology, but accumulation of CFSE^{high} erythrocytes was strongly correlated to the proportion of SME detected using IFC. Quantification of CFSE^{high} RBC only requires a standard flow cytometer: a technology available in both clinical and research laboratories. The staining protocol is fairly simple and therefore has the potential to be adapted and standardized for use in the quality control of red cell concentrates.

Carboxyfluorescein Diacetate Succinimidyl Ester staining reactivity is a new marker of storage lesion that allows quantification and sorting of morphologically altered stored RBC. Future research using this method will explore the SME cellular properties and should help better understand the storage lesion and RBC senescence.

DATA AVAILABILITY STATEMENT

The raw data supporting the conclusions of this article will be made available by the authors, without undue reservation.

ETHICS STATEMENT

Ethical review and approval was not required for the study on human participants in accordance with the local legislation and institutional requirements. Written informed consent for

participation was not required for this study in accordance with the national legislation and the institutional requirements.

AUTHOR CONTRIBUTIONS

MM, SP, YH, SG, and MD performed the experiments. MM, SP, YH, SG, MD, CR, OH, PR, PB, and PA analyzed the data. MM, CR, OH, PB, and PA designed the research. MM, SP, and PA wrote the manuscript. PB edited the manuscript. All authors read and approved the manuscript.

FUNDING

This work was supported by State funding from the Agence Nationale de la Recherche under “Investissements d’Avenir” program (ANR-10-IAHU-01, ANR-11-LABX-0051, and ANR-18-IDEX-0001), Association Recherche et Transfusion grant 181, and National Heart, Lung and Blood Institute grant R01HL148151.

ACKNOWLEDGMENTS

We thank EFS Hauts-de-France-Normandie and EFS Ile-de-France for providing RBC concentrates.

SUPPLEMENTARY MATERIAL

The Supplementary Material for this article can be found online at: <https://www.frontiersin.org/articles/10.3389/fphys.2022.838138/full#supplementary-material>

Supplementary Figure 1 | SME that accumulate during pretransfusion storage are intensely fluorescent. **(A)** Representative projected surface area frequency plot, obtained by imaging flow cytometry (IFC), of unstained (black line) and CFDA-SE stained (purple line) long-stored RBC. The bimodal distribution shows the segregation into subpopulations of either SME (orange) or normal erythrocytes (blue) subpopulations by the nadir point of the bimodal distribution. **(B)** Comparison of the mean projected surface area of SME and normal erythrocytes subpopulation determined as in **(A)**, from eight red cell concentrates (RCC) stored 42 days. **(C)** Representative CFSE intensity frequency plots of unstained (black line) and the SME (orange line) and normal erythrocytes (blue line) subpopulations previously selected in **(A)**. **(D)** Comparison of the mean CFSE fluorescence intensities of each SME and normal erythrocytes subpopulations determined as in **(C)** obtained from eight RCC stored 42 days. Results are presented as mean \pm SD in **(B,D)** and tests of Wilcoxon for non-parametric and paired data were applied to compare groups between each other ($*p = 0.0078$).

Supplementary Figure 2 | Gating strategies to quantify morphologically altered CFSE^{high} and morphologically normal CFSE^{low} subpopulations of stored RBC. **(A)** Representative imaging flow cytometry (IFC) dot plot of projected surface area and fluorescence intensity of CFDA-stained RBC after 42 days of storage. Selection using only CFSE fluorescence intensity (vertical dotted black line) shows that **(B)** CFSE^{low} subpopulation contains some SME and that **(C)** CFSE^{high} subpopulation contains morphologically normal erythrocytes. **(D)** Selection on morphological (projected surface area by IFC) and fluorescence (CFSE intensity) criteria (oblique dotted black line) improves the gating specificity.

REFERENCES

- Antonelou, M. H., Tzounakas, V. L., Velentzas, A. D., Stamoulis, K. E., Kriebardis, A. G., and Papassideri, I. S. (2012). Effects of pre-storage leukoreduction on stored red blood cells signaling: a time-course evaluation from shape to proteome. *J. Proteom.* 76, 220–238. doi: 10.1016/j.jprot.2012.06.032
- Banks, H. T., Choi, A., Huffman, T., Nardini, J., Poag, L., and Thompson, W. C. (2013). Quantifying CFSE label decay in flow cytometry data. *Appl. Math. Lett.* 26, 571–577. doi: 10.1016/j.aml.2012.12.010
- Bardyn, M., Rappaz, B., Jaferzadeh, K., Crettaz, D., Tissot, J.-D., Moon, I., et al. (2017). Red blood cells ageing markers: a multi-parametric analysis. *Blood Transfus.* 15, 239–248. doi: 10.2450/2017.0318-16
- Berezina, T. L., Zaets, S. B., Morgan, C., Spillert, C. R., Kamiyama, M., Spolarics, Z., et al. (2002). Influence of storage on red blood cell rheological properties. *J. Surg. Res.* 102, 6–12. doi: 10.1006/jsre.2001.6306
- Bessis, M. (1972). Red cell shapes. an illustrated classification and its rationale. *Nouv. Rev. Fr. Hematol.* 12, 721–745.
- Bessis, M. (1974). *Corpuscles*. Berlin: Springer, doi: 10.1007/978-3-642-65657-6
- Blasi, B., D'Alessandro, A., Ramundo, N., and Zolla, L. (2012). Red blood cell storage and cell morphology. *Transfus. Med.* 22, 90–96. doi: 10.1111/j.1365-3148.2012.01139.x
- Bordbar, A., Johansson, P. I., Paglia, G., Harrison, S. J., Wichuk, K., Magnusdottir, M., et al. (2016). Identified metabolic signature for assessing red blood cell unit quality is associated with endothelial damage markers and clinical outcomes. *Transfusion* 56, 852–862. doi: 10.1111/trf.13460
- Burger, P., Kostova, E., Bloem, E., HilariusStokman, P., Meijer, A. B., and Berg, T. K. (2013). Potassium leakage primes stored erythrocytes for phosphatidylserine exposure and shedding of pro-coagulant vesicles. *Br. J. Haematol.* 160, 377–386. doi: 10.1111/bjh.12133
- Chen, Y., Feng, Y., Wan, J., and Chen, H. (2018). Enhanced separation of Aged RBCs by designing channel cross section. *Biomicrofluidics* 12:024106. doi: 10.1063/1.5024598
- Ciana, A., Achilli, C., and Minetti, G. (2017). Spectrin and other membrane-skeletal components in human red blood cells of different age. *Cell Physiol. Biochem.* 42, 1139–1152. doi: 10.1159/000478769
- D'Alessandro, A., D'Amici, G. M., Vaglio, S., and Zolla, L. (2012). Time-course investigation of sagem-stored leukocyte-filtered red blood cell concentrates: from metabolism to proteomics. *Haematologica* 97, 107–115. doi: 10.3324/haematol.2011.051789
- D'Alessandro, A., Kriebardis, A. G., Rinalducci, S., Antonelou, M. H., Hansen, K. C., Papassideri, I. S., et al. (2015). An update on red blood cell storage lesions, as gleaned through biochemistry and omics technologies. *Transfusion* 55, 205–219. doi: 10.1111/trf.12804
- Diaz, C., Morkowski, J., and Schroit, A. J. (1996). Generation of phenotypically aged phosphatidylserine-expressing erythrocytes by dilauroylphosphatidylcholine-induced vesiculation. *Blood* 87, 2956–2961.
- Doan, M., Sebastian, J. A., Caicedo, J. C., Siegert, S., Roch, A., Turner, T. R., et al. (2020). Objective assessment of stored blood quality by deep learning. *Proc. Natl. Acad. Sci. USA* 117, 21381–21390. doi: 10.1073/pnas.2001227117
- Högman, C. F., Verdier, C.-H. D., Ericson, A., Hedlund, K., and Sandhagen, B. (1985). Studies on the mechanism of human red cell loss of viability during Storage at +4°C in Vitro. *Vox. Sanguin.* 48, 257–268. doi: 10.1111/j.1423-0410.1985.tb00181.x
- Hunsicker, O., Hessler, K., Krannich, A., Boemke, W., Braicu, I., Sehouli, J., et al. (2018). Duration of storage influences the hemoglobin rising effect of red blood cells in patients undergoing major abdominal surgery. *Transfusion* 58, 1870–1880. doi: 10.1111/trf.14627
- Lelubre, C., and Vincent, J.-L. (2013). Relationship between red cell storage duration and outcomes in adults receiving red cell transfusions: a systematic review. *Crit. Care* 17:R66. doi: 10.1186/cc12600
- Lu, M., and Shevchoplyas, S. S. (2020). Dynamics of shape recovery by stored red blood cells during washing at the single cell level. *Transfusion* 60, 2370–2378. doi: 10.1111/trf.15979
- Luten, M., Roerdinkholder-Stoelwinder, B., Schaap, N. P. M., de Grip, W. J., Bos, H. J., and Bosman, G. J. G. M. (2008). Survival of red blood cells after transfusion: a comparison between red cells concentrates of different storage periods. *Transfusion* 48, 1478–1485. doi: 10.1111/j.1537-2995.2008.01734.x
- Lyons, A. B., Blake, S. J., and Doherty, K. V. (2013). Flow cytometric analysis of cell division by dilution of CFSE and Related Dyes. *Curr. Protoc. Cytom.* 9:64. doi: 10.1002/0471142956.cy0911s64
- McQuilten, Z. K., French, C. J., Nichol, A., Higgins, A., and Cooper, D. J. (2018). Effect of age of red cells for transfusion on patient outcomes: a systematic review and meta-analysis. *Transfus. Med. Rev.* 32, 77–88. doi: 10.1016/j.tmr.2018.02.002
- McQuilten, Z. K., French, C. J., Nichol, A., Higgins, A., and Cooper, D. J. (2020). Corrigendum to “effect of age of red cells for transfusion on patient outcomes: a systematic review and meta-analysis”. *Transfus. Med. Rev.* 34, 138–139. doi: 10.1016/j.tmr.2020.03.002
- Mykhailova, O., Olafson, C., Turner, T. R., D'Alessandro, A., and Acker, J. P. (2020). Donor-dependent aging of young and old red blood cell subpopulations: metabolic and functional heterogeneity. *Transfusion* 60, 2633–2646. doi: 10.1111/trf.16017
- Owusu, B. Y., Stapley, R., Honavar, J., and Patel, R. P. (2013). Effects of erythrocyte aging on nitric oxide and nitrite metabolism. *Antioxid. Redox. Signal* 19, 1198–1208. doi: 10.1089/ars.2012.4884
- Paglia, G., D'Alessandro, A., Rolfsson, O., Sigurjonsson, O. E., Bordbar, A., Palsson, S., et al. (2016). Biomarkers defining the metabolic age of red blood cells during cold storage. *Blood* 128, e43–e50. doi: 10.1182/blood-2016-06-721688
- Rapido, F., Brittenham, G. M., Bandyopadhyay, S., LaCarpia, F., McMahon, D. J., Rebbaa, A., et al. (2018). Prolonged red cell storage before transfusion increases extravascular hemolysis. *J. Clin. Invest.* 127, 375–382. doi: 10.1172/JCI90837
- Reinhart, W. H., Piety, N. Z., Deuel, J. W., Makhro, A., Schulzki, T., Bogdanov, N., et al. (2015). Washing stored red blood cells in an albumin solution improves their morphologic and hemorheologic properties. *Transfusion* 55, 1872–1881. doi: 10.1111/trf.13052
- Reisz, J. A., Wither, M. J., Dzieciatkowska, M., Nemkov, T., Issaian, A., Yoshida, T., et al. (2016). Oxidative modifications of glyceraldehyde 3-phosphate dehydrogenase regulate metabolic reprogramming of stored red blood cells. *Blood* 128, e32–e42. doi: 10.1182/blood-2016-05-714816
- Roubinian, N. H., Plimier, C., Woo, J. P., Lee, C., Bruhn, R., Liu, V. X., et al. (2019). Effect of donor, component, and recipient characteristics on hemoglobin increments following red blood cell transfusion. *Blood* 134, 1003–1013. doi: 10.1182/blood.2019000773
- Roubinian, N. H., Reese, S. E., Qiao, H., Plimier, C., Fang, F., Page, G. P., et al. (2022). Donor genetic and nongenetic factors affecting red blood cell transfusion effectiveness. *JCI Insight* 7:152598. doi: 10.1172/jci.insight.152598
- Roussel, C., Dussiot, M., Marin, M., Morel, A., Ndour, P. A., Duez, J., et al. (2017). Spherocytic shift of red blood cells during storage provides a quantitative whole cell-based marker of the storage lesion. *Transfusion* 57, 1007–1018. doi: 10.1111/trf.14015
- Roussel, C., Morel, A., Dussiot, M., Marin, M., Colard, M., Fricot-Monsinjon, A., et al. (2021). Rapid clearance of storage-induced microerythrocytes alters transfusion recovery. *Blood* 137, 2285–2298. doi: 10.1182/blood.202008563
- Rydén, J., Clements, M., Hellstrom-Lindberg, E., Hoglund, P., and Edgren, G. A. (2019). Longer duration of red blood cell storage is associated with a lower hemoglobin increase after blood transfusion: a cohort study. *Transfusion* 59, 1945–1952. doi: 10.1111/trf.15215

- Simionato, G., Hinkelmann, K., Chachanidze, R., Bianchi, P., Fermo, E., van Wijk, R., et al. (2021). Red blood cell phenotyping from 3d confocal images using artificial neural networks. *PLoS Comput. Biol.* 17:e1008934. doi: 10.1371/journal.pcbi.1008934
- Tchir, J. D. R., Acker, J. P., and Holovati, J. L. (2013). Rejuvenation of ATP during storage does not reverse effects of the hypothermic storage lesion. *Transfusion* 53, 3184–3191. doi: 10.1111/trf.12194
- Tuo, W.-W., Wang, D., Liang, W.-J., and Huang, Y.-X. (2014). How cell number and cellular properties of blood-banked red blood cells of different cell ages decline during storage. *PLoS One* 9:e105692. doi: 10.1371/journal.pone.0105692
- Yoshida, T., Prudent, M., and D'Alessandro, A. (2019). Red blood cell storage lesion: causes and potential clinical consequences. *Blood Transfus.* 17, 27–52. doi: 10.2450/2019.0217-18
- Zehnder, L., Schulzki, T., Goede, J. S., Hayes, J., and Reinhart, W. H. (2008). Erythrocyte Storage in Hypertonic (SAGM) or Isotonic (PAGGSM) conservation medium: influence on cell properties. *Vox. Sang.* 95, 280–287. doi: 10.1111/j.1423-0410.2008.01097.x
- Conflict of Interest:** PA is funded in part by New Health Science. MM, SP, MD, CR, PB, and PA declare that the European patent application EP21306765 was filed on December 12th, 2021.
- The remaining authors declare that the research was conducted in the absence of any commercial or financial relationships that could be construed as a potential conflict of interest.
- Publisher's Note:** All claims expressed in this article are solely those of the authors and do not necessarily represent those of their affiliated organizations, or those of the publisher, the editors and the reviewers. Any product that may be evaluated in this article, or claim that may be made by its manufacturer, is not guaranteed or endorsed by the publisher.
- Copyright © 2022 Marin, Peltier, Hadjou, Georgeault, Dussiot, Roussel, Hermine, Roingeard, Buffet and Amireault. This is an open-access article distributed under the terms of the Creative Commons Attribution License (CC BY). The use, distribution or reproduction in other forums is permitted, provided the original author(s) and the copyright owner(s) are credited and that the original publication in this journal is cited, in accordance with accepted academic practice. No use, distribution or reproduction is permitted which does not comply with these terms.



Reticulocyte Maturation and Variant Red Blood Cells

Christian J. Stevens-Hernandez^{1,2,3}, Joanna F. Flatt^{1,2}, Sabine Kupzig¹ and Lesley J. Bruce^{1,2,3*}

¹ Bristol Institute for Transfusion Sciences, NHS Blood and Transplant, Bristol, United Kingdom, ² School of Biochemistry, University of Bristol, Bristol, United Kingdom, ³ Component Development Laboratory, NHS Blood and Transplant, Long Road, Cambridge Biomedical Campus, Cambridge, United Kingdom

The bone marrow produces billions of reticulocytes daily. These reticulocytes mature into red blood cells by reducing their plasma membrane by 20% and ejecting or degrading residual internal organelles, membranes and proteins not required by the mature cell. This process occurs by autophagy, protein degradation and vesiculation but is not well understood. We previously reported that Southeast Asian Ovalocytic RBCs demonstrate incomplete reticulocyte maturation and we have now extended this study to a number of other variant RBCs. By comparing the profile of a pure reticulocyte preparation of cultured red cells with these variant cells, we show that the largest of these cells, the overhydrated hereditary stomatocytosis cells, are the least mature, they barely reduced their plasma membrane and contain large amounts of proteins that should have been reduced or removed. Intermediate sized variant RBCs appear to be more mature but retain some endoplasmic reticulum and residual membrane proteins. We propose that the size and composition of these variant cell types correlate with the different stages of reticulocyte maturation and provide insight into the reticulocyte maturation process.

Keywords: reticulocyte maturation, stomatocytosis, OHSt, hereditary spherocytosis, Southeast Asian ovalocytosis, cryohydrocytosis, stomatin, erythropoiesis

OPEN ACCESS

Edited by:

Giampaolo Minetti,
University of Pavia, Italy

Reviewed by:

Benoit Malleret,
National University of Singapore,
Singapore
Alessandro Matte',
University of Verona, Italy

*Correspondence:

Lesley J. Bruce
Lesley.bruce@nhsbt.nhs.uk

Specialty section:

This article was submitted to
Red Blood Cell Physiology,
a section of the journal
Frontiers in Physiology

Received: 13 December 2021

Accepted: 15 February 2022

Published: 07 March 2022

Citation:

Stevens-Hernandez CJ, Flatt JF,
Kupzig S and Bruce LJ (2022)
Reticulocyte Maturation and Variant
Red Blood Cells.
Front. Physiol. 13:834463.
doi: 10.3389/fphys.2022.834463

INTRODUCTION

On average, 200 billion reticulocytes are produced every day in the bone marrow of healthy individuals. These immature red blood cells (RBCs) must go through a process of maturation to form mature RBCs. Immediately post-enucleation reticulocytes are large (120–140 fL) and multi-lobular. This stage is known as an R1 reticulocyte as classified by Mel et al., 1977. R1 reticulocytes are motile and are found in the bone marrow; they still contain substantial amounts of RNA giving the cell a reticulo-filamentous appearance and its name. R1 reticulocytes also contain residual mitochondria, ribosomes, endoplasmic reticulum (ER) and other internal membranes that are not required by the mature RBC. They have excess plasma membrane, which must be reduced by 20%, plus numerous superfluous proteins, e.g., the transferrin receptor (TfR) and various integrins, to be removed from the mature RBC (Koury et al., 1989; Wickrema et al., 1994; Liu et al., 2010). This initial stage of maturation occurs by membrane rearrangement via autophagic, proteolytic, and vesicle-based mechanisms (Minetti et al., 2020) and results in the R2 reticulocytes that are released into the circulation where they mature further.

Studies have shown that during maturation the level of RNA, as measured by thiazole orange (TO), and TfR in the reticulocyte reduces and these levels are often used to define the different stages of maturation from R1 (nascent reticulocyte, high CD71, high RNA) to R2 (intermediate reticulocyte, low CD71, low RNA) to R3 (mature RBC, CD71 negative, RNA negative)

(Malleret et al., 2013). Recently, another method for classifying different stages of reticulocyte maturation has been described that uses changes in mitochondrial membrane potential (Du et al., 2020). Despite all these classifications, exactly how the nascent reticulocyte matures into a RBC is not fully understood. However, one fact is clear, as the nascent reticulocyte matures it becomes smaller. This is due to the loss of plasma membrane and volume via vesicle release.

The nascent reticulocyte begins life at 120–140 fL, then loses membrane forming an R2 reticulocyte of about 100–120 fL, further membrane is lost to form a mature RBC of about 86–98 fL. This final maturation stage is probably the least understood and must involve the membrane and cytoskeleton “clicking” into their final arrangement, forming a perfect deformable biconcave disk. Interestingly, there are a number of variant RBCs that have mean cell volumes (MCV) of similar sizes to R1 and R2 reticulocytes. These variants cause conditions that affect RBC cation permeability. Overhydrated hereditary stomatocytic (OHSt) RBCs have the most severe cation leak of the HSt group (40x normal) and a MCV of 120–140 fL (Gallagher et al., 2003; Bruce et al., 2009). OHSt is caused by variants of *RHAG*, the gene encoding the Rh-associated glycoprotein (RhAG). OHSt RBCs also lack stomatin, although no gene defect was found in *STOM* to account for this loss (Fricke et al., 2003). Southeast Asian Ovalocytosis (SAO), cryohydrocytosis (CHC) and stomatin-deficient CHC (sdCHC) have an intermediate cation leak (4–10x normal) and MCVs between 100–120 fL. SAO and CHC are caused by variants of *SLC4A1*, the gene encoding band 3 [anion exchanger 1 (AE1)], and have a cation leak of about four times normal (Tanner et al., 1991; Bruce et al., 1999, 2005; Guizouarn et al., 2011). sdCHC is caused by variants of *SLC2A1*, the gene encoding glucose transporter 1 (GLUT1), and these RBCs have a cation leak about ten times normal (Flatt et al., 2011; Bawazir et al., 2012). sdCHC RBCs also lack stomatin although again there is no associated gene defect in *STOM*. We reported previously that SAO RBCs appeared to have a defect in reticulocyte maturation (Flatt et al., 2020). Consequently, we decided to investigate the degree of defective reticulocyte maturation in all of these variant RBCs to determine whether this correlated with their MCV and potentially with the MCV of the different stages of reticulocyte maturation.

MATERIALS AND METHODS

Patient Samples

Control RBC, with no known RBC defects, were isolated from United Kingdom blood donor samples. Variant RBC samples were from an OHSt patient (heterozygous Phe65Ser variant in *RHAG*; rs863225468) first reported by Lock et al., 1961, then again as patient Stockport-A-II-1 (Bruce et al., 2009); a hereditary spherocytosis (HS) patient (heterozygous g > t mutation in the donor splice site of intron 12 of *SLC4A1*; unpublished, see **Supplementary Case** study); an HS patient with incomplete distal renal tubular acidosis (dRTA) (homozygous Ser667Phe variant in *SLC4A1*), previously reported (Toye et al., 2008); a CHC patient (heterozygous Ser731Pro variant in *SLC4A1*;

rs863225461), previously reported as patient CHC2 (Bruce et al., 2005); an sdCHC patient (heterozygous Gly286Asp variant in *SLC2A1*; rs864309514) first reported (Fricke et al., 2004 patient D-II-2, later in Flatt et al., 2011); an SAO sample (heterozygous deletion Ala400–Ala408 in *SLC4A1*; rs769664228) mother of the homozygous SAO child reported (Picard et al., 2014, later in Flatt et al., 2020). Cultured RBCs (cRBCs) were grown *in vitro* from CD34⁺ cells isolated from peripheral blood of United Kingdom blood donors.

All blood samples were collected with informed consent, obtained in accordance with the Declaration of Helsinki. This study is part of a larger study approved by the National Health Service National Research Ethics Service South West entitled “*In Vitro* Studies of Erythropoiesis in Health and Disease.”

Culture of CD34⁺ Cells

CD34⁺ cells were isolated from cones, a by-product of platelet apheresis, and cultured as described (Griffiths et al., 2012a). Typically, a culture begins with $\sim 2 \times 10^6$ CD34⁺ cells and expands to $\sim 5.25 \times 10^9$ cells (erythroblasts & reticulocytes) in a 3 liter culture (final volume). Briefly, cells were cultured in IMDM supplemented with 3% (v/v) AB serum (Merck), 2 mg/ml HSA (Irvine Scientific), 10 μ g/ml insulin (Merck), 3 U/ml Erythropoietin (Roche), 500 μ g/ml holotransferrin (R&D Systems), 10 ng/ml SCF (Medsafe), 1 ng/ml IL3 (R&D Systems), 3 IU/ml heparin (Merck) from day 0–10, from day 11–13 as above but without IL-3, then from day 14 onward as for days 11–13 but without SCF. Cultures were kept in vented flasks followed by spinner flasks at 37°C, 5% CO₂.

Filtration of Cultured Cells

Cell cultures were filtered, to remove residual nucleated cells and pyrenocytes, using a standard leucofilter (LXT; Macopharma) around day 21, once the enucleated cells were at > 60%. The pure cRBC preparation was resuspended in saline, adenine, glucose and mannitol solution (SAG-M; Macopharma) or SAG-M + 10% human serum albumin (HSA) and stored for 10 days at 4°C.

Scanning Electron Microscopy

Cells were prepared for scanning electron microscopy as described in Griffiths et al., 2012a. For further details, see **Supplementary Methods**.

Erythrocyte Membrane Protein Analysis

RBC ghost membrane preparations were prepared according to the hemolysis method (Dodge et al., 1963), with some modifications (see **Supplementary Methods**). SDS-PAGE (reducing conditions) and Western blotting analysis were performed as described (Bruce et al., 2003). Blots were analyzed using semi-quantitative scanning densitometry with the Kodak Gel100 system software or LI-COR Image Studio software. Densitometry analysis was carried out using Image J (v1.50i) (**Supplementary Table 1**).

Antibodies Used for Immunoblotting

Antibodies were used against the following proteins. The voltage dependent anion channel 1 (VDAC1; Abcam, ab15895) and

stomatin like protein 2 (SLP2; in-house rabbit polyclonal) were used as markers of residual mitochondrial membranes, calreticulin (Abcam, ab2908) as an endoplasmic reticulum marker, lysosomal associated membrane protein 2 (LAMP-2; Abcam ab25631) as a lysosomal membrane marker and transferrin receptor (TfR; Abcam, ab84036) and CD147 (Abcam, ab108308) as markers of proteins that are significantly reduced during reticulocyte maturation (Gronowicz et al., 1984; Griffiths et al., 2012a; Malleret et al., 2013; Flatt et al., 2020). β -spectrin (BRAC65; IBGRL, Bristol, United Kingdom) was used as a loading control. It was not possible to use β -actin, a common loading control, as β -actin has a similar molecular weight to some of the test proteins. The level of stomatin (STOM, in-house rabbit polyclonal IDML) was assessed because some of the variant RBCs are known to have reduced levels of stomatin (Bruce et al., 2009; Flatt et al., 2011).

Reprobing Immunoblots

Immunoblots were probed and reprobed in sequence. It was possible to probe for all the proteins of interest, given their different apparent molecular weights, using a limited number of blots. One blot was probed first with anti-VDAC1 (35kDa, 37 kDa) then anti-SLP2 (44 kDa). Another blot was probed first with anti-LAMP2 (~80 kDa) then anti-calreticulin (55 kDa) then anti-STOM (31 kDa). A further blot was probed first with anti-CD147 (30 kDa) (non-glycosylated) and 42-65 kDa (glycosylated) then anti-TfR [98 kDa (monomer), 200 kDa (dimer)]. Between each probing the blot was wetted with methanol, washed with phosphate-buffered saline (PBS; 137mM NaCl, 10mM Phosphate, 2.7mM KCl pH 7.4) Tween solution [PBS-0.2%Tween 20 (Merck)], then re-blocked in 5% milk, PBS-Tween solution and probed. All blots were reprobed with anti- β -spectrin (220 kDa) as a loading control.

RESULTS

Production of Normal Human Reticulocytes

The culture conditions used in our laboratory differentiate the CD34⁺ cells, in a fairly synchronized manner, through to reticulocytes. Using standard blood donor (non-variant) cells we usually achieve 70-80% enucleation and, post-filtration, produce a pure population of cRBCs. Scanning electron micrograph images of the different stages of cell development in culture, from pre-enucleation through to the mature RBC, are shown in **Figure 1**. Pure cRBCs are a mixture of R1 (**Figure 1iii**) and R2 (**Figure 1iv**) reticulocytes plus a small number of more mature cells (**Figure 1v**) resembling fully mature erythrocytes (**Figure 1vi**).

Comparative Mean Cell Volume of Reticulocytes Versus Variant RBCs

The phenotype and properties of the variant RBCs used in this study are shown in **Table 1**. The mean cell volume (MCV) of standard donor RBCs ranges from 86-98fL whereas reticulocytes

have a much larger MCV, ranging from 120-140fL. This reflects the fact that reticulocytes must lose about 20% of their membrane area during the maturation process. RBC variant cells were selected with MCVs intermediate between these two (**Table 1**). The MCV for the heterozygous SAO sample was in fact lower than the standard range (78fL). MCVs for SAO RBCs in the literature vary enormously and this is because very often SAO is reported in conjunction with other conditions, e.g., thalassemia, where the MCV is low (Yamsri et al., 2021) or distal renal tubular acidosis where the MCV is high (Gunaratne et al., 2020). However, it is clear from heterozygous SAO RBC films that the double stoma, macro-ovalocytes are large (100-120fL; Garnett and Bain, 2013).

Immunoblotting Analysis of Cultured Red Blood Cell Membrane Proteins

Cell membranes were isolated from standard donor RBCs and from cRBCs by hypotonic lysis, the proteins separated by SDS-PAGE and analyzed by immunoblotting. As expected, immunoblotting analysis of the cRBC membrane proteins showed large amounts of the proteins associated with mitochondria (VDAC1 & SLP2), with ER (calreticulin) and with lysosomes (LAMP2) compared to vanishingly small amounts of these proteins in the mature donor RBC membranes (**Figure 2**). Membrane proteins that are usually reduced during reticulocyte maturation (TfR & CD147) were also present in large amounts in the cRBC membranes compared to the donor RBC membranes (**Figure 2**). The unglycosylated form of CD147 was much increased in the cRBC membranes as was a 200 kDa band in the TfR immunoblot, presumed to be the TfR dimer (**Figure 2**). Proteins that are known to be present in both reticulocyte and donor RBC membranes (stomatin & β -spectrin) were found to be present in equal amounts in the membranes from both cell types (**Figure 2**).

Immunoblotting Analysis of Variant Red Blood Cell Membrane Proteins

Immunoblotting analysis of variant RBC membranes displayed varying levels of the above mentioned proteins, more commonly associated with reticulocytes, suggesting that the variant RBCs may undergo incomplete reticulocyte maturation to different degrees.

Overhydrated Hereditary Stomatocytosis Red Blood Cells

Immunoblotting of OHSt RBC membranes gave a profile more similar to that of the cRBC membranes than mature RBC membranes (**Figures 2A,B**). The OHSt membranes contained VDAC1, SLP2, calreticulin and LAMP2, at about 12-94% the level found in cRBC membranes (**Supplementary Table 1**) showing that the OHSt RBCs have incomplete clearance of mitochondrial, ER and lysosomes. There was also incomplete clearance of the proteins that are usually reduced during reticulocyte maturation, CD147 and TfR (note that the TfR OHSt blot in **Figure 2A** is a 1:10 dilution); and the unglycosylated form of CD147 and dimeric form of TfR were both increased (**Figures 2A,B**).

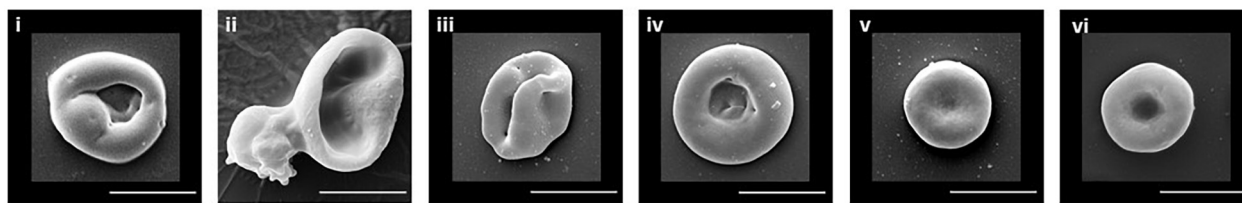


FIGURE 1 | SEM of erythroid cells. Illustrative examples of the typical cell morphology of the different stages of erythrocyte maturation are shown. **(i)** Orthochromatic reticulocyte. **(ii)** Enuclating reticulocyte. **(iii)** R1 reticulocyte. **(iv)** R2 reticulocyte. **(v)** Mature reticulocyte/RBC. **(vi)** Donor RBC. Scale bar 5 μ m.

TABLE 1 | RBC properties.

Cell type (sex)	RBC ($\times 10^{12}/L$)	Hb (g/dL)	MCV fL	MCHC (g/dL)	Retic%	Other complications	References
RBC (normal range)	4.5-5.5 (M) 3.8-4.8 (F)	12.5-18.0 (M) 11.5-15.8 (F)	86-98	30.8-35.3 (adults)	0.5 -1.5 (adults)	N/A	N/A
cRBC	N/A	5.4-6.3	120-140	23.3-37.4	100	N/A	Present study
OHSt (M)	Not reported	9.0-11.0	136.5-139.0	25.3, 27.0	10-20	Compensated hemolytic anemia, stomatocytes, loss of stomatin	Fricke et al., 2003; Bruce et al., 2009
sdCHC (M)	Not reported	12.7	121.3	31.4	1.4	Neurological disorder and cataracts, hemolytic anemia, loss of stomatin	Fricke et al., 2004
CHC (M)	Not reported	15.0	91.2, 87.7	37.3, 38.3	8-09, 8-99	Mild hemolytic anemia, stomatocytes, gall stones, jaundice.	Coles et al., 1999. (B-III-2)
SAO (F)	5.95 [#]	13.9 [#]	78 [#]	30.2 [#]	1.6 [#]	Heterozygous 3.7 kb α -thalassemia trait; sickle cell trait (HBB c.20 C > T)	FBC (Picard, unpublished [†]); Picard et al., 2014
HS-het (F)	4.07*	12.2*	90.7*	33*	Not available*	Heterozygous <i>SLC4A1</i> variant g > t at c.1431 + 1 affecting the splice donor site of intron 12 and causing HS	Present study (see supplemental data)
HS-hom. (M)	0.94	3.8	100.6	35.9	17.2	Homozygous <i>SLC4A1</i> variant (Ser667Phe) causing both HS and dRTA.	Toye et al., 2008

Full blood counts (FBC) were measured for the cRBC preparations using an automated hematology analyzer (Horiba, United Kingdom). FBC was measured for HS-het patient using hematology analyzer (Sysmex, United Kingdom).

[#]The FBC for the SAO was measured in 2011. The MCV for this individual is below the normal range probably due to co-inheritance of the heterozygous 3.7 kb α -thalassemia trait and sickle cell trait (HBB c.20 C > T) (Picard et al., 2014). Indeed, the MCV of heterozygous SAO RBCs often falls within or below the normal range probably due to conditions inherited with SAO. However, SAO RBCs consist of two populations of RBCs, a population of normal sized cells and a population of macro-ovalocytes (100-120 fL; Garnett and Bain, 2013). Note, the SAO reticulocyte count is also normal. SAO individuals rarely have reticulocytosis, unless it is associated with other secondary conditions. However neonatal anemia is associated with SAO (Laosombat et al., 2005).

*The FBC for the HS-het was measured in 2011 post-splenectomy. The reticulocyte count is no longer available but the patient was referred to the Hematology Department with anemia.

[†]Picard, V., (2022) Personal communication of FBC.

OHSt RBC membranes contained normal levels of spectrin but very low levels of stomatin as expected (Figures 2A,B). The same high level of these proteins (VDAC1, SLP2, calreticulin, LAMP2, CD147 & TfR) was found in a second OHSt sample, confirming that this profile is typical of the OHSt phenotype (data not shown).

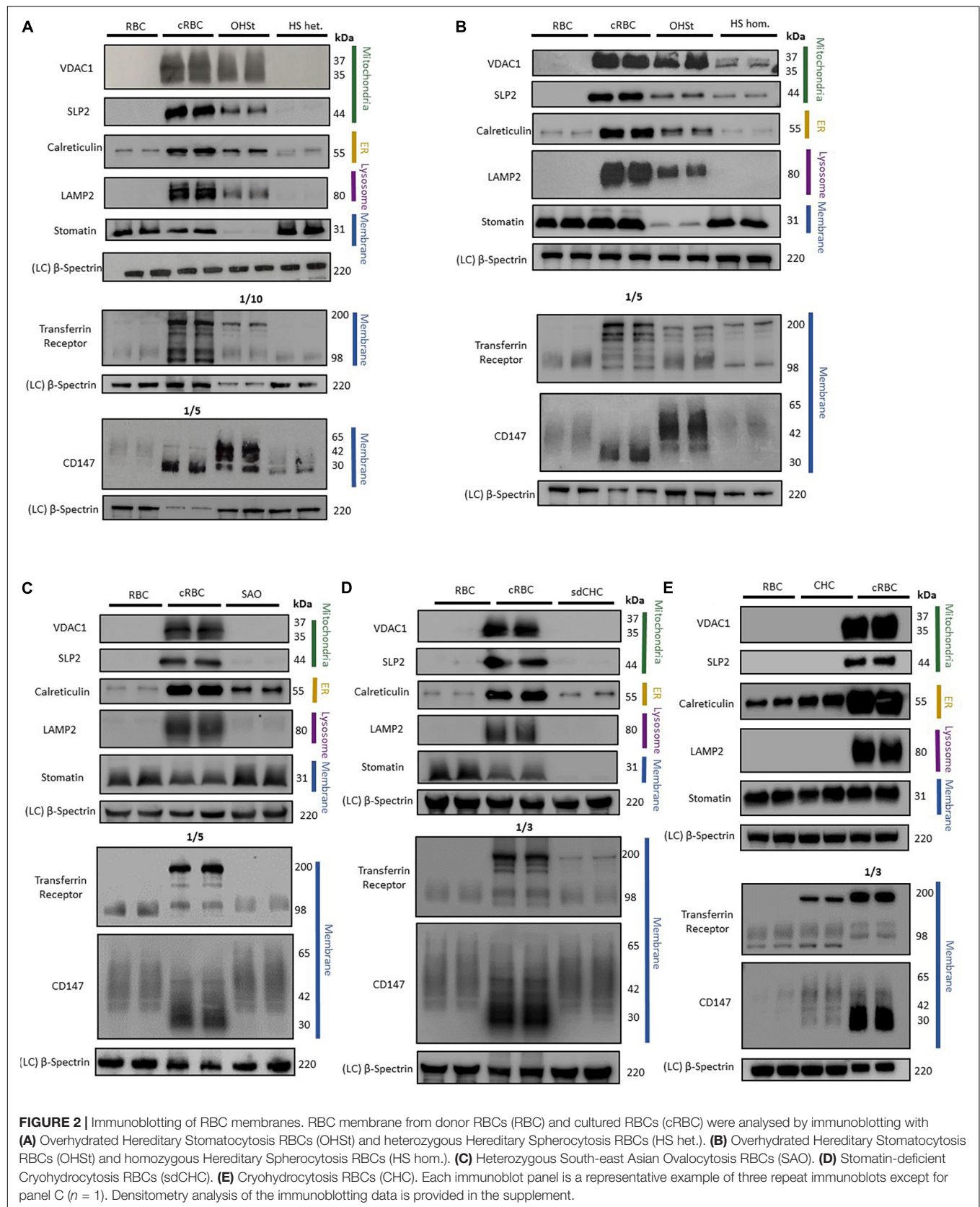
Hereditary Spherocytosis Red Blood Cells

In contrast, immunoblotting of heterozygous HS RBC membranes gave a similar profile to that of control donor RBC membranes, clearing most internal membranes and containing only residual amounts of calreticulin (ER), TfR and CD147 (Figure 2A and Supplementary Table 1), about the same level as found in the mature RBC membranes, suggesting that HS RBCs complete reticulocyte maturation normally and that the RBC defect occurs later during RBC circulation. Homozygous HS RBC membranes did contain slightly more residual mitochondrial membrane proteins (VDAC1 and SLP2) than

donor RBC membranes (Figure 2B and Supplementary Table 1) but this sample has a homozygous *SLC4A1* variant causing low *SLC4A1* expression, a trafficking defect and hemolytic anemia (Toye et al., 2008). Both heterozygous and homozygous HS RBC membranes contained normal levels of spectrin and stomatin (Figures 2A,B).

South-East Asian Ovalocytosis, Stomatin-Deficient Cryohydrocytosis and Cryohydrocytosis

As reported previously (Flatt et al., 2020), SAO RBCs failed to clear calreticulin as efficiently as control donor RBCs, suggesting greater retention of ER membranes, although mitochondrial membrane proteins (VDAC1 and SLP2) and lysosomal membrane protein (LAMP2) appeared to clear normally (Figure 2C and Supplementary Table 1). CD147 was not cleared as well from SAO membranes as from the control donor RBC membranes and migrated more slowly in SDS-PAGE, whereas TfR was cleared slightly



better from SAO compared to control RBC membranes (**Figure 2C** and **Supplementary Table 1**). Stomatin and spectrin were present in normal amounts in SAO membranes (**Figure 2C**).

The sdCHC and CHC RBC membranes gave a similar profile to that of the SAO RBC membranes. Both cleared residual mitochondrial and lysosomal membranes to the same degree as the mature donor RBCs but retained more ER membranes than the donor RBCs (**Figures 2D,E** and **Supplementary Table 1**). Both had increased amounts of the monomeric and dimeric forms of TfR relative to the donor RBC membranes (**Figures 2D,E**). CD147 was increased in the CHC compared to donor RBCs (**Figures 2D,E** and **Supplementary Table 1**). Both contained normal levels of spectrin but, as expected, stomatin was reduced in the sdCHC RBCs (**Figures 2D,E** and **Supplementary Table 1**).

DISCUSSION

The culture conditions used in our laboratory differentiate CD34⁺ cells, in a fairly synchronized manner, through to reticulocytes. The ultimate goal is to mature these cells *in vitro* into erythrocytes but, as far as we know, no one has managed to achieve this yet. Native reticulocytes, isolated from peripheral blood, can be matured *in vitro* (Koury et al., 2005). Indeed, we have also shown that native reticulocytes, when incubated in either plasma or media at 37°C for ten days, reduce their levels of RNA and TfR and develop an increased ratio of R2:R1 reticulocytes (data not shown). Cultured reticulocytes can be induced to begin the maturation process when put under shear stress (Moura et al., 2019) and appear to mature fully in the circulation of a mouse model (Kupzig et al., 2017) but completing the maturation process *in vitro* has yet to be achieved. Proteomic analysis comparing native reticulocytes to cultured reticulocytes shows their proteomic profile to be very similar (Moura et al., 2018) but there must be an essential factor missing from the cRBCs (perhaps a plasma protein or the lack of macrophages) that restricts their development *in vitro*. There is a great deal of interest in understanding the mechanism of reticulocyte maturation. Numerous laboratories worldwide are growing cRBCs and these cells have the potential for many future applications, e.g. in drug delivery or therapeutics or even as a future blood component if scale-up and cost-reduction are achieved. However, storage of cRBCs is a problem, as cRBCs are much less stable than mature erythrocytes in cold-storage, but if cRBCs could be matured to erythrocytes then their full potential could be realized.

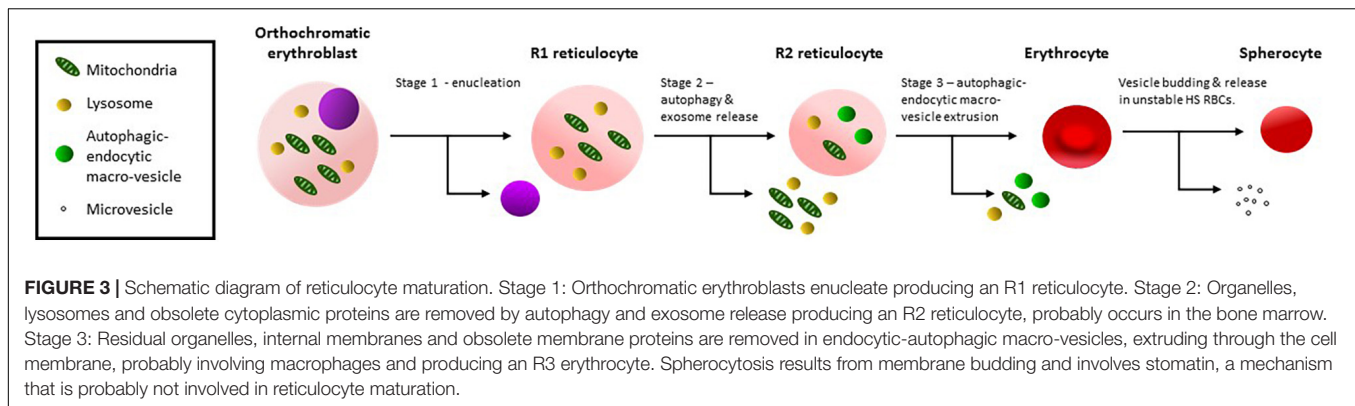
The process of reticulocyte maturation involves a reduction in size and clearance of residual organelles, internal membranes and proteins that are superfluous to the function of the mature RBC. There have been a number of cellular mechanisms identified. Autophagic organelle clearance is thought to begin pre-enucleation and continue through reticulocyte maturation. Autophagosomes deliver cytoplasmic proteins or organelles to lysosomes for degradation (Mei et al., 2021). This involves the autophagy proteins LC3, ATG4 and ATG7 (Zhang et al., 2009; Betin et al., 2013). Mitophagy has been shown to be inhibited

in ATG7-deficient erythroid cells however removal of ribosomes and endoplasmic reticulum continues in the absence of ATG7 and may involve a different mechanism (Zhang et al., 2009). Indeed, ubiquitin proteasome-mediated proteolysis degrades ribosomal proteins as well as other non-ribosomal targets, such as histone H2B and may be the mechanism used for degradation of much of the obsolete cytoplasmic proteins (Nguyen et al., 2017). Removal or reduction of membranes proteins involves endocytosis. Following endocytosis, the endosome invaginates to form exosomes, containing the obsolete membranes proteins, and either fuses with the plasma membrane, discharging its content, or fuses with a lysosome where the proteins are digested.

Levels of CD71 and RNA/reticulins gradually reduce throughout the maturation process and this clearance may involve all of the above mechanisms. However, reduction of TfR from the circulating R2 reticulocyte appears to require the interaction of splenic macrophages (Rhodes et al., 2016) and is probably separate from the mitochondrial clearance stage (Zhang et al., 2019). In late stages of maturation, the final organelle and membrane remnants, together with residual obsolete proteins, are collected in large vacuolar compartments that comprise part endosome that label strongly with glycophorin A (GPA) and part autophagosome that label with LC3 (Griffiths et al., 2012b). These autophagic-endocytic macro-vesicles then squeeze out through the plasma membrane, by a mechanism yet to be determined, and are removed by phagocytes (Mankelov et al., 2016). These large macro-vesicles can be seen inside reticulocytes and partially protruding from reticulocytes and RBCs, in splenectomized individuals, and label positively for phosphatidylserine, a phospholipid usually restricted to the inner membrane leaflet (Mankelov et al., 2016).

Variant Cells

In this study we have compared the degree of defective reticulocyte maturation in the variant RBCs as measured by their size (MCV) and the levels of proteins, that should have been cleared by the maturation process, remaining in their membranes. We hypothesize that these attributes correlate with the size and reticulocyte-like protein patterns of the different stages of reticulocyte maturation. As expected, post-enucleation cRBC membranes contain large amounts of residual internal membranes, e.g., mitochondria, ER and lysosomes as can be seen by the presence of VDAC1, SLP2, calreticulin and LAMP2 (**Figure 2**) plus large amounts of TfR and CD147 (**Figure 2**). Mature donor RBC membranes, for the most part, lack these internal membranes and have only residual amounts of ER, TfR and CD147 (**Figure 2**). We have reported previously that residual amount of monomeric TfR (98 kDa) can be detected by immunoblotting in mature donor RBC membranes (Flatt et al., 2020). As the controls used in the immunoblots were prepared from red cell concentrates (RCC) this is unlikely to be due to residual reticulocytes (see **Supplementary Figure 2**). The heterozygous and homozygous HS samples were included in this study as controls because these patients had reticulocytosis (**Table 1**). Some of the patients studied in this report had some level of reticulocytosis (**Table 1**) and we needed to show that the residual reticulocyte proteins in the variant samples were not simply due to increased reticulocyte count. Interestingly, we show



here that both heterozygous and homozygous HS RBCs appear to mature normally; the heterozygous HS RBC membranes have much the same protein profile as the control RBC membranes (**Figure 2A** and **Supplementary Table 1**). The homozygous HS RBC membranes do contain some residual mitochondrial proteins and increased amounts of dimeric TfR compared to the control RBC membranes (**Figure 2B**) but this is probably due to the trafficking defect found in these homozygous HS cells (Toye et al., 2008) or it may reflect the high (17.5%) reticulocyte count in this sample (the HS-hom. sample shows the level of these reticulocyte proteins to be expected in the RBC membrane from a sample with a high reticulocyte count). However, overall the data indicates that the RBCs (non-reticulocytes) in these HS samples mature normally although, as HS RBCs vesiculate and lose plasma membrane continually in the circulatory system, we cannot rule out the possibility that mitochondrial, lysosomal and ER membranes, CD147 and TfR have been lost in these vesicles.

The largest variant RBC studied was OHSt which are similar in size to nascent R1 reticulocytes (**Table 1**). These cells were the least mature of the variants studied and contained large amounts of mitochondrial, ER and lysosomal proteins (**Figures 2A,B** and **Supplementary Table 1**). The OHSt RBCs also contained large amounts of TfR, including the presumed dimeric form found in cRBCs, and CD147, including the unglycosylated form found in cRBCs (**Figures 2A,B**). Together these results suggest that the OHSt RBCs have not matured much further than the R1 stage. Next in size are the sdCHC, CHC and SAO variant RBCs (**Table 1**). These cells all cleared the mitochondrial and lysosomal proteins but retained more ER membranes and the SAO and CHC RBCs had slightly more CD147 than the controls (**Figures 2C-E** and **Supplementary Table 1**). The sdCHC and CHC RBC membranes contained more dimeric TfR than controls however as previously reported (Flatt et al., 2020) the SAO RBC membranes contained less TfR than the donor control RBC membranes (**Figure 2C**). We previously showed that SAO band 3 accumulates in SAO erythroblasts in internal vesicles disrupting cytokinesis and enucleation and blocking the intracellular milieu with vesicle aggregates that may affect the recycling of TfR (Flatt et al., 2020). Nonetheless, this group of variants, with MCVs that match the average size of an R2 reticulocyte, all matured further than the OHSt RBCs, clearing mitochondrial and lysosomal proteins. The maturation of R2 reticulocytes to mature RBCs is known to involve the final clearance of ER and other membrane

fragments and excess proteins (TfR, CD147 etc.) and a final reduction in size involving the expulsion of autophagic-endocytic vesicles (Mankelov et al., 2016). This is probably followed by further dehydration and cytoskeleton rearrangement (**Figure 3**).

The Role of Stomatin

Interestingly, the presence or absence of stomatin appeared to have little effect on the ability of the reticulocyte to mature. CHC and sdCHC RBCs matured to much the same level despite the near absence of stomatin in the sdCHC RBCs (**Figure 2D**). Stomatin is known to be involved in membrane budding as occurs in the circulation and during RBC storage (Salzer et al., 2008). Our data suggests that the budding mechanism of vesiculation is not employed in reticulocyte maturation. However, stomatin is also involved in the formation of the autophagic-endocytic vesicles produced in the final stages of reticulocyte maturation (Mankelov et al., 2016) and lack of stomatin, depending on when it is lost in these variant cells, may affect this process.

CONCLUSION

We describe here a number of variant RBCs whose size appears to correlate with their level of reticulocyte maturation. The sizes of the variant cells are also similar to the sizes of reticulocytes at different stages of reticulocyte maturation. Numerous mechanisms of reticulocyte maturation have been described but it has been unclear as to whether these occur simultaneously or in stages. Our data, and that of others (Mel et al., 1977; Koury et al., 2005; Mankelov et al., 2016; Rhodes et al., 2016; Du et al., 2020; Mei et al., 2021), suggests that different mechanisms of maturation occur at different stages. Mitochondria and lysosomes predominantly being lost early probably through an autophagy and exosome release mechanism. Residual ER, TfR and CD147 predominantly lost later probably through the autophagic-endocytic macrovesicle mechanism (**Figure 3**). Stomatin does not appear to be required, although lack of stomatin may affect maturation in OHSt RBCs, but the membrane budding mechanism of vesiculation that occurs in RBC storage is probably not involved in reticulocyte maturation. No doubt all of these mechanisms overlap to some

extent throughout the process but we believe this data provides a unique insight into the process of reticulocyte maturation and may also be useful in understanding the hemolytic anemia experienced by individuals with these conditions.

DATA AVAILABILITY STATEMENT

Publicly available datasets were analyzed in this study. This data can be found here: <https://www.ncbi.nlm.nih.gov/snp/rs863225468>, <https://www.ncbi.nlm.nih.gov/snp/rs769664228>, <https://www.ncbi.nlm.nih.gov/snp/rs864309514>, and <https://www.ncbi.nlm.nih.gov/snp/rs863225461>.

ETHICS STATEMENT

The studies involving human participants were reviewed and approved by National Health Service National Research Ethics Service South West. The patients/participants provided their written informed consent to participate in this study.

AUTHOR CONTRIBUTIONS

CS-H and JF designed and performed the immunoblotting experiments. CS-H analyzed the data. SK conducted the electron

microscopy experiments. LB designed the study, analyzed data, and wrote the manuscript. All authors edited the manuscript.

FUNDING

This study was supported by the National Institute for Health Research Blood and Transplant Research Unit (NIHR BTRU) in Red Cell Products (IS-BTU-1214-10032) and by the UK National Health Service R&D Directorate.

ACKNOWLEDGMENTS

We thank Gordon W. Stewart, Jean Delaunay, Graham Standen, Caroline Thomas and Veronique Picard for providing patient samples and the patients and their families for their participation.

SUPPLEMENTARY MATERIAL

The Supplementary Material for this article can be found online at: <https://www.frontiersin.org/articles/10.3389/fphys.2022.834463/full#supplementary-material>

REFERENCES

- Bawazir, W. M., Gevers, E. F., Flatt, J. F., Ang, A. L., Jacobs, B., Oren, C., et al. (2012). An infant with pseudohyperkalemia, hemolysis, and seizures: cation-leaky GLUT1-deficiency syndrome due to a SLC2A1 mutation. *J. Clin. Endocrinol. Metab.* 97, E987–E993. doi: 10.1210/jc.2012-1399
- Betin, V. M., Singleton, B. K., Parsons, S. F., Anstee, D. J., and Lane, J. D. (2013). Autophagy facilitates organelle clearance during differentiation of human erythroblasts: evidence for a role for ATG4 paralogs during autophagosome maturation. *Autophagy* 9, 881–893. doi: 10.4161/auto.24172
- Bruce, L. J., Beckmann, R., Ribeiro, M. L., Peters, L. L., Chasis, J. A., Delaunay, J., et al. (2003). A band 3-based macrocomplex of integral and peripheral proteins in the RBC membrane. *Blood* 101, 4180–4188. doi: 10.1182/blood-2002-09-2824
- Bruce, L. J., Guizouarn, H., Burton, N. M., Gabillat, N., Poole, J., Flatt, J. F., et al. (2009). The monovalent cation leak in overhydrated stomatocytic red blood cells results from amino acid substitutions in the Rh-associated glycoprotein. *Blood* 113, 1350–1357. doi: 10.1182/blood-2008-07-171140
- Bruce, L. J., Ring, S. M., Ridgwell, K., Reardon, D. M., Seymour, C. A., Van Dort, H. M., et al. (1999). South-east asian ovalocytic (SAO) erythrocytes have a cold sensitive cation leak: implications for in vitro studies on stored SAO red cells. *Biochim. Biophys. Acta* 1416, 258–270. doi: 10.1016/s0005-2736(98)00231-4
- Bruce, L. J., Robinson, H. C., Guizouarn, H., Borgese, F., Harrison, P., King, M. J., et al. (2005). Monovalent cation leaks in human red cells caused by single amino-acid substitutions in the transport domain of the band 3 chloride-bicarbonate exchanger, AE1. *Nat. Genet.* 37, 1258–1263. doi: 10.1038/ng1656
- Coles, S. E., Chetty, M. C., Ho, M. M., Nicolaou, A., Kearney, J. W., Wright, S. D., et al. (1999). Two British families with variants of the 'cryohydrocytosis' form of hereditary stomatocytosis. *Br. J. Haematol.* 105, 1055–1065. doi: 10.1046/j.1365-2141.1999.01444.x
- Dodge, J. T., Mitchell, C., and Hanahan, D. J. (1963). The preparation and chemical characteristics of hemoglobin-free ghosts of human erythrocytes. *Arch. Biochem. Biophys.* 100, 119–130. doi: 10.1016/0003-9861(63)90042-0
- Du, R., Bei, H., Jia, L., Huang, C., Chen, Q., Wang, J., et al. (2020). A low-cost, accurate method for detecting reticulocytes at different maturation stages based on changes in the mitochondrial membrane potential. *J. Pharmacol. Toxicol. Methods* 101:106664. doi: 10.1016/j.vascn.2019.106664
- Flatt, J. F., Guizouarn, H., Burton, N. M., Borgese, F., Tomlinson, R. J., Forsyth, R. J., et al. (2011). Stomatin-deficient cryohydrocytosis results from mutations in SLC2A1: a novel form of GLUT1 deficiency syndrome. *Blood* 118, 5267–5277. doi: 10.1182/blood-2010-12-326645
- Flatt, J. F., Stevens-Hernandez, C. J., Cogan, N. M., Eggleston, D. J., Haines, N. M., Heesom, K. J., et al. (2020). Expression of South East Asian Ovalocytic Band 3 Disrupts Erythroblast Cytokinesis and Reticulocyte Maturation. *Front. Physiol.* 11:357. doi: 10.3389/fphys.2020.00357
- Fricke, B., Argent, A. C., Chetty, M. C., Pizzey, A. R., Turner, E. J., Ho, M. M., et al. (2003). The "stomatin" gene and protein in overhydrated hereditary stomatocytosis. *Blood* 102, 2268–2277. doi: 10.1182/blood-2002-06-1705
- Fricke, B., Jarvis, H. G., Reid, C. D., Aguilar-Martinez, P., Robert, A., Quittet, P., et al. (2004). Four new cases of stomatin-deficient hereditary stomatocytosis syndrome: association of the stomatin-deficient cryohydrocytosis variant with neurological dysfunction. *Br. J. Haematol.* 125, 796–803. doi: 10.1111/j.1365-2141.2004.04965.x
- Gallagher, P. G., Chang, S. H., Rettig, M. P., Neely, J. E., Hillery, C. A., Smith, B. D., et al. (2003). Altered erythrocyte endothelial adherence and membrane phospholipid asymmetry in hereditary hydrocytosis. *Blood* 101, 4625–4627. doi: 10.1182/blood-2001-12-0329
- Garnett, C., and Bain, B. J. (2013). South-East Asian ovalocytosis. *Am. J. Hematol.* 88:328.
- Griffiths, R. E., Kupzig, S., Cogan, N., Mankelov, T. J., Betin, V. M., Trakarnsanga, K., et al. (2012a). Maturing reticulocytes internalize plasma membrane in glycophorin A-containing vesicles that fuse with autophagosomes before exocytosis. *Blood* 119, 6296–6306. doi: 10.1182/blood-2011-09-376475
- Griffiths, R. E., Kupzig, S., Cogan, N., Mankelov, T. J., Betin, V. M., Trakarnsanga, K., et al. (2012b). The ins and outs of human reticulocyte maturation: autophagy and the endosome/exosome pathway. *Autophagy* 8, 1150–1151. doi: 10.4161/auto.20648
- Gronowicz, G., Swift, H., and Steck, L. (1984). Maturation of the reticulocyte in vitro. *J. Cell Sci.* 71, 177–179.

- Guizouarn, H., Borgese, F., Gabillat, N., Harrison, P., Goede, J. S., McMahon, C., et al. (2011). South-east Asian ovalocytosis and the cryohydrocytosis form of hereditary stomatocytosis show virtually indistinguishable cation permeability defects. *Br. J. Haematol.* 152, 655–664. doi: 10.1111/j.1365-2141.2010.08454.x
- Gunaratne, W., Dissanayake, D., Jayaratne, K., Premawardhana, N. P., and Siribaddana, S. (2020). A case series of distal renal tubular acidosis, Southeast Asian ovalocytosis and metabolic bone disease. *BMC Nephrol.* 21:327. doi: 10.1186/s12882-020-01959-7
- Koury, M. J., Koury, S. T., Kopsombut, P., and Bondurant, M. C. (2005). In vitro maturation of nascent reticulocytes to erythrocytes. *Blood* 105, 2168–2174. doi: 10.1182/blood-2004-02-0616
- Koury, S. T., Koury, M. J., and Bondurant, M. C. (1989). Cytoskeletal distribution and function during the maturation and enucleation of mammalian erythroblasts. *J. Cell Biol.* 109, 3005–3013. doi: 10.1083/jcb.109.6.3005
- Kupzig, S., Parsons, S. F., Curnow, E., Anstee, D. J., and Blair, A. (2017). Superior survival of *ex vivo* cultured human reticulocytes following transfusion into mice. *Haematologica* 102, 476–483. doi: 10.3324/haematol.2016.154443
- Laosombat, V., Dissaneevate, S., Wongchanchailert, M., and Satayasevana, B. (2005). Neonatal anemia associated with Southeast Asian ovalocytosis. *Int. J. Hematol.* 82, 201–205. doi: 10.1532/IJH97.A20505
- Liu, J., Guo, X., Mohandas, N., Chasis, J. A., and An, X. (2010). Membrane remodeling during reticulocyte maturation. *Blood* 115, 2021–2027. doi: 10.1182/blood-2009-08-241182
- Lock, S. P., Smith, R. S., and Hardisty, R. M. (1961). Stomatocytosis: a hereditary red cell anomaly associated with haemolytic anemia. *Br. J. Haematol.* 7, 303–314. doi: 10.1111/j.1365-2141.1961.tb00341.x
- Malleret, B., Xu, F., Mohandas, N., Suwanarus, R., Chu, C., Leite, J. A., et al. (2013). Significant biochemical, biophysical and metabolic diversity in circulating human cord blood reticulocytes. *PLoS One.* 8:e76062. doi: 10.1371/journal.pone.0076062
- Mankelaw, T. J., Griffiths, R. E., Trompeter, S., Flatt, J. F., Cogan, N. M., Massey, E. J., et al. (2016). The ins and outs of reticulocyte maturation revisited: the role of autophagy in sickle cell disease. *Autophagy* 12, 590–591. doi: 10.1080/15548627.2015.1125072
- Mei, Y., Liu, Y., and Ji, P. (2021). Understanding terminal erythropoiesis: an update on chromatin condensation, enucleation, and reticulocyte maturation. *Blood Rev.* 46:100740. doi: 10.1016/j.blre.2020.100740
- Mel, H. C., Prenant, M., and Mohandas, N. (1977). Reticulocyte motility and form: studies on maturation and classification. *Blood* 49, 1001–1009.
- Minetti, G., Bernecker, C., Dorn, I., Achilli, C., Bernuzzi, S., Perotti, C., et al. (2020). Membrane Rearrangements in the Maturation of Circulating Human Reticulocytes. *Front. Physiol.* 11:215. doi: 10.3389/fphys.2020.00215
- Moura, P. L., Hawley, B. R., Mankelaw, T. J., Griffiths, R. E., Dobbe, J. G. G., Streekstra, G. J., et al. (2018). Non-muscle myosin II drives vesicle loss during human reticulocyte maturation. *Haematologica* 103, 1997–2007. doi: 10.3324/haematol.2018.199083
- Moura, P. L., Lizarralde Iragorri, M. A., François, O., Le Pioufle, B., Dobbe, J. G. G., Streekstra, G. J., et al. (2019). Reticulocyte and red blood cell deformation triggers specific phosphorylation events. *Blood Adv.* 3, 2653–2663. doi: 10.1182/bloodadvances.2019000545
- Nguyen, A. T., Prado, M. A., Schmidt, P. J., Sendamarai, A. K., Wilson-Grady, J. T., Min, M., et al. (2017). UBE2O remodels the proteome during terminal erythroid differentiation. *Science* 357:eaan0218. doi: 10.1126/science.aan0218
- Picard, V., Proust, A., Eveillard, M., Flatt, J. F., Couec, M. L., Caillaux, G., et al. (2014). Homozygous Southeast Asian ovalocytosis is a severe dyserythropoietic anemia associated with distal renal tubular acidosis. *Blood* 123, 1963–1965. doi: 10.1182/blood-2014-01-548149
- Rhodes, M. M., Koury, S. T., Kopsombut, P., Alford, C. E., Price, J. O., and Koury, M. J. (2016). Stress reticulocytes lose transferrin receptors by an extrinsic process involving spleen and macrophages. *Am. J. Hematol.* 91, 875–882. doi: 10.1002/ajh.24421
- Salzer, U., Zhu, R., Luten, M., Isobe, H., Pastushenko, V., Perkmann, T., et al. (2008). Vesicles generated during storage of red cells are rich in the lipid raft marker stomatin. *Transfusion* 48, 451–462. doi: 10.1111/j.1537-2995.2007.01549.x
- Tanner, M. J., Bruce, L., Martin, P. G., Rearden, D. M., and Jones, G. L. (1991). Melanesian hereditary ovalocytes have a deletion in red cell band 3. *Blood* 78, 2785–2786. doi: 10.1182/blood.v78.10.2785.bloodjournal7810.2785
- Toye, A. M., Williamson, R. C., Khanfar, M., Bader-Meunier, B., Cynober, T., Thibault, M., et al. (2008). Band 3 Courcouronnes (Ser667Phe): a trafficking mutant differentially rescued by wild-type band 3 and glycophorin A. *Blood* 111, 5380–5389. doi: 10.1182/blood-2007-07-099473
- Wickrema, A., Koury, S. T., Dai, C. H., and Krantz, S. B. (1994). Changes in cytoskeletal proteins and their mRNAs during maturation of human erythroid progenitor cells. *J. Cell Physiol.* 160, 417–426. doi: 10.1002/jcp.1041600304
- Yamsri, S., Kawon, W., Duereh, A., Fucharoen, G., and Fucharoen, S. (2021). Southeast Asian Ovalocytosis and Hemoglobinopathies in Newborns: Prevalence, Molecular, and Hematologic Analyses. *J. Pediatr. Hematol. Oncol.* 43, e341–e345. doi: 10.1097/MPH.0000000000001920
- Zhang, J., Randall, M. S., Loyd, M. R., Dorsey, F. C., Kundu, M., Cleveland, J. L., et al. (2009). Mitochondrial clearance is regulated by Atg7-dependent and -independent mechanisms during reticulocyte maturation. *Blood* 114, 157–164. doi: 10.1182/blood-2008-04-151639
- Zhang, Q., Steensma, D. P., Yang, J., Dong, T., and Wu, M. X. (2019). Uncoupling of CD71 shedding with mitochondrial clearance in reticulocytes in a subset of myelodysplastic syndromes. *Leukemia* 33, 217–229. doi: 10.1038/s41375-018-0204-z

Author Disclaimer: The views expressed are those of the authors and not necessarily those of the National Health Service, NIHR, or the Department of Health and Social Care.

Conflict of Interest: The authors declare that the research was conducted in the absence of any commercial or financial relationships that could be construed as a potential conflict of interest.

Publisher's Note: All claims expressed in this article are solely those of the authors and do not necessarily represent those of their affiliated organizations, or those of the publisher, the editors and the reviewers. Any product that may be evaluated in this article, or claim that may be made by its manufacturer, is not guaranteed or endorsed by the publisher.

Copyright © 2022 Stevens-Hernandez, Flatt, Kupzig and Bruce. This is an open-access article distributed under the terms of the Creative Commons Attribution License (CC BY). The use, distribution or reproduction in other forums is permitted, provided the original author(s) and the copyright owner(s) are credited and that the original publication in this journal is cited, in accordance with accepted academic practice. No use, distribution or reproduction is permitted which does not comply with these terms.



The Relation Between Extracellular Vesicles Released From Red Blood Cells, Their Cargo, and the Clearance by Macrophages

Duc Bach Nguyen^{1*}, Hanh Triet Tran², Lars Kaestner^{3,4} and Ingolf Bernhardt^{5*}

¹ Department of Molecular Biology, Faculty of Biotechnology, Vietnam National University of Agriculture, Hanoi, Vietnam,

² Division of Aquacultural Biotechnology, Biotechnology Center of Ho Chi Minh City, Ho Chi Minh City, Vietnam, ³ Theoretical Medicine and Biosciences, Medical Faculty, Saarland University, Homburg, Germany, ⁴ Dynamics of Fluids, Experimental Physics, Saarland University, Saarbruecken, Germany, ⁵ Laboratory of Biophysics, Faculty of Natural and Technical Sciences, Saarland University, Saarbruecken, Germany

OPEN ACCESS

Edited by:

Wassim El Nemer,
French Blood Establishment (EFS),
France

Reviewed by:

Angelo D'Alessandro,
University of Colorado, Denver,
United States
Elie Nader,
Université Claude Bernard Lyon 1,
France

*Correspondence:

Duc Bach Nguyen
ndbach@vnua.edu.vn
Ingolf Bernhardt
i.bernhardt@mx.uni-saarland.de

Specialty section:

This article was submitted to
Red Blood Cell Physiology,
a section of the journal
Frontiers in Physiology

Received: 25 September 2021

Accepted: 14 February 2022

Published: 31 March 2022

Citation:

Nguyen DB, Tran HT, Kaestner L
and Bernhardt I (2022) The Relation
Between Extracellular Vesicles
Released From Red Blood Cells, Their
Cargo, and the Clearance by
Macrophages.
Front. Physiol. 13:783260.
doi: 10.3389/fphys.2022.783260

Extracellular vesicles (EVs) are cell-derived membrane particles that include exosomes, ectosomes, microvesicles, microparticles, apoptotic bodies, and other EV subsets. EVs are involved in intercellular communication and the transport of macromolecules between cells. Here, we propose and test the ability of red blood cell (RBC)-derived EVs (RBC-EVs) as putative drug carriers. EVs were produced by treating RBCs with Phorbol-12-myristate-13-acetate (PMA) and separating from the cells by differential centrifugation steps. RBC-EVs were characterized by size determination, flow cytometry, and scanning electron microscopy (SEM). EVs were loaded with DNA plasmids coding for the green fluorescent protein (GFP) by electroporation. The DNA-loaded EVs (DNA-EVs) were used to transfect THP-1-derived macrophages and analyzed by fluorescence microscopy and flow cytometry. The results showed that RBC-EVs had an almost spherical shape and a polydispersity in their size with an average of 197 ± 44 nm and with a zeta potential of -36 ± 8 mV. RBC-EVs were successfully loaded with DNA but associated with an increase of the polydispersity index (Pdl) and showed a positive signal with Picogreen. DNA-EVs were almost completely taken up by macrophages within 24 h, however, resulting in the expression of the GFP in a subpopulation of macrophages. As the way, we designed that RBC-EVs could be potential nucleic acid carriers when the immune system was addressed. This study may contribute to the understanding of the role of EVs in the development of microvesicle-based vehicles.

Keywords: human red blood cells, macrophages, THP-1 cells, cell-based vehicles, extracellular vesicles, clearance

INTRODUCTION

In 1987, extracellular vesicles (EVs) were firstly described in erythropoietic cells by Johnstone et al. (1987) when cultured sheep reticulocytes *in vitro*. Later EVs were found released from blood cells, body fluids of animals, and also from bacteria and plant cells (Akuma et al., 2019; Macia et al., 2020). Under physiological and pathological conditions, various cell types secrete EVs

(Raposo and Stoorvogel, 2013; L tvall et al., 2014; Antonyak and Cerione, 2015; Witwer et al., 2017; Van Niel et al., 2018; Murphy et al., 2019; Thangaraju et al., 2020). Recently, all secreted membrane-enclosed vesicles are collectively called EVs, which include exosomes, ectosomes, microvesicles, microparticles, apoptotic bodies, and other EV subsets (L tvall et al., 2014; Witwer et al., 2017).

Red blood cell (RBC)-derived EVs (RBC-EVs) are secreted during erythropoiesis, cellular aging, such as stored blood (Bosman et al., 2008; Kriebardis et al., 2008; Thangaraju et al., 2020), or in response to activated conditions, such as an increase of intracellular Ca^{2+} or activation of protein kinase C (PKC) (Nguyen et al., 2016, 2017; Bernhardt et al., 2020), and disease conditions (Alaarg et al., 2013; Mantel et al., 2013; Leal et al., 2018). Under physiological and pathological conditions, RBC-EVs could be loaded with proteins, lipids, and miRNAs might be vital for homeostasis. RBC-EVs are also involved in the communication between RBCs and endothelium to regulate NO and O_2 , redox balance, immunomodulation, and the pro-coagulant effects in several disease states (Van der Meijden et al., 2012; Thangaraju et al., 2020). In addition, RBC-EVs are involved in inducing the secretion of proinflammatory cytokines and chemokines (Danesh et al., 2014; Zecher et al., 2014).

Recently, RBC-EVs have received much attention in respect to intercellular communication (Nguyen et al., 2016; Noubouossie et al., 2020). It has been reported that RBC-EVs can be applied for RNA delivery in gene therapy (Usman et al., 2018). As the number of RBCs exceeds that of all other cell types, therefore, the number of EVs released from RBC is myriad in the whole blood (Wu et al., 2017). Current theories mainly focus on the removal of senescent RBCs and their EVs as a part of the homeostasis governed by macrophages (de Back et al., 2014). Therefore, the understanding and application of RBC-EVs as novel vehicles for drugs delivery or treatment is of utmost importance. So far, limited data are available about using RBC-EVs as vehicles for the transport of macromolecules and also the knowledge about the fate of RBC-EVs in circulation is not available. In addition, the information about the loading of macromolecules into RBC-EVs and the delivery of loaded RBC-EVs are limited.

In the last decades, the development of nanoparticle-based vehicles has improved the therapeutic efficacy of certain drugs by allowing controlled access and administration to target cells. However, several problems associated with synthetic nanoparticles have been observed, such as cell cytotoxicity, immunogenicity, rapid elimination by the phagocytic mononuclear system, and the specific sites of action (Lee et al., 2012; Murphy et al., 2019; Gutierrez-Millan et al., 2021). Because EVs possess nanoscale dimensions and a variety of adhesion proteins presenting on their surface that support the specific interaction with targeted cell types, they are qualified as potential vehicles for drug delivery (Maas et al., 2017; Bunggulawa et al., 2018; Elsharkasy et al., 2020; Gutierrez-Millan et al., 2021). Therefore, EV can be a means of transport for drugs or macromolecules open a new approach for targeted drug delivery and treatment (Kanada et al., 2015; Balachandran et al., 2019; Li C. et al., 2019; Li X. et al., 2019; Butreddy et al., 2021; Gutierrez-Millan et al., 2021). Recent studies have proposed that EVs play a role in intercellular communication and transport

molecules, such as mRNA, miRNA, and proteins between cells (Chitoiu et al., 2020; Gurung et al., 2021).

Within this study, we produced RBC-EVs, characterized them physically, and loaded them with DNA. Furthermore, we investigated the ability of EVs to carry DNA and the interaction between EVs and macrophages differentiated from THP-1 cells. The study contributes to the understanding of RBC-EVs properties and encourages the further development of microvesicle-based vehicles as a new approach for targeted drug delivery and treatment (such as gene therapy). The study also suggests that the macrophages may limit the applicability of RBC-EVs *in vivo*.

MATERIALS AND METHODS

Blood and Solutions

Fresh human venous blood from healthy donors was withdrawn by venipuncture into citrate-coated tubes or with heparin as an anticoagulant, kept at 4 C, and used on the same day. Fresh whole blood was centrifuged at 2,000 g for 5 min at room temperature and the plasma, and buffy coat was removed by aspiration. Subsequently, RBCs were washed 3 times in N-2-hydroxyethylpiperazine-N'-2-ethanesulfonic acid (HEPES)-buffered solution (HPS) containing (mM): NaCl 145, KCl 7.5, glucose 10, HEPES 10, pH 7.4, and finally, RBCs were resuspended in HPS and kept at 4 C for experiments.

Stimulation of Red Blood Cells and Isolation of Extracellular Vesicles

Red blood cells were suspended in HPS at a hematocrit of 0.5% in the presence of 2 mM CaCl_2 . Phorbol 12-myristate 13-acetate (PMA, Sigma-Aldrich, St. Louis, United States) was added at a concentration of 6 μM and the cell suspension was incubated for 2 h at 37 C with occasional shaking. Subsequently, cell suspensions were subjected to differential centrifugation. First, a centrifugation step at 1,500 g for 10 min was applied followed by centrifugation at 3,000 g for 15 min twice to remove intact cells, cell debris, and apoptotic blebs. The supernatants were collected and further centrifuged at 25,000 g for 1 h at 4 C to harvest large size EVs. Subsequently, the collected supernatants were transferred to new tubes and ultra-centrifuged at 35,000 rpm (corresponding to $\sim 200,000$ g) for 2 h at 4 C for the isolation of small size EVs (Beckman Coulter, Swinging Bucket rotor SW40 Ti, k-factor 137). Pellets obtained after each centrifugation step were resuspended in Milli-Q water (ultra-pure) for morphological, size, and zeta potential measurements (Nguyen et al., 2016).

Loading of DNA Plasmids Into Extracellular Vesicles

DNA plasmid (pEGFP-C3, Clontech, United States) was transformed into competent *Escherichia coli* DH5  cells and cloned in the DH-5 alpha competent cells. It was cultured overnight on lysogeny broth (LB) agar medium (22700025, Thermo Fisher Scientific, United Kingdom) containing a final concentration of 30 $\mu\text{g/ml}$ kanamycin. The resulting

colonies were individually selected and cultured in LB liquid medium (12780052, LB Broth Base, Thermo Fisher Scientific, United Kingdom) shaken at 37°C for 16 h. The plasmid was extracted using a Plasmid Midi Kit (12143, Qiagen, United Kingdom). Purified DNA plasmid DNA quantification using a NanoDrop® (ND-1000 UV-Vis spectrophotometer, Thermo Fisher Scientific, United Kingdom).

In this study, DNA plasmid (dsDNA) was loaded into small size EVs by electroporation. To load DNA into EVs, a 10 µl DNA plasmid (1.0 µg/µl) aliquot was added into 1 ml freshly isolated EVs [suspended in phosphate-buffered saline (PBS) buffer, containing (mM): (NaCl 137.0, KCl 2.7, Na₂HPO₄ 10, KH₂PO₄ 1.8, CaCl₂·2H₂O 1.0), pH 7.4] at a concentration of about 10⁷ particles/ml. DNA plasmid and EVs were mixed throughout gently by pipetting. The mixture of EVs and DNA was prepared as described and transferred (200 µl) to the electroporation cuvettes (T-25714-02, Eppendorf, United Kingdom) gap width 2 mm, then electroporated for 5.0 ms at 2,000 V (Multiporator 36205-10, Eppendorf® Electroporation Systems, United Kingdom). The electroporation was carried out for several batches to obtain enough DNA-loaded EVs (DNA-EVs) for experiments. The efficiency of the transformation of DNA plasmid into EVs was investigated by flow cytometry with specific fluorescent dyes for (dsDNA).

THP-1 Cell Culture

The human monocytic leukemia cell line, THP-1, was grown in Roswell Park Memorial Institute (RPMI) 1640 medium supplemented with 10% Fetal Bovine Serum (FBS, Gibco™, Thermo Fisher Scientific, United Kingdom), 10 mM HEPES (#15630-056, Gibco™, Thermo Fisher Scientific, United Kingdom), 1% L-glutamine, and 50 µg/ml of cefotaxime (Sigma, St. Louis, United States)/ml. THP-1 monocytes are differentiated into macrophages following a modified procedure by incubation with 100 nM PMA for 24 h (Genin et al., 2015). After washing in PBS to remove PMA, cells were transferred to PMA-free RPMI 1640 medium for 48 h resting. Macrophage M2 polarization was obtained by incubation with interleukin 4 (20 ng/ml) for 48 h. After being washed in PBS twice, differentiated THP-1 cells were seeded at a density of 5.105 cells/well in 24-well plates and cultured for 24 h in RPMI media containing 10% FBS, and 50 µg/ml of cefotaxime before transfection with EVs.

Transfection Experiments

The differentiated THP-1 cells were infected with DNA-EVs treated or untreated with annexin V. For each well, the same amount of DNA-EVs (~10⁷ EVs/µl) was added to the cell culture. The remaining EVs in cell culture were observed by fluorescence microscopy, DNA-EVs were loaded with propidium iodide (PI) (stock solution of 1 mg/ml in distilled water). The remaining EVs after 0, 6, 12, 18, and 24 h of transfection were also analyzed by flow cytometry. The suspensions containing EVs were collected by centrifugation at 10,000 g for 10 min at 4°C to remove cells. The concentration of EVs in solutions was measured by flow cytometry with 100,000 events using the following parameters: (i) the number of events in the gate of EVs, and (ii) the volume of sample used in the counting process. The number of EVs remaining in the solution reflected the uptake of differentiated

THP-1 cells during the transfection. Data are presented as percent of remaining EVs relative to the controls.

Cell Viability (Trypan Blue Assay)

THP-1 monocytes were seeded at 180,000 cells/well in 24 well plates and differentiated in macrophages as described. Before being transfected with EVs, cells were tested for viability using trypan blue. In short, cells were detached from the flask by trypsinization and centrifuged the cell suspension for 5 min at 1,000 g (Eppendorf 5415R, Germany). Subsequently, cells were resuspended in 1 ml of culture medium using a pipette to obtain a single-cell suspension. In total, 100 µl of trypan blue solution (0.4%) was added to 100 µl of cell suspension and incubated for 5 min to stain the dead cells. The cells were counted using a hemocytometer and a light microscope (Eclipse Ei, Nikon, Japan). The percentage of viability and number of cells in the culture were calculated by considering the final dilution factor (Piccinini et al., 2017).

Flow Cytometry

Samples were analyzed using a Beckman-Coulter FC500 cytometer (High Wycombe, United Kingdom). For each sample, a minimum of 20,000 events were analyzed. All acquisition and analysis were carried out in log mode. The parameters were set up using a standard calibration kit (BD Calibrite™, BD Calibrate 3 Beads, BD Biosciences, United States). Parameters of both forward and side scatter were adjusted to remove instrument noise (dust). The gating process was carried out using a combination of sheath fluid (blank), samples of stimulated RBCs, isolated EVs stained with the fluorescent probes annexin V-FITC for phosphatidylserine (PS), and Dil stain {1,1'-Diiodo-3,3',3'-tetramethylindocarbocyanine Perchlorate ['DiI'; DiIC18(3)]} as the lipophilic tracer. Freshly washed RBCs were used in the calibration and gating to localize the noise events. The concentration of EVs (as number of EVs/ml) was calculated based on the gating and counting the number of events showing a positive signal with annexin V-FITC and Dil stain in the gate of EVs.

Morphological Analysis Using Scanning Electron Microscopy

RBCs stimulated by PMA were fixed with 2% glutaraldehyde at room temperature for 10 min and washed by PBS-TWEEN® solution (1 tablet per liter to yield 140 mM NaCl, 3 mM KCl, 0.05% TWEEN 20 detergent, 10 mM phosphate buffer, pH 7.4 at 25°C) (PBS-TWEEN® tablets, Calbiochem- Merck, Darmstadt, Germany) to remove glutaraldehyde by centrifugation at 5,000 g for 5 min at room temperature. The pellets were resuspended in Milli-Q water and immediately applied on glass slides and air-dried for 1 h. The slides were dipped quickly and gently washed stepwise with ethanol from 50, 70, and 90–100% for dehydration. For SEM analysis, the prepared slides were sputtered with a gold layer of 15 nm thickness before SEM imaging (Sputter coater: Quorum Q150R ES, Quorum Technologies Ltd., East Grinstead, United Kingdom) and kept in a closed box at room temperature.

To prepare samples of EVs for SEM analysis, 0.5 ml EVs (about 10^7 particles/ml) were fixed with glutaraldehyde at a final concentration of 2% for 5 min at room temperature. Subsequently, the samples were washed in PBS-TWEEN solution by an ultracentrifuge step at 200,000 g for 30 min at 4°C. Further steps were performed similarly to the preparation of stimulated RBCs described above. For SEM imaging (EVO HD15, Carl Zeiss Microscopy GmbH, Jena, Germany), several randomly selected frames from each sample were captured for morphological observation and statistical purposes. SEM imaging was carried out using a 5 kV acceleration voltage and a secondary electron (SE) detector.

Size and Zeta Potential Measurement

Zetasizer Nano ZS (Malvern, Worcestershire, United Kingdom) was used for EVs size and zeta potential measurement. Uniform polystyrene particles of 100, 200, and 400 nm diameter (Bangs Laboratories, Thermo Fishers Scientific, United States) at 0.01% in PBS were used to verify instrument operation. For size measurement, the EV samples were diluted in Milli-Q water (attenuator index position in the range from 7 to 9) and analyzed using the standard operation procedure (SOP) as follows: sample refractive index 1.43 (phospholipid liposomes), dispersant refractive index 1.33 (water), system temperature at 25°C, and sample equilibration time for 60 s. One millimeter of each sample was measured in disposable polystyrene (DTS0012, Malvern Instruments, Worcestershire, United Kingdom) with a path length of 10 mm. Observed populations of particles were characterized by associated Z-average size (nm) and polydispersity index (PDI).

For zeta potential measurement, the disposable capillary cell DTS1070 (Malvern Instruments, United Kingdom) was used. Samples were measured in PBS-TWEEN solution. The SOP was set up similarly as described above. Each sample was measured 3 times with a maximum of 100 runs in automatic mode. Observed populations of particles were characterized by associated phase (rad) and zeta potential (mV). The Malvern Zetasizer software v7.03 was used to collect and analyze the data.

Statistics

All experiments were repeated at least three times. Data were presented as the mean values \pm SD of at least 3 independent experiments. Statistical analysis was performed using Student's *t*-test when Gaussian distributed. Differences were considered significant when $p < 0.05$ or $p < 0.01$, otherwise, a Mann-Whitney test was performed.

RESULTS

Stimulation, Isolation, and Characterization of Red Blood Cell-Extracellular Vesicles

To produce adequate RBC-EVs, RBCs (0.5% hematocrit) were treated with PMA as described. After 10 min of PMA treatment in the presence or absence of Ca^{2+} , RBCs were

deformed (**Figure 1A**) and changed their shapes to stomatocytes (**Figure 1B**). The stomatocyte shape was stable and correlated with the formation and shedding of EVs on the surface of the RBCs. The formation of EVs could be observed under a transmission light microscope after 10 min of stimulation, and the number of EVs was increased over time (**Figure 1C**). The stimulated RBCs and EVs adhered together to form a clot with EVs extruding on the outer surface (**Figure 1D**). SEM analysis showed that the EVs released from RBCs had an almost spherical shape and polydispersity in their size. Statistical analysis revealed that the size of EVs was in the range of 100–300 nm at an average value of about 200 nm (**Figure 1E**).

The EVs were collected by differential centrifugation as described above. After 60 min stimulated by PMA, the cell suspension was centrifuged at 1,500 g for 10 min to collect the EVs and remove intact cells. Size distribution analysis showed high heterogeneity in size in this fraction (**Figure 2A**). Size distribution of the fractions of EVs was ultracentrifuged at 200,000 g for 2 h at 4°C that showed an average value of 196.6 ± 43.4 nm (**Figure 2B**). Zeta potential analysis of EVs suspended in Milli-Q water (ultra-pure) showed a negative charge with an average value of -36.4 ± 7.8 mV (**Figure 2C**).

Loading Red Blood Cell-Extracellular Vesicles With DNA

The next step was to load the RBC-EVs with DNA plasmids by electroporation as described in “Materials and Methods” section. These DNA-EVs were investigated by the NanoSizer and by flow cytometry. For the NanoSizer analysis, the size distributions of RBC-EVs under different conditions were investigated. The effect of electroporation changed the size of EVs in the presence and absence of DNA plasmid (cp. **Figures 3A,B**) and also the DNA plasmid itself (cp. **Figures 3D,E**). There was a significant change in the size distribution of EVs after electroporation in the presence of DNA plasmid. The population of EVs or DNA-EVs included sub-populations with sizes in the ranges of 200, 700, and 6,000 nm (**Figure 3C**).

Flow cytometry analysis showed that electroporation was an effective approach for loading DNA into EVs. Under 2,000 V for 5 ms, the EVs showed positive fluorescent signals with Dil (**Figure 4Biii**) with a change of the structure in side scatter (**Figure 4B**) when compared with the control (**Figure 4A**). The positive signal of EVs with Picogreen suggested that these EVs were carrying DNA plasmid (**Figure 4Cii**). The double staining with both Picogreen and Dil showed that EVs could be loaded with DNA (DNA-EVs) and that electroporation was an effective loading procedure.

Transfection of Extracellular Vesicles With THP-1 Cell Lines

To test the ability of the DNA-EVs to release their cargo at putative target cells, M2 macrophages derived from THP-1 cells (as macrophage M2) were transfected with DNA-EVs (**Figure 5**). There was no significant fluorescence signal of green fluorescent protein (GFP) observed except the autofluorescence of cells during the transfection time up to 96 h (**Figure 5B**). During the

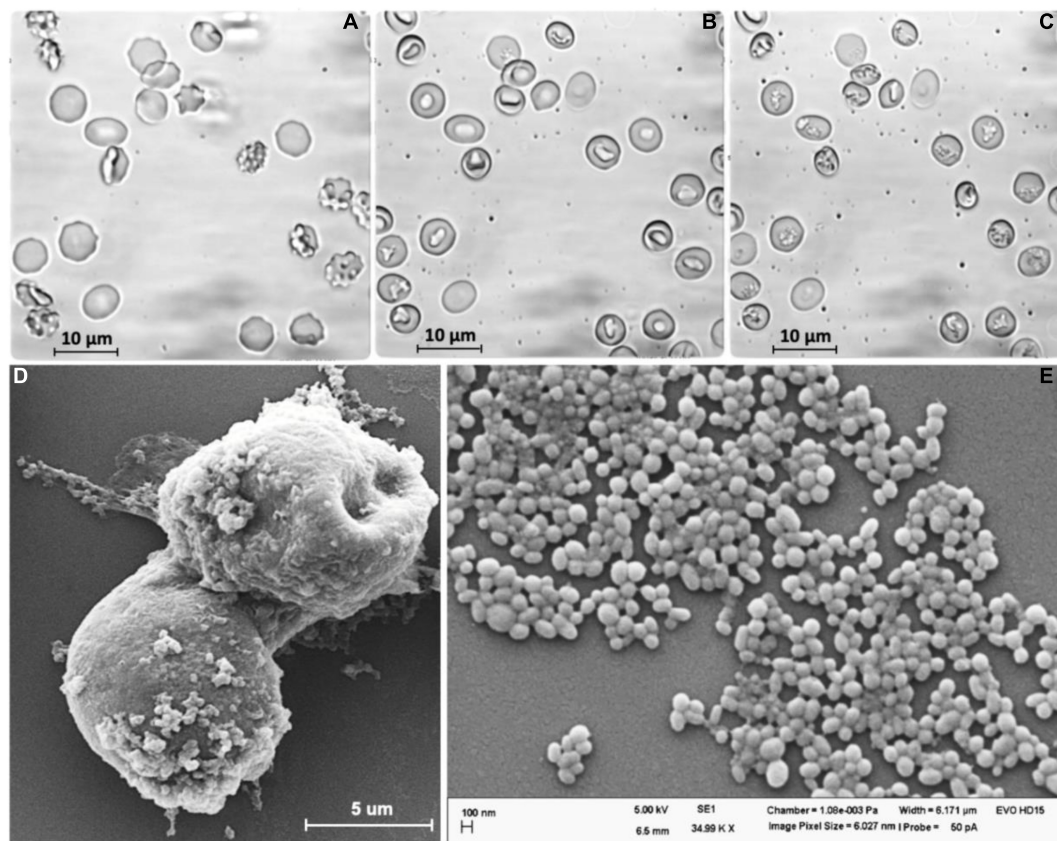


FIGURE 1 | Extracellular vesicles (EVs) were released from human red blood cells (RBCs) stimulated by PMA (6 μ M) after (A) 0 min, (B) 15 min, and (C) 60 min. (D) SEM analysis of stimulated RBCs treated by PMA after 60 min. (E) EVs released from RBCs.

culture, macrophages attached to cell culture surfaces showed the amoeboid movement with stretching filopodia to engulf surrounding particles (**Figure 5D**). In addition, the ratio of dead cells stained with trypan blue was relatively low within 72 h under experimental conditions. However, after 96 h of transfection, some macrophages showed apoptotic signals, such as cytoplasmic vacuolization, swollen endoplasmic reticulum, and cell blebbing (**Figure 5I**). Although the expression of GFP was observed in a sub-population of cells, however, the expression was not stable. In many trials, the transfection efficiency was low and the expression was significantly reduced after 48 h (**Figure 5E**).

Although we could show that DNA-EVs can be taken up by the phagocytic active macrophages, it would be interesting to see if this uptake could be reduced by treating the EVs with annexin V protein. This should shield the “eat me signal” by the exposure of PS on the outer membrane leaflet of the EVs. As shown in **Figure 6**, the treatment with annexin V protein could not prevent the DNA-MV uptake by the macrophages, as the number of remaining EVs after different time intervals. The controls (DNA-EVs) were stable and slightly reduced within 48 h. However, after 12 h of transfection with macrophages M2, the number of EVs in the culture was reduced tremendously, the remaining DNA-EVs and DNA-EVs-AnV were about 60 and 62%, respectively. After 24 h, EVs were almost captured and

engulfed by macrophages. There was no significant difference between the number of remaining DNA-EVs and DNA-EVs-AnV for all the time courses of transfection ($p > 0.05$; **Figure 6**).

DISCUSSION

During erythropoiesis, physiological cellular aging, disease conditions, and in response to environmental stressors, RBCs release EVs that include both endosome-derived exosomes and plasma-membrane-derived microvesicles (Thangaraju et al., 2020). Mature RBCs are anucleated cells without membrane-enclosed organelles. Therefore, RBC-EVs can be potentially used as a vehicle for DNA transport. It has been known that the formation of EVs is triggered by shedding of cell membrane caused by various factors, such as increased intracellular Ca^{2+} concentration, activation of PKC (Tissot et al., 2013; Nguyen et al., 2016; Thangaraju et al., 2020), disruption of erythrocyte skeleton-membrane attachment, aging-associated oxidative stress, ATP depletion (Asaro et al., 2018; Sudnitsyna et al., 2020), storage lesion (Leal et al., 2018; Prudent et al., 2018; Hashemi Tayer et al., 2019; Yoshida et al., 2019; Freitas Leal et al., 2020), and certain diseases (Regev-Rudzki et al., 2013; Jansen et al., 2017).

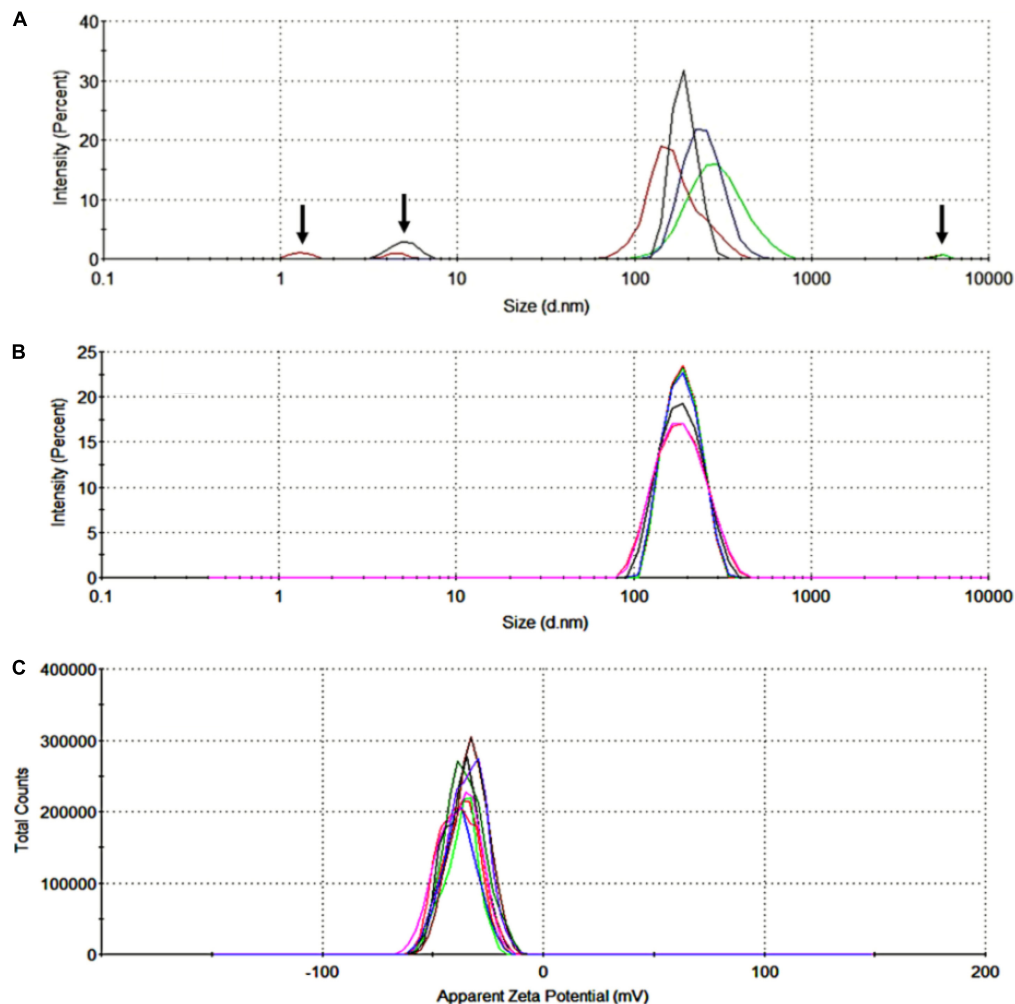


FIGURE 2 | Size distribution and zeta potential of red blood cell-derived extracellular vesicles (RBC-EVs) stimulated by PMA. **(A)** The highly heterogeneous in size of RBC-EVs, the arrows indicated large particles (cell debris or apoptotic blebs) and fine particles (dust or noise), **(B)** size distribution by the intensity of EVs collected in the fractions of ultra-centrifuged at 200,000 g for 2 h (overlay of 6 separated measurements), **(C)** zeta potential distribution of EVs (overlay of 10 separated measurements).

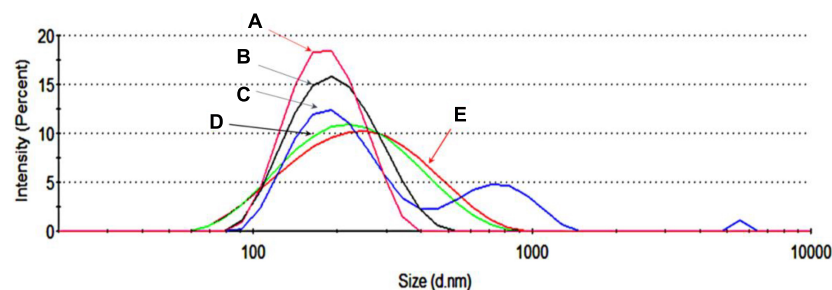


FIGURE 3 | Size distribution by the intensity of extracellular vesicles (EVs) under different conditions. **(A)** EVs in PBS-TWEEN solution. **(B)** Electroporated EVs without DNA. **(C)** Electroporated EVs with DNA. **(D)** DNA dissolved in MQ water. **(E)** Electroporated DNA without EVs.

In the case of RBCs, the formation of EVs *in vivo* is believed as a homeostatic process to remove damaged cell constituents, such as oxidized hemoglobin and damaged membrane constituents,

thereby prolonging their lifespan (Leal et al., 2018). However, it has been proved that RBC-derived EVs are not homogeneous in their size and content (Tissot et al., 2013; Marcoux et al., 2016;

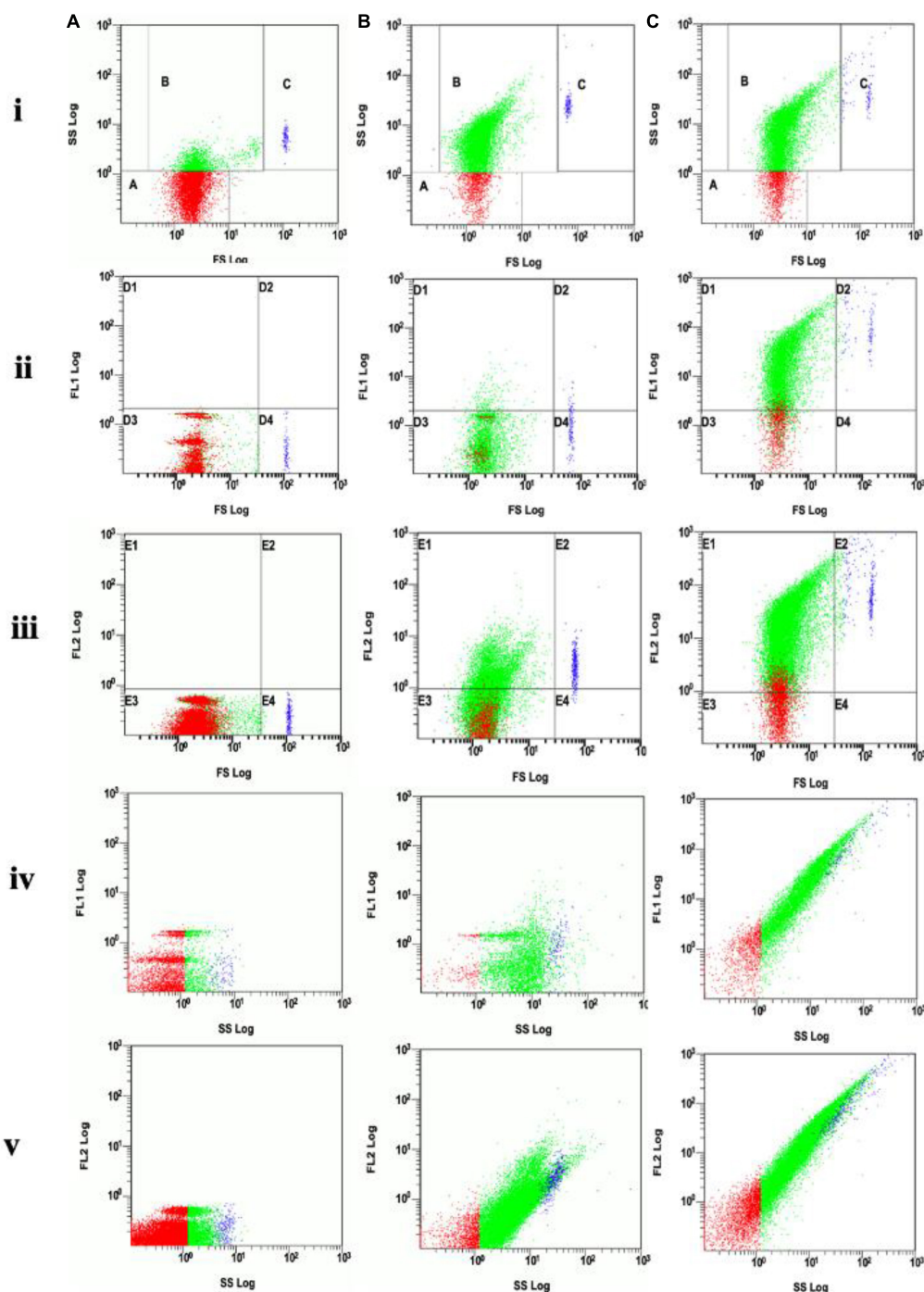


FIGURE 4 | (A) Analysis of EVs without electroporation (control). **(B)** Analysis of DNA-electroporated extracellular vesicles (EVs) stained with lipophilic DiI fluorescent dye, the EVs showing positive fluorescence signal was distributed in gates E1 and E2 of the FL2 channel. **(C)** Analysis of DNA-electroporated EVs double-stained with both Picogreen and lipophilic DiI fluorescent dyes. EVs showing positive fluorescence signal distributed in gates D1 and D2 in the FL1 channel (for Picogreen) and in gates E1 and E2 in the FL2 channel (for DiI). On each row, **(i)** the forward scatter (FS) vs. side scatter (SS), gate A containing dust/noise, gate B containing EVs and gate C containing large or aggregated EVs, **(ii)** FL1 vs. FS, **(iii)** FL2 vs. FS, **(iv)** FL1 vs. SS, and **(v)** FL2 vs. SS.

Freitas Leal et al., 2020). In this study, RBC-EVs were artificially produced by stimulating RBCs with PMA with a sufficient number within 2 h in a reproducible manner. Activation of PKC

by PMA led to the formation and release of EVs from human RBCs and could be observed after 10 min treatment and the density of EVs significantly increased within 60 min (**Figure 1**).

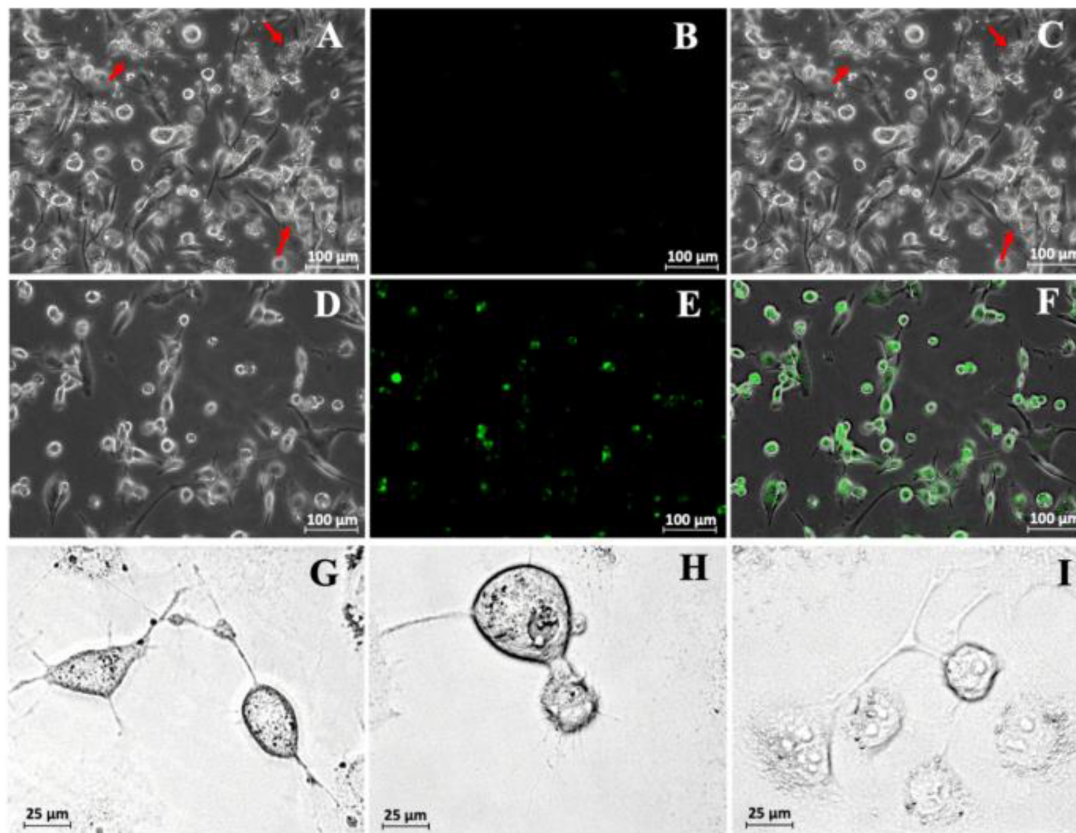


FIGURE 5 | (A) Transfection of THP-1-derived macrophage M2 with DNA-extracellular vesicles (EVs). A bright-field image was taken just after the infection of DNA-EVs. The red arrows indicate the DNA-EVs adhered together with macrophages and also on cell culture surfaces. (B) Fluorescence image with no green signal. (C) Overlay of bright-field and fluorescence images. Further images were taken after 36 h transfection: bright field (D), fluorescence (E), overlay (F). Images to see the stretch of macrophage arms to capture EVs on the cell culture surfaces were taken after 6 h (G), 12 h (H), and 96 h (I) transfection.

This process likely involved the activity of the PKC α and the TRPC6 channel (Wagner-Britz et al., 2013; Wang et al., 2021).

It has been known that mature RBCs do not have organelles, so RBC-EVs can be considered as the ideal vehicle for carrying and transporting macromolecules or therapeutic drugs to target cells. As RBCs are the most abundant cells in our body, representing above 80% of all the cells in an average adult human being (Kuo et al., 2017; Della Pelle and Kostevšek, 2021), therefore, it is relatively simple and rapid to prepare a large amount of EVs for research and treatment without requiring cell culture. In addition, this becomes more advantageous in the case of personalized medicine when the EVs can be isolated directly from individual patients. Currently, RBC-EVs are also provided by Cellarcus Biosciences Inc., as research materials with an average size of 140 nm (in the range from 80 to 210 nm). The Cellarcus' human red blood cell-derived vesicles are prepared from RBCs induced by a Ca²⁺ selective ionophore. Vesicles are isolated from cells and debris *via* centrifugation and provided at a concentration of 10⁷ vesicles/ μ l.

At present, the classification of the subsets of EVs is still difficult due to the lack of EV-specific “markers” that enable to distinguish these subsets from each other (Lötvall et al., 2014;

Witwer et al., 2017; Witwer and Théry, 2019). Because RBC-EVs are highly heterogeneous in size, morphology, and metabolomic components (Tissot et al., 2013; Lötvall et al., 2014; Murphy et al., 2019) and there is no currently “gold-standard” method to isolate or purify EVs. Therefore, in some cases, the isolated EVs may contain a mixture of different subsets of EVs (Cvjetkovic et al., 2014; Lötvall et al., 2014).

For a period of time, RBC-EVs have been thought to be cellular garbage sacs, however, various types of microRNAs were recently found in RBCs and their released EVs (Sun et al., 2020). Therefore, the roles of RBC-EVs could go far beyond the current understanding. However, in our study, the recognition and clearance of RBC-EVs by M2 macrophages (Figures 5, 6) suggested that the erythrophagocytosis by macrophages could be a barrier to the application of RBC-EVs in practice.

In the era of gene therapy, the delivery of nucleic acids, such as the small interfering RNA (siRNA), mRNA, or plasmid DNA in target cells, is a challenge with numerous implementations under development (Kaestner et al., 2015). Liposomes have been most widely applied as carriers because they are easy to synthesize and modify their characters to change their form, rigidity, permeability, retention, or conjugation with stealth

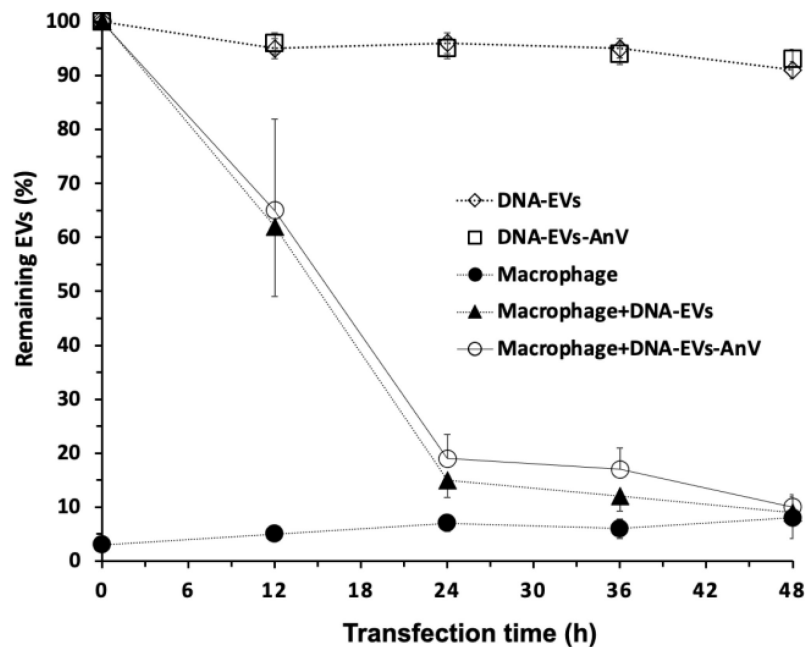


FIGURE 6 | Remaining EVs after infection to THP-1 cells. (♦) DNA-extracellular vesicles (EVs; (EVs containing DNA plasmids) were stable within 48 h. (◻) DNA-EVs treated with Annexin V protein. (●) THP-1-derived macrophages M2. (▴) DNA-EVs infected with macrophages M2. (○) DNA-EVs coated with Annexin V protein infected to THP-1 cells.

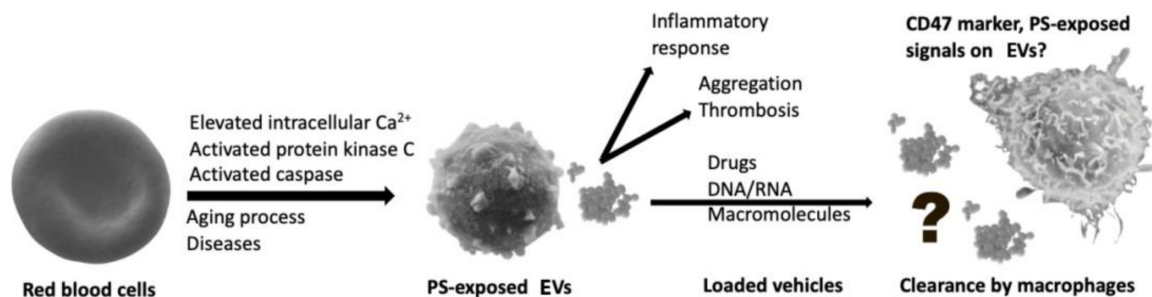


FIGURE 7 | Macrophages act as a barrier to recognize and eliminate red blood cell-derived extracellular vesicles (RBC-EVs).

polymers (Della Pelle and Kostevšek, 2021). Recently, the mRNA vaccines against severe acute respiratory syndrome coronavirus 2 (SARS-CoV-2) of Pfizer/BioNTech and Moderna were protected and delivered effectively to the target cells by 1,2-dimyristoyl-sn-glycero-3-phosphocholine liposomes. Doxorubicin (Doxil® or Caelyx®) and amphotericin B (under commercial name AmBisome®, and MM-398®/Onivyde) were also encapsulated by liposomes. However, artificial nanoparticles prepared by polymeric, dendrimeric, liposomal, or combinatory approaches are often recognized as non-self by the immune system (antibody or macrophages) (Della Pelle and Kostevšek, 2021). So far, it is difficult to synthesize inert nano-carriers, therefore, an effort to prepare nano-bio materials as vehicles for macromolecules or drug transport should be focused on. At present, most nucleic acid carriers have a cationic charge to maximize the stability of the formulation and to enhance cell delivery

(Jiang and Thayumanavan, 2020), while there are some concerns about toxicity. Therefore, neutral or mildly anionic materials to entrap or carry nucleic acid have been started to be investigated, to ensure better biocompatibility, and broaden the application range (Della Pelle and Kostevšek, 2021).

Although liposome formulations remain the most used, cell-based drug-delivery systems, EVs could bring friendly vehicles or even be self-originated for personal medicine (Ryu et al., 2014). Using the vehicle structures from the body's cells, as drug delivery systems is a promising strategy to overcome the limitations of existing drug-delivery approaches. RBC ghosts have been studied for intracellular delivery of genetic materials, drug delivery as a vascular carrier (Muzykantov, 2010). As empty sacs, biotherapeutic agents can be encapsulated in and the cell membrane may serve as a surface to reduce immune reaction to these agents or protect from pathways of

inactivation (Villa et al., 2016). The membrane of ghost cells can be considered, from the drug delivery system point of view, perfect stealth, biocompatible, highly elastic, and deformable made of phospholipids and cholesterol. As particles shed directly from the cell membrane and possess a small size at the nanoscale, spherical shape, surface potential, and membrane permeability, the vesicles can be exploited to deliver particular molecules by loading them *ex vivo* (Zhang et al., 2018; Zipkin, 2020). RBC-EVs draw the attention of the scientific community due to their ability to cargo nucleic acid, drugs, or biotherapeutic agents (Sun et al., 2020).

One of the focusing points for developing a reliable, stable drug delivery system is the loading of nucleic acid, drug, or bioactive compounds into the EVs. Recent studies showed that the exosome is an outstanding platform candidate for cargo delivery (Mandal, 2016; Maas et al., 2017; Usman et al., 2018; Gangadaran and Anh, 2020; Della Pelle and Kostevšek, 2021; Gutierrez-Millan et al., 2021). Various strategies have been developed for loading materials into exosomes, e.g., by incubation, the desired cargo can be diffused across membrane structures and packaged within exosomes (Fu et al., 2020; Han et al., 2021). Nucleic acids can be loaded into EVs by transfection-based strategy or physical treatments, such as electroporation, sonication, and surfactant treatment that facilitate cargo loading (Fu et al., 2020; Xu et al., 2020; Han et al., 2021). For the present study, electroporation at 2 kV for 5 s was suitable for loading of DNA plasmid to RBC-EVs (Figure 3). However, electroporation led to an increase of PdI that indicated the broad size distribution of DNA-EVs or contained large particles or aggregates (Figure 3C). Another study also proved that electroporation providing extra electrical fields produces micropores on the membrane of EVs to enhance permeability (Alvarez-Erviti et al., 2011). In our study, electroporation showed a simple and effective approach to load DNA plasmids into RBC-EVs that was proved by flow cytometry analysis with the fluorescent dyes Dil and Picogreen (Figure 4). Freeze-thaw treatment, extrusion, and dialysis may be applied to load cargo into EVs (Fu et al., 2020).

A general limitation of delivery systems is the recognition and elimination of foreign substances by the immune system. Biomimetic vehicles, such as cell membrane-derived carriers, may disguise cargo and escape from macrophage in the immune systems (Li et al., 2018; Sudnitsyna et al., 2020). CD47 was reported to involve the inhibition of phagocytosis of RBCs through the receptor signal regulatory protein alpha (SIRP α) (Hatherley et al., 2008; Kriebardis et al., 2008; D'Alessandro et al., 2010; Tissot et al., 2013; de Back et al., 2014). Another report also noted that CD47 did not only function as a “do not eat me” signal for uptake but can also act as an “eat me” signal (Burger et al., 2012). Therefore, it is questionable whether CD47 supports the escape of EVs from the clearance by macrophages. In the present study, the DNA-EVs were eliminated by macrophages M2 after 24–48 h transfection (Figure 5). In our study, although the signal of GFP was observed, the expression was observed in a subpopulation of cells. In addition, the expression was not constitutive and stable in many experiments, which might be due to the transient expression, low transfection efficiency, or

the erythrophagocytosis. In addition, the mechanism of the DNA uptake by THP-1 cells is still the question. It could be either whole EV taken up in an endocytotic manner or/and the EVs fused with the membrane and showing a transient expression in a sub-population of M2 macrophages was still a question. In reports, the transfection to THP-1 cells was more effective *via* viral transduction, such as a process mediated by lentivirus or herpes simplex virus (Ferreira et al., 2019; Venuti et al., 2019), and in some cases, the electroporation (nucleofection) would be also preferred (Maeß et al., 2014). To date, the mechanism of DNA carried by EVs and gene expression in THP-1 cells after EVs interacted with these cells remains to be elucidated.

In our study, the engulfment and clearance of EVs by macrophages M2 required further investigation in future research. A study on the efferocytosis of exosomes derived from T-cells by monocytes explained the clearance of those exosomes by the PS-related pathway (Wei et al., 2016). Treatment with annexin V inhibited the uptake of apoptotic cells by macrophages due to masking the exposure of PS (Bennett et al., 1995). In a study in mice, the treatment of exosomes with annexin V protein significantly reduced the clearance of macrophages up to 66% (Matsumoto et al., 2017). However, in our study, there was only a slight reduction of the density of EVs with no significant difference between EVs treated and untreated with annexin V protein ($p > 0.05$) (Figure 6).

It is worthwhile to mention that in contrast to the aforementioned finding, our study was performed *in vitro*. *In vivo* and *in vitro* conditions represent completely different interaction scenarios (flow vs. stasis) and different surrounding media (blood plasma vs. cell culture medium). Therefore, we cannot present an uptake mechanism and its putative regulation, which will be the subject of further research. Although the recognition and uptake of exosomes by macrophages have been investigated, studies on the interaction between receptors of macrophages with membrane proteins, PS, and other lipids of EVs require a better understanding (Mulcahy et al., 2014; Birge et al., 2016; Naeini et al., 2020; Figure 7).

Therefore, further studies should be carried out to clarify the roles of EVs in the homeostasis of RBCs and cell communication. Although RBC-EVs are vehicle structures from the body's cells, the use of these vehicles to cargo macromolecules for therapy or treatment is still a challenge. However, the GFP-coding plasmid resulted in a GFP expression in the macrophages. Although we have to admit that it was not the goal of our study, we could show that RBC-EVs in the way we designed them can be used as nucleic acid carriers if the immune system is addressed.

Further studies, e.g., using stable fluorescent dyes or radioactive isotopes to labeled DNA molecules, bioactive compounds, or drugs loaded into RBC-EVs are required to underline the fate of EVs and the delivery of cargos to the target cells. In addition, a study on the modification of RBC-EVs to hide from recognition and elimination of macrophages would contribute to developing cell-based systems for drug delivery or even self-originated for personalized medicine. In conclusion, the present study provides information for the physiological functions of RBC-EVs as well the potential for the application of these EVs as a cell-based delivery system.

DATA AVAILABILITY STATEMENT

The raw data supporting the conclusions of this article will be made available by the authors, without undue reservation.

ETHICS STATEMENT

The studies involving human participants were reviewed and approved by the Research Ethics Committees of the Saarland University (approval 63/11). Written informed consent for participation was not required for this study in accordance with the national legislation and the institutional requirements. The animal study was reviewed and approved by the Research Ethics Committees of the Saarland University (approval 63/11).

AUTHOR CONTRIBUTIONS

DN and IB conceived the idea. DN and HT designed the study, wrote the first manuscript draft, and analyzed the data. LK and IB provided materials and support. All authors contributed to write the manuscript. All authors

contributed to the article and approved the submitted version.

FUNDING

Furthermore, we acknowledge support by the Deutsche Forschungsgemeinschaft (DFG, German Research Foundation) and Saarland University within the funding program Open Access Publishing. The research has been funded by the Vietnam National University of Agriculture (VNUA), National Foundation for Science and Technology Development (NAFOSTED) under grant no. 106-YS.06-2013.16, and Researcher Links Travel Grant from British Council.

ACKNOWLEDGMENTS

We are grateful to the British Council for the travel grant and the hospitality support from the School of Life and Health Sciences, Aston University, Aston Triangle, Birmingham, United Kingdom. We thank to Y. Perrie and A. Devitt for their kindness in providing the biological material and scientific advice.

REFERENCES

- Akuma, P., Okagu, O. D., and Udenigwe, C. C. (2019). Naturally occurring exosome vesicles as potential delivery vehicle for bioactive compounds. *Front. Sustain. Food Syst.* 3:23. doi: 10.3389/fsufs.2019.00023
- Alaarg, A., Schiffelers, R. M., Van Solinge, W. W., and Van Wijk, R. (2013). Red blood cell vesiculation in hereditary hemolytic anemia. *Front. Physiol.* 4:365. doi: 10.3389/fphys.2013.00365
- Alvarez-Erviti, L., Seow, Y., Yin, H., Betts, C., Lakhal, S., and Wood, M. J. (2011). Delivery of siRNA to the mouse brain by systemic injection of targeted exosomes. *Nat. Biotechnol.* 29, 341–345. doi: 10.1038/nbt.1807
- Antonyak, M. A., and Cerione, R. A. (2015). Emerging picture of the distinct traits and functions of microvesicles and exosomes. *Proc. Natl. Acad. Sci. U.S.A.* 112, 3589–3590. doi: 10.1073/pnas.1502590112
- Asaro, R. J., Zhu, Q., and Cabrales, P. (2018). Erythrocyte aging, protection via vesiculation: an analysis methodology via oscillatory flow. *Front. Physiol.* 9:1607. doi: 10.3389/fphys.2018.01607
- Balachandran, B., Yuana, Y., and Schumacher, U. (2019). Extracellular vesicles-based drug delivery system for cancer treatment. *Cogent Med.* 6, 241–349. doi: 10.1080/2331205X.2019.1635806
- Bennett, M. R., Gibson, D. F., Schwartz, S. M., and Tait, J. F. (1995). Binding and phagocytosis of apoptotic vascular smooth muscle cells is mediated in part by exposure of phosphatidylserine. *Circ. Res.* 77, 1136–1142. doi: 10.1161/01.res.77.6.1136
- Bernhardt, I., Nguyen, D. B., Wesseling, M. C., and Kaestner, L. (2020). Intracellular Ca²⁺ concentration and phosphatidylserine exposure in healthy human erythrocytes in dependence on in vivo cell age. *Front. Physiol.* 10:1629. doi: 10.3389/fphys.2019.01629
- Birge, R. B., Boeltz, S., Kumar, S., Carlson, J., Wanderley, J., Calianese, D., et al. (2016). Phosphatidylserine is a global immunosuppressive signal in efferocytosis, infectious disease, and cancer. *Cell Death Differ.* 23, 962–978. doi: 10.1038/cdd.2016.11
- Bosman, G. J., Lasonder, E., Luten, M., Roerdinkholder-Stoelwinder, B., Novotný, V. M., Bos, H., et al. (2008). The proteome of red cell membranes and vesicles during storage in blood bank conditions. *Transfusion* 48, 827–835. doi: 10.1111/j.1537-2995.2007.01630.x
- Bunggulawa, E. J., Wang, W., Yin, T., Wang, W., Yin, T., Wang, N., et al. (2018). Recent advancements in the use of exosomes as drug delivery systems. *J. Nanobiotechnol.* 16:81. doi: 10.1186/s12951-018-0403-9
- Burger, P., Hilarius-Stokman, P., de Korte, D., van den Berg, T. K., and van Bruggen, R. (2012). CD47 functions as a molecular switch for erythrocyte phagocytosis. *Blood* 119, 5512–5521. doi: 10.1182/blood-2011-10-386805
- Butreddy, A., Kommineni, N., and Dudhipala, N. (2021). Exosomes as naturally occurring vehicles for delivery of biopharmaceuticals: insights from drug delivery to clinical perspectives. *Nanomaterials (Basel, Switzerland)* 11:1481. doi: 10.3390/nano11061481
- Chitoiu, L., Dobranici, A., Gherghiceanu, M., Dinescu, S., and Costache, M. (2020). Multi-omics data integration in extracellular vesicle biology-Utopia or future reality? *Int. J. Mol. Sci.* 21:8550. doi: 10.3390/ijms21228550
- Cvjetkovic, A., Lötvall, J., and Lässer, C. (2014). The influence of rotor type and centrifugation time on the yield and purity of extracellular vesicles. *J. Extracell. Vesicles* 3:1. doi: 10.3402/jev.v3.23111
- D'Alessandro, A., Righetti, P. G., and Zolla, L. (2010). The red blood cell proteome and interactome: an update. *J. Proteome Res.* 9, 144–163. doi: 10.1021/pr900831f
- Danesh, A., Inglis, H. C., Jackman, R. P., Wu, S., Deng, X., Muench, M. O., et al. (2014). Exosomes from red blood cell units bind to monocytes and induce proinflammatory cytokines, boosting T-cell responses in vitro. *Blood* 123, 687–696. doi: 10.1182/blood-2013-10-530469
- de Back, D., Kostova, E., van Kraaij, M., van den Berg, T., and van Bruggen, R. (2014). Of macrophages and red blood cells; a complex love story. *Front. Physiol.* 5:9. doi: 10.3389/fphys.2014.00009
- Della Pelle, G., and Kostevšek, N. (2021). Nucleic acid delivery with red blood cell-based carriers. *Int. J. Mol. Sci.* 22:5264. doi: 10.3390/ijms22105264
- Elsharkasy, O. M., Nordin, J. Z., Hagey, D. W., de Jong, O. G., Schiffelers, R. M., Andalousi, S. E. L., et al. (2020). Extracellular vesicles as drug delivery systems: why and how? *Adv. Drug. Deliv. Rev.* 159, 332–343. doi: 10.1016/j.addr.2020.04.004
- Ferreira, C. B., Sumner, R. P., Rodriguez-Plata, M. T., Rasaiyaah, J., Milne, R. S., Thrasher, A. J., et al. (2019). Lentiviral vector production titer is not limited in HEK293T by induced intracellular innate immunity. *Mol. Ther. Methods. Clin. Dev.* 17, 209–219. doi: 10.1016/j.omtm.2019.11.021

- Freitas Leal, J. K., Lasonder, E., Sharma, V., Schiller, J., Fanelli, G., Rinalducci, S., et al. (2020). Vesiculation of red blood cells in the blood bank: a multi-omics approach towards identification of causes and consequences. *Proteomes* 8:6. doi: 10.3390/proteomes8020006
- Fu, S., Wang, Y., Xia, X., and Zheng, J. C. (2020). Exosome engineering: current progress in cargo loading and targeted delivery. *NanoImpact* 20:100261. doi: 10.1016/j.impact.2020.100261
- Gangadaran, P., and Anh, B. C. (2020). Extracellular vesicle- and extracellular vesicle mimetics-based drug delivery systems: new perspectives, challenges, and clinical developments. *Pharmaceutics* 12:442. doi: 10.3390/pharmaceutics12050442
- Genin, M., Clement, F., Fattaccioni, A., Raes, M., and Michiels, C. (2015). M1 and M2 macrophages derived from THP-1 cells differentially modulate the response of cancer cells to etoposide. *BMC Cancer* 15:577. doi: 10.1186/s12885-015-1546-9
- Gurung, S., Perocheau, D., Touramanidou, L., and Baruteau, J. (2021). The exosome journey: from biogenesis to uptake and intracellular signalling. *Cell Commun. Signal.* 19:47. doi: 10.1186/s12964-021-00730-1
- Gutierrez-Millan, C., Calvo, D. C., Lanao, J. M., and Colino, C. I. (2021). Advances in exosomes-based drug delivery systems. *Macromol. Biosci.* 21:e2000269. doi: 10.1002/mabi.202000269
- Han, Y., Jones, T. W., Dutta, S., Zhu, Y., Wang, X., Narayanan, S. P., et al. (2021). Overview and update on methods for cargo loading into extracellular vesicles. *Processes* 9:356. doi: 10.3390/pr9020356
- Hashemi Tayer, A., Amirizadeh, N., Ahmadinejad, M., Nikougoftar, M., Deyhim, M. R., and Zolfaghari, S. (2019). Procoagulant activity of red blood cell-derived microvesicles during red cell storage. *Transfus. Med. Hemother.* 46, 224–230. doi: 10.1159/000494367
- Hatherley, D., Graham, S. C., Turner, J., Harlos, K., Stuart, D. I., and Barclay, A. N. (2008). Paired receptor specificity explained by structures of signal regulatory proteins alone and complexed with CD47. *Mol. Cell.* 31, 266–277. doi: 10.1016/j.molcel.2008.05.026
- Jansen, F., Nickenig, G., and Werner, N. (2017). Extracellular vesicles in cardiovascular disease: potential applications in diagnosis, prognosis, and epidemiology. *Circ. Res.* 120, 1649–1657. doi: 10.1161/CIRCRESAHA.117.310752
- Jiang, Z., and Thayumanavan, S. (2020). Noncationic material design for nucleic acid delivery. *Adv. Ther.* 3:1900206. doi: 10.1002/adtp.201900206
- Johnstone, R. M., Adam, M., Hammond, J. R., Orr, L., and Turbide, C. (1987). Vesicle formation during reticulocyte maturation. Association of plasma membrane activities with released vesicles (exosomes). *J. Biol. Chem.* 262, 9412–9420.
- Kaestner, L., Scholz, A., and Lipp, P. (2015). Conceptual and technical aspects of transfection and gene delivery. *Bioorg. Med. Chem. Lett.* 25, 1171–1176. doi: 10.1016/j.bmcl.2015.01.018
- Kanada, M., Bachmann, M. H., Hardy, J. W., Frimannson, D. O., Bronsart, L., Wang, A., et al. (2015). Differential fates of biomolecules delivered to target cells via extracellular vesicles. *Proc. Natl. Acad. Sci. U.S.A.* 112, E1433–E1442. doi: 10.1073/pnas.1418401112
- Kriebardis, A. G., Antonelou, M. H., Stamoulis, K. E., Economou-Petersen, E., Margaritis, L. H., and Papassideri, I. S. (2008). RBC-derived vesicles during storage: ultrastructure, protein composition, oxidation, and signaling components. *Transfusion* 48, 1943–1953. doi: 10.1111/j.1537-2995.2008.01794.x
- Kuo, W. P., Tigges, J. C., Toxavidis, V., and Ghiran, I. (2017). Red blood cells: a source of extracellular vesicles. *Methods Mol. Biol.* 1660, 15–22. doi: 10.1007/978-1-4939-7253-1_2
- Leal, J. K. F., Adjubo-Hermans, M. J. W., and Bosman, G. J. C. G. M. (2018). Red blood cell homeostasis: mechanisms and effects of microvesicle generation in health and disease. *Front. Physiol.* 9:703. doi: 10.3389/fphys.2018.00703
- Lee, Y., El Andaloussi, S., and Wood, M. J. (2012). Exosomes and microvesicles: extracellular vesicles for genetic information transfer and gene therapy. *Hum. Mol. Genet.* 21, R125–R134. doi: 10.1093/hmg/dd3317
- Li, C., Wang, J., Wang, Y., Gao, H., Wei, G., Huang, Y., et al. (2019). Recent progress in drug delivery. *Acta Pharm. Sin. B* 9, 1145–1162. doi: 10.1016/j.apsb.2019.08.003
- Li, S. P., Lin, Z. X., Jiang, X. Y., and Yu, X. Y. (2018). Exosomal cargo-loading and synthetic exosome-mimics as potential therapeutic tools. *Acta Pharmacol. Sin.* 39, 542–551. doi: 10.1038/aps.2017.178
- Li, X., Corbett, A. L., Taatizadeh, E., Tasnim, N., Little, J. P., Garnis, C., et al. (2019). Challenges and opportunities in exosome research-perspectives from biology, engineering, and cancer therapy. *APL Bioeng.* 3:011503. doi: 10.1063/1.5087122
- Lötvall, J., Hill, A. F., Hochberg, F., Buzás, E. I., Di Vizio, D., Gardiner, C., et al. (2014). Minimal experimental requirements for definition of extracellular vesicles and their functions: a position statement from the International Society for Extracellular Vesicles. *J. Extracell. Vesicles* 3:26913. doi: 10.3402/jev.v3.26913
- Maas, S. L. N., Breakefield, X. O., and Weaver, A. M. (2017). Extracellular vesicles: unique intercellular delivery vehicles. *Trends Cell. Biol.* 27, 172–188. doi: 10.1016/j.tcb.2016.11.003
- Macia, L., Nanan, R., Hosseini-Beheshti, E., and Grau, G. E. (2020). Host- and microbiota-derived extracellular vesicles, immune function, and disease development. *Int. J. Mol. Sci.* 21:107. doi: 10.3390/ijms21010107
- Maeß, M. B., Wittig, B., and Lorkowski, S. (2014). Highly efficient transfection of human THP-1 macrophages by nucleofection. *J. Vis. Exp.* 90:e51960. doi: 10.3791/51960
- Mandal, S. (2016). Curcumin, a promising anticancer therapeutic: its bioactivity and development of the drug delivery vehicles. *Int. J. Drug Res. Technol.* 6:2. doi: 10.1039/C3RA46396F
- Mantel, P. Y., Hoang, A. N., Goldowitz, I., Potashnikova, D., Hamza, B., Vorobjev, I., et al. (2013). Malaria-infected erythrocyte-derived microvesicles mediate cellular communication within the parasite population and with the host immune system. *Cell Host Microbe* 13, 521–534. doi: 10.1016/j.chom.2013.04.009
- Marcoux, G., Duchez, A. C., Cloutier, N., Provost, P., Nigrovic, P. A., and Boilard, E. (2016). Revealing the diversity of extracellular vesicles using high-dimensional flow cytometry analyses. *Sci. Rep.* 6:35928. doi: 10.1038/srep35928
- Matsumoto, A., Takahashi, Y., Nishikawa, M., Sano, K., Morishita, M., Charoenviriyakul, C., et al. (2017). Role of phosphatidylserine-derived negative surface charges in the recognition and uptake of intravenously injected B16BL6-derived exosomes by macrophages. *J. Pharm. Sci.* 106, 168–175. doi: 10.1016/j.xphs.2016.07.022
- Mulcahy, L. A., Pink, R. C., and Carter, D. R. (2014). Routes and mechanisms of extracellular vesicle uptake. *J. Extracell. Vesicles* 3:10.3402/jev.v3.24641. doi: 10.3402/jev.v3.24641
- Murphy, D. E., de Jong, O. G., Brouwer, M., Wood, M. J., Lavie, G., Schiffelers, R. M., et al. (2019). Extracellular vesicle-based therapeutics: natural versus engineered targeting and trafficking. *Exp. Mol. Med.* 51, 1–12. doi: 10.1038/s12276-019-0223-5
- Muzykantor, V. R. (2010). Drug delivery by red blood cells: vascular carriers designed by mother nature. *Expert Opin. Drug. Deliv.* 7, 403–427. doi: 10.1517/17425241003610633
- Naeini, M. B., Bianconi, V., Pirro, M., and Sahebkar, A. (2020). The role of phosphatidylserine recognition receptors in multiple biological functions. *Cell Mol. Biol. Lett.* 25:23. doi: 10.1186/s11658-020-00214-z
- Nguyen, D. B., Ly, T. B., Wesseling, M. C., Hittinger, M., Torge, A., Devitt, A., et al. (2016). Characterization of microvesicles released from human red blood cells. *Cell Physiol. Biochem.* 38, 1085–1099. doi: 10.1159/000443059
- Nguyen, D. B., Ly, T. B. T., and Bernhardt, I. (2017). “Microvesicles released from human red blood cells: properties and potential applications,” in *Novel Implications of Exosomes in Diagnosis and Treatment of Cancer and Infectious Diseases*, ed. J. Wang (London: InTechOpen). doi: 10.5772/intechopen.69599
- Noubouossie, D. F., Henderson, M. W., Mooberry, M., Ilich, A., Ellsworth, P., Piegore, M., et al. (2020). Red blood cell microvesicles activate the contact system, leading to factor IX activation via 2 independent pathways. *Blood* 135, 755–765. doi: 10.1182/blood.2019001643
- Piccinini, F., Tesi, A., Arienti, C., and Bevilacqua, A. (2017). Cell counting and viability assessment of 2D and 3D cell cultures: expected reliability of the trypan blue assay. *Biol. Proced. Online* 19:8. doi: 10.1186/s12575-017-0056-3
- Prudent, M., Delobel, J., Hübner, A., Benay, C., Lion, N., and Tissot, J. D. (2018). Proteomics of stored red blood cell membrane and storage-induced microvesicles reveals the association of flotillin-2 with band 3 complexes. *Front. Physiol.* 9:421. doi: 10.3389/fphys.2018.00421

- Raposo, G., and Stoorvogel, W. (2013). Extracellular vesicles: exosomes, microvesicles, and friends. *J. Cell. Biol.* 200, 373–383. doi: 10.1083/jcb.201211138
- Regev-Rudzki, N., Wilson, D. W., Carvalho, T. G., Sisquella, X., Coleman, B. M., Rug, M., et al. (2013). Cell-cell communication between malaria-infected red blood cells via exosome-like vesicles. *Cell* 153, 1120–1133. doi: 10.1016/j.cell.2013.04.029
- Ryu, J. H., Lee, S., Son, S., Kim, S. H., Leary, J. F., Choi, K., et al. (2014). Theranostic nanoparticles for future personalized medicine. *J. Control. Release* 190, 477–484. doi: 10.1016/j.jconrel.2014.04.027
- Sudnitsyna, J., Skverchinskaya, E., Dobrylko, I., Nikitina, E., Gambaryan, S., and Mindukshev, I. (2020). Microvesicle formation induced by oxidative stress in human erythrocytes. *Antioxidants* 9:929. doi: 10.3390/antiox9100929
- Sun, L., Yu, Y., Niu, B., and Wang, D. (2020). Red blood cells as potential repositories of microRNAs in the circulatory system. *Front. Genet.* 11:442. doi: 10.3389/fgene.2020.00442
- Thangaraju, K., Neerukonda, S. N., Katneni, U., and Buehler, P. W. (2020). Extracellular vesicles from red blood cells and their evolving roles in health, coagulopathy and therapy. *Int. J. Mol. Sci.* 22:153. doi: 10.3390/ijms22010153
- Tissot, J. D., Canellini, G., Rubin, O., Angelillo-Scherrer, A., Delobel, J., Prudent, M., et al. (2013). Blood microvesicles: from proteomics to physiology. *Transl. Proteomics* 1, 38–52. doi: 10.1016/j.trprot.2013.04.004
- Usman, W. M., Pham, T. C., Kwok, Y. Y., Vu, L. T., Ma, V., Peng, B., et al. (2018). Efficient RNA drug delivery using red blood cell extracellular vesicles. *Nat. Commun.* 9:2359. doi: 10.1038/s41467-018-04791-8
- Van der Meijden, P. E. J., Van Schilfgaarde, M., Van Oerle, R., Renné, T., ten Cate, H., and Spronk, H. M. H. (2012). Platelet- and erythrocyte-derived microparticles trigger thrombin generation via factor XIIa. *J. Thromb. Haemost.* 10, 1355–1362. doi: 10.1111/j.1538-7836.2012.04758.x
- Van Niel, G., D'Angelo, G., and Raposo, G. (2018). Shedding light on the cell biology of extracellular vesicles. *Nat. Rev. Mol. Cell Biol.* 19, 213–228. doi: 10.1038/nrm.2017.125
- Venuti, A., Musarra-Pizzo, M., Pennisi, R., Tankov, S., Medici, M. A., Mastino, A., et al. (2019). HSV-1/EGFP stimulates miR-146a expression in a NF-κB-dependent manner in monocytic THP-1 cells. *Sci. Rep.* 9:5157. doi: 10.1038/s41598-019-41530-5
- Villa, C. H., Anselmo, A. C., Mitragotri, S., and Muzykantov, V. (2016). Red blood cells: supercarriers for drugs, biologicals, and nanoparticles and inspiration for advanced delivery systems. *Adv. Drug Deliv. Rev.* 106(Pt A), 88–103. doi: 10.1016/j.addr.2016.02.007
- Wagner-Britz, L., Wang, J., Kaestner, L., and Bernhardt, I. (2013). Protein kinase Cα and P-type Ca channel CaV2.1 in red blood cell calcium signalling. *Cell. Physiol. Biochem.* 31, 883–891. doi: 10.1159/000350106
- Wang, J., Hertz, L., Ruppenthal, S., El Nemer, W., Connes, P., Goede, J. S., et al. (2021). Lysophosphatidic acid-activated calcium signaling is elevated in red cells from sickle cell disease patients. *Cells* 10:456. doi: 10.3390/cells10020456
- Wei, X., Liu, C., Wang, H., Wang, L., Xiao, F., Guo, Z., et al. (2016). Surface phosphatidylserine is responsible for the internalization on microvesicles derived from hypoxia-induced human bone marrow mesenchymal stem cells into human endothelial cells. *PLoS One* 11:e0147360. doi: 10.1371/journal.pone.0147360
- Witwer, K. W., Soekmadji, C., Hill, A. F., Wauben, M. H., Buzás, E. I., Di Vizio, D., et al. (2017). Updating the MISEV minimal requirements for extracellular vesicle studies: building bridges to reproducibility. *J. Extracell. Vesicles* 6:1396823. doi: 10.1080/20013078.2017.1396823
- Witwer, K. W., and Théry, C. (2019). Extracellular vesicles or exosomes? On primacy, precision, and popularity influencing a choice of nomenclature. *J. Extracell. Vesicles* 8:1648167. doi: 10.1080/20013078.2019.1648167
- Wu, M., Ouyang, Y., Wang, Z., Zhang, R., Huang, P. H., Chen, C., et al. (2017). Isolation of exosomes from whole blood by integrating acoustics and microfluidics. *Proc. Natl. Acad. Sci. U.S.A.* 114, 10584–10589. doi: 10.1073/pnas.1709210114
- Xu, M., Yang, Q., Sun, X., and Wang, Y. (2020). Recent advancements in the loading and modification of therapeutic exosomes. *Front. Bioeng. Biotechnol.* 8:586130. doi: 10.3389/fbioe.2020.586130
- Yoshida, T., Prudent, M., and D'Alessandro, A. (2019). Red blood cell storage lesion: causes and potential clinical consequences. *Blood Transfus.* 17, 27–52. doi: 10.2450/2019.0217-18
- Zeicher, D., Cumpelik, A., and Schifferli, J. A. (2014). Erythrocyte-derived microvesicles amplify systemic inflammation by thrombin-dependent activation of complement. *Arterioscler. Thromb. Vasc. Biol.* 34, 313–320. doi: 10.1161/ATVBAHA.113.302378
- Zhang, D. X., Kiomourtzis, T., Lam, C. K., and Le, M. T. N. (2018). “The biology and therapeutic applications of red blood cell extracellular vesicles,” in *Erythrocyte*, ed. A. Tombak (London: IntechOpen). doi: 10.5772/intechopen.81758
- Zipkin, M. (2020). Big pharma buys into exosomes for drug delivery. *Nat. Biotechnol.* 38, 1226–1228. doi: 10.1038/s41587-020-0725-7

Conflict of Interest: The authors declare that the research was conducted in the absence of any commercial or financial relationships that could be construed as a potential conflict of interest.

Publisher's Note: All claims expressed in this article are solely those of the authors and do not necessarily represent those of their affiliated organizations, or those of the publisher, the editors and the reviewers. Any product that may be evaluated in this article, or claim that may be made by its manufacturer, is not guaranteed or endorsed by the publisher.

Copyright © 2022 Nguyen, Tran, Kaestner and Bernhardt. This is an open-access article distributed under the terms of the Creative Commons Attribution License (CC BY). The use, distribution or reproduction in other forums is permitted, provided the original author(s) and the copyright owner(s) are credited and that the original publication in this journal is cited, in accordance with accepted academic practice. No use, distribution or reproduction is permitted which does not comply with these terms.



Membrane Localization of Piezo1 in the Context of Its Role in the Regulation of Red Blood Cell Volume

Bojan Božič¹ and Saša Svetina^{1,2*}

¹Institute of Biophysics, Faculty of Medicine, University of Ljubljana, Ljubljana, Slovenia, ²Jožef Stefan Institute, Ljubljana, Slovenia

Piezo1 is a membrane nonspecific cation channel involved in red blood cells (RBCs) in the regulation of their volume. Recently, it was shown that it is distributed on the RBC membrane in a nonuniform manner. Here it is shown that it is possible to interpret the lateral distribution of Piezo1 molecules on RBC membrane by the curvature dependent Piezo1—bilayer interaction which is the consequence of the mismatch between the intrinsic principal curvatures of the Piezo1 trimer and the principal curvatures of the membrane at Piezo1's location but without its presence. This result supports the previously proposed model for the role of Piezo1 in the regulation of RBC volume.

OPEN ACCESS

Edited by:

Giampaolo Minetti,
University of Pavia, Italy

Reviewed by:

Egee Stéphane,
UMR8227 Laboratoire de Biologie
Intégrative des Modèles Marins,
France

Robert Asaro,
University of California, San Diego,
United States

*Correspondence:

Saša Svetina
sasa.svetina@mf.uni-lj.si

Specialty section:

This article was submitted to
Red Blood Cell Physiology,
a section of the journal
Frontiers in Physiology

Received: 18 February 2022

Accepted: 29 April 2022

Published: 20 May 2022

Citation:

Božič B and Svetina S (2022)
Membrane Localization of Piezo1 in the
Context of Its Role in the Regulation of
Red Blood Cell Volume.
Front. Physiol. 13:879038.
doi: 10.3389/fphys.2022.879038

Keywords: lateral distribution, membrane curvature, channel, intrinsic curvature, discocyte, membrane permeability, spontaneous curvature

INTRODUCTION

Piezo1 is a mechanosensitive nonspecific cation membrane channel present in a variety of tissues where it plays a significant role in various physiological processes (Murthy et al., 2017; Lai et al., 2021). In the red blood cell (RBC) it is involved in regulating cell's volume, as evidenced by the fact that mutations resulting in its gain of function cause hereditary xerocytosis, a disease characterized by the subnormal RBC volume (Zarychanski et al., 2012). RBC volume depends on cell's content of potassium ions (K^+) established by the balance between their Na^+-K^+ -ATPase driven influx and their passive efflux (Hoffmann et al., 2009). It has been demonstrated that Piezo1 affects the latter, in a manner such that its transient opening causes an influx of calcium ions that subsequently activate the specific K^+ permeating Gárdos channels (Cahalan et al., 2015). Recently, it was revealed, by high-resolution atomic force and confocal microscopy studies, that the area density of Piezo1 molecules varies along the RBC discocyte membrane in a nonuniform manner, in that it is larger than the average in regions of its poles (in dimples) and smaller than the average in the region of its rim (Dumitru et al., 2021).

A similar nonuniform lateral distribution of Piezo1 as revealed by Dumitru et al. (2021) was a crucial element of the model of a possible mechanism of the Piezo1—governed regulation of the RBC volume (Svetina et al., 2019; Svetina, 2020). The latter model was based on previously established effect of Piezo1 on the RBC efflux of potassium ions and the assumption that the Piezo1—born permeability for cations depends, on average, on the curvature of the membrane at Piezo1's location but without its presence. The reason for such dependence was sought in the mismatch between the membrane principal curvatures and the intrinsic principal curvatures of the Piezo1 trimer. According to this type of mismatch, the Piezo1 molecules would i), because of their curved structure (Ge et al., 2012; Guo and MacKinnon, 2017; Saotome et al., 2018; Zhao et al., 2018), tend to accumulate in the RBC discocyte shape in the region of its poles, and ii), have a smaller probability to transform into their permeable state. The model predicted the establishment of a

negative feedback loop between the RBC reduced volume (volume divided by the volume of a sphere with its surface area equal to the area of RBC membrane) and the average permeability of RBC membrane for the potassium ions. In this model, the action of Piezo1 on K^+ efflux depends on the RBC discoid shape.

The aim of the present work is to demonstrate the consistency between the basic assumptions of the noted model (Svetina et al., 2019) and the observed Piezo1 membrane localization (Dumitru et al., 2021). In addition, the magnitude of the parameters that describe the interaction between Piezo1 and its bilayer environment will be estimated. The coupling between RBC shape and the lateral distribution of Piezo1 molecules will be analyzed by minimizing the membrane energy involving the bending energy of the membrane and the free energy of the freely moving membrane inclusions by a procedure developed earlier (Božič et al., 2006). In the free energy of inclusions the Piezo1—bilayer interaction will be described by the general phenomenological inclusion—bilayer interaction term (Kralj-Iglič et al., 1999) adapted for this specific case.

The section Theory and Methods will be devoted to a description of the applied theory. In Results we will first show the dependence of the system's behavior on model parameters. The consistency of the model of Piezo1 regulated RBC volume (Svetina et al., 2019) will be checked by investigating the dependence of RBC shape on the reduced volume by using the parameters giving rise to the Piezo1 lateral distribution that agrees with the experimentally determined Piezo1 membrane location (Dumitru et al., 2021). It will be shown how the discocyte RBC shape causes Piezo1 molecules to distribute along membrane in a nonuniform manner and, also, that there is a consequent modification of the cell shape. Finally, we will comment on how these results relate to the role of Piezo1 in the regulation of RBC volume.

THEORY AND METHODS

In the present analysis we follow the approach developed for studying shape behavior of vesicles whose membranes contain inclusions that are free to move in the plane of the membrane (Božič et al., 2006). Vesicle shape and the corresponding lateral distribution of inclusions are obtained by solving the shape equation that is the result of the minimization of the sum of the bending energy of the membrane (W_b) and the free energy of inclusions comprising a term describing their interaction with the surrounding membrane and a term due to the entropy of mixing (F_N).

Membrane bending energy is defined (Canham, 1970; Helfrich, 1973) as

$$W_b = 2k_c \int H^2 dA \quad (1)$$

where k_c is the bending modulus, H the mean membrane curvature, defined as the mean of the sum of membrane principal curvature C_1 and C_2

$$H = \frac{1}{2} (C_1 + C_2), \quad (2)$$

and integration runs over the cell membrane area (A).

The free energy of N membrane inclusions can be, in the limit of an ideal gas, expressed as (Kralj-Iglič et al., 1996)

$$F_N = \int n \left(E_{int} + k_B T \ln \frac{n}{\bar{n}} \right) dA \quad (3)$$

where n is inclusion area density, \bar{n} its average value (N/A), E_{int} the inclusion—bilayer interaction, k_B the Boltzmann constant and T the temperature. The limit of ideal gas for the entropy of the mixing term is appropriate because RBC proteome analysis has shown that its membrane contains about 170 (166 ± 109) Piezo1 monomers (Gautier et al., 2018). This means that there may be, on the RBC membrane area of $A \sim 140 \mu m^2$, only a little more than 50 Piezo1 trimers that form the channels. The interaction E_{int} can be described by the phenomenological energy term based on the mismatch between the intrinsic curvatures of the inclusion ($C_{1,inc}$ and $C_{2,inc}$) and membrane curvatures at Piezo1's location but without its presence (C_1 and C_2). By definition, a curvature is positive when it is convex with respect to the cell interior. The general expression for the corresponding energy term, at the limit of a rigid inclusion, has been formulated by Kralj-Iglič et al. (1999) as

$$E_{int} = \frac{\kappa}{2} (H - H_{incl})^2 + \frac{\kappa^*}{2} [\Delta H^2 - 2\Delta H \Delta H_{incl} \cos(2\omega) + \Delta H_{incl}^2] \quad (4)$$

where $H_{incl} = (C_{1,inc} + C_{2,inc})/2$ is the mean intrinsic curvature of Piezo1 and $\Delta H_{incl} = (C_{1,inc} - C_{2,inc})/2$ is a measure of the difference between the two channel intrinsic principal curvatures, $\Delta H = (C_1 - C_2)/2$ is a measure of the difference between the two membrane principal curvatures, κ and κ^* independent interaction constants, and the angle ω defines the mutual orientation of the coordinate systems of the intrinsic principal curvatures of the channel and the principal curvatures of the membrane.

Expression 4 (implemented in our previous analysis (Svetina et al., 2019)) is the minimal general expression for the inclusion—membrane interaction encompassing different symmetry situations with regard to intrinsic principal curvatures of the inclusion and principal curvatures of the bilayer (Svetina, 2015). In the case of Piezo1, the middle term of its second part only counts for its conformations in which $\Delta H_{incl} \neq 0$, i.e., for example, when one of its arms has a different structure. Here we restrict the analysis to the lateral distribution of Piezo1 in its axisymmetric resting state. Expression 4 thus involves only three curvature dependent terms which are proportional to H^2 , $H_{incl}H$, and ΔH^2 . It can be further simplified because the intrinsic curvatures of the Piezo1 trimer are about three orders of magnitude larger than the principal curvatures of the membrane of the RBC discocyte. Namely, the mean curvature of the Piezo1 molecule is $100 \mu m^{-1}$ (Guo and MacKinnon, 2017) and that of the discocyte shape predicted by the minimization of membrane bending energy for the reduced volume 0.6 and membrane area $140 \mu m^2$ is in the range of

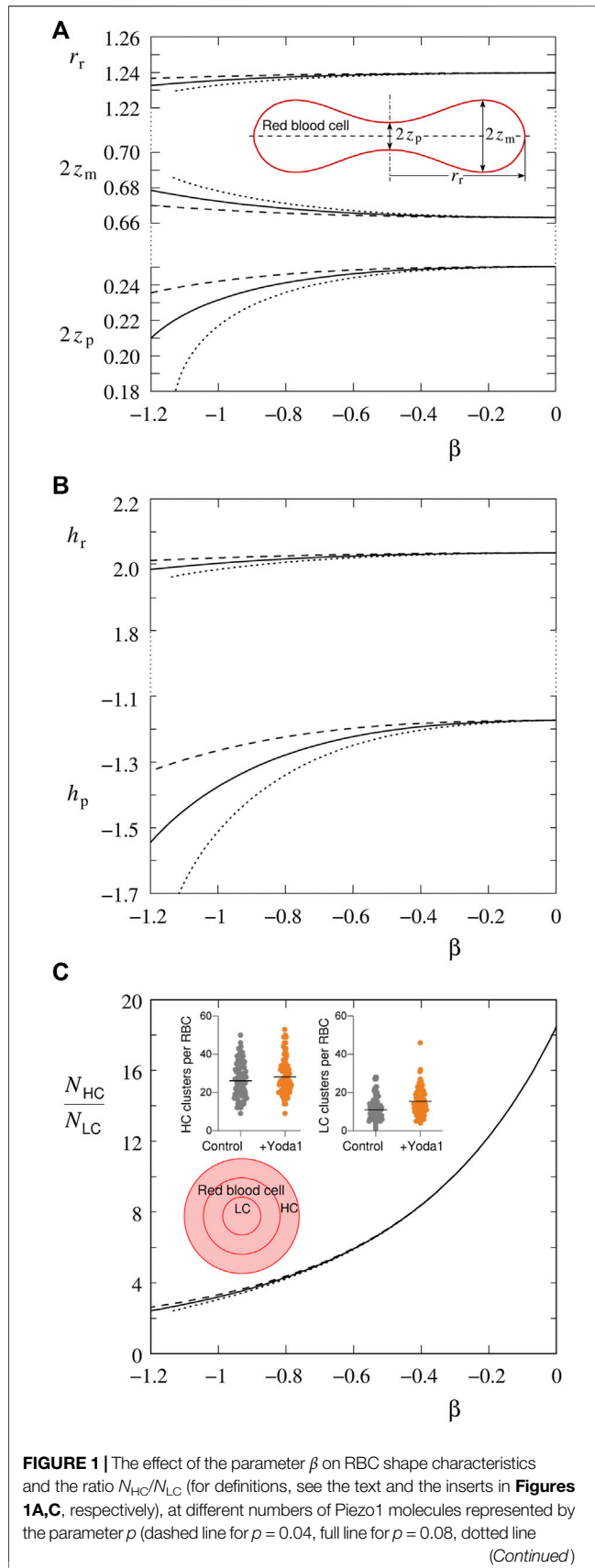


FIGURE 1 | for $p = 0.12$. RBC reduced volume is $v = 0.6$. The distances and curvatures are given relative to $R_s = (A/4\pi)^{1/2}$. **(A)** The dependences of the reduced distance between the poles ($2z_p$), the largest reduced distance between the membrane above and below the discocyte symmetry plane ($2z_m$) and the reduced radius of the rim (r_r) on the parameter β . The insert shows the contour of the RBC axial cross-section obtained by minimization of **Eqn. 1** at $v = 0.6$. The essential geometrical shape characteristics are indicated. **(B)** The reduced mean curvature at the pole (h_p) and at the rim (h_r). **(C)** The ratio between numbers of Piezo1 molecules in the rim region and in the pole regions ($N_{\text{HC}}/N_{\text{LC}}$). As the insert are presented slightly adapted **Figures 3A,E,F** of Dumitru et al. (2021). It is shown how the 2D horizontal projection of the RBC surface is divided by three concentric circles with radii $r_r/3$, $2r_r/3$ and r_r that define the inner area (LC) (dimple regions), median area, and outer area (HC) (rim region). The other two pictures show, in the diction of the corresponding caption, “the abundance of Piezo1 clusters in HC and LC areas for control and Yoda1-treated RBCs”.

$-0.34 \mu\text{m}^{-1}$ to $0.62 \mu\text{m}^{-1}$ (Svetina and Žekš, 1989). Therefore, assuming the same order of magnitude of the interaction constants κ and κ^* , the terms with H^2 and ΔH^2 can be neglected. The leading term of **Eqn. 4** is thus $-\kappa H_{\text{incl}}H$, and we can, for the interaction term, simply take

$$E_{\text{int}} = -bH, \quad (5)$$

its only parameter being $b = \kappa H_{\text{incl}}$.

It is convenient to minimize the described energy functional ($W_{\text{tot}} = W_b + F_N$) in its reduced form in which all energy terms are divided by the bending energy of a spherical vesicle ($8\pi\kappa_c$) (denoted by the corresponding small letters), and all distances reduced with respect to the radius of the sphere with the membrane area A , i.e., $R_s = (A/4\pi)^{1/2}$. Then

$$w_{\text{tot}} = w_b + p \int \frac{n}{\bar{n}} \left(-\beta h + \ln \frac{n}{\bar{n}} \right) da \quad (6)$$

Where $h = R_s H$, $da = dA/4\pi R_s^2$,

$$p = \frac{Nk_B T}{8\pi\kappa_c} \quad (7)$$

and

$$\beta = \frac{b}{k_B T R_s} \quad (8)$$

The derivation of the corresponding shape equation and how it is solved for axisymmetrical shapes was described in Božič et al. (2006). The solution of the shape equation (at given values of the RBC reduced volume and the parameters p and β) comprises the axial contour of the shape (see the insert in **Figure 1A**) and the dependence of the relative inclusion density (n/\bar{n}) as the function of the distance from the axis, as it is for instance presented in **Figure 2B**.

RESULTS

Analysis has been performed in three consecutive steps, first by looking at how an RBC discocyte shape and the corresponding lateral distribution of Piezo1 channels depend, at a given

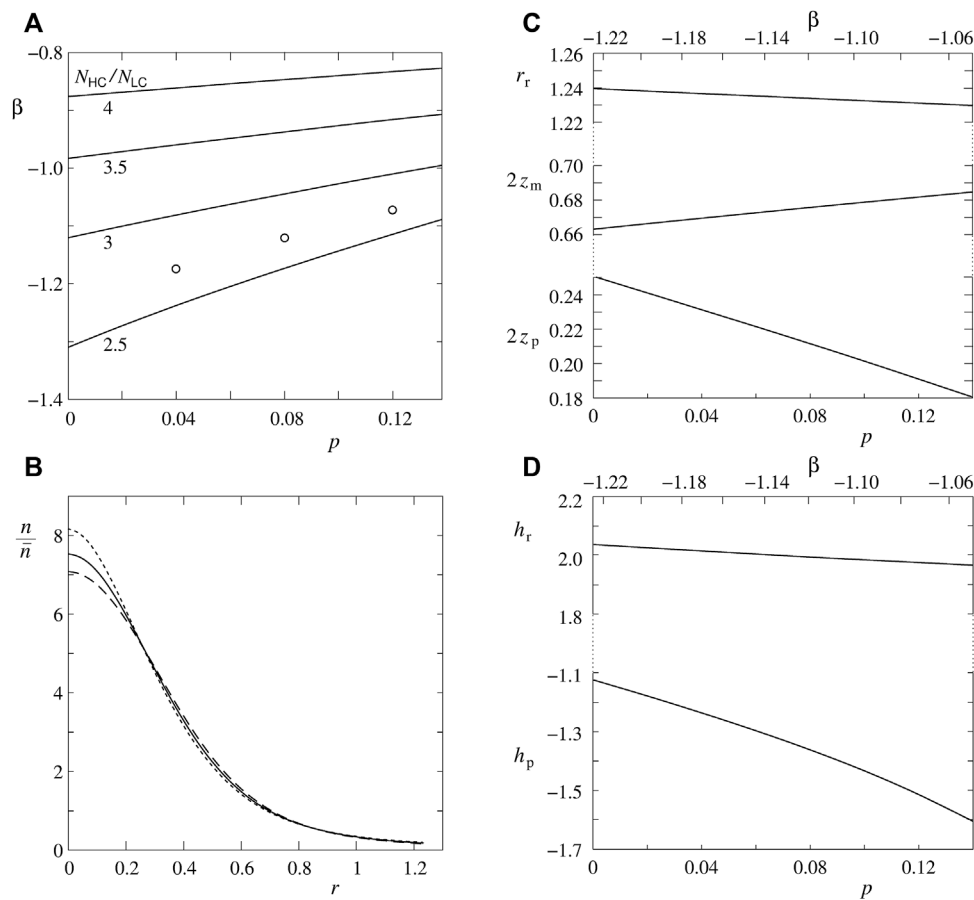
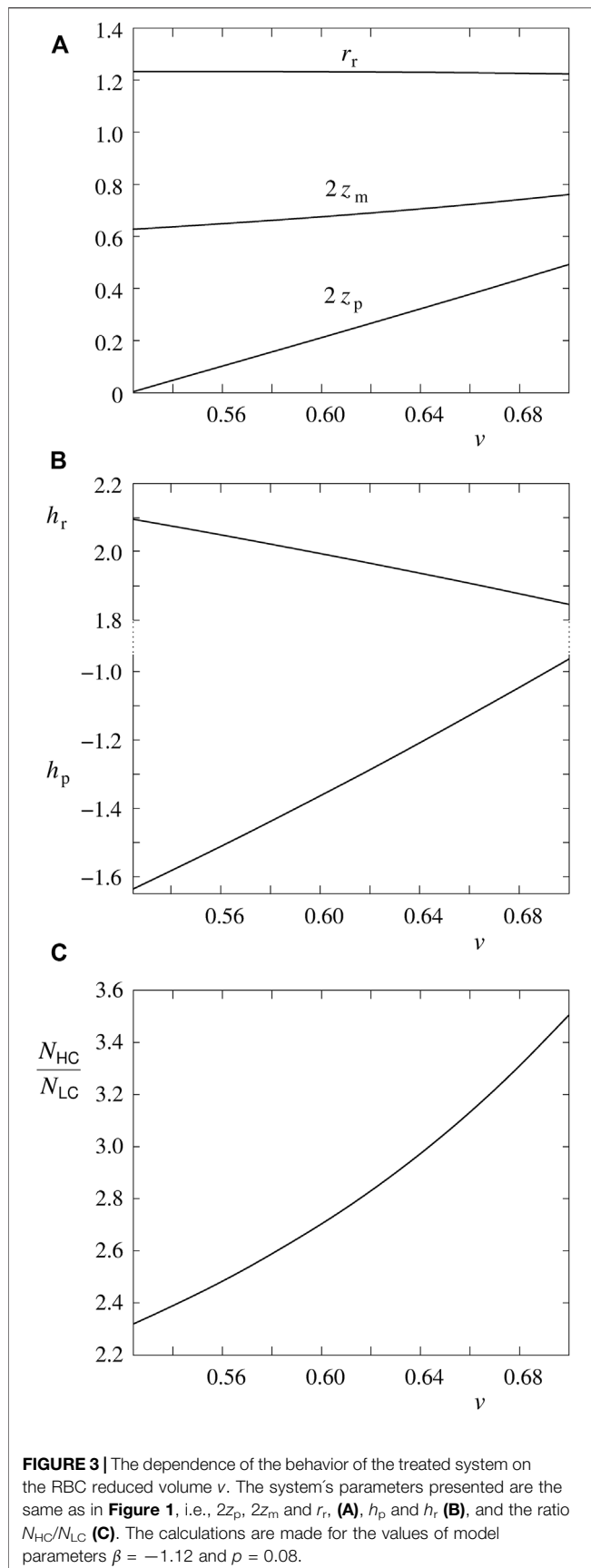


FIGURE 2 | Model predictions for the effect of Piezo1–bilayer interaction on RBC shape and Piezo1 lateral distribution. **(A)** Combinations of model parameters p and β that give the indicated values of the ratio N_{HC}/N_{LC} . The three points indicate values of parameters p and β employed in further analyses. **(B)** Relative area density of Piezo1 molecules (n/\bar{n} where \bar{n} is the average area density) in dependence on the reduced distance from the shape axis (r) at reduced volume 0.6 and at $N_{HC}/N_{LC} = 2.7$ for three combinations of the parameter p (0.04, 0.08 and 0.12) and interaction constant ($\beta = -1.17, -1.12$ and -1.07), respectively. Type of lines is the same as for the same values of the parameter p in **Figure 1**. **(C)** RBC discocyte characteristic parameters ($2z_p$, $2z_m$ and r_r) obtained at reduced volume 0.6 and the ratio $N_{HC}/N_{LC} = 2.7$ in dependence on the number of RBC Piezo1 trimers represented by the parameter p . **(D)** The corresponding dependence of the RBC mean curvature at the poles (h_p) and at the rim (h_r). In the latter two graphs the line on their top gives the corresponding scale for the parameter β .

reduced volume ($v = 3V/4\pi R_s^3$, where V is the volume of RBC), on their number and on the strength of their interaction with the surrounding bilayer. They are represented in **Eqn. 6** by the parameters p and β , respectively. This has been followed by a search of combinations of these two parameters that could give rise to the fit of the experimental results of Dumitru et al. (2021). Finally, we have observed how the system's behavior, with the thus obtained parameters, depends on the RBC reduced volume. In this study it is assumed that Piezo1 molecules are in their low energy state as revealed by cryoEM structural analysis (Guo and MacKinnon, 2017; Saotome et al., 2018; Zhao et al., 2018).

The physiologically relevant representative RBC reduced volume is $v = 0.6$. RBC discocyte shape at and around this reduced volume is well characterized by the distance between poles ($2z_p$), the maximal distance between the membrane above and below of the discocyte mirror plane ($2z_m$), the distance from the rotational axis to the rim (r_r), and the mean curvatures at

poles (h_p) and the rim (h_r) (see the insert in **Figure 1A** showing the axial cross-section of the RBC discocyte). In **Figures 1A,B** it is demonstrated how these shape characteristics depend on the interaction between Piezo1 and the surrounding bilayer. The increase of its strength (the absolute value of the parameter β) causes the pole-to-pole distance to be shorter. The radius of the rim also diminishes but to a much less relative extent. Correspondingly, in the investigated interval of the parameter β , the membrane mean curvature at the poles becomes more negative, and the mean curvature at the rim does not change appreciably (**Figure 1B**). All these dependences are more pronounced at larger number of Piezo1 channels (N), represented by the parameter of the model p , and thus also at larger value of their average areal number density (\bar{n}). The chosen three values of the parameter p are supposed to lie within a realistic range of RBC membrane bending stiffness, k_c , and a realistic range of the number of Piezo1 molecules, N . For example, by taking $k_c = 2.0 \cdot 10^{-19}$ J (Hwang and Waugh, 1997) and $p = 0.08$,



we get at $T = 300$ K (see **Eqn. 7**) the number of Piezo1 trimers $N = 100$ which is within the range obtained by the proteome analysis (Gautier et al., 2018). Piezo1 lateral inhomogeneity is manifested, as evidenced by Dumitru et al. (2021), by the ratio between the number of Piezo1 molecules in the rim region (N_{HC}) and dimple regions (N_{LC}) (see the insert in **Figure 1C**). The numbers N_{HC} and N_{LC} are obtained by the integrals of the areal number density (n) over the corresponding areas ($\int n dA$). The ratio N_{HC}/N_{LC} is, as a function of the absolute value of the parameter β , decreasing (**Figure 1C**). Here it has to be noted that, at zero interaction constant where the distribution is uniform, the plotted value 18.5 reflects the ratio between the respective membrane areas (A_{HC}/A_{LC}). Interestingly, the ratio N_{HC}/N_{LC} is, except for rather large absolute values of the parameter β , practically independent on the number of molecules.

The next set of figures (**Figure 2**) is devoted to the estimate of model parameters β and p for which the ratio between the number of Piezo1 molecules in the rim and pole regions N_{HC}/N_{LC} agrees with the measured value of Dumitru et al. (2021). In **Figure 2A** are shown combinations of model parameters β and p for which are obtained the same ratios N_{HC}/N_{LC} . In accord with the dependence of N_{HC}/N_{LC} on β (**Figure 1C**), the effect of the number of Piezo1 molecules is not very significant at smaller absolute values of the parameter β , however, the situation becomes different below its value of about -0.8 . At larger number of Piezo1 molecules the same ratio N_{HC}/N_{LC} is obtained at much smaller absolute values of the parameter β . The results of Dumitru et al. (2021) show the numbers N_{HC} and N_{LC} (by assuming that these numbers are proportional to the number of detected Piezo1 clusters) to be in different cells of the RBC population considerably different (see the insert in **Figure 1C**). However, it is possible to use for the measure of the ratio N_{HC}/N_{LC} its value obtained for a hypothetical “average” cell that has the numbers N_{HC} and N_{LC} proportional to the corresponding experimentally determined average values of the numbers of Piezo1 clusters. These values are for the controls (grey points in the insert of **Figure 1C** presented pictures) 27 for HC and 10 for LC, so that $N_{HC}/N_{LC} = 2.7$. By accepting this value and taking $p = 0.08$, the parameter β is estimated to be -1.12 . In **Figure 2A** the location of this point is shown by a circle. The other two points in **Figure 2A** indicate the values of the parameter β for $N_{HC}/N_{LC} = 2.7$ at $p = 0.04$ and $p = 1.2$. It is of interest to see how different combinations of parameters p and β which predict the same ratio N_{HC}/N_{LC} affect the predicted Piezo1 lateral distribution and RBC shape. This is shown in **Figures 2B–D**. The choice of parameters β and p affects the predicted Piezo1 areal density the most in the region of poles (**Figure 2B**). This is also reflected in the pole-to-pole distance ($2z_p$) (**Figure 2C**) and the pole curvature (h_p) (**Figure 2D**) which depend on the constant N_{HC}/N_{LC} combination of parameters β and p much stronger than the discocyte shape characteristics pertaining to the rim region. The described dependences are additional evidence that, with respect to the number of RBC Piezo1 channels, the most sensitive part of the RBC discocyte shape is its dimple region.

The last set of figures (**Figure 3**) shows the dependence of the behavior of the treated system on the RBC reduced volume. We

choose for the parameters $\beta = -1.12$ and $p = 0.08$. The range of interest for the reduced volume is from $v = 0.7$ to its value where, in this case, the distance between poles becomes zero ($v = 0.522$). The results accord with expectations: pole-to-pole distance is decreasing (**Figure 3A**), the mean curvature at poles is becoming more negative while the one at the rim is becoming more positive (**Figure 3B**). The ratio between the number of Piezo1 molecules in the rim and pole regions is, in dependence on v , decreasing (**Figure 3C**).

DISCUSSION

We first comment on the presented graphs and then, in a more general sense, put this study in the frame of some other recent related analyses.

The results in **Figure 1** show that the interaction between Piezo1 and the bilayer has an effect both on RBC shape and the lateral distribution of channels. Piezo1 molecules thus act as shape sensing and shape forming entities. Such a mutual effect on each other of vesicle shape and lateral distribution of membrane inclusions or membrane binding molecules has been studied a lot for shapes composed of sections with constant curvatures. An example is a cylindrical tether pulled out of a vesicle aspirated into a pipette, where it is possible to describe shape by a simple geometrical model (Simunovic et al., 2016). RBC discocyte exhibits a continuously varying mean curvature from its negative value at poles to its positive value at the rim. The results in **Figure 1** show why it is, in such cases, crucial to apply the theoretical approach developed for general axisymmetrical shapes of vesicles with inclusions (Božič et al., 2006). The effect of Piezo1 on the shape is, in the region of the rim, much less pronounced than in the dimple region where there is also a much larger area density of Piezo1 molecules.

The results presented in **Figure 2** imply that it is possible to interpret the distribution of Piezo1 molecules observed by Dumitru et al. (2021) over the RBC membrane solely on the basis of the curvature dependent interaction between Piezo1 molecules and the surrounding bilayer. The system's behavior depends on the parameters β and p which represent the strength of the Piezo1–bilayer interaction, and the effects of the contribution of its entropy, respectively. The estimated value of the ratio between the number of Piezo1 molecules in the rim region and dimple regions ($N_{\text{HC}}/N_{\text{LC}}$) is in the range of the values of parameters β and p where its value (2.7) can be obtained by a wide range of their combinations (**Figure 2A**). A better estimate of the values of parameters β and p could be obtained by measuring Piezo1 areal density with a better spatial resolution. From the comparison of the three predicted areal density distributions of Piezo1 molecules (**Figure 2B**) it can be concluded that the densities mostly differ within the regions of poles. A better spatial resolution should therefore be applied primarily within these regions.

The Piezo1–bilayer interaction was, in this work, described in terms of a phenomenological interaction term. It will be informative to relate this term to different basic contributions to the energy of the system. Such interactions have been studied theoretically, for example by determining due to the inclusion

increased bilayer bending energy (Phillips et al., 2009). Up to now the Piezo1–bilayer interaction term has been, in this sense, calculated for a Piezo1 molecule embedded into a flat tensed membrane (Haselwandter and MacKinnon, 2018). It was shown how, due to the curved structure of Piezo1, a membrane footprint is formed that extends far beyond the size of a molecule. The extension of this theory to cases where Piezo1 is embedded in an already curved membrane could give an estimate of the value of the parameter β .

The results presented in **Figure 3** are relevant with regard to the recently proposed model of the role of Piezo1 in the regulation of RBC volume (Svetina et al., 2019; Svetina, 2020). The crucial element of this model was the nonuniform distribution of Piezo1 molecules due to their curvature dependent interaction with the surrounding bilayer. Due to lack of the appropriate data, the procedure was simplified by the assumption that Piezo1 molecules sense the curvature at the discocyte poles. **Figure 3C** is an indication that the system behaves, in qualitative terms, in the same manner. In consequence, instead of relying on an assumption, it will be possible, in further development of this modeling, to apply the Piezo1 area distribution obtained experimentally (Dumitru et al., 2021). Another improvement of the model would be the predicted effect of the Piezo1 lateral distribution on the pole-to-pole distance (**Figure 1A**). In this respect it is important to note that, in the treated case, the distribution and discocyte shape act on each other in a manner of a positive feedback. The more Piezo1 molecules reside in the region of poles, the larger is the absolute value of the pole curvature; the larger is the latter, the more Piezo1 molecules tend to reside in this region.

The occurrence of the nonuniform distribution of Piezo1 molecules implies strongly that they are laterally mobile. This appears to be in conflict with the notion of the effect of a spectrin network on their mobility (Dumitru et al., 2021). However, it can be assumed that Piezo1 molecules are, because of the formed footprint (Haselwandter and MacKinnon, 2018), corralled by the spectrin network which can cause their effective diffusion constant on the RBC membrane to be considerably smaller than in membranes without such a skeleton.

This analysis is a strong indication that it is the curvature dependent Piezo1–bilayer interaction that is responsible for the observed Piezo1 lateral distribution on the RBC membrane. Nevertheless, one has to be aware of its possible limitations. For example, the described simple system seems to be inadequate for the interpretation of the effect Yoda1 on the discocyte lateral distribution of Piezo1 (Dumitru et al., 2021). In the presence of Yoda1 the ratio $N_{\text{HC}}/N_{\text{LC}}$ extracted from the mean values of counted Piezo1 clusters (insert in **Figure 1C**) is smaller (1.9) than in the control (2.7) which could be understood as an indication that Yoda1 causes Piezo1 to be curved more than in its absence, contrary to the common view that it causes Piezo1 structure to transform in the direction of its less curved open state. This discrepancy could be the result of our assumption that all Piezo1 molecules reside in their state with the lowest energy, as revealed by cryoEM (Guo and MacKinnon, 2017; Saotome et al., 2018; Zhao et al., 2018). But it could also happen that a Piezo1 molecule embedded in a curved membrane at a given curvature switches

into one of its other stable conformations with smaller intrinsic curvatures. A hypothesis can thus be made that Yoda1 causes a shift of such a critical membrane curvature. However, at present there is not enough data on structures of other than the resting state of Piezo1 to confirm this interpretation. Furthermore, it is also necessary to take into consideration that there are several other factors that have an effect on the RBC discocyte shape. One is the difference between the areas of the two bilayer leaflets. It is known, from theoretical analyses, that the pole-to-pole distance increases as a function of such an area difference (Svetina and Žekš, 1989). Recently it has been revealed that the pole-to-pole distance also depends on the activity of the RBC's actin-myosin system (Smith et al., 2018). In these respects the part of the present analysis related to the establishment of the RBC discocyte shape is far from complete.

In relation to the present work, the effects of the actin-myosin system deserve special attention. It has been shown that actins and myosins are denser in the region of the RBC dimple (Alimohamadi et al., 2020). The present study suggests that this property could be the consequence of the accumulation of Piezo1 molecules in this region. The formation of membrane footprints (Haselwandter and MacKinnon, 2018) indicates that the effective lateral compressibility of the membrane is larger than in their absence. Consequently, it varies along the RBC membrane in correspondence to the Piezo1 lateral distribution. Under condition of the lateral compression of the membrane involving Piezo1 footprints, it can thus be expected that it causes the increase of their extra membrane area, implying that membrane lateral compressibility has a component proportional to the Piezo1 area density.

The mismatch principle can be considered as one of the ways to interpret consequences of the interaction between membrane bilayer and shape sensing and forming membrane proteins (reviewed in Tsai et al., 2021). In this study it has been realized that, in the case of RBC Piezo1, because of the intrinsic mean curvature of Piezo1 being orders of magnitude larger than that of the RBC membrane, its product with the interaction constant (parameter b) matters more than this constant (H_{incl}) by itself. The interaction term thus involves only a single constant, which can be considered as a macroscopic material constant. The sum of the bending

energy (Eqn. 1) and contributions of the interaction term (Eqn. 5) can be transformed in this case into an expression for the area density of the bending energy of a membrane $2k_c(H - C_0^{\text{eff}}/2)^2$, by $C_0^{\text{eff}} = nb/k_c$ considered as a laterally variable effective spontaneous curvature. "Effective" because it is the result of the strength of the interaction and is not related to a certain real radius of a sphere. It has also to be pointed out that the calculations presented here belong to the "mismatch" type and not to the "spontaneous curvature" type modeling (Tsai et al., 2021), because the energy functional to be minimized (Eqn. 6) still involves the entropy part of the free energy of inclusions. However, the concept of spontaneous curvature modeling could be applied if the location of inclusions were fixed, for example if shape transformations would occur in times much shorter than is the characteristic time for the system's equilibration, due to Piezo1 lateral diffusion.

DATA AVAILABILITY STATEMENT

The raw data supporting the conclusions of this article will be made available by the authors, without undue reservation.

AUTHOR CONTRIBUTIONS

The authors contributed to this work equally.

FUNDING

The study was partly supported by the Slovenian Research Agency through Grant P1-0055.

ACKNOWLEDGMENTS

The authors thank Professor Roger H. Pain for critical reading of the manuscript.

REFERENCES

- Alimohamadi, H., Smith, A. S., Nowak, R. B., Fowler, V. M., and Rangamani, P. (2020). Non-uniform Distribution of Myosin-Mediated Forces Governs Red Blood Cell Membrane Curvature through Tension Modulation. *PLoS Comput. Biol.* 16. e1007890. doi:10.1371/journal.pcbi.1007890
- Božič, B., Kralj-Iglič, V., and Svetina, S. (2006). Coupling between Vesicle Shape and Lateral Distribution of Mobile Membrane Inclusions. *Phys. Rev. E* 73.041915. doi:10.1103/PhysRevE.73.041915
- Cahalan, S. M., Lukacs, V., Ranade, S. S., Chien, S., Bandell, M., and Patapoutian, A. (2015). Piezo1 Links Mechanical Forces to Red Blood Cell Volume. *eLife* 4. e07370. doi:10.7554/eLife.07370
- Canham, P. B. (1970). The Minimum Energy of Bending as a Possible Explanation of the Biconcave Shape of the Human Red Blood Cell. *J. Theor. Biol.* 26, 61–81. doi:10.1016/s0022-5193(70)80032-7
- Dumitru, A. C., Stommen, A., Koehler, M., Cloos, A.-S., Yang, J., Leclercqz, A., Tyteca, D., and Alsteens, D. (2021). Probing PIEZO1 Localization upon Activation Using High-Resolution Atomic Force and Confocal Microscopy. *Nano Lett.* 21, 4950–4958. doi:10.1021/acs.nanolett.1c00599
- Gautier, E.-F., Leduc, M., Cochet, S., Bailly, K., Lacombe, C., Mohandas, N., Guillonnet, F., Nemer, W. E., and Mayeux, P. (2018). Absolute Proteome Quantification of Highly Purified Populations of Circulating Reticulocytes and Mature Erythrocytes. *Blood Adv.* 2, 2646–2657. doi:10.1182/bloodadvances.2018023515
- Ge, J., Li, W., Zhao, Q., Li, N., Chen, M., Zhi, P., Li, R., Gao, N., Xiao, B., and Yang, M. (2015). Architecture of the Mammalian Mechanosensitive Piezo1 Channel. *Nature* 527, 64–69. doi:10.1038/nature15247
- Guo, Y. R., and MacKinnon, R. (2017). Structure-based Membrane Dome Mechanism for Piezo Mechanosensitivity. *eLife* 6. e33660. doi:10.7554/eLife.33660
- Haselwandter, C. A., and MacKinnon, R. (2018). Piezo's Membrane Footprint and its Contribution to Mechanosensitivity. *eLife* 7. e41968. doi:10.7554/eLife.41968
- Helfrich, W. (1973). Elastic Properties of Lipid Bilayers: Theory and Possible Experiments. *Z. Naturforsch.* 28, 693–703. doi:10.1515/znc-1973-11-1209

- Hoffmann, E. K., Lambert, I. H., and Pedersen, S. F. (2009). Physiology of Cell Volume Regulation in Vertebrates. *Physiol. Rev.* 89, 193–277. doi:10.1152/physrev.00037.2007
- Hwang, W. C., and Waugh, R. E. (1997). Energy of Dissociation of Lipid Bilayer from the Membrane Skeleton of Red Blood Cells. *Biophys. J.* 72, 2669–2678. doi:10.1016/S0006-3495(97)78910-0
- Kralj-Iglič, V., Svetina, S., and Žekš, B. (1996). Shapes of Bilayer Vesicles with Membrane Embedded Molecules. *Eur. Biophys. J.* 24, 311–321.
- Kralj-Iglič, V., Heinrich, V., Svetina, S., and Žekš, B. (1999). Free Energy of Closed Membrane with Anisotropic Inclusions. *Eur. Phys. J. B* 10, 5–8.
- Lai, A., Cox, C. D., Sekar, N. C., Thurgood, P., Jaworowski, A., Peter, K., and Baratchi, S. (2021). Mechanosensing by Piezo1 and its Implications for Physiology and Various Pathologies. *Biol. Rev.* 97(2):604–614. doi:10.1111/bvr.128110.1111/bvr.12814
- Murthy, S. E., Dubin, A. E., and Patapoutian, A. (2017). Piezos Thrive under Pressure: Mechanically Activated Ion Channels in Health and Disease. *Nat. Rev. Mol. Cell Biol.* 18, 771–783. doi:10.1038/nrm.2017.92
- Phillips, R., Ursell, T., Wiggins, P., and Sens, P. (2009). Emerging Roles for Lipids in Shaping Membrane-Protein Function. *Nature* 459, 379–385. doi:10.1038/nature08147
- Saotome, K., Murthy, S. E., Kefauver, J. M., Whitwam, T., Patapoutian, A., and Ward, A. B. (2017). Structure of the Mechanically Activated Ion Channel Piezo1. *Nature* 554, 481–486. doi:10.1038/nature25453
- Simunovic, M., Prévost, C., Callan-Jones, A., and Bassereau, P. (2016). Physical Basis of Some Membrane Shaping Mechanisms. *Phil. Trans. R. Soc. A* 374, 20160034. doi:10.1098/rsta.2016.0034
- Smith, A. S., Nowak, R. B., Zhou, S., Giannetto, M., Gokhin, D. S., Papoin, J., Ghiranf, I. C., Blance, L., Wanb, J., and Fowler, V. M. (2018). Myosin IIA Interacts with the Spectrin-Actin Membrane Skeleton to Control Red Blood Cell Membrane Curvature and Deformability. *Proc. Natl. Acad. Sci. U. S. A.* 115, E4377–E4385. doi:10.1073/pnas.1718285115
- Svetina, S., and Žekš, B. (1989). Membrane Bending Energy and Shape Determination of Phospholipid Vesicles and Red Blood Cells. *Eur. Biophys. J.* 17, 101–111. doi:10.1007/bf00257107
- Svetina, S., Švelc Kebe, T., and Božič, B. (2019). A Model of Piezo1-Based Regulation of Red Blood Cell Volume. *Biophys. J.* 116, 151–164. doi:10.1016/j.bpj.2018.11.3130
- Svetina, S. (2015). Curvature-dependent Protein-Lipid Bilayer Interaction and Cell Mechanosensitivity. *Eur. Biophys. J.* 44, 513–519. doi:10.1007/s00249-015-1046-5
- Svetina, S. (2020). Theoretical Bases for the Role of Red Blood Cell Shape in the Regulation of its Volume. *Front. Physiol.* 11, 544. doi:10.3389/fphys.2020.00544
- Tsai, F.-C., Simunovic, M., Sorre, B., Bertin, A., Manzi, J., Callan-Jones, A., and Bassereau, P. (2021). Comparing Physical Mechanisms for Membrane Curvature-Driven Sorting of BAR-Domain Proteins. *Soft Matter* 17, 4254–4265. doi:10.1039/d0sm01573c
- Zarychanski, R., Schulz, V. P., Houston, B. L., Maksimova, Y., Houston, D. S., Smith, B., Rinehart, J., and Gallagher, P. G'. (2012). Mutations in the Mechanotransduction Protein PIEZO1 Are Associated with Hereditary Xerocytosis. *Blood* 120, 1908–1915. doi:10.1182/blood-2012-04-422253
- Zhao, Q., Zhou, H., Chi, S., Wang, Y., Wang, J., Geng, J., Wu, K., Liu, W., Zhang, T., Dong, M.-Q., Wang, J., Li, X., and Xiao, B. (2018). Structure and Mechanogating Mechanism of the Piezo1 Channel. *Nature* 554, 487–492. doi:10.1038/nature25743

Conflict of Interest: The authors declare that the research was conducted in the absence of any commercial or financial relationships that could be construed as a potential conflict of interest.

Publisher's Note: All claims expressed in this article are solely those of the authors and do not necessarily represent those of their affiliated organizations, or those of the publisher, the editors and the reviewers. Any product that may be evaluated in this article, or claim that may be made by its manufacturer, is not guaranteed or endorsed by the publisher.

Copyright © 2022 Božič and Svetina. This is an open-access article distributed under the terms of the Creative Commons Attribution License (CC BY). The use, distribution or reproduction in other forums is permitted, provided the original author(s) and the copyright owner(s) are credited and that the original publication in this journal is cited, in accordance with accepted academic practice. No use, distribution or reproduction is permitted which does not comply with these terms.



Light and Scanning Electron Microscopy of Red Blood Cells From Humans and Animal Species Providing Insights into Molecular Cell Biology

Gheorghe Benga^{1,2*} and Guy Cox^{3*}

¹Romanian Academy, Cluj-Napoca, Romania, ²School of Life and Environmental Sciences, Faculty of Science, University of Sydney, Darlington, NSW, Australia, ³Australian Centre for Microscopy & Microanalysis, University of Sydney, Darlington, NSW, Australia

OPEN ACCESS

Edited by:

Anna Bogdanova,
University of Zurich, Switzerland

Reviewed by:

Umberto Laforenza,
University of Pavia, Italy
Nicolas Montalbetti,
University of Pittsburgh, United States

*Correspondence:

Gheorghe Benga
gheorghe.benga@academia-cj.ro
Guy Cox
guy.cox@sydney.edu.au

Specialty section:

This article was submitted to
Red Blood Cell Physiology,
a section of the journal
Frontiers in Physiology

Received: 17 December 2021

Accepted: 22 March 2022

Published: 01 July 2022

Citation:

Benga G and Cox G (2022) Light and Scanning Electron Microscopy of Red Blood Cells From Humans and Animal Species Providing Insights into Molecular Cell Biology. *Front. Physiol.* 13:838071. doi: 10.3389/fphys.2022.838071

We reviewed the many discoveries in cell biology, made since the 17th century, which have been based on red blood cells (RBCs). The advances in molecular and structural biology in the past 40 years have enabled the discovery with these cells, most notably, of the first water channel protein (WCP) called today aquaporin1 (AQP1). The main aim of our work reviewed was to examine by light and electron microscopy a very wide range of RBCs from reptiles, birds, monotremes, marsupials and placentals, in order to estimate from these images the RBC cell volume and surface area. The diffusional water permeability of the RBC membrane from these species has further been measured with a nuclear magnetic resonance (NMR) spectroscopy technique. The significance of the observed permeability of RBCs to water and possible influences on the whole body are discussed.

Keywords: erythrocyte, microscopy, marsupial, monotreme, placental mammal, NMR

RED BLOOD CELLS AS OBJECTS OF STUDIES IN CELL AND MOLECULAR BIOLOGY OVER CENTURIES

Naked-eye inspection of blood at phlebotomy as part of medical diagnosis was practiced at least 2,000 years ago. However, only after the explosion of interest in microscopy in the 17th century did the examination of the constituents of blood become possible and RBCs were seen. The Dutch microscopist, Antoni van Leeuwenhoek (1632–1723), is credited by many (e.g., De Robertis, 1970) with this discovery. In a critical analysis of the discovery of blood cells, Hajdu, (2003) concluded that the Dutch naturalist Jan Swammerdam (1637–1680) was the first person to observe RBCs under the microscope. However, Antoni van Leeuwenhoek described the size and shape of “red corpuscles” and rendered the first illustration of them in a letter in 1665 to Swammerdam (Letter 42 of Arcana Natura, 1695). The dispute over priority for the initial discovery emphasizes the difficulty in establishing such claims and yet the correct position today is to consider who and when a fact is reported in the formal refereed scientific literature.

Over the centuries, various (and sometimes unexpected) discoveries about living systems have been made in experiments and observations on RBCs. Specifically, it was noted that the sizes of RBCs in various species display much smaller variations compared to the large or even huge differences in body size (mass), considering for example small animals like the mouse or bilby, versus much larger ones like the horse or elephant. Extrapolated to various organs in the body, it became obvious that the total mass of the organ is due to the number and not the volume of each cell. This led to the so called “Law of constant volume”, that was formulated in the 19th century (De Robertis, 1970). The first

isolation protocols of nucleic acids were developed in 1869 in Tübingen by the German scientist Friedrich Miescher. He and his supervisor, Professor Felix Hoppe-Seyler are now recognized as the discoverers of DNA. They found it in the biological material called “nuclein”. Their work involved RBCs among other cells. In 1871 the first publications of Miescher and Hoppe-Seyler describing the “nuclein” appeared (Miescher, 1871). In addition, another student of Hoppe-Seyler, P. Plósz, (1871), reported the presence of “nuclein” in the hemolyzed nucleated erythrocytes from birds and snakes. The story of the work performed in Tübingen at this time is reviewed by His, (1897). Dahm, (2005) published a more complete history of the discovery of DNA, while Hajdu, (2003) mentioned the discovery in the 19th century of the medical implications of RBCs and the foundation of a new medical specialty, hematology.

The RBC membrane was the main one to reveal the essential features of the structure and function of virtually all cell membranes. Specifically, (1) the “Lipid bilayer model” proposed by the Dutch scientists Gorter and Grendel, (1925); the model proposed in 1935 by the Americans Danielli and Davson, revised in 1943, to include proteins on both surfaces of the lipid bilayer, and also the idea of protein “pores” through the lipid bilayer to allow solute exchange (Davson and Danielli, 1943); the “Fluid mosaic model” proposed in 1972 by Americans Singer and Nicolson: it includes so called “intrinsic membrane proteins” (embedded in the lipid bilayer) and the proteins attached on both sides of the membrane (Singer and Nicolson, 1972); (2) the analysis of membrane proteins by sodium dodecyl sulphate polyacrylamide gel electrophoresis (SDS-PAGE), the analysis of lipids by chromatography, and the study of protein-lipid interactions; (3) the visualization of glycoproteins and glycolipids in the glycocalix; (4) the interactions between the intrinsic membrane proteins and the proteins located inside the cell, in the cytoskeleton; (5) the identification of proteins with roles as antigens (beginning with the blood group antigens). Such aspects are presented in many publications (e.g., De Robertis, 1970; Kummerow et al., 1983; Benga et al., 1984; Benga and Holmes, 1984; Benga et al., 1985a; Benga et al., 1985b; Benga et al., 1985c; Benga et al., 1987a; Benga et al., 1987b; Benga and Tager, 1988; Benga et al., 1989; Benga et al., 1990; Benga et al., 1991; Sperelakis, 2001; Alberts et al., 2008).

THE TRANSPORT PROCESSES ACROSS THE RBC MEMBRANE AND THE DISCOVERY OF THE FIRST WATER CHANNEL PROTEIN, LATER CALLED AQUAPORIN1 (AQP1)

The permeability of the RBC membrane to water, ions, micromolecules has been investigated for decades, as reviewed in several books (e.g., House, 1974; Benga et al., 1985a; Benga et al., 1985b; Benga et al., 1985c; Stein, 1986; Benga, 1989a; Benga, 1989b). The start point for the discovery in the RBC membrane of the first water channel protein (WCP), later called aquaporin1 (AQP1), was the comparative NMR measurements of water

permeability of the RBC from children with epilepsy and control children performed in 1976 in Cluj-Napoca, Romania, by Gheorghe Benga, Vasile V. Morariu, Ileana Benga and Cornelia Morariu. The results of the study were published in *Nature* (Benga and Morariu, 1977). The complete story of the discovery was also recently presented (Benga, 2021).

The water permeability of RBCs in children with epilepsy compared with control children was measured by the NMR method of Conlon and Outhred, (1972). The method involves addition of a paramagnetic solution (MnCl_2) to the plasma and measurement of the spin-spin relaxation time (T_2) of the RBC water proton. The spin-spin relaxation time of water inside the isolated RBCs is about 140 ms and is much longer than the time required for water to exchange across the membrane (the water exchange time, T_{ae}), which is about 10 ms. The value of T_{ae} is inversely related to the water permeability (P_d) of RBCs. If the relaxation time in plasma is made much shorter than the exchange time (by adding the paramagnetic ion Mn^{2+}) the observed relaxation time of the RBC (T_{2b}) is dominated by the exchange process through the membrane. The spin-spin relaxation time is evaluated from a logarithmic plot of the nuclear spin-echo as a function of the time interval 2τ where τ is the time interval between the radiofrequency pulses. When the system is characterized by a single relaxation time, the plot is a straight line and the relaxation time is the reciprocal of the slope. For a system characterized by two relaxation times (as for the blood doped with Mn^{2+}) the plot consists of two lines and the relaxation times are calculated from the slopes of these lines; see **Figure 1** in ref. Morariu and Benga, (1977), which can be accessed on Google Chrome following two steps:

https://scholar.google.ro/scholar?q=Morariu+Benga+Biochimica+Biophysica+Acta+1977&hl=ro&as_sdt=0&as_vis=1&oi=scholar; then click on [PDF]Academia.edu.

The paper published by Benga and Morariu, (1977) can also be accessed on Google Chrome following two steps: <https://af.booksc.eu/book/10454413/a8b701>; followed by click on [PDF]. The values of T_{ae} were measured in 24 children with epilepsy (aged 1–12 years) and 24 controls (children aged 2–16 years). In all children with epilepsy the exchange time of water through the RBC membrane (T_{ae}) was longer than in control subjects. In other words decreased values of the water permeability were found in case of RBCs from children with epilepsy. There were no significant differences in T_{ae} values between idiopathic and focal epilepsies. High values of T_{ae} were found in patients who had seizures every day and in whom the attacks were poorly controlled by anticonvulsant therapy. It was also found that the value of T_{ae} during the seizure was not higher than in the interictal period. This indicated that the low water permeability of RBCs in epilepsy is a permanent alteration (not a transient one). The abnormal water permeability was found in both untreated and treated patients, i. e. was not related to the anticonvulsant therapy. An alteration (decrease) of the permeability to water of RBCs in children with epilepsy was the most likely explanation for the findings. Gh. Benga, Vasile Morariu, Ileana Benga and Cornelia Morariu realized immediately the important significance of findings, as they had already studied extensively

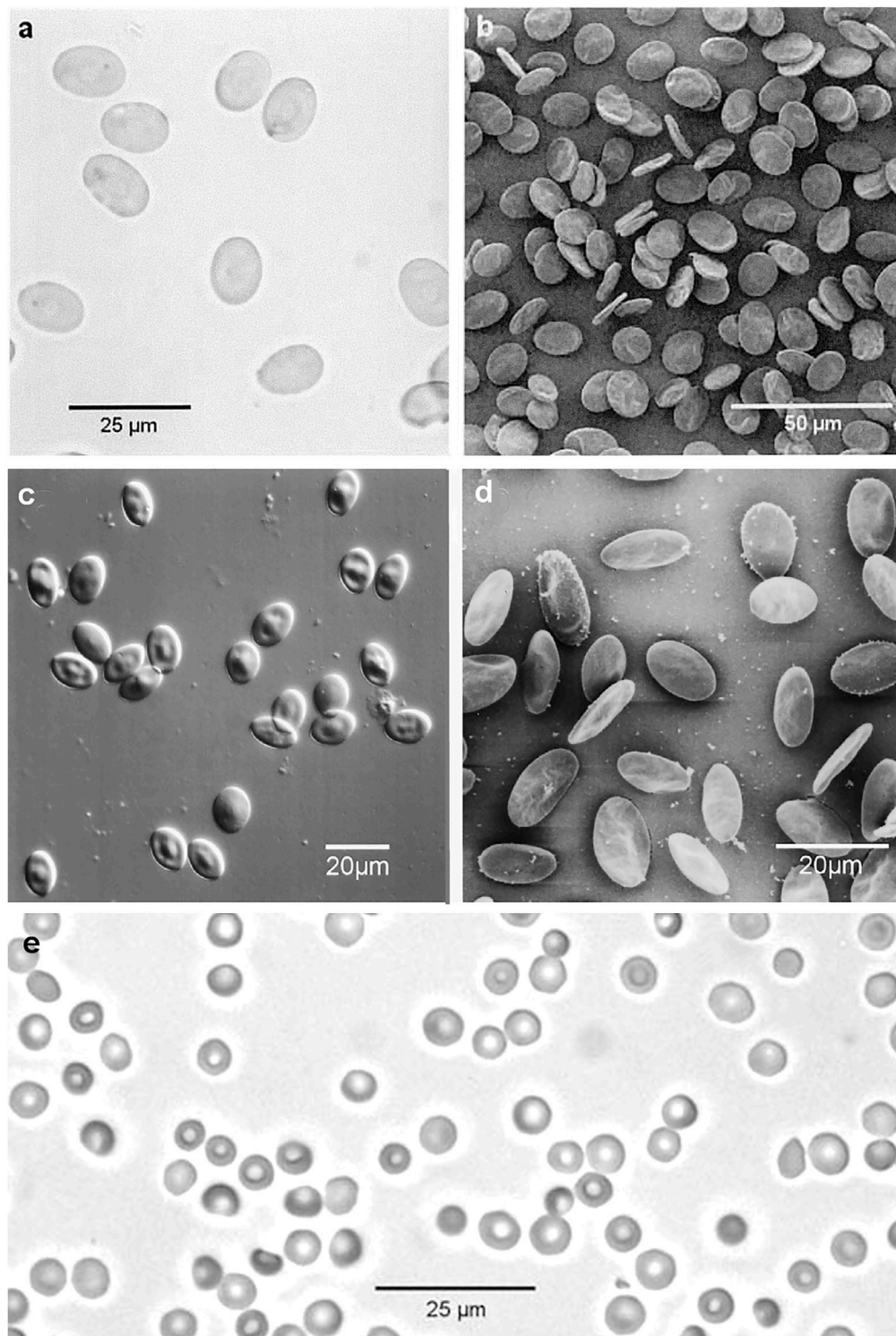


FIGURE 1 | Reptiles, birds and monotremes: **(A)** Green Sea Turtle (*Chelonia mydas*) RBCs, bright field optical micrograph (Nikon Eclipse E800 Plan Apo $\times 40$ 0.95NA objective); **(B)** Green Sea Turtle RBCs, secondary electron SEM image (Jeol JSM-6300f); **(C)** Little Penguin (*Eudyptula minor*) RBCs, DIC optical micrograph (Nikon Eclipse E800 Plan Apo $\times 40$ 0.95NA objective); **(D)** Little Penguin RBCs, secondary electron SEM image (Jeol JSM-6300f); **(E)** Platypus (*Ornithorhynchus anatinus*) RBCs, bright field optical micrograph. (Nikon Eclipse E800 Plan Apo $\times 40$ 0.95NA objective). The original images were published by (Benga, 1994; Benga, 2003; Benga et al., 2015).

the publications regarding the NMR (Vasile Morariu) and epilepsy (Gheorghe and Ileana Benga). In October 1976 a manuscript was sent to Nature, in December 1976 was accepted to be published without change and in February 1977 it appeared (Benga and Morariu, 1977). The authors concluded that “decreased permeability in erythrocytes of epileptics may reflect a membrane defect in all tissues and may be an expression of the individual predisposition in epilepsy; it might be of particular importance in the nervous system. Further studies on erythrocyte membranes in epilepsy may give clues to the understanding of the membrane defect in molecular terms (Benga and Morariu, 1977; Morariu et al., 1981).” Subsequent studies of Morariu and Benga, (1984) on the effects of temperature allowed the calculation of the activation energy ($E_{a,d}$) of the RBC membrane diffusional permeability (P_d) to water and showed that the water diffusion time (T_e), is related with P_d by the expression involving the cell water volume (V) and the cell surface area (A):

$$P_d = V/A \times 1/T_e \quad (1)$$

Gh. Benga, working at The “Iuliu Hațieganu” University of Medicine and Pharmacy (abbreviated as U.M.F.) Cluj-Napoca, Romania, started an extensive program of research aimed to identify the pathway by which the water molecules cross the membrane. Several important aspects had to be studied until the final goal was achieved: NMR measurements of the effects on P_d of various inhibitors and of chemical modifications of membrane proteins, measurements on resealed ghosts (prepared by a special procedure: hemolysis to remove hemoglobin and then restoring the membrane integrity, as described by Schwach and Passow, 1973), labelling of the protein involved in water permeability by a radioactive inhibitor ^{203}Hg -PCMBs, - PCMBs being an abbreviation of *p*-(Chloromercuri) benzenesulfonate, and finally the identification of this protein by SDS-PAGE. After almost a decade of hard work, the water channel protein (WCP) in the human RBC membrane was identified by Gh. Benga’s group. The discovery was reported in two landmark publications (Benga et al., 1986a,b). The discovery of the first WCP was really achieved in 1985 when the first landmark paper was sent for publication to the prestigious American journal *Biochemistry*, which accepted the publication without change (Benga et al., 1986a). In this paper it was stated: “previous labelling experiments with sulfhydryl-reactive reagents did not correlate binding with inhibition of water transport. The binding pattern of PCMBs that was observed in correlation with the inhibition of water diffusion suggests that either or both band 3 and 4.5 proteins could be associated with water channels. Polypeptides migrating in these regions have already been identified in other transport functions, notably anion exchange and the transport of glucose and nucleosides. To date, however, there is no evidence that a specific inhibitor of one of these processes will inhibit water transport. It remains possible that a minor membrane protein that binds PCMBs is involved in water transport.” Finally, it was also indicated how the final confirmation could be achieved. “We believe the best way to clarify the role of bands 3 and 4.5 in water transport will ultimately be through studies on the reconstitution of purified proteins in liposomes.” The second landmark paper was published in 1986 in

a well known European journal (Benga et al., 1986b). The title of this paper clearly indicated that Benga’s group has identified the proteins present in the RBC membrane implicated in water transport.

Gh. Benga presented the novelty of the discovery of his group in reviews published before 1990 (Benga, 1989a; Benga, 1989b; Benga, 1989c) and in many publications in the following years (Benga and Borza, 1995; Benga, 2003; Benga, 2009; Benga, 2012a; Benga, 2012b; Benga, 2012c). It should be emphasized that previous “labelling studies” (Brown et al., 1975; Sha’afi and Feinstein, 1977) pointed to band 3 protein (“a major protein”, known to be the anion transporter in the RBC membrane) to also be the water channel. For the first time Gh. Benga considered the possibility that “a minor protein” in the RBC membrane could be a specific water channel.

In 1988 the protein identified by Benga et al. (1986a), Benga et al. (1986b) was by serendipity purified by Peter Agre’s group working at The Johns Hopkins University, School of Medicine, Baltimore, United States (Denker et al., 1988). Agre confessed on several occasions (cited by Allewa et al., 2012): “Our laboratory got into the water channel field by accident”. In 1988 he and his coworkers had no idea of the function of the purified protein, which they called CHIP28, from *CH*annel forming integral membrane protein of 28 kDa (Denker et al., 1988). In addition to the 28 kDa component, the protein had a 35–60 kDa glycosylated component, i.e., the one previously detected by Benga et al. (1986a), Benga et al. (1986b) as the binding site of PCMBs under conditions for the inhibition of water transport across the RBC membrane. In their paper Agre and coworkers (Denker et al., 1988) have cited one of Benga’s group articles (Benga et al., 1983a): “the characteristics of CHIP28 are consistent with other known features of water channels, e.g., CHIP28 proteins in intact RBCs are impervious to proteolytic digestion (Denker et al., 1988; Smith and Agre, 1991) as are water channels (Benga et al., 1983a).” However, they have not cited the two landmark papers previously published by Gh. Benga’s group Benga et al. (1986a), Benga et al. (1986b).

Following the advice of Prof. John C. Parker (Agre’s Clinical Mentor at The Univ. of North Carolina at Chapel Hill) that CHIP28 could be a water channel, Agre’s group performed an experiment which proved that oocytes from *Xenopus laevis* microinjected with in vitro-transcribed CHIP28 RNA exhibited increased osmotic water permeability. This was inhibited by mercuric chloride, therefore, it was suggested that CHIP28 is a functional unit of membrane water channels (Preston et al., 1992). However, they recognized that “the possibility exists that CHIP28 may function as a water channel regulator, rather than the water channel itself.” The final proof that CHIP28 is the water channel itself rather than a water channel regulator was demonstrated by reconstitution in liposomes and direct measurements of osmotic water permeability by the collaboration of Mark Zeidel’s group (from Harvard Medical School) with Peter Agre’s group (Zeidel et al., 1992). This was already suggested by Gh. Benga’s group in the first landmark paper (Benga et al. (1986a).

The protein identified in Cluj-Napoca was the first water channel discovered. Other WCPs were discovered in 1993: in a plant (Maurel et al., 1993) and in the kidney (Fushimi et al., 1993). The name of

aquaporins was proposed for the WCPs (Agre et al., 1993) and CHIP28 was named aquaporin 1 (AQP1). In a few years it became obvious that a large family of WCPs exists, with three subfamilies: aquaporins (AQPs), aquaglyceroporins, and S-aquaporins. Moreover, it was discovered that actually the WCP family (with all three subfamilies) belongs to a superfamily of Membrane Intrinsic Proteins (MIPs). MIP is an acronym first used for MIP 26 (Major Intrinsic Protein of 26 kDa) of lens fiber cells in the eye (Gorin et al., 1984). Later, the presence and roles of such proteins in all kinds of species on Terra (from prokaryotes to plants, animals and humans) have been revealed. Lots of papers, special issues of prestigious journals, multi-authored books, were dedicated to the newly discovered proteins (Heymann and Engel, 1999; Benga, 2005; Zardoya, 2005; Gonen and Walz, 2006; Kuchel, 2006; Benga, 2009; Benga, 2012a; Yang, 2017).

In 2003, Peter Agre was awarded the Nobel Prize in Chemistry, which he shared with Roderick MacKinnon for their “discoveries concerning structure and function of channels in cell membranes”.

Agre introduced his Nobel Lecture with these words: “I wish to discuss the background in order to give credit to the individuals who were in this field long before we joined the field. The current view is that the lipid bilayer has a finite permeability for water, but, in addition, a set of proteins exists that we now refer to as “aquaporins”. Their existence was suggested by a group of pioneers in the water transport field who preceeded us by decades—people including Arthur K. Solomon in Boston, Alan Finkelstein in New York, Robert Macey in Berkeley, Gheorghe Benga in Romania, Guillermo Whittumbury in Venezuela, Mario Parisi in Argentina—who by biophysical methods predicted that water channels must exist in certain cell types with high water permeability as renal tubules, salivary glands, and red cells (Agre, 2004).” Some comments regarding the 2003 Nobel Prize in Chemistry appeared in 2003 and afterwards (Balaban et al., 2006; Cucuianu, 2006; Haulică, 2006).

George Emil Palade (1974 Nobel Laureate in Physiology of Medicine) sent on December 2003 a message by fax supporting the recognition of the priority of Gh. Benga:

“Dear Doctor Benga,

I did not expect The Nobel Committee for Chemistry to select water channels as area to give prominence this year and I did not realize either how close is your work to that of Peter Agre.

The idea of a petition has the merit of attracting the attention to the scientific community in the regrettable mistake of your omission from the group of laureates this year.

In any case I signed the petition received from you, I wish you enough courage and strength to carry through this battle and I remain sincerely,

George E. Palade”

Wed, 19 November 2003 To: Gheorghe Benga <gbenga@clujnapoca.ro> From Naoyuki Taniguchi <proftani@biochem.med.osaka-u.ac.jp> Subject: I regret very much.

Dear Professor Benga: I was really surprized to know that you are not awarded even though you are the first scientist who discovered aquaporin 1. It is my also great regret to hear that one of the Nobel Laureates did not cite your work which is really unfair. I do not know what kind of politics existed in these processes [...] Sincerely yours, Naoyuki Taniguchi M.D. Ph.D.,

Professor and Chairman, Dept. of Biochemistry, Osaka Univ. Medical School, Osaka University Graduate School of Medicine, Room B-1, 2-2 Yamadaoka Suita Osaka 565-0871 Japan.

“In the late 1980s, Peter Agre, while working on the rhesus blood group antigens at Johns Hopkins University serependipitously discovered a new membrane protein that he called CHIP28 (*channel integral protein of molecular weight 28 kD*). At the time he had no idea that its function was ... Previously and independently, Gheorghe Benga and his group in Romania had shown that the water transport inhibitor *p*-chloromercuribenzenesulfonate selectively bound to a protein in red blood cell membranes ... Subsequent studies showed that this was a glycosylated form of CHIP28 (Vandenberg and Kuchel, 2003).”

“The detection of water-specific membrane channels in red blood cells belong to the fundamental discoveries in biology of the 20th century ... In 1986 and 1988, the independent groups of Gheorghe Benga and Peter Agre, respectively, discovered the water channel proteins which later were called aquaporins (Wolburg et al., 2011).”

“The 2003 Nobel prize in chemistry was awarded for the discovery of “porins”—protein channels that transport molecules through cell membranes. It went to the Americans Peter Agre for aquaporins, or water channels, and Roderick MacKinnon for potassium channels. But aquaporins were first described in 1986 by Gheorghe Benga, in what was then communist Romania. There is no doubt that Agre told us much more about aquaporins than Benga did, but I can’t believe Benga would have been excluded from the award had he been working in a Western nation (Cox, 2014).”

Consequently, looking in retrospect, asking the crucial question, when was the first water channel protein, aquaporin 1, discovered, a fair and clear cut answer would be: the first water channel protein, now called aquaporin 1, was identified or “seen” *in situ* in the human RBC membrane by Benga and coworkers in 1986 (Benga et al. (1986a), Benga et al. (1986b)). It was again “seen” when it was by chance purified by Agre and coworkers in 1988 (Denker et al., 1988), and was again identified when its main feature, the water transport property was found by Agre, Zeidel and coworkers in 1992 (Preston et al., 1992; Zeidel et al., 1992). The discovery of AQP1 laid the ground for the identification of other water channel family members by homology cloning and other means, which has led to the understanding that aquaporins play essential roles in water transport in tissues. Today almost 400,000 articles are indexed under the tag water channel proteins in PubMed (<http://www.ncbi.nlm.nih.gov/pubmed>).

COMPARATIVE LIGHT AND SCANNING ELECTRON MICROSCOPIC ASPECTS OF RBCS FROM HUMANS AND VARIOUS ANIMAL SPECIES AND NMR STUDIES OF RBC WATER PERMEABILITY

In September 1989 at an international event on RBCs organized in what was then The “East Berlin” Gh. Benga had the chance to meet Professor Philip Kuchel (The University of Sydney), who

was aware of the papers published in 1977 by Benga and Morariu (mentioned above). The idea of a comparative program of studies of water permeability of RBCs in various animals occurred in the discussion. Gh. Benga mentioned that in Cluj-Napoca such studies have already been started and it would be very interesting to compare the characteristics of water permeability of RBCs from animal species living in Europe with those living only in Australia or introduced from Europe to Australia. A collaborative program of research of Gh. Benga's group in Romania with Philip Kuchel, Guy Cox and other distinguished Australian scientists whose names are listed in the Dedication (The Australian group) was established after 1990, when the "communist" regime collapsed in Romania. The two groups achieved exchange working visits, performing studies of the RBC water permeability of over 30 species and the program is still active.

Samples of blood were obtained from: "Iuliu Hațieganu" University of Medicine and Pharmacy Cluj-Napoca, Romania; Taronga Zoo, Sydney, NSW; Dubo Zoo, NSW; University of New England, Armidale, NSW; CSIRO McMaster Laboratory, Sydney, NSW; CSIRO Wildlife and Ecology Division, Canberra, ACT; Department of Veterinary Physiology, University of Sydney, NSW.

Species studied were: **Placentals:** man (*Homo sapiens*), mouse (*Mus musculus*), rat (*Rattus norvegicus*), sheep (*Ovis aries*), dog (*Canis familiaris*), dingo (*Canis lupus dingo*), horse (*Equus ferus caballus*), cow (*Bos taurus*), guinea pig (*Cavia porcellus*), rabbit (*Chinchilla*) (*Oryctolagus cuniculus*), alpaca (*Lama pacos*), camel (*Camelus dromaderius*), elephant (*Elephas maximus*). **Marsupials:** bilby (*Macrotis lagotis sagitta*), bandicoot (*Isodon macrourus*), Tasmanian devil (*Sarcophilus harrisi*), koala (*Phascolarctus cinereus*), brushtail possum (*Trichosurus vulpecula*), Godfellow's tree kangaroo (*Dendrolagus goodfellowi*), Bennett's wallaby (*Macropus rufogriseus*), parma wallaby (*Macropus parma*), swamp wallaby (*Wallabia bicolor*), tammar wallaby (*Macropus eugenii*), whiptail wallaby (*Macropus paryi*), Eastern grey kangaroo (*Macropus giganteus*), red kangaroo (*Macropus rufus*). **Monotremes:** platypus (*Ornithorhynchus anatinus*), echidna (*Tachyglossus aculeatus*). **Birds:** little penguin (*Eudyptula minor*), chicken (*Gallus domesticus*). **Reptiles:** green sea turtle (*Chelonia mydas*), saltwater crocodile (*Crocodyllis porosus*). Human RBCs were used as reference materials.

Blood was collected into heparinised tubes (~15 IU/ml), refrigerated within 30 min and used within 72 h. The RBCs were isolated by centrifugation, washed three times in medium S (150 mMNaCl, 5.5 mM glucose, 5 mM Hepes [4-(2-hydroxy-ethyl)-1-piperazine ethanesulphonic acid], pH 7.4. Finally, the erythrocytes were suspended in medium S (supplemented with 0.5% bovine serum albumin) at a hematocrit of 30–50%.

The mean cell volumes were calculated from the measurements of hematocrits and mean cell counts, using a Sysmex-CC 130 Microcell counter (Tao Medical Electronics Co. Ltd., Kobe, Japan).

The cell water content was determined by drying samples of RBCs at 105°C to constant weight (~15 h) and calculating the cell water volume as a fraction of cell volume.

The cell surface areas were calculated from the mean cell diameters when the cells were swollen to spheres in hypotonic NaCl solutions containing 0.5% (w/v) albumin as previously described (Benga et al., 1993a). The measurements were performed using an image analyzer (Tracor Northern TN 8502, Madison, WI, United States).

For scanning electron microscopy (SEM), samples of sedimented washed RBCs were fixed using 1% glutaraldehyde in medium S. After 90 min at 0°C the cells were sedimented and washed twice in 150 mM-phosphate buffer, pH 7.2. They were then post-fixed in 1% osmium tetroxide, dehydrated and critical-point dried from CO₂. After mounting and sputter-coating with gold, samples were examined and photographed in a Hitachi HU-11A (in Romania) and a Jeol JSM-6300 f scanning electron microscope (in Australia). The diameters of RBCs were measured on photographs using a binocular enlarging system with a calibrated eye piece. The measurements were performed only on cells lying completely flat or exactly on edge. Other details of the SEM analyses were previously described (Benga et al., 1992b; Benga et al., 1999; Benga et al., 2000a; Benga et al., 2003; Benga et al., 2010a; Benga et al., 2010b; Benga et al., 2015).

A selection of optical micrographs and SEM images of RBCs from humans and some animal species are presented in **Figures 1–3**. Some aspects of RBCs from these Figures need to be discussed. A first important aspect is the *presence of nucleus* in the RBCs of reptiles and birds: Green Sea Turtle (*Chelonia mydas*), respectively Little Penguin (*Eudyptula minor*) presented in **Figure 1**. As mentioned in the Introduction, P. Plósz, (1871) reported the presence of "nuclein" in the hemolyzed nucleated erythrocytes from birds and snakes and this was actually a crucial step in the discovery of DNA.

The second aspect is the correlation between the *size* of RBCs with the whole *body size (mass)* of various organisms. In **Figure 2** RBCs from nine species of marsupials are presented: bandicoot (*Isodon macrourus*), bilby (*Macrotis lagotis sagitta*), koala (*Phascolarctus cinereus*), red kangaroo (*Macropus rufus*), Bennett's wallaby (*Macropus rufogriseus*), parma wallaby (*Macropus parma*), swamp wallaby (*Wallabia bicolor*), Tammar wallaby (*Macropus eugenii*), whiptail wallaby (*Macropus paryi*). The RBCs of these species have a rather similar size, although the whole body size is highly variable (from the small sizes in bilby and bandicoot to the large sizes of wallabies and kangaroos). The relationship between the size of RBCs and the body size (mass) is also easy to be seen in the case of the Indian elephant (*Elephas maximus*) compared with humans (*Homo sapiens*) (**Figure 3**). The diameter of the elephant RBC is ~9.3 μm, which is ~1.4 μm larger than that for the human RBC (Benga et al., 2000a). The difference between the whole body size (mass) of these two species is huge. As mentioned in the Introduction such observations led to the so called "Law of constant volume", formulated in the 19th century (De Robertis, 1970).

The third aspect is the *shape* of RBCs. The human RBCs, and the RBCs of the majority of animal species are biconcave disks. This is true for: 1) the RBCs of monotremes: platypus (*Ornithorhynchus anatinus*) in **Figure 1**; 2) the RBCs of all marsupials; 3) the RBCs of some placentals: humans (in

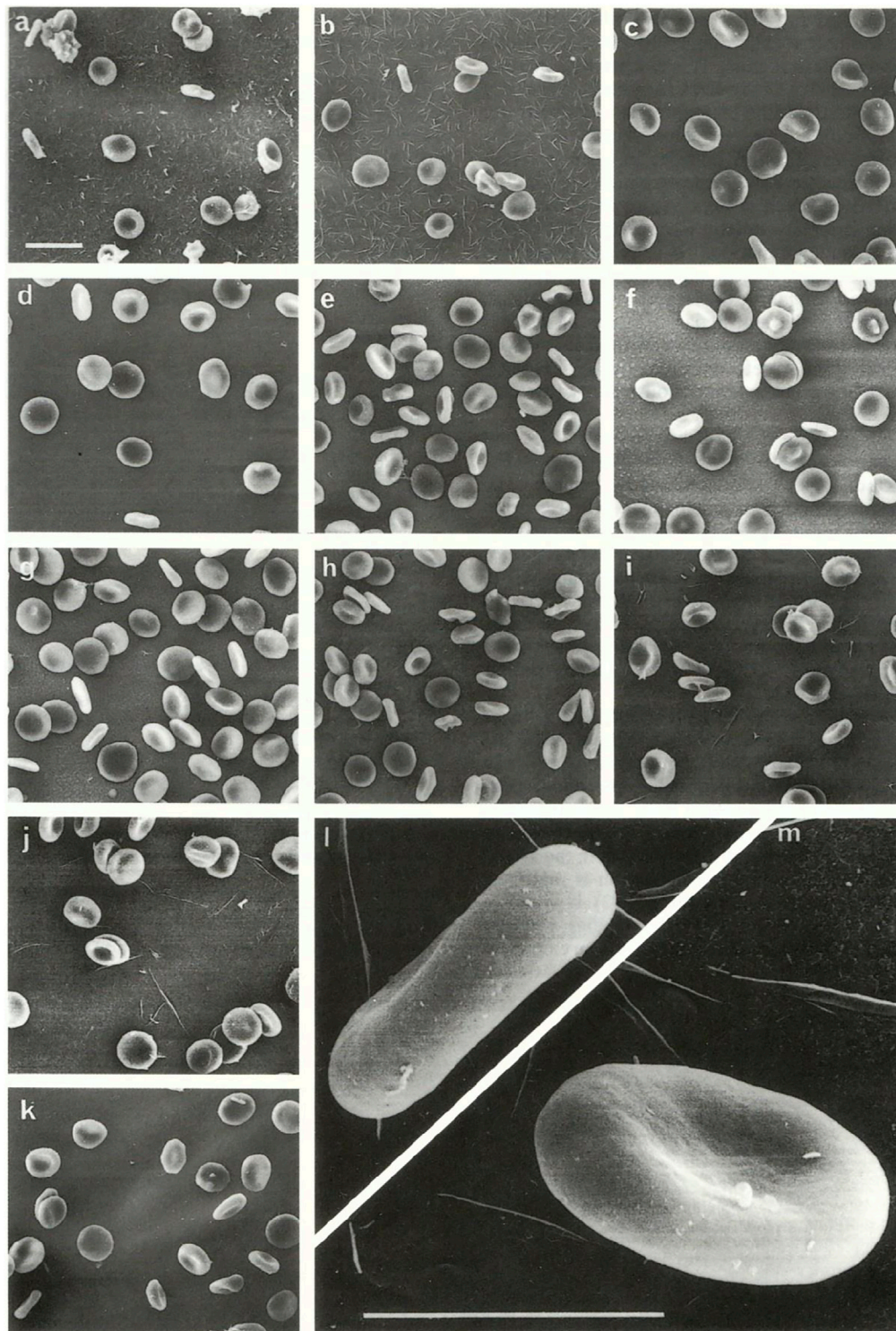


FIGURE 2 | Marsupials. Scanning electron microscopic appearance of red blood cells from **(A)** bandicoot; **(B)** bilby; **(C)** koala; **(D)** red kangaroo; **(E)** Bennett's wallaby; **(F)** parma wallaby; **(G)** swamp wallaby; **(H)** Tammar wallaby; **(I,J)** whiptail wallaby; and **(K-M)** man. **(A-K)** original magnification $\times 2,000$, scale bar 5 μm ; **I, m** original magnification $\times 10,000$, scale bar 5 μm . The original images were published by (Benga et al., 1992b).

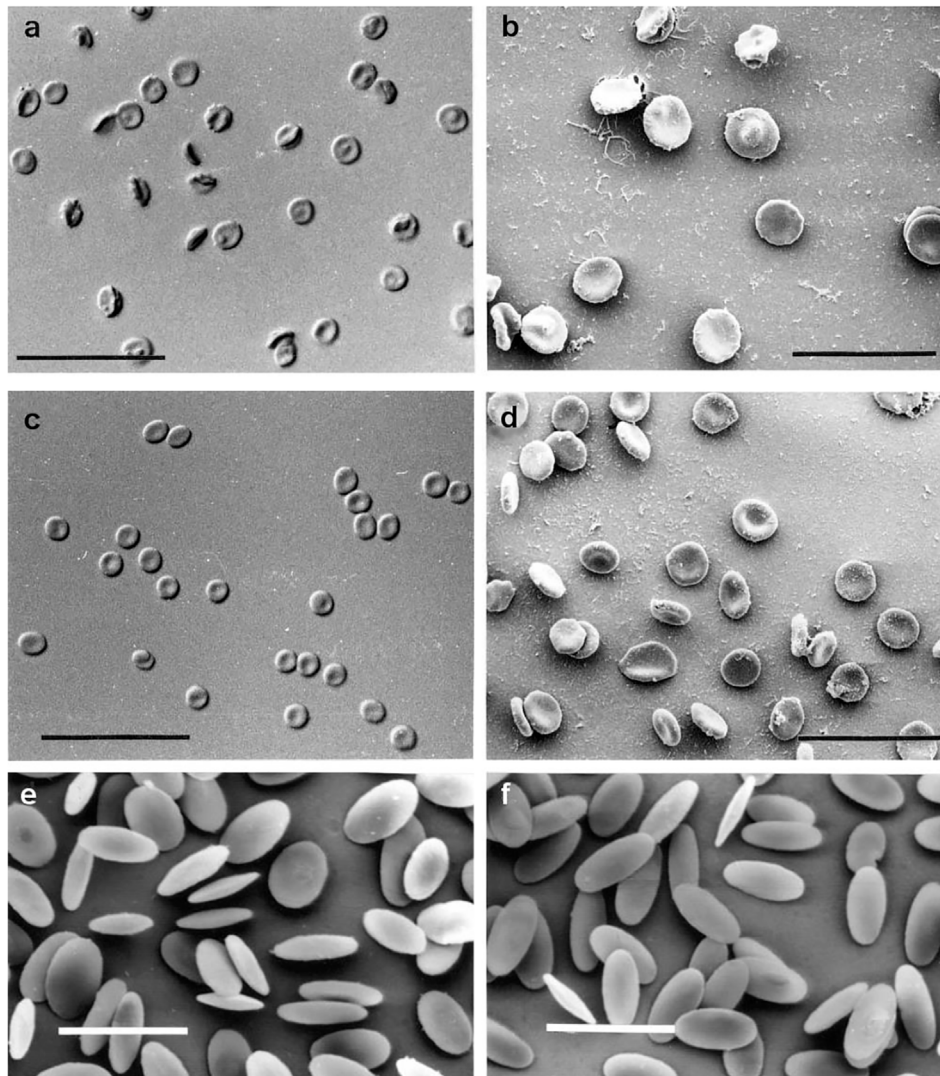


FIGURE 3 | (A) DIC optical micrograph of Indian elephant (*Elephas maximus*) RBCs. Scale bar = 50 μ m (Nikon Eclipse E800 Plan Apo $\times 40$ 0.95NA objective); **(B)** Secondary electron SEM image of Indian elephant RBCs. Scale bar = 22 μ m (Jeol JSM-6300f); **(C)** DIC optical micrograph of human (*Homo sapiens*) RBCs. Scale bar = 50 μ m (Nikon Eclipse E800 Plan Apo $\times 40$ 0.95NA objective.); **(D)** Secondary electron SEM image of human RBCs. Scale bar = 22 μ m (Jeol JSM-6300f); **(E)** Secondary electron SEM image of washed RBCs from camel (*Camelus dromedarius*). Scale bar = 10 μ m (JEOL JSM-6300f); **(F)** Secondary electron SEM image of washed RBCs from alpaca (*Lama pacos*). Scale bar = 10 μ m (JEOL JSM-6300f). The original images were published by Benga et al., 1999; Benga et al., 2000a.

Figures 2, 3), Indian elephant (*Elephas maximus*) in **Figure 3**. On the other hand there are placentals which have ellipsoidal RBCs. This is the case of RBCs from camelids: camel (*Camelus dromedarius*) and alpaca (*Lama pacos*) (**Figure 3**). It is probably related to their ability to swell rapidly when a dehydrated camel rehydrates and thereby avoid haemolysis (Benga et al., 1999).

Samples of sedimented washed RBCs were fixed using 1% glutaraldehyde in medium S. After 90 min at 0 °C the cells were sedimented and washed twice in 150 mM-phosphate buffer, pH 7.2. They were then post-fixed in 1% osmium tetroxide, dehydrated and critical-point dried from CO₂. After mounting and sputter-coating with gold, samples were examined and photographed in a Hitachi HU-11A (in Romania) and a Jeol

JSM-6300 f scanning electron microscope (in Australia). The diameters of RBCs were measured on photographs using a binocular enlarging system with a calibrated eye piece. The measurements were performed only on cells lying completely flat or exactly on edge. The details of the SEM analyses were previously described (Benga et al., 1992b; Benga et al., 1999; Benga et al., 2000a; Benga et al., 2003; Benga et al., 2010a; Benga et al., 2010b; Benga et al., 2015). The values are mean \pm standard deviations.

Samples of elephant (*Elephas maximus*) blood were obtained from Taronga Zoo, Sydney, New South Wales; the donor was a female, aged 43 years and weighing 3500 kg. Blood samples were collected into heparin (15 IU/ml), refrigerated within 30 min and used within 72 h. The last sample had a haematocrit of 48%, mean

TABLE 1 | Diameters of animal RBC compared with human RBC, measured by electron microscopy.

Species	Number of cells measured	Diameter (μm)	
		Observed	Corrected
Bandicoot (<i>Isodon macrourus</i>)	40	4.66 ± 0.15	7.12 ± 0.22
Bilby (<i>Macrotis lagotis sagitta</i>)	70	4.59 ± 0.23	7.01 ± 0.36
Tasmanian devil (<i>Sarcophilus harrisii</i>)	24	4.43 ± 0.19	6.77 ± 0.29
Koala (<i>Phascolarctus cinereus</i>)	45	5.63 ± 0.20	8.60 ± 0.31
Bennet's wallaby (<i>Macropus rufogriseus</i>)	71	5.27 ± 0.15	8.05 ± 0.23
Parma wallaby (<i>Macropus parma</i>)	108	5.23 ± 0.19	8.00 ± 0.29
Swamp wallaby (<i>Wallabia bicolor</i>)	108	5.61 ± 0.15	8.57 ± 0.23
Whiptail wallaby (<i>Macropus paryi</i>)	37	5.48 ± 0.18	8.38 ± 0.27
Tammar wallaby (<i>Macropus eugenii</i>)	98	5.07 ± 0.12	7.76 ± 0.18
Goodfellow's tree kangaroo (<i>Dendrolagus goodfellowi</i>)	37	4.82 ± 0.14	7.30 ± 0.21
Red kangaroo (<i>Macropus rufus</i>)	75	5.46 ± 0.11	8.35 ± 0.17
Man (<i>Homo sapiens</i>)	77	5.24 ± 0.18	8.00 ± 0.22

TABLE 2 | Diameter of elephant RBC compared with human RBC.

Species	Technique	Number of cells	Diameter (μm)	Corrected
		Measured	Observed	
Elephant	Light microscopy	26	9.3 ± 0.7	9.3 ± 0.7
	SEM	46	7.8 ± 0.6	
Man	Light microscopy	29	8.0 ± 0.4	8.0 ± 0.6
	SEM	31	6.7 ± 0.4	

whole-blood haemoglobin concentration of 172 g/l whole blood, a mean corpuscular haemoglobin concentration of 358 g/l RBC and a mean corpuscular volume of 126 fl. The RBCs were isolated by centrifugation, washed three times in medium S (150 mM NaCl, 5.5 mM glucose, 5 mM Hepes [4-(2-hydroxy-ethyl)-1-piperazine ethanesulphonic acid]), pH 7.4. Finally, the erythrocytes were suspended in medium S (supplemented with 0.5% bovine serum albumin) at a hematocrit of 30–50%. For light microscopy, samples of RBCs were fixed for 90 min in 1% (w/v) glutaraldehyde in with medium S, followed by three washes in isotonic phosphate buffer, pH 7.2. The suspended cells were then placed on a clean microscope slide, a cover slip was placed over them and they were examined using a Nikon Eclipse 800 microscope (Nikon Corporation, Tokyo, Japan) using the differential interference contrast (DIC) technique. Image acquisition was performed using a charge-coupled device (CCD) Imaging Sensicam (PCO Computer Optics, GmbH, Kelheim, Germany) at 1280×1024 pixels. A stage micrometer

was used as a size reference. For scanning electron microscopy (SEM) the samples were prepared as described above and examined and photographed using a Philips XL30 scanning electron microscope. The results are presented in **Tables 1, 2**. The original results were published by Benga et al., 1992b; Benga et al., 2000a.

The results of our comparative NMR studies of water permeability of RBCs from humans and various animal species were published in many papers (Benga et al., 1992a; Benga et al., 1992b; Benga et al., 1993a; Benga et al., 1993b; Benga et al., 1993c; Benga et al., 1993d; Benga et al., 1993e; Benga et al., 1994a; Benga et al., 1994b; Benga et al., 1995; Benga and Borza, 1995; Benga et al., 1996; Benga et al., 1999; Benga et al., 2000a; Benga et al., 2000b; Benga et al., 2002a; Benga et al., 2002b; Benga et al., 2003; Benga et al., 2009; Benga et al., 2010a; Benga et al., 2015). We express here (in **Figures 4–6**) only a brief overview of our studies, previously published (Benga et al., 1992b;

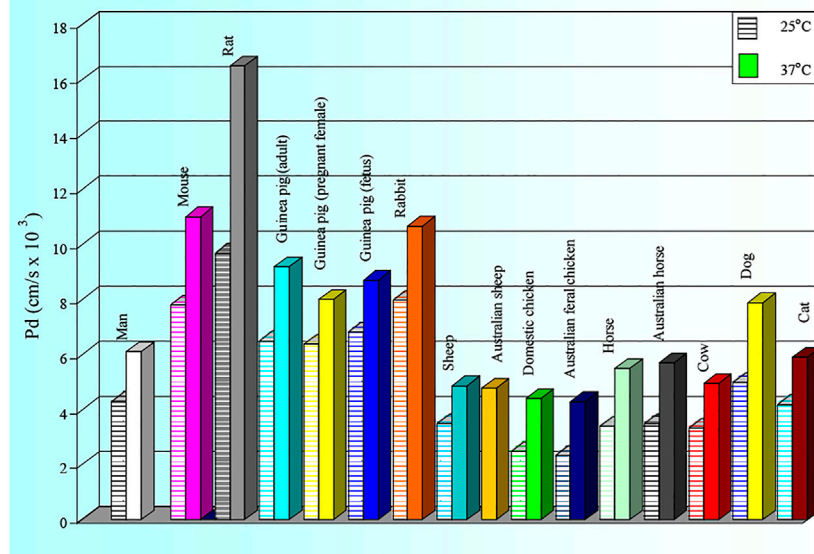


FIGURE 4 | Values of the membrane diffusional permeability (P_d) to water of RBCs of man and several animal species. The SD values are: Man: 25 °C: 0.50; 37 °C: 0.12; Mouse: 25 °C: 0.30; 37 °C: 0.81; Rat: 25 °C: 0.23; 37 °C: 0.21; Guinea pig (adult): 25 °C: 1.31; 37 °C: 2.02; Guinea pig (pregnant female): 25 °C: 1.31; 37 °C: 2.02; Guinea pig (fetus): 25 °C: 0.66; 37 °C: 1.16; Rabbit: 25 °C: 0.68; 37 °C: 1.77; Sheep: 25 °C: 0.54; 37 °C: 0.86; Australian sheep: 25 °C: 0.75; 37 °C: 1.06; Domestic chicken: 25 °C: 0.25; 37 °C: 0.21; Australian feral chicken: 25 °C: 0.37; 37 °C: 0.55; Horse: 25 °C: 0.87; 37 °C: 0.75; Australian horse: 25 °C: 1.07; 37 °C: 1.02; Cow: 25 °C: 0.54; 37 °C: 0.86; Dog: 25 °C: 0.20; 37 °C: 0.22; Cat: 25 °C: 0.50; 37 °C: 0.72.

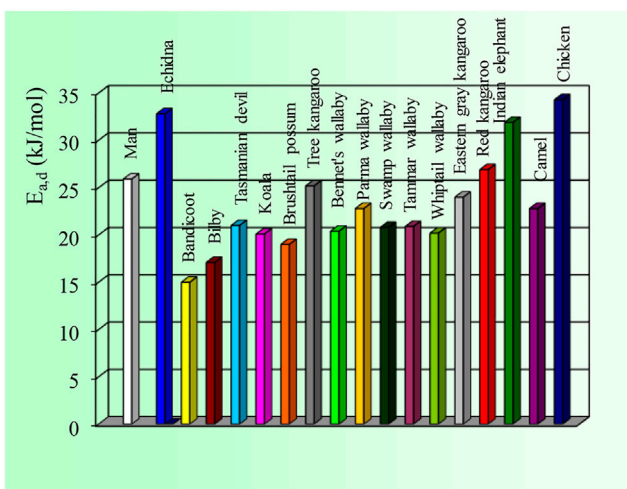


FIGURE 5 | Values of the activation energy of water diffusion through the RBC membrane of man and several animal species. The SD values are: Man: 2.9; Echidna: 6.2; All Marsupials: 1.9–2.0; Elephant: 0.6; Camel: 1.8; Chicken: 7.0. The original results were published previously (Benga et al., 1992b; Benga and Borza, 1995; Benga et al., 1999; Benga et al., 2000a; Benga et al., 2003; Benga et al., 2010a; Benga et al., 2010b; Benga, 2013; Benga et al., 2015).

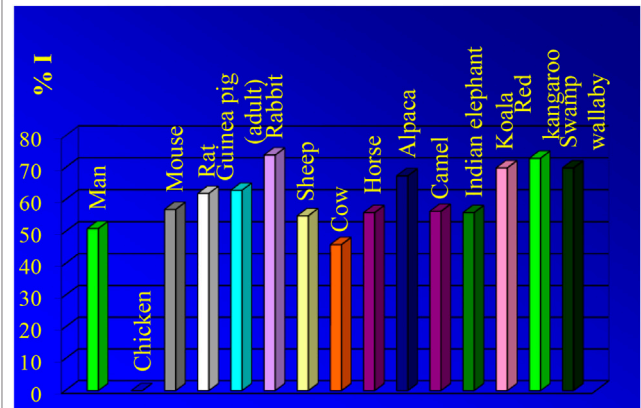


FIGURE 6 | Effects of PCMBs (inhibitor) of water channel proteins on water diffusion through the RBC membrane of man and several animal species. The highest value of inhibition is presented for each species. The original results were published previously (Benga et al., 1992b; Benga and Borza, 1995; Benga et al., 1999; Benga et al., 2000a; Benga et al., 2003; Benga et al., 2010a; Benga et al., 2010b; Benga, 2013; Benga et al., 2015).

Benga and Borza, 1995; Benga et al., 1999; Benga et al., 2000a; Benga et al., 2003; Benga et al., 2010a; Benga et al., 2010b; Benga, 2013; Benga et al., 2015).

As shown in **Figure 4** and **Figure 5** the RBC water permeability (P_d and $E_{a,d}$) are species characteristics, as there are no changes correlated with the marked alteration in the habitat of the species introduced to Australia (rat, rabbit, sheep, chicken) compared with their European counterpart. Human RBCs have P_d values of $\sim 4 \times 10^{-3} \text{ cm s}^{-1}$ at 25 °C and $\sim 7 \times 10^{-3} \text{ cm s}^{-1}$ at 37 °C with a

value of $E_{a,d} \sim 25 \text{ kJ mol}^{-1}$. The chicken and echidna RBCs have the lowest P_d values ($\sim 2 \times 10^{-3} \text{ cm s}^{-1}$) and the highest values of $E_{a,d}$ (over 30 kJ mol^{-1}). This indicates that no functional AQPs are present in chicken and echidna RBCs. Large and less-active animals (cow, sheep, horse and elephant) have lower values of P_d . In contrast, small and active animals (mouse, rat, guinea pig, rabbit, small marsupials) have P_d values significantly higher with lower $E_{a,d}$ values (from 15 to 22 kJ mol^{-1}).

The original results were published previously (Benga et al., 1992b; Benga and Borza, 1995; Benga et al., 1999; Benga et al., 2000a; Benga et al., 2003; Benga et al., 2010a; Benga et al., 2010b; Benga, 2013; Benga et al., 2015).

We measured the effects of various inhibitors on water diffusion through the RBC membrane of man and several animal species. As previously described, the water channels are blocked by PCMBs: *p*-(Chloromercuri) benzenesulfonate. As shown in **Figure 3** PCMBs has no effects in case of chicken RBCs. This indicates that no functional AQPs are present in chicken RBCs.

Kuchel and Benga, (2003), Kuchel and Benga, (2005) provided two new explanations for the physiological “raison d’être” of AQPs in RBC. The first is the “oscillating sieve explanation”: the high water permeability of RBC membrane favours the energy driven membrane undulations (or oscillations) of the RBC membrane, a phenomenon also called “flickering” (Morariu et al., 1966; Brochard and Lennon, 1975); these movements consume a minimum of energy in simply displacing water. Such membrane undulations perform a valuable role in movement of cells through capillaries. The second is the “water displacement explanation”: when ions, such as Cl^- and HCO_3^- , and solutes, such as glucose, are entering into the cells, the water molecules are displaced and exit rapidly the cell, thus obviating a change in cell volume. The molecular volume of these ions and molecules are significantly higher than that of water. Kuchel and Benga, (2003), Kuchel and Benga, (2005) that AQPs in RBCs ensure the rate of exchange of water across the membrane required in various animals in relation to their physical activity, metabolic rate and the mean rate of circulation of their blood. Whether there is a correlation between the macroscopic whole-body activity and the cellular-membrane fluctuations, and hence the requirement (according to the above hypothesis) for differences in water exchange rate, is as yet unknown, and begs new investigations.

REFERENCES

- Agre, P., Sasaki, S., and Chrispeels, M. J. (1993). Aquaporins: a Family of Water Channel Proteins. *Am. J. Physiology-Renal Physiology* 265, F461. doi:10.1152/ajprenal.1993.265.3.f461
- Agre, P. (2004). Nobel Lecture. Aquaporin Water Channels. *Biosci. Rep.* 24, 127–163. doi:10.1007/s10540-005-2577-2
- Alberts, B., Johnson, A., Lewis, J., Morgan, D., Raff, M., Roberts, K., et al. (2008). *Molecular Biology of the Cell*. Sixth edition. New York, Abingdon: Garland Science, Taylor & Francis Group.
- Allewa, K., Chara, O., and Amodeo, G. (2012). Aquaporins: Another Piece in the Osmotic Puzzle. *FEBS Lett.* 586, 2991–2999. doi:10.1016/j.febslet.2012.06.013

CONCLUSION

Many discoveries in cell biology have been based on RBCs. Advances in molecular and structural biology in the past 40 years, have enabled the discovery with these cells, most notably, of the water channel protein, called today aquaporin1 (AQP1). It appears that AQPs in RBCs ensure the rate of exchange of water across the membrane required in various animals in relation to their physical activity, metabolic rate and the mean rate of circulation of their blood.

DEDICATIONS

We dedicate this paper to the people from Australia (Bogdan E. Chapman, Clifford H. Gallagher), Romania (Adriana Hodârnu, Victoria Borza, Vasile V. Morariu, Dorin Poruțiu, Petre T. Frangopol) and United Kingdom (John Wigglesworth, William Ferdinand), who contributed essentially to the work on RBC water permeability over the decades and have now passed away.

AUTHOR CONTRIBUTIONS

GhB—planning, physiology, microscopy, final mss. GC—optical and electron microscopy, final mss.

ACKNOWLEDGMENTS

The comments of Professor Philip Kuchel (School of Life and Environmental Sciences, Faculty of Science, University of Sydney) are acknowledged. The excellent SEM work of Tony Romeo (Australian Centre for Microscopy & Microanalysis, University of Sydney) and of Anthony Brain (Laboratory of Electron Microscopy, King’s College, University of London) are also acknowledged. The authors thank Ciprian-Valentin Mihali, BSc, MBIol, PhD, Cell and Molecular Biology/Electron Microscopy, “Vasile Goldiș” Western University of Arad and Molecular Biology Laboratory, Research and Development Station for Bovine, Arad, for arranging **Figures 1–3**.

- Balaban, A. T., Haiduc, I., Matasa, C. G., and Sha’afi, R. I. (2006). Who Discovered the Water Channels (Aquaporins)? *Cell Mol. Biol. (Noisy-le-grand)* 52, 6–7.
- Benga, G., Popescu, O., and Pop, V. I. (1983a). Water Exchange Through Erythrocyte Membranes. V. Incubation With Papain Prevents the *p*-Chloromercuribenzenesulfonate Inhibition of Water Diffusion Studied by a Nuclear Magnetic Resonance Technique. *Cell Biol. Int. Rep.* 7, 807–818.
- Benga, Gh., and Borza, T. (1995). Diffusional Water Permeability of Mammalian Red Blood Cells. *Comp. Biochem. Physiology Part B Biochem. Mol. Biol.* 112, 653–659. doi:10.1016/0305-0491(95)00116-6
- Benga, Gh., and Holmes, R. P. (1984). “Interactions Between Components in Biological Membranes and Their Implications for Membrane Function,”. Editor T. L. Blundell, 43, 195–257. doi:10.1016/0079-6107(84)90014-2 *Prog. Biophysics Mol. Biol.*

- Benga, Gh., and Morariu, V. V. (1977). Membrane Defect Affecting Water Permeability in Human Epilepsy. *Nature* 265, 636–638. doi:10.1038/265636a0
- Benga, Gh., and Tager, J. M. (1988). *Biomembranes: Basic and Medical Research*. Berlin: Springer-Verlag.
- Benga, Gh., Baum, H., and Kummerow, F. A. (1984). *Membrane Processes: Molecular Biology and Medical Applications*. New York: Springer-Verlag.
- Benga, Gh., Popescu, O., Pop, V. I., and Holmes, R. P. (1986a). P-(Chloromercuri) benzenesulfonate Binding by Membrane Proteins and the Inhibition of Water Transport in Human Erythrocytes. *Biochemistry* 25, 1535–1538. doi:10.1021/bi00355a011
- Benga, G., Popescu, O., Borza, V., Pop, V. I., Muresan, A., Mocsy, I., et al. (1986b). Water Permeability in Human Erythrocytes: Identification of Membrane Proteins Involved in Water Transport. *Eur. J. Cell Biol.* 41, 252–262.
- Benga, G., Brain, A., Pop, V., Hodárnău, A., and Wrighlesworth, J. (1987a). Freeze-fracture Electron Microscopic Observations on the Effects of Sulphydryl Group Reagents on Human Erythrocyte Membranes. *Cell Biol. Int. Rep.* 11, 679–687. doi:10.1016/0309-1651(87)90103-2
- Benga, G., Pop, V. I., Popescu, O., Hodárnău, A., Borza, V., and Presecan, E. (1987b). Effects of Temperature on Water Diffusion in Human Erythrocytes and Ghosts - Nuclear Magnetic Resonance Studies. *Biochimica Biophysica Acta (BBA) - Biomembr.* 905, 339–348. doi:10.1016/0005-2736(87)90462-7
- Benga, G., Popescu, O., Borza, V., Pop, V. I., and Hodárnău, A. (1989). Water Exchange through Erythrocyte Membranes: Biochemical and Nuclear Magnetic Resonance Studies Re-evaluating the Effects of Sulphydryl Reagents and of Proteolytic Enzymes on Human Membranes. *J. Membr. Biol.* 108, 105–113. doi:10.1007/BF01871022
- Benga, G., Pop, V. I., Popescu, O., and Borza, V. (1990). The Basal Permeability to Water of Human Red Blood Cells Evaluated by a Nuclear Magnetic Resonance Technique. *Biosci. Rep.* 10, 31–36. doi:10.1007/bf01116848
- Benga, G., Popescu, O., BorzaHodárnău, V. A., Hodárnău, A., Ioan Pop, V., and Wrighlesworth, J. (1991). Water Transport in Human Red Cells: Effects of 'non-Inhibitory' Sulphydryl Reagents. *Biochimica Biophysica Acta (BBA) - Biomembr.* 1061, 309–312. doi:10.1016/0005-2736(91)90297-1
- Benga, G., Popescu, O., Pop, V. I., Hodor, P., and Borza, T. (1992a). Effects on Water Diffusion of Inhibitors Affecting Various Transport Processes in Human Red Blood Cells. *Eur. J. Cell Biol.* 59, 219–223.
- Benga, G., Porutiu, D., Ghiran, I., Kuchel, P. W., Gallagher, C. H., and Cox, G. C. (1992b). Scanning Electron Microscopy of Red Blood Cells from Eleven Species of Marsupial. *Comp. Haematol. Int.* 2, 227–230. doi:10.1007/bf00216099
- Benga, G., Matei, H., Borza, T., Porutiu, D., and Lupse, C. (1993a). Comparative Nuclear Magnetic Resonance Studies on Water Diffusional Permeability of Red Blood Cells from Mice and Rats. *Comp. Biochem. Physiology Part A Physiology* 104, 491–495. doi:10.1016/0300-9629(93)90453-b
- Benga, G., Borza, T., Popescu, O., Porutiu, D., and Matei, H. (1993b). Comparative Nuclear Magnetic Resonance Studies of Diffusional Water Permeability of Red Blood Cells from Sheep and Cow. *Comp. Biochem. Physiology Part B Comp. Biochem.* 104, 589–594. doi:10.1016/0305-0491(93)90286-e
- Benga, G., Matei, H., Borza, T., Porutiu, D., and Lupse, C. (1993c). Comparative Nuclear Magnetic Resonance Studies of Diffusional Water Permeability of Red Blood Cells from Different Species. V-Rabbit (*Oryctolagus Cuniculus*). *Comp. Biochem. Physiology Part B Comp. Biochem.* 106, 281–285. doi:10.1016/0305-0491(93)90301-k
- Benga, G., Chapman, B. E., Gallagher, C. H., Cooper, D., and Kuchel, P. W. (1993d). NMR Studies of Diffusional Water Permeability of Red Blood Cells from Macropodid Marsupials (Kangaroos and Wallabies). *Comp. Biochem. Physiology Part A Physiology* 104, 799–803. doi:10.1016/0300-9629(93)90157-y
- Benga, G., Chapman, B. E., Gallagher, C. H., Agar, N. S., and Kuchel, P. W. (1993e). Nmr Studies of Diffusional Water Permeability of Erythrocytes from Eight Species of Marsupial. *Comp. Biochem. Physiology Part A Physiology* 106, 515–518. doi:10.1016/0300-9629(93)90246-z
- Benga, G., Ralston, G. B., Borza, T., Chapman, B. E., Gallagher, C. H., and Kuchel, P. W. (1994a). NMR Studies of Diffusional Water Permeability of Red Blood Cells from the Echidna *Tachyglossus aculeatus*. *Comp. Biochem. Physiology Part B Comp. Biochem.* 107, 45–50. doi:10.1016/0305-0491(94)90223-2
- Benga, G., Chapman, B. E., Hinds, L., and Kuchel, P. W. (1994b). Comparative NMR Studies of Diffusional Water Permeability of Erythrocytes from Some Animals Introduced to Australia: Rat Rabbit and Sheep. *Comp. Haematol. Int.* 4, 232–235. doi:10.1007/bf00185179
- Benga, G., Borza, T., Matei, H., Hodor, P., Frențescu, L. L., Ghiran, I., et al. (1995). Comparative Nuclear Magnetic Resonance Studies of Diffusional Water Permeability of Red Blood Cells from Different Species. VIII. Adult and Fetal guinea Pig (*Cavia Procellus*). *Comp. Haematol. Int.* 5, 106–111. doi:10.1007/bf00638928
- Benga, G., Matei, H., Chapman, B. E., Bulliman, B. T., Gallagher, C. H., Agar, N. S., et al. (1996). Comparative Nuclear Magnetic Resonance Studies of Diffusional Water Permeability of Red Blood Cells from Different Species. IX. Australian Feral Chicken and Domestic Chicken (*Gallus domesticus*). *Comp. Haematol. Int.* 6, 92–95. doi:10.1007/bf00426048
- Benga, G., Grieve, S. M., Chapman, B. E., Gallagher, C. H., and Kuchel, P. W. (1999). Comparative NMR Studies of Diffusional Water Permeability of Red Blood Cells from Different Species. X. Camel (*Camelus dromedarius*) and Alpaca (*Lama pacos*). *Comp. Haematol. Int.* 9, 43–48. doi:10.1007/bf02585521
- Benga, G., Kuchel, P. W., Chapman, B. E., Cox, G. C., Ghiran, I., and Gallagher, C. H. (2000a). Comparative Cell Shape and Diffusional Water Permeability of Red Blood Cells from Indian Elephant (*Elephas maximus*) and Man (*Homo sapiens*). *Comp. Haematol. Int.* 10, 1–8. doi:10.1007/s005800070020
- Benga, G., Matei, H., Frențescu, L., Chapman, B. E., and Kuchel, P. W. (2000b). Comparative Nuclear Magnetic Resonance Studies of Diffusional Water Permeability of Red Blood Cells from Different Species. XI. Horses Introduced to Australia and European Horses (*Equus caballus*). *Comp. Haematol. Int.* 10, 138–143. doi:10.1007/s005800070005
- Benga, G., Ghiran, I., Matei, H., Frențescu, L., and Florea, A. (2002a). Comparative Nuclear Magnetic Resonance Studies of Diffusional Water Permeability of Red Blood Cells from Different Species. XII. Dog (*Canis familiaris*) and Cat (*Felis Domestica*). *Comp. Clin. Pathol.* 11, 246–255. doi:10.1007/s005800200026
- Benga, G., Chapman, B. E., Matei, H., and Cox, G. C. (2002b). Effects of P-chloromercuribenzenesulfonate on Water Transport across the Marsupial Erythrocyte Membrane. *J. Comp. Physiology B Biochem. Syst. Environ. Physiology* 172, 513–518. doi:10.1007/s00360-002-0277-9
- Benga, G., Chapman, B. E., Cox, G. C., and Kuchel, P. W. (2003). Comparative NMR Studies of Diffusional Water Permeability of Red Blood Cells from Different Species: XIV. Little Penguin, *Eudyptula minor*. *Cell Biol. Int.* 27, 921–928. doi:10.1016/j.cellbi.2003.07.005
- Benga, G., Chapman, B. E., and Kuchel, P. W. (2009). Comparative NMR Studies of Diffusional Water Permeability of Red Blood Cells from Different Species. *Comp. Biochem. Physiology Part A Mol. Integr. Physiology* 154, 105–109. doi:10.1016/j.cbpa.2009.05.008
- Benga, G., Chapman, B. E., Matei, H., Cox, G. C., Romeo, T., Mironescu, E., et al. (2010a). Comparative NMR Studies of Diffusional Water Permeability of Red Blood Cells from Different Species: XVI Dingo (*Canis familiaris* Dingo) and Dog (*Canis familiaris*). *Cell Biol. Int.* 34, 373–378. doi:10.1042/cbi20090006
- Benga, G., Chapman, B. E., Cox, G. C., and Kuchel, P. W. (2010b). Comparative NMR Studies of Diffusional Water Permeability of Red Blood Cells from Different Species: XVIII Platypus (*Ornithorhynchus anatinus*) and Saltwater Crocodile (*Crocodylus Porosus*). *Cell Biol. Int.* 34, 703–708. doi:10.1042/cbi20090430
- Benga, G., Chapman, B. E., Romeo, T., Cox, G. C., and Kuchel, P. W. (2015). Morphology and Water Permeability of Red Blood Cells from Green Sea Turtle (*Chelonia mydas*). *Protoplasma* 252, 1181–1185. doi:10.1007/s00709-014-0747-4
- Benga, G. (1985a). *Structure and Properties of Cell Membranes*. A survey of molecular aspects of membrane structure and function, I. Boca Raton: CRC Press.
- Benga, G. (1985b). *Structure and Properties of Cell Membranes*. Molecular basis of selected transport systems, II. Boca Raton: CRC Press.
- Benga, G. (1985c). *Structure and Properties of Cell Membranes*. Methodology and properties of membranes, III. Boca Raton: CRC Press.
- Benga, G. (1989a). Water Exchange through the Erythrocyte Membrane. *Int. Rev. Cytol.* 114, 273–316. doi:10.1016/s0074-7696(08)60864-5
- Benga, G. (1989b). Permeability through Pores and Holes. *Curr. Opin. Cell Biol.* 1, 771–774. doi:10.1016/0955-0674(89)90047-1
- Benga, Gh. (1989c). "Membrane Proteins Involved in the Water Permeability of Human Erythrocytes." From cells to multicellular barrier systems in *Water Transport in Biological Membranes*. Editor G. Benga (Boca Raton: CRC Press), II, 41–62.
- Benga, G. (1994). Water Channels in Membranes. *Cell Biol. Int.* 18, 829–834. doi:10.1006/cbir.1994.1116
- Benga, G. (2003). Birth of Water Channel Proteins-The Aquaporins. *Cell Biol. Int.* 27, 701–709. doi:10.1016/s1065-6995(03)00171-9

- Benga, G. (2005). Water Channel Proteins: from Their Discovery in 1985 in Cluj-Napoca, Romania, to the 2003 Nobel Prize in Chemistry. *Cell Mol. Biol. (Noisy-le-grand)* 52, 10–19.
- Benga, G. (2009). Water Channel Proteins (Later Called Aquaporins) and Relatives: Past, Present, and Future. *IUBMB Life* 61, 112–133. doi:10.1002/iub.156
- Benga, G. (2012a). Foreword to the Special Issue on Water Channel Proteins (Aquaporins and Relatives) in Health and Disease: 25 Years after the Discovery of the First Water Channel Protein, Later Called Aquaporin 1. *Mol. Aspects Med.* 33, 511–513. doi:10.1016/j.mam.2012.06.002
- Benga, G. (2012b). On the Definition, Nomenclature and Classification of Water Channel Proteins (Aquaporins and Relatives). *Mol. Aspects Med.* 33, 514–517. doi:10.1016/j.mam.2012.04.003
- Benga, G. (2012c). The First Discovered Water Channel Protein, Later Called Aquaporin 1: Molecular Characteristics, Functions and Medical Implications. *Mol. Aspects Med.* 33, 518–534. doi:10.1016/j.mam.2012.06.001
- Benga, G. (2013). Comparative Studies of Water Permeability of Red Blood Cells from Humans and over 30 Animal Species: an Overview of 20 Years of Collaboration with Philip Kuchel. *Eur. Biophys. J.* 42, 33–46. doi:10.1007/s00249-012-0868-7
- Benga, I. (2021). Implications of Water Channel Proteins (Aquaporins and Relatives) in Epilepsies. *Stud. UBB Chem. LXVI*, 27–47.
- Brochard, F., and Lennou, J. F. (1975). Frequency Spectrum of the Flicker Phenomenon in Erythrocytes. *J. Phys. Fr.* 36, 1035–1047. doi:10.1051/jphys:0197500360110103500
- Brown, P. A., Feinstein, M. B., and Sha'afi, R. I. (1975). Membrane Proteins Related to Water Transport in Human Erythrocytes. *Nature* 254, 523–525. doi:10.1038/254523a0
- Conlon, T., and Outhred, R. (1972). Water Diffusion Permeability of Erythrocytes Using an NMR Technique. *Biochimica Biophysica Acta (BBA) - Biomembr.* 288, 354–361. doi:10.1016/0005-2736(72)90256-8
- Cox, G. (2014). Opinion Letters. *New Sci.* 30, 26.
- Cucuianu, M. (2006). The Discovery by Gh. Benga of the First Water Channel Protein in 1986 in Cluj-Napoca. *Rom. J. Intern. Med.* 44, 323–334.
- Dahm, R. (2005). Friedrich Miescher and the Discovery of DNA. *Dev. Biol.* 278, 274–288. doi:10.1016/j.ydbio.2004.11.028
- Davson, A., and Danielli, J. F. (1943). *The Permeability of Natural Membranes*. Cambridge: Cambridge University Press.
- De Robertis, E. D. P. (1970). *Cell Biology*. Philadelphia, London, Toronto: W. B. Saunders.
- Denker, B. M., Smith, B. L., Kuhajda, F. P., and Agre, P. (1988). Identification, Purification, and Partial Characterization of a Novel Mr 28,000 Integral Membrane Protein from Erythrocytes and Renal Tubules. *J. Biol. Chem.* 263, 15634–15642. doi:10.1016/s0021-9258(19)37635-5
- Fushimi, K., Uchida, S., Harat, Y., Hirata, Y., Marumo, F., and Sasaki, S. (1993). Cloning and Expression of Apical Membrane Water Channel of Rat Kidney Collecting Tubule. *Nature* 361, 549–552. doi:10.1038/361549a0
- Gonen, T., and Walz, T. (2006). The Structure of Aquaporins. *Quart. Rev. Biophys.* 39, 361–396. doi:10.1017/s0033583506004458
- Gorin, M. B., Yancey, S. B., Cline, J., Revel, J.-P., and Horwitz, J. (1984). The Major Intrinsic Protein (MIP) of the Bovine Lens Fibre Membrane: Characterization and Structure Based on cDNA Cloning and Membrane Characterization and Structure Based on a DNA Cloning. *Cell* 39, 49–59. doi:10.1016/0092-8674(84)90190-9
- Gorter, E., and Grendel, F. (1925). On Bimolecular Layers of Lipoids on the Chromocytes of the Blood. *J. Exp. Med.* 41, 439–443. doi:10.1084/jem.41.4.439
- Hajdu, S. I. (2003). The Discovery of Blood Cells. *Ann. Clin. Lab. Sci.* 33, 237–238.
- Haulică, I. (2006). A Regrettable Mistake in the Award of the 2003 Nobel Prize in Chemistry: the Omission of Gheorghe Benga, the First Discoverer of the First Water Channel Protein in the Red Blood Cell Membrane. *Cell. Mol. Biol. (Noisy-Le-Grand)* 52, 8–9.
- Heymann, J. B., and Engel, A. (1999). Aquaporins: Phylogeny, Structure, and Physiology of Water Channels. *Physiology* 14, 187–193. doi:10.1152/physiologyonline.1999.14.5.187
- His, W. (1897). *Die Histochemischen und Physiologischen Arbeiten von Friedrich Miescher*, I. Leipzig: F.C.W.Vogel.
- House, C. R. (1974). *Water Transport in Cells and Tissues*. London: Edward Arnold Publishers Ltd.
- Kuchel, P. W., and Benga, Gh. (2003). Why Is the Transmembrane Exchange of Water in the Red Blood Cell So Fast? *Bull. Mol. Med.* 15–16, 29–34.
- Kuchel, P. W., and Benga, G. (2005). Why Does the Mammalian Red Blood Cell Have Aquaporins? *Biosystems* 82, 189–196. doi:10.1016/j.biosystems.2005.07.002
- Kuchel, P. W. (2006). The Story of the Discovery of Aquaporins: Convergent Evolution of Ideas-But Who Got There First? *Cell Mol. Biol. (Noisy-le-grand)* 52, 2–5.
- Kummerow, F. A., Benga, Gh., and Holmes, R. P. (1983). *Biomembranes and Cell Function*, 414. New York: Annals of New York Academy of Sciences.
- Maurel, C., Reizer, J., Schroeder, J. I., and Chrispeels, M. J. (1993). The Vacuolar Membrane Protein Gamma-TIP Creates Water Specific Channels in Xenopus Oocytes. *EMBO J.* 12, 2241–2247. doi:10.1002/j.1460-2075.1993.tb05877.x
- Miescher, F. (1871). Ueber die chemische Zusammensetzung der Eiterzellen. *Med.-Chem. Unters.* 4, 441–460.
- Morariu, V. V., and Benga, G. Gh. (1977). Evaluation of a Nuclear Magnetic Resonance Technique for the Study of Water Exchange through Erythrocyte Membranes in Normal and Pathological Subjects. *Biochimica Biophysica Acta (BBA) - Biomembr.* 469, 301–310. doi:10.1016/0005-2736(77)90166-3
- Morariu, V. V., and Benga, G. (1984). “Water Diffusion through Erythrocyte Membranes in Normal and Pathological Subjects: Nuclear Magnetic Resonance Investigations,” in *Membrane Processes: Molecular Biology and Medical Applications*. Editors G. Benga, H. Baum, and F. A. Kummerow (New York: Springer-Verlag), 121–139. doi:10.1007/978-1-4613-8274-4_7
- Morariu, V. V., Chis, A. M., and Znamirovski, V. (1966). Fluctuations in Red Cell Membranes. *Cytobios* 86, 53–64.
- Morariu, V. V., Pop, V. I., Popescu, O., and Benga, G. (1981). Effects of Temperature and pH on the Water Exchange through Erythrocyte Membranes: Nuclear Magnetic Resonance Studies. *J. Membr. Biol.* 62, 1–5. doi:10.1007/bf01870194
- Plósz, P. (1871). Ueber das chemische Verhalten der Kerne der Vogel- und Schlangenblutkörperchen. *Med.-Chem. Unters.* 4, 461–462.
- Preston, G. M., Carroll, T. P., Guggino, W. B., and Agre, P. (1992). Appearance of Water Channels in Xenopus Oocytes Expressing Red Cell CHIP28 Protein. *Science* 256, 385–387. doi:10.1126/science.256.5055.385
- Schwoch, G., and Passow, H. (1973). Preparation and Properties of Human Erythrocyte Ghosts. *Mol. Cell Biochem.* 2, 197–218. doi:10.1007/BF01795474
- Sha'afi, R. I., and Feinstein, M. B. (1977). “Membrane Water Channels and SH-Groups,” in *Membrane Toxicity*. Editors M. V. Miller and A. E. Shamoo (New York: Plenum Press), 67–80.
- Singer, S. V., and Nicolson, G. L. (1972). The Fluid Mosaic Model for the Structure of Biological Membranes. *Science* 175, 720–731.
- Sperelakis, N. (2001). *Cell Physiology Sourcebook. A Molecular Approach*. Third edition. San Diego, London: Academic Press.
- Stein, W. (1986). *Transport and Diffusion across Cell Membranes*. London: Academic Press Inc. Ltd.
- Vandenberg, J. I., and Kuchel, P. W. (2003). Nobel Prizes for Magnetic Resonance Imaging and Channel Proteins. *Med. J. Aust.* 179, 611–613. doi:10.5694/j.1326-5377.2003.tb05718.x
- Wolburg, H., Wolburg-Buchholz, K., Fallier-Becker, P., Noell, S., and Mack, A. F. (2011). Structure and Functions of Aquaporin-4-Based Orthogonal Arrays of Particles. *Int. Rev. Cell. Mol. Biol.* 287, 1–41. doi:10.1016/b978-0-12-386043-9.00001-3
- Yang, B. (2017). “Aquaporins,” in *Advances in Experimental Medicine and Biology* (Dordrecht: Springer Science+Business Media B.V.).
- Zardoya, R. (2005). Phylogeny and Evolution of the Major Intrinsic Protein Family. *Biol. Cell* 97, 397–414. doi:10.1042/bc20040134
- Zeidel, M. L., Ambudkar, S. V., Smith, B. L., and Agre, P. (1992). Reconstitution of Functional Water Channels in Liposomes Containing Purified Red Cell CHIP28 Protein. *Biochemistry* 31, 7436–7440. doi:10.1021/bi00148a002

Conflict of Interest: The authors declare that the research was conducted in the absence of any commercial or financial relationships that could be construed as a potential conflict of interest.

Publisher's Note: All claims expressed in this article are solely those of the authors and do not necessarily represent those of their affiliated organizations, or those of the publisher, the editors and the reviewers. Any product that may be evaluated in this article, or claim that may be made by its manufacturer, is not guaranteed or endorsed by the publisher.

Copyright © 2022 Benga and Cox. This is an open-access article distributed under the terms of the Creative Commons Attribution License (CC BY). The use, distribution or reproduction in other forums is permitted, provided the original author(s) and the copyright owner(s) are credited and that the original publication in this journal is cited, in accordance with accepted academic practice. No use, distribution or reproduction is permitted which does not comply with these terms.



OPEN ACCESS

EDITED BY

Eitan Fibach,
Hadassah Medical Center, Israel

REVIEWED BY

Alessandro Matte',
University of Verona, Italy
Joanne Yacobovich,
Schneider Children's Medical Center,
Israel
Marianna H. Antonelou,
National and Kapodistrian University of
Athens, Greece

*CORRESPONDENCE

Carina Levin,
levin_c@cclalit.org.il,
Levincarina@gmail.com

[†]These authors have contributed equally
to this work

SPECIALTY SECTION

This article was submitted to Red Blood
Cell Physiology,
a section of the journal
Frontiers in Physiology

RECEIVED 17 October 2021

ACCEPTED 02 August 2022

PUBLISHED 29 August 2022

CITATION

Peretz S, Livshits L, Pretorius E,
Makhro A, Bogdanova A, Gassmann M,
Koren A and Levin C (2022), The
protective effect of the spleen in sickle
cell patients. A comparative study
between patients with asplenia/
hyposplenism and hypersplenism.
Front. Physiol. 13:796837.
doi: 10.3389/fphys.2022.796837

COPYRIGHT

© 2022 Peretz, Livshits, Pretorius,
Makhro, Bogdanova, Gassmann, Koren
and Levin. This is an open-access article
distributed under the terms of the
[Creative Commons Attribution License](#)
(CC BY). The use, distribution or
reproduction in other forums is
permitted, provided the original
author(s) and the copyright owner(s) are
credited and that the original
publication in this journal is cited, in
accordance with accepted academic
practice. No use, distribution or
reproduction is permitted which does
not comply with these terms.

The protective effect of the spleen in sickle cell patients. A comparative study between patients with asplenia/hyposplenism and hypersplenism

Sari Peretz^{1,2†}, Leonid Livshits^{1,3†}, Ethersia Pretorius⁴,
Asya Makhro³, Anna Bogdanova^{3,5}, Max Gassmann³,
Ariel Koren¹ and Carina Levin^{1,2*}

¹Pediatric Hematology Unit, Emek Medical Center, Afula, Israel, ²The Ruth and Bruce Rappaport Faculty of Medicine, Technion-Israel Institute of Technology, Haifa, Israel, ³Red Blood Cell Research Group, Vetsuisse Faculty, Institute of Veterinary Physiology, University of Zurich, Zürich, Switzerland, ⁴Department of Physiological Sciences, Faculty of Science, Stellenbosch University, Stellenbosch, South Africa, ⁵The Zurich Center for Integrative Human Physiology (ZIHP), Zürich, Switzerland

Sickle cell disease (SCD) is caused by a point mutation in the beta-globin gene. SCD is characterized by chronic hemolytic anemia, vaso-occlusive events leading to tissue ischemia, and progressive organ failure. Chronic inflammatory state is part of the pathophysiology of SCD. Patients with SCD have extremely variable phenotypes, from mild disease to severe complications including early age death. The spleen is commonly injured in SCD. Early splenic dysfunction and progressive spleen atrophy are common. Splenomegaly and hypersplenism can also occur with the loss of the crucial splenic function. Acute, life-threatening spleen-related complications in SCD are well studied. The association of laboratory parameters with the spleen status including hyposplenism, asplenia, and splenomegaly/hypersplenism, and their implication in vaso-occlusive crisis and long-term complications in SCD remain to be determined. We evaluated the association between the spleen status with clinical and laboratory parameters in 31 SCD patients: Group a) Patients with asplenia/hyposplenism (N = 22) (including auto-splenectomy and splenectomized patients) vs. Group b) patients with splenomegaly and or hypersplenism (N = 9). Laboratory studies included: Complete Blood Count, reticulocyte count, iron metabolism parameters, C Reactive Protein (CRP), Hb variant distribution, and D-dimer. Metabolic and morphological red blood cell (RBC) studies included: density gradient (by Percoll), glucose consumption, lactate release, and K⁺ leakage, fetal RBC (F-Cells) and F-Reticulocytes, annexinV+, CD71+, oxidative stress measured by GSH presence in RBC and finally Howell Jolly Bodies count were all analyzed by Flow Cytometry. Scanning electron microscopy analysis of RBC was also performed. Patients with asplenia/hyposplenism showed significantly higher WBC, platelet, Hematocrit, hemoglobin S, CRP, D-dimer, Gamma Glutamyl Transferase (GGT), cholesterol, transferrin, annexin V+ RBCs, CD71+ RBCs, together with a markedly lower F Reticulocyte levels in comparison with splenomegaly/hypersplenism patients. In summary, important differences were also found

between the groups in the studied RBCs parameters. Further studies are required to elucidate the effect of the spleen including hyper and hyposplenism on laboratory parameters and in clinical manifestations, vascular pathology, and long-term complications of SCD. The benefits and risks of splenectomy compared to chronic transfusion need to be evaluated in clinical trials and the standard approach managing hypersplenism in SCD patients should be re-evaluated.

KEYWORDS

hypersplenism, asplenia, fetal hemoglobin, reticulocytes, sickle cell disease, hyposplenism

Introduction

Sickle cell disease (SCD) is the most frequent worldwide hereditary hemoglobinopathy (Piel et al., 2013; Ware et al., 2017). The disorder is caused by the inheritance of abnormal beta-globin alleles carrying the sickle mutation on the HBB gene (HBB: c:20T>A- Glu6Val, β S). SCD results either by the homozygous state HbSS or by the combination of HbS with another abnormal HBB variants, mostly β^+ or β^0 thalassemia, both resulting in sickle red blood cells (RBC) (Bain 2008; Ware et al., 2017). Polymerization of deoxy-HbS generates abnormal dense and dehydrated RBC that play a central role in the acute and chronic manifestations of SCD. Intravascular sickling leads to impaired blood flow and vaso-occlusion with ischemic/reperfusion injury (Franceschi et al., 2011). Some organs, such as the spleen, are prone to be specifically vulnerable and damaged from HbS polymerization in SCD patients at early life (Platt 2000). Hyposplenism, asplenia, and progressive spleen atrophy (auto-splenectomy) are common. On the other hand, hypersplenism is characterized by an enlarged spleen (splenomegaly) which causes rapid and premature destruction of blood cells, resulting in thrombocytopenia, anemia, and or leukopenia, (Laws et al., 1979; Lv et al., 2016; Ladu et al., 2021). Splenomegaly and or hypersplenism can coexist with loss of function (Pearson 1969; O'Brien et al., 1976; Eichner 1979; Pearson et al., 1979; Serjeant et al., 1979; Zago et al., 1980; Brown et al., 1994).

In SCD, splenic dysfunction and hypersplenism are regularly observed during infancy; followed, in most cases, by spleen atrophy. In those cases, after repeated episodes of infarctions, the spleen is reduced to a fibrotic nodule (Diggs and Memphis 1935; Pearson et al., 1979). Another common and dangerous complication of SCD in young children is the sudden enlargement of the spleen defined as acute splenic sequestration crisis, associated with rapid decrease in hemoglobin levels of at least 2 g/dl, without signs of hemolysis (Leshner et al., 2009; Samuk et al., 2019).

Despite several postoperative complications, surgical splenectomy is recommended to treat the effects of

hypersplenism in SCD subjects (Emond et al., 1984; Kyaw et al., 2006; Leone and Pizzigallo 2015; Iolascon et al., 2017; Luu et al., 2019; Tahir et al., 2020; Yacobovich et al., 2020).

One of the indicators for splenic dysfunction is the presence of Howell-Jolly bodies (HJB) inside RBCs. HJB are DNA inclusions that are usually formed at low frequency. Normally RBC containing HJB are removed from the peripheral blood by the spleen. In SCD patients, with functional asplenia, HJB are present in a higher amount than in healthy individuals. In addition to complete blood count (CBC), the presence of HJB is used as a splenic dysfunction marker (Harrod et al., 2007; El Hoss et al., 2019). Those results can provide a fast evaluation of spleen status.

Maintenance of normal spleen function is crucial in the prevention of morbidity and mortality in SCD patients. Since the spleen is involved in immune response and the clearance of senescent and aberrant blood cells, noninvasive, quantitative, and qualitative measurements of spleens' function are required. In this study, we compared blood parameters and RBC properties of SCD patients and compared the results between SCD patients with asplenia, to patients with splenomegaly/hypersplenism. In addition, we implemented novel, non-routinely used methods for the evaluation of the functional status of the spleen in those patients.

Materials and methods

Patients

The study included 31 SCD patients treated at the Pediatric Hematology Unit, Emek Medical Center, (EMC), Afula, Israel. To get a better understanding of the spleen influence in SCD, the studied group was divided into two subgroups: patients with asplenia/hyposplenism [group (a)] which included patients with non-visualization of the spleen on ultrasound or no palpable spleen or patients after surgical total splenectomy. In this sub group we included young patients with splenic abnormal function and patients that probably underwent auto-splenectomy, both conditions well known in patients with SCD and patients that underwent surgical splenectomy. The

TABLE 1 Patients' characteristics. Demographic and clinical features of 31 SCD patients enrolled in this study and divided into two groups: Asplenia/hyposplenism and Hypersplenism. Events of VOC and hospitalizations presented here are per year prior to the study.

	Asplenia/hyposplenism <i>n</i> = 22	Hypersplenism <i>n</i> = 9
	Average \pm STD	Average \pm STD
Age (years)	25.1 \pm 12.9	16.8 \pm 10.3
Gender female/male	12/10	6/3
Hb SS Genotype	12	4
Hb S/ β Genotype	10	5
Splenectomized	7	—
Acute events VOC/study year ^a	10 (45%)	2 (22%)
Hospitalizations (admissions) ^b	14 (63%)	4 (44%)

^aVOC: Asplenia/hyposplenism- 10 events (1 patient had 3 crises, 2 patients had 2 crises and another 2 had one crisis each); hypersplenism- 2 events (1 patient had 2 crisis).

^bHospitalizations: Asplenia/hyposplenism- 14 events (2 patients had 3 hospitalizations, 2 patients had 2 hospitalizations and 4 patients had one hospitalization each); hypersplenism- 4 events (2 patients had 2 hospitalizations).

second group, [group (b)], included patients with splenomegaly and/or hypersplenism. This group included patients with an enlarged spleen, palpable by physical examination and/or detected by ultrasound, with or without cytopenias, persistent for more than 6 months of follow-up.

The asplenia/hyposplenism group (group a) included 22 patients: 12 females; mean age 25.1 \pm 12.9 years; 12 HbSS genotype and 9 HbS/ β -genotype [1- β^+ , 8- β^0 and another one probably β^0 based on High-performance liquid chromatography (HPLC) results], one HbS/D-genotype and seven patients after surgical total splenectomy. The hypersplenism group (group b) included 9 patients: 6 females; mean age 16.8 \pm 10.3 years (4 HbSS and 5 HbS/ β -genotype (4- β^0 and one- β^+), patient characteristics are presented in (Table 1). RBC membrane permeability and metabolic properties studied in 14 healthy individuals and, Percoll density gradients studied in 21 healthy individuals were used as control values for comparison with the results of the study groups.

All subjects were under stable doses of hydroxyurea treatment (500–2,000 mg/daily, 22.8 \pm 9.6 mg/kg with no significant differences between the cohorts). Any of the patients were receiving routine blood transfusions or sporadic blood transfusions for at least 3 months before the study's tests. Informed consent was obtained from all patients or their parents and the study received the approval of the local Helsinki Committee (Registry Nos. EMC-0071-17 and EMC-0120-17).

Laboratory tests

Patients' complete blood count (CBC) and blood biochemistry were analyzed on Advia2120 analyzer (SIEMENS, Germany) and AU5800 (Beckman Coulter, United States) and Clinical Chemistry Set-ups, respectively, at the EMC laboratory within 1 h after collection. High-

performance liquid chromatography (HPLC) analysis of hemoglobin variant distribution was performed by Variant II analyzer (BIO-RAD, United States). The presented normal ranges are as accepted at the EMC, if not indicated differently.

Separation on percoll density gradient levels

A whole blood sample was fractionated on a Percoll-based gradient as described (Makhro et al., 2013) with some modifications. Briefly, whole blood sample was layered over a Percoll solution (90% commercial Percoll (17-0891-01, GE Healthcare) and 10% of the concentrated plasma-like medium (1.4 M NaCl, 40 mM KCl, 7.5 mM MgSO₄, 100 mM glucose, 0.15 mM ZnCl₂, 2 mM Glycine, 2 mM Sodium Glutamate, 2 mM Alanine, 1 mM Arginine, 6 mM Glutamine, 1% BSA, 200 mM HEPES imidazole, pH 7.4) supplemented with 2 mM CaCl₂, and then centrifuged at 18,514 g for 60 min (minimal acceleration/deceleration) at 30°C (Eppendorf Centrifuge 5810R, F-34-6-38 Rotor supplemented with specific adapter for 15 ml Falcon tubes). Then, the distribution of blood components was captured by the 16 Mp camera (installed in the Samsung Galaxy S6 Model SM-G920F mobile phone (Samsung Electronics Co.) and further analyzed by the free Windows version of the ImageJ software (downloaded from <https://imagej.nih.gov/ij/download.html>). The total visualized fraction was divided to equal ten stations and the intensity of each subfraction was measured.

Glucose consumption, lactate release, and K⁺ leakage studies

Isolated RBC samples were incubated in the plasma-like medium (140 mM NaCl, 4 mM KCl, 0.75 mM MgSO₄, 10 mM

glucose, 0.015 mM ZnCl₂, 0.2 mM Glycine, 0.2 mM Sodium Glutamate, 0.2 mM Alanine, 0.1 mM Arginine, 0.6 mM Glutamine, 0.1% BSA, 20 mM HEPES imidazole, pH 7.4) supplemented with 2 mM CaCl₂ as described previously (Makhro et al., 2017) for 4 h at 37°C in gentle shake (14,000 rpm). The medium's concentrations of potassium, glucose, and lactate were measured prior (time 0 h s) and after incubation (4 h s) by GEM® Premier™ 4,000 blood gas analyzer. The 4 vs. 0 h s difference was normalized with total hemoglobin concentration measured simultaneously.

Red blood cells flow cytometry studies

Morphological characteristics of RBC and reticulocytes, phosphatidylserine (PS) exposure on outer membrane leaflet representing early apoptotic RBCs was measured by annexin V+ RBCs, intracellular Ca²⁺ and oxidative stress measured by reduced glutathione (GSH) levels in RBC were investigated by FC as described elsewhere (Kuypers et al., 1996; Kämpf et al., 2019). Briefly, 2 µl of whole blood suspended in a 1 ml plasma-like medium was loaded with 1.5 µl of either:

- Intracellular Ca²⁺ dye, Fluo-4 AM [1 mM stock, (Thermo Fisher Scientific)].
- GSH binding dye, monobromobimane (MBBR) (100 mM stock, Thermo Fisher Scientific).
- Anti-CD71-FITC (TfR) antibody (IQP-152F, IQ Products) for identification of reticulocyte fraction.
- eBioscience™ Annexin V Apoptosis Detection Kit eFluor 450 dye (Thermo Fisher Scientific) for PS externalization test.

The stained cells were incubated for 45 min in dark before FC measurements.

RBC sizes and morphology were examined in unstained samples.

In addition, the presence of DNA inclusions inside the RBCs, the Howell-Jolly bodies—HJB) (El Hoss et al., 2018) and fetal RBC (F-Cells), F Reticulocytes (representing early changes in HbF cells), were also examined using FC. HbF and F-Cells are used to monitor SCD patients' response to Hydroxyurea treatment and to evaluate their chances to suffer from SCD-related complications (Lebman et al., 1982; Kono et al., 2009; Sato et al., 2010).

In brief, 20 µl of whole blood in an EDTA tube fixed in 1 ml of 25% glutaraldehyde solution (Sigma, United States) for 10 min. Immediately after fixation, 100 µl of the suspension was permeabilized in a new tube by resuspension in 400 µl of 0.1% TRITON X-100 (Sigma, United States) for 4 min. Following permeabilization, 20 µl of the suspension was taken in a new tube with 5 µl of 5 µM Hoechst 33342 (Sigma, United States), 5 µl 7-AAD (7-amino-actinomycin D) (Invitrogen, United States), 5 µl anti CD71 (transferrin receptor) APC conjugate (Invitrogen,

United States), 5 µl intercellular anti-human fetal Hb (MHFH01) FITC conjugate (Life technologies, United States) and 70 µl PBS. After vortex and dark incubation for 15 min, 400 µl of PBS was added and gentle vortex before FC measurement.

The fluorescence intensity was measured on RBC gate using Navios EX flow cytometer (Beckman Coulter, United States). Double measurements (>50,000 total cells/measurement) were performed and averaged for each condition. All data were analyzed using Kaluza Analysis Software (Beckman Coulter, United States <https://www.beckman.co.il/flow-cytometry/software/kaluza>).

Scanning electron microscopy imaging of blood components

10 µl of whole blood was pipetted into a 10 mm round glass microscope cover slip and dried for 2 min at room temperature. The glass microscope cover slips were placed in a 24-well culture flask for further washing; PBS was added and removed after 15 min. Next, 4% formaldehyde was added to the sample for fixation for a minimum of 30 min. After three washes with PBS one drop of osmium tetra-oxide (OT) (Sigma, United States) was added directly onto the cover slip and then covered with dH₂O for 15 min. Right after, the samples were washed three times with PBS for 3 min each wash. Next, dehydration was performed by a series of Ethanol-dH₂O mixtures (30%, 50%, 70%, 90%, and finally 100%) for 3 min. The last wash with 100% ethanol was repeated twice. At this stage, the well plate was sealed with parafilm, and the samples were stored for 24–48 h. Next, the samples were covered with 99.9% hexamethyldisilazane (HMDS) (Sigma, United States) for 30 min. Then, the open plate was left overnight to evaporate HMDS. The prepared samples were coated with carbon and viewed with a Zeiss MERLIN field emission-SEM with the InLens detector using 1 kV (Carl Zeiss Microscopy, Munich, Germany).

Statistics

Data for the entire study was analyzed using GraphPad 5 software. Differences between SCD patients with Asplenia/hyposplenism vs. Hypersplenism were tested using the Mann-Whitney test. For all analyses, a two-tailed test with $p < 0.05$ was accepted as statistically significant.

Results

Patient laboratory characteristics

Comparison of the CBC and biochemistry parameters revealed significant differences between hypersplenic and asplenic/hyposplenic SCD subjects (Table 2).

TABLE 2 CBC and biochemistry parameters in asplenic/hyposplenic compared to hypersplenic SCD subjects. Normal ranges are presented in accordance with the criteria accepted by the EMC Lab divisions. The data is presented as average \pm Standard Deviation (SD); Significance was calculated using the two-tailed Mann-Whitney as $p < 0.05$. WBC, White blood count, ANC, Absolute Neutrophil count, ALC, Absolute lymphocyte count, AMC, Absolute monocyte count, AEC, Absolute eosinophil count, ABC, Absolute basophil count, Hb, Hemoglobin, HCT, Hematocrit, Hypo, Hypochromic Red Cells, PLT, Platelet, RET: Reticulocyte, HbF, Fetal hemoglobin, HbS, S hemoglobin, LDH, Lactic dehydrogenase, GGT, Gamma Glutamyl Transferase, CRP, C reactive protein. RBC, Red blood cells.

Parameter (Units)	Normal range	Asplenia/Hyposplenism $n = 22^a$	Hypersplenism $n = 9^a$	p -value
WBC (K/ μ l)	4.5–11.5	10.06 \pm 3.568	4.674 \pm 2.093	0.0002
ANC (K/ μ l)	1.5–6	5.526 \pm 2.416	2.486 \pm 1.007	0.0005
ALC (K/ μ l)	1.5–6	3.160 \pm 1.193	1.719 \pm 0.987	0.0031
AMC (K/ μ l)	0.1–0.8	0.705 \pm 0.536	0.237 \pm 0.213	0.0005
AEC (K/ μ l)	0–0.8	0.287 \pm 0.168	0.090 \pm 0.038	0.0009
ABC (K/ μ l)	0–0.2	0.078 \pm 0.044	0.017 \pm 0.017	0.0001
Hb (g/dl)	M:14–17; F: 12–15	9.718 \pm 1.279	8.006 \pm 0.949	0.0025
HCT (%)	M: 40–54; F: 37–47	29.83 \pm 3.968	25.02 \pm 2.508	0.0036
Hypo (%)	0–2.5	6.609 \pm 5.471	12.70 \pm 6.968	0.0313
PLT K/ μ l	150–450	501.2 \pm 194.3	156.2 \pm 54.48	<0.0001
RET absolute (K/ μ l)	20–100	208.0 \pm 86.37 (19)	181.1 \pm 88.87 (9)	ns
HbF (%)	0.5–1.5	17.67 \pm 7.185	22.26 \pm 8.156	ns
HbS (%)	0	71.42 \pm 11.01	59.87 \pm 12.54	0.0124
D-Dimer (ng/ml)	0–500	1451 \pm 990.4 (14)	439.2 \pm 83.17 (5)	0.0014
Albumin (g/dl)	3.5–5.2	4.328 \pm 0.310 (21)	4.131 \pm 0.168 (9)	0.0374
LDH (U/L)	230–480	783.6 \pm 353.2	937.0 \pm 325.8	ns
Cholesterol (mg/dl)	<200	120.2 \pm 23.16 (21)	83.28 \pm 12.54 (9)	0.0004
GGT: (U/L)	M:0–55; F: 0–38	58.60 \pm 73.04 (16)	9.944 \pm 2.698 (5)	0.0028
Serum Potassium (mM/dl)	3.5–5.1	4.318 \pm 0.286	3.868 \pm 0.230	0.0006
Serum Calcium (mM/dl)	8.5–10.5	9.468 \pm 0.3737	9.148 \pm 0.1905	0.0066
Ferritin (ng/ml)	M:22–322; F: 10–291	579.1 \pm 644.1	960.9 \pm 1065	ns
Serum iron (μ g/dl)	M:60–160; F: 40–145	103.8 \pm 64.14	68.53 \pm 29.12	ns
Transferrin (mg/dl)	200–360	240.9 \pm 44.47 (17)	183.8 \pm 23.92 (4)	0.0224
CRP (mg/dl)	0.00–0.50	1.445 \pm 1.986 (20)	0.371 \pm 0.341 (9)	0.0360

^aNumber of patients studied when not all the patients in this group were analyzed.

We found a significantly lower hematocrit and hemoglobin levels (approximately 2 g/dl reduction) in the hypersplenism vs. asplenia/hyposplenism group ($p < 0.05$) that was accompanied by an almost two-fold increase in the percentage of hypochromic RBC in the hypersplenism group ($p = 0.03$).

Lower white blood cell (WBC) and platelet counts were found in the hypersplenism group compared to the asplenia/hyposplenism group ($p < 0.001$), similarly to all the subsets of leukocytes (Table 2). The mean percent of HbF was higher in the hypersplenism group (an increase of 5%) but this difference was not significant. The mean percent of HbS was significantly lower in hypersplenism compared with the asplenia/hyposplenism group ($p = 0.01$).

The D-Dimer was significantly lower in the hypersplenism group but within the normal range, while in the asplenia/hyposplenism was increased ($p < 0.05$).

Serum Lactic dehydrogenase (LDH) levels were elevated in both groups, representing the chronic hemolytic state, with no

differences between the groups (Table 2). Serum albumin, cholesterol, calcium, and potassium levels were within normal values in both groups but were significantly lower in the hypersplenism than in the asplenia/hyposplenism group ($p = 0.05$).

The CRP levels, representing the inflammation state, were within the normal range in the hypersplenism group, while in the asplenia/hyposplenism group were abnormally increased ($p < 0.05$).

No significant differences between the groups were found in ferritin and serum iron, however, the transferrin level was lower in the hypersplenism group ($p < 0.05$).

Metabolic and morphological characteristics of red blood cells

To specify the RBCs-related differences between the groups, blood samples were fractionated on Percoll density gradient as

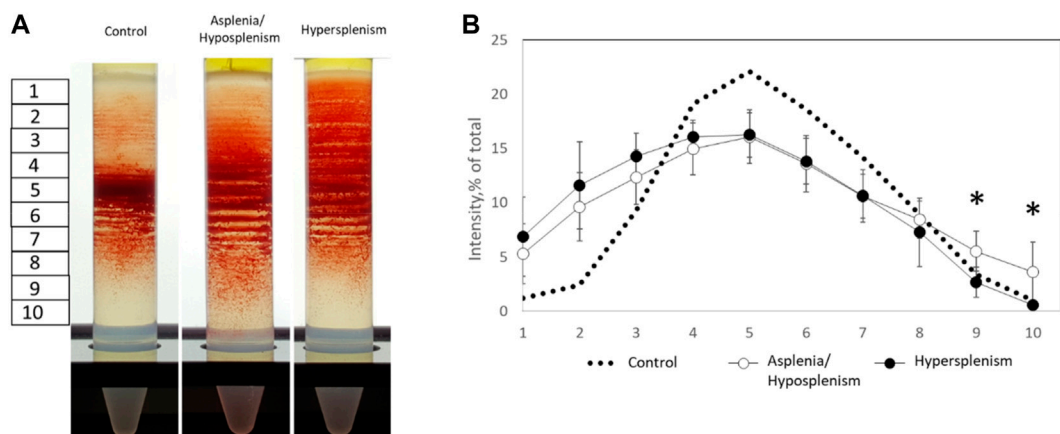


FIGURE 1
Percoll density gradients of control and SCD subjects for dense and hydrated RBC fractions. **(A)** Representative Percoll gradients for control, asplenic/hyposplenic, and hypersplenic subjects are demonstrated. **(B)** The RBC content in each station was estimated as a percentage from a sum of all sub-fraction intensity values. The correspondent examination of RBCs obtained from control subjects ($n = 21$; 10M/11F; 46.8 ± 14.2 years) was made. The data is presented in average \pm SD; the significance is < 0.05 .

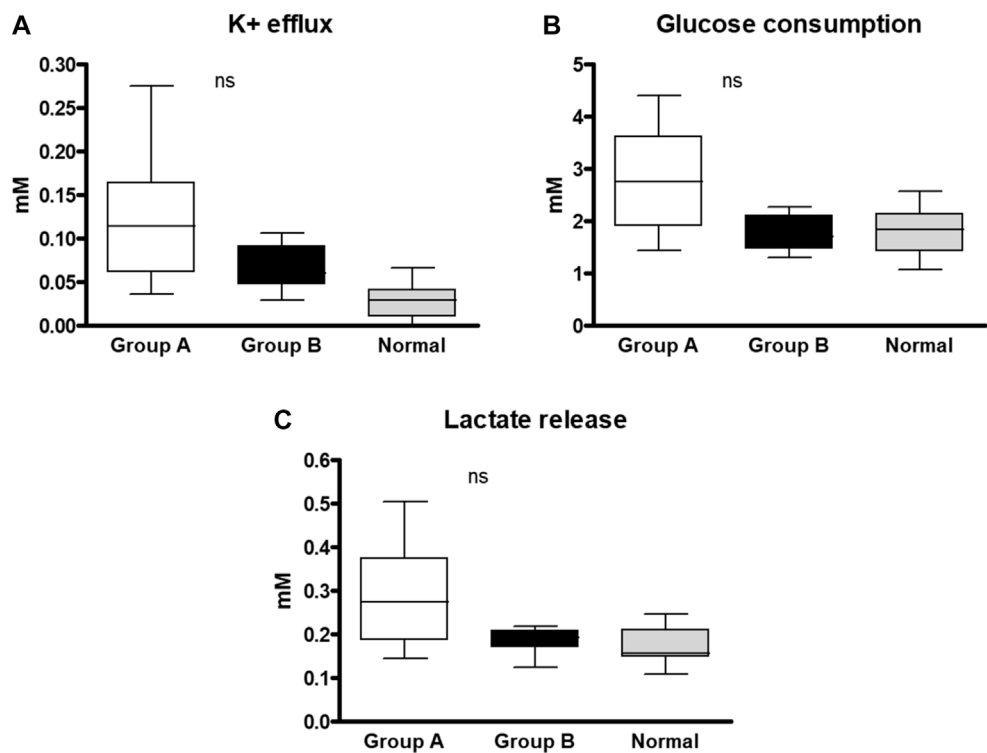


FIGURE 2
RBC membrane permeability and metabolic properties of SCD subjects and healthy control. Samples of each group were incubated for 4 h in a plasma-like medium and examined for: **(A)** K⁺ efflux, **(B)** Glucose consumption, and **(C)** Lactate release. The 4 vs. 0 h difference was normalized with total hemoglobin concentration. The correspondent examination of RBCs obtained from control subjects ($n = 14$; 8M/6F; 34.1 ± 16.1 years) was made. The data is presented in average \pm SD; the significance is < 0.05 . Group (A) patients with asplenia/hyposplenism, Group (B) patients with hypersplenism.

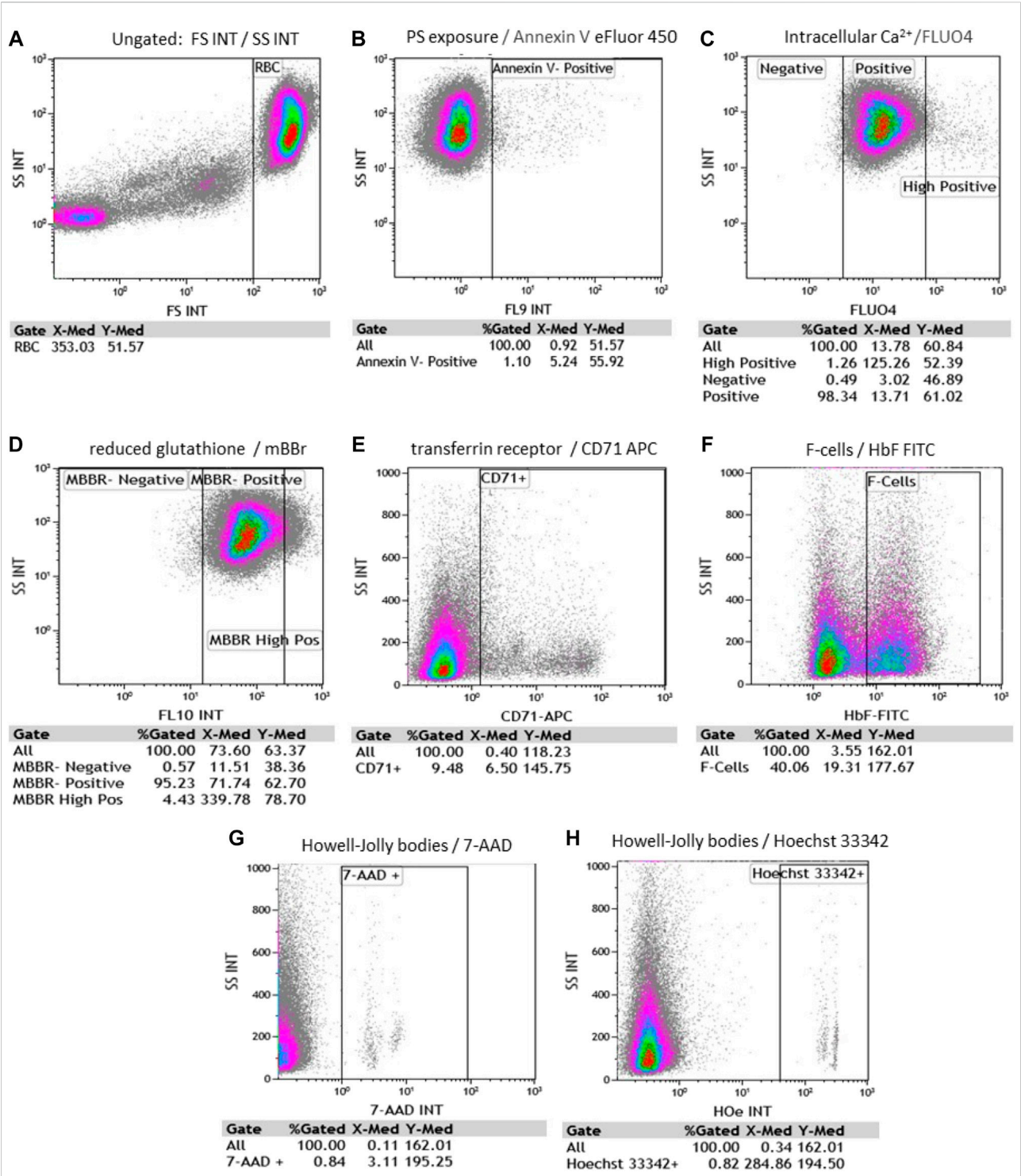


FIGURE 3 Representative flow cytometry scatter plots and gating strategy for RBC. Each evaluates % gated cells and median fluorescence intensity (MFI). (A) RBC side and forward scattering of unstained cells (SS and FS, accordingly); (B) Annexin V-positive RBC; (C) fluo-4 positive and fluo-4 high-positive RBC; (D) MBBR-positive and MBBR high-positive RBC; (E) CD71 positive RBC; (F) F- RBC (F-cells) positive fraction (G) 7-AAD (7-amino-actinomycin D) positive RBC and (H) Hoechst 33342 positive RBC. [(B–H) plots were all gated on RBC].

described. We found a significant reduction of dense/senescent RBC fractions (lower stations 9 and 10) in the hypersplenism compared with the asplenia/hyposplenism group. This demonstrates that the hypersplenism group contains more hydrated and less dense/dehydrated and sickled RBCs when compared to the asplenia/hyposplenism group (Figure 1).

Our next target was to study RBC membrane permeability and metabolic properties (Figure 2). We found no significant difference in the RBCs membrane permeability between the two groups measured by K^+ leak and lactate released from RBCs. Also, the RBCs glucose consumption was similar in the two groups, however, the values in the hypersplenism group were lower than in the asplenia/hyposplenism group and approximates to normal values of healthy controls.

Red blood cells flow cytometry characteristics and percentage HbF by high-performance liquid chromatography

Using FC, we evaluated RBC and reticulocytes morphological characteristics, phosphatidylserine (PS) exposure on outer membrane leaflet, intracellular Ca^{2+} , oxidative stress measured by reduced glutathione (GSH), reticulocytes identification, F- cells, and HJB levels. Representative scatter plots and gating strategy for RBC were shown for all fluorophores (Figure 3).

Side scatter (SSC) and forward scatter (FSC) median fluorescence intensity (MFI) of unstained RBC were 55.39 ± 5.6 and 399.6 ± 39.64 ; respectively in the hypersplenism group. and 64.29 ± 6.24 and 407.3 ± 45.89 ; respectively in the asplenia/hyposplenism group.

We found a lower percentage of Annexin V+ RBCs, in the hypersplenism group compared to the results in the asplenia/hyposplenism group (mean $0.34 \pm 0.2\%$ vs. $0.82 \pm 0.5\%$ respectively, $p = 0.05$). We also found lower, but not statistically significant, RBC intracellular Ca^{2+} levels as measured by fluo-4-high-positive RBCs, in the hypersplenism group compared to asplenia/hyposplenism (mean % 0.63 ± 0.3 vs. 1.63 ± 0.95 ; respectively $p = ns$. and MFI 96.56 ± 10.48 vs. 87.73 ± 44.88 ; respectively $p = ns$). Additionally, we observed decreased trend of MBRR-high-positive RBC in the hypersplenism group vs. the asplenia/hyposplenism group (mean % 0.97 ± 0.49 vs. 1.75 ± 0.93 ; respectively $p = ns$ and MFI 356.66 ± 95.49 vs. 495.37 ± 107.81 ; respectively $p = ns$). Also, the total MBRR positive population MFI was lower in the hypersplenism group vs. the asplenia/hyposplenism group (mean MFI 68.23 ± 22.79 vs. 103.61 ± 28.04 ; respectively $p = 0.04$) (Figure 4).

We found that the percent of immature RBCs CD71⁺, reticulocytes expressing the transferrin receptor on the cell surface was lower in the hypersplenism vs. asplenia/

hyposplenism group (mean % 1.5 ± 0.4 vs. 4.2 ± 2.1 ; respectively, $p = 0.013$). These results correlate with a decreased trend in total reticulocyte count in the CBC in the hypersplenism group (Figure 4).

We found a higher, but not statistically significant, level of HbF measured by HPLC in the hypersplenism group compared to asplenia/hyposplenism (mean HbF % 22.26 ± 8.15 vs. 17.67 ± 7.18 ; respectively $p = ns$) (Table 2), and percent of F-Cells measured by FC (Mean % 64.01 ± 19 vs. 52.77 ± 20 ; respectively $p = ns$). We show a positive correlation between these two parameters (Spearman, $r = 0.8457$) (Figure 5). Since reticulocytes circulate in the peripheral blood for 7 days, the calculation of F- reticulocyte can serve as a unique and important value for patient's follow-up and treatment response. We found significantly higher F-reticulocyte counts in the hypersplenism compared to the asplenia/hyposplenism group (mean 33.2 ± 14.1 vs. $55.1 \pm 12.6\%$; respectively $p = 0.011$) (Figure 5).

Splenic dysfunction examined by the presence of HJB in the RBCs using FC revealed, as expected, a significantly lower count of HJB in the hypersplenism group compared to asplenia/hyposplenism patients in both nucleotides' dyes; Hoechst 33342 and 7-AAD (0.27 ± 0.2 and 0.26 ± 0.2 vs. 0.43 ± 0.2 and 0.43 ± 0.2 respectively $p = 0.01$) (Figure 6).

Representative SEM images of RBCs from healthy and SCD subjects were shown including sickle shape RBC and RBCs with fibrin clot net in a patient with asplenia (Figure 7).

Discussion

The spleen has several functions including clearance of damaged blood cells and antibodies production (Lewis et al., 2019). On the one hand, SCD patients without a spleen suffer from the presence of damaged RBC which can increase the risk of vaso-occlusive crises and overwhelming severe bacterial infections (el Hoss and Brousse, 2019). On the other hand, the negative consequences of hypersplenism are associated with the increased clearance of blood cells and blood-borne antigens, leading to cytopenia and some degree of immunodeficiency caused by the leukopenia (Brousse et al., 2014). Excessive destruction of RBCs in SCD children with prolonged hypersplenism may lead to subsequent growth impairment and bone marrow hyperplasia. Also, transfusion efficiency is usually reduced in SCD patients with hypersplenism (Laws et al., 1979; Lv et al., 2016; Ladu et al., 2021). One of the targets of our study was to use simple tests to monitor spleen status in SCD patients. For example, the use of DNA dyes and the easy handling FC method can serve as a good alternative for HJB count, instead of a labore microscope examination.

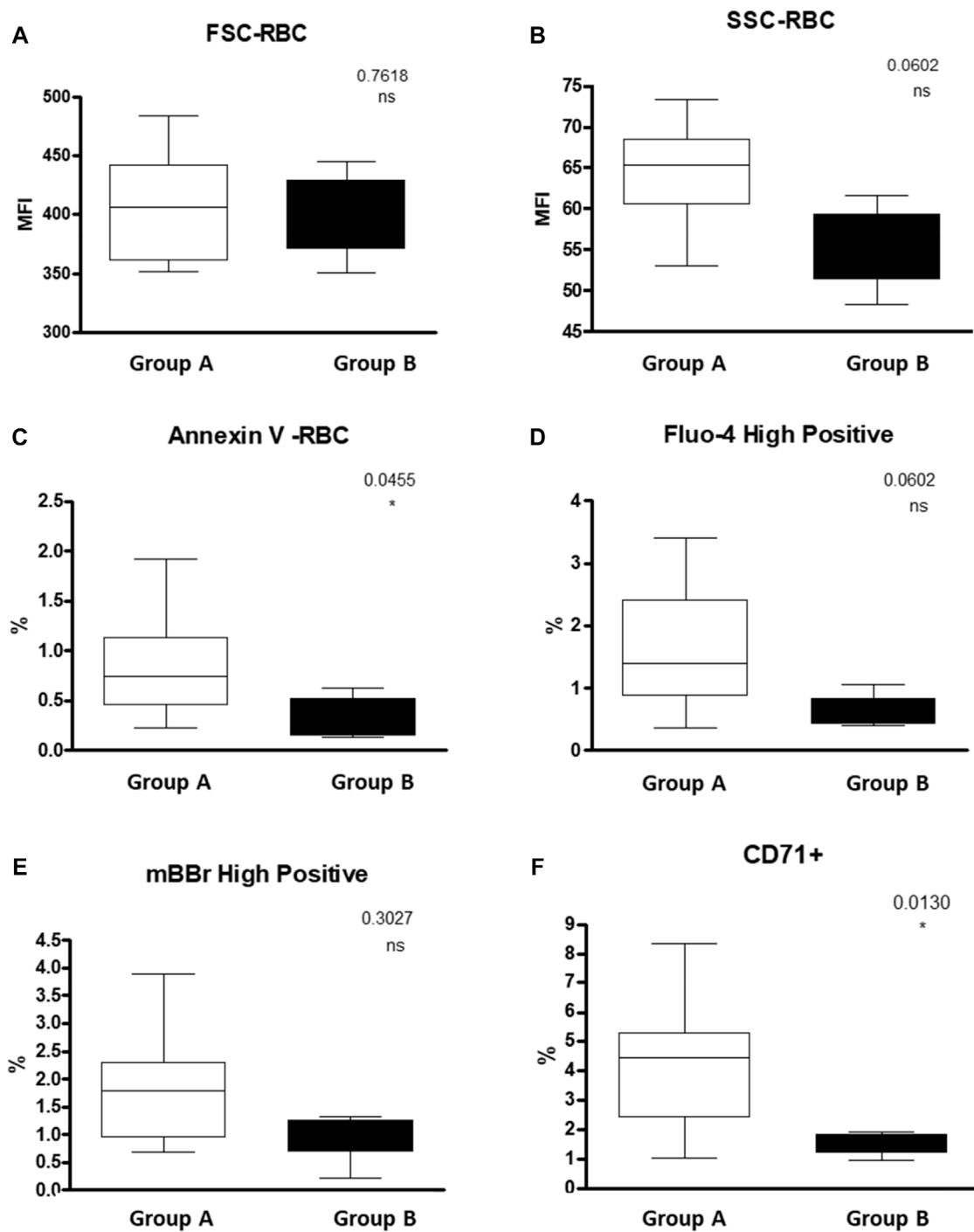


FIGURE 4

RBC properties of SCD patients Asplenic/hyposplenic compared to Hypersplenic using Flow cytometry: (A) + (B) FSC and SSC of RBC; (C) Annexin V positive RBC; (D) fluo-4 high-positive RBC; (E) MBBR high-positive RBC; (F) CD71 positive RBC. Group (A) patients with asplenia/hyposplenism, Group (B) patients with hypersplenism.

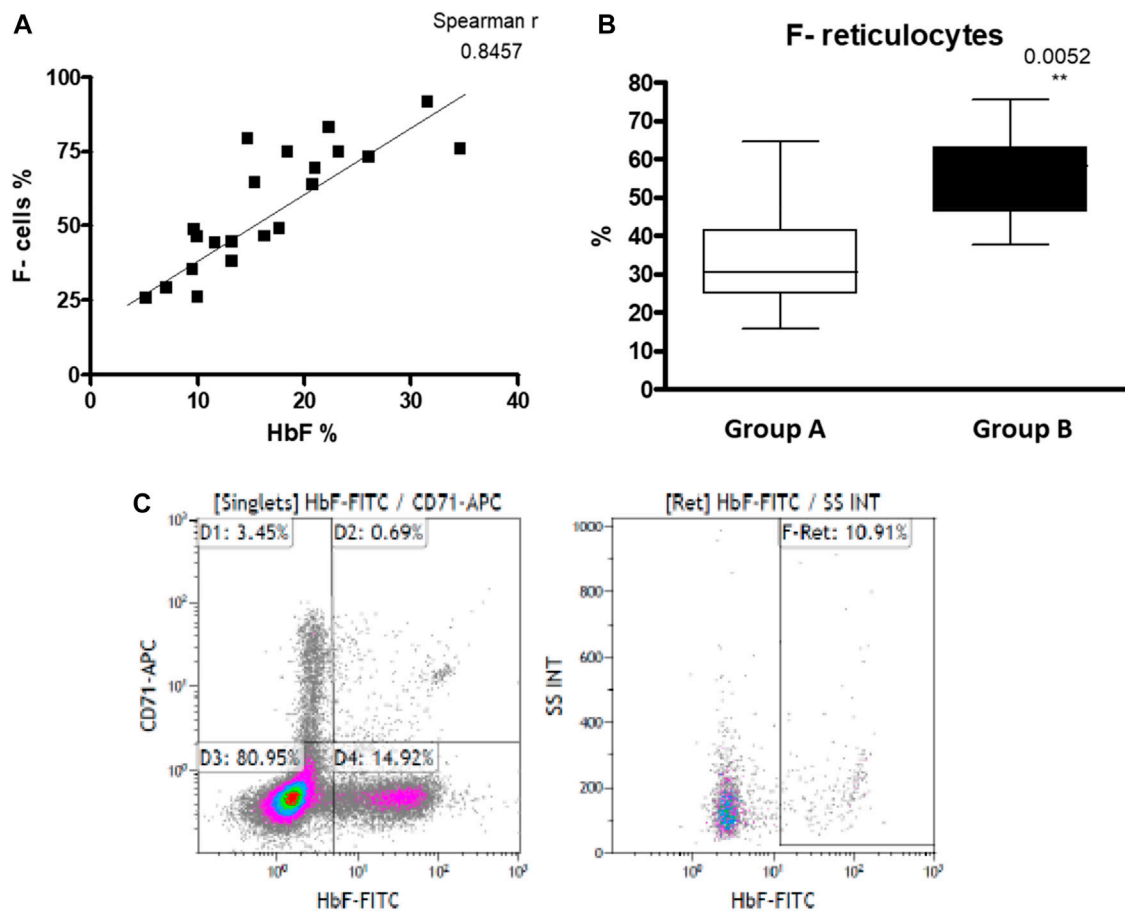


FIGURE 5

HbF in RBC of SCD patients: (A) HbF measured by HPLC and F- cells measured by FC positively correlates ($n = 21$). (B) F- reticulocytes count in asplenic/hyposplenic ($n = 14$) vs. hypersplenic ($n = 7$) SCD subjects. (C) representative FC gating strategy for F- Reticulocytes. Group (A) patients with asplenia/hyposplenism, Group (B) patients with hypersplenism.

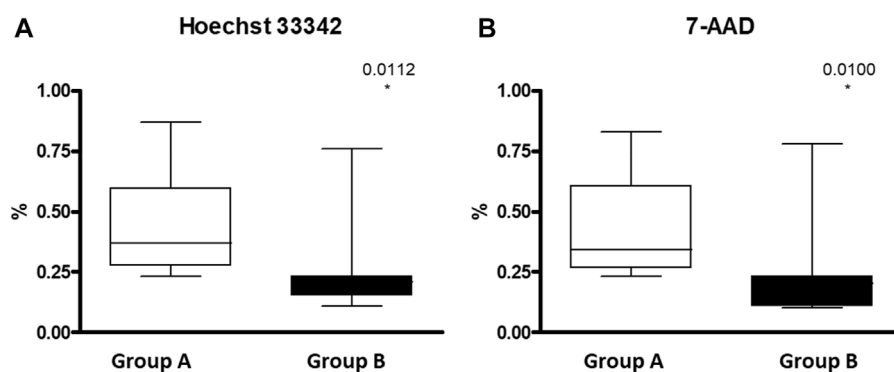
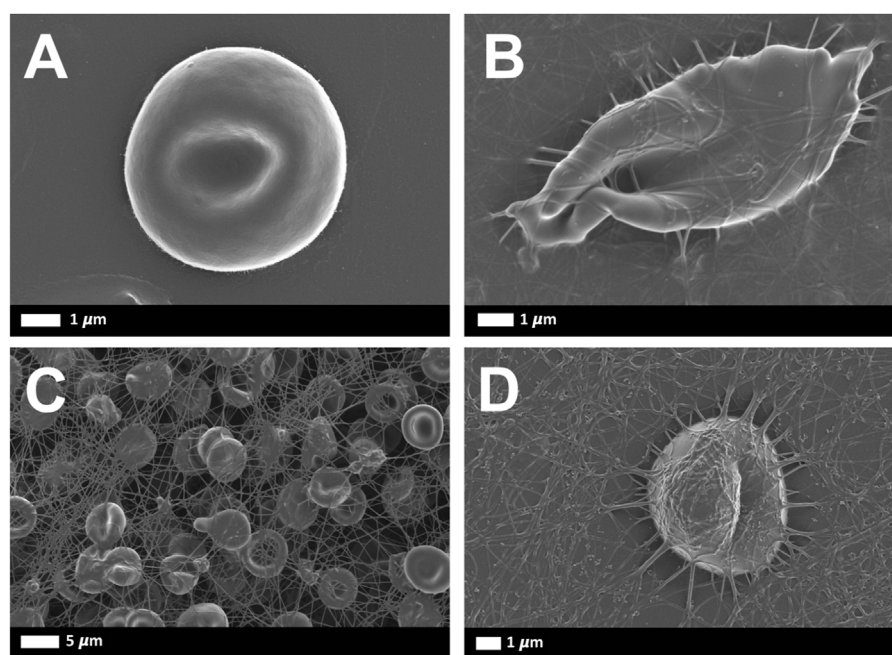


FIGURE 6

HJB inside RBC measured by FC in asplenic/hyposplenic vs. hypersplenic SCD subjects: (A) Hoechst 33342 for A and T nucleotides and (B) 7-AAD (7-amino-actinomycin D) for C and G nucleotides. Group (A) patients with asplenia/hyposplenism, ($n = 13$). Group (B) patients with hypersplenism, ($n = 7$).

**FIGURE 7**

Representative scanning electron microscopy images of RBCs from healthy and SCD subjects: (A) Representative RBC from a healthy individual (B) Sick RBC, (C) RBCs with fibrin net (D) single RBC with fibrin net that spontaneously formed.

Laboratory tests

The findings of the low Hb, HCT total WBC, WBC subtypes, and platelets in the hypersplenism group can be explained by spleen clearance of blood cells. On the other hand, the relative thrombocytosis in the asplenia/hyposplenism group is related to the lack of platelet clearance by the absent or nonfunctional spleen. Our results related to the blood cells counts confirm most of the previously reported data (al-Salem et al., 1996; Fasola and Adekanmi 2019; el Hoss and Brousse, 2019).

Lower percent of HbS in hypersplenism group compared with the asplenia/hyposplenism group, is probably related to the more effective clearance of sickled RBC by the spleen (Brousse et al., 2014). It is well known that the HbS content and the percentage of HbF are the main modulators of clinical severity in SCD, and even small changes in sickle RBCs hemoglobin composition may reduce or delay polymerization with great significance on clinical manifestations (Hebert et al., 2020). The slightly higher mean percent of HbF and the F-Cells in the hypersplenism group suggest less Hb polymerization.

Chronic inflammatory state that is part of the pathophysiology of the SCD (Adekile 2013), we observed increased acute-phase reactant proteins in patients with non-functional spleen, the asplenia/hyposplenism group. Among those findings we can mention the higher D Dimer the lower transferrin that are common in anemia of chronic diseases

(Costa et al., 2008), and the higher and abnormally elevated CRP and ferritin levels all observed in the asplenia/hyposplenism group.

Also, the high abnormal D-Dimer that we found in the asplenia/hyposplenism group probably indicated a prothrombotic state and not only a marker of inflammation. It is known that in a healthy individual, the main clotting plasma protein, fibrinogen, is in a soluble state. In those subjects' fibrin network formation can be induced if thrombin is added to whole blood (Palta et al., 2014). Fibrin deposits that form without the addition of thrombin are only noted during pathological clotting (Lipinski et al., 2012). However, in the presence of circulating inflammatory molecules, in inflammatory conditions, the plasma proteins may be induced to form spontaneous fibrin networks, without the presence of thrombin. Since SCD is a chronic inflammatory state, fibrin production can be spontaneously seen (Figures 7C,D). Hypercoagulation and clotting pathologies are well-known accompaniments to inflammatory conditions (Pretorius et al., 2017; Olumuyiwa-Akeredolu et al., 2019; Randeria et al., 2019).

In the current study, we observed normal electrolyte values in our SCD patients, however, the serum potassium and calcium were lower in the hypersplenism group compared to the asplenia/hyposplenism, group probably reflecting reduced intravascular hemolysis. The increase in serum potassium has been described

in sickle cell patients, with higher levels during an acute crisis (Pandey et al., 2012; Mansoor et al., 2021). In addition to an increased release caused by the chronic hemolysis, serum K^+ abnormalities may be related to the status of hydration, the degree of acidosis during acute events, abnormalities in renal function, and alterations in RBCs ion transporting systems. Some of these RBCs systems such as the Gardos channel, K-Cl cotransporter, and the Na/K pump are directly involved in the maintenance of RBC hydration; their increased activity contributes to RBC dehydration in SCD subjects (Vitoux et al., 1989; Gibson et al., 1998; Izumo et al., 1987; Luthra and Sears 1982; Hannemann et al., 2015).

Separation on percoll density gradient levels

Percoll density gradient was used as an indication of RBCs dehydration-rehydration state (Hänggi et al., 2014). The reduction of dense/senescent RBC fractions observed in patients with hypersplenism compared with the asplenia/hyposplenism group demonstrates that the hypersplenism group contains more hydrated and less sickled RBCs; which can be considered a beneficial effect related to increased clearance of abnormal RBCs by the spleen.

Red blood cells flow cytometry studies: Oxidative stress

Nicotinamide adenine dinucleotide (NAD) is a ubiquitous oxidation-reduction (redox) cofactor in RBCs. The synthesis of NAD and its reduced form, NADH, play major roles in maintaining redox balance (Zerez et al., 1988). Sick RBCs have a lower redox ratio $[(NADH):(NAD^+ + NADH)]$ than normal RBCs. Increased reduced glutathione (GSH) availability can decrease oxidative stress status and potentially reduce sickled RBC (Niihara et al., 2018). MBBR interaction with GSH forms a highly fluorescent derivative detected by FC. Here we showed decreased MBBR-high-positive RBC both percentage and MFI in the hypersplenism group compared with the asplenia/hyposplenism group. These results were contrary to what we expected and to the literature. One of our study limitations is the low sample size in both groups. We believe that increasing the sample size can reveal more genuinely the MBBR results and then facilitate explaining those facts. In addition, since reticulocytes contain increased amounts of reduced glutathione than mature RBC (Roth et al., 1979) and we found a 3-fold increase of reticulocytes count in the asplenia/hyposplenism group compared to hypersplenism, we hypothesize that the clearance of reticulocyte by the spleen of hypersplenic patients may have led to decreased MBBR-high-positive RBC which also included reticulocytes.

Red blood cells flow cytometry studies: Morphology

Regarding the results of the flow cytometry analysis, as previously done (Warang et al., 2011; More et al., 2020), we used SSC and FSC values to assess the RBCs size.

Here we observed an interesting tendency for the RBC hypochromia and a decrease in RBC side scatter value, in patients with hypersplenism compared with the asplenia/hyposplenism group. This suggests on the one hand a reduced number of sickled and hyperchromic RBCs. And on the other hand, less senescent RBCs, normally removed by the spleen, appear to be selectively cleared by the spleen in patients with hypersplenism (Girasole et al., 2012).

This is in line with the significantly lower number of early apoptotic RBCs (annexin V+) in this patient group. Additionally, we show that these morphological changes appear in view of the decrease in the dense RBCs at lower fractions of Percoll density gradient separation as well as with a decrease in the number of RBCs high-positive intracellular Ca^{2+} concentrations. These findings confirm the previously reported data of higher intracellular Ca^{2+} content in dense RBCs than in light RBC fractions (Romero et al. 1997). Furthermore, such an increase of RBCs with elevated Ca^{2+} may be directly connected with the correspondent increase in PS-exposing erythrocytes as shown by Wesseling (Wesseling et al., 2016).

Normally, PS is confined to the cytoplasmic RBC membrane leaflet, PS external expression represents a signal for clearance and early apoptosis of RBCs, known to be increased in SC RBCs (Hannemann et al., 2018; Thiagarajan et al., 2021; Anke). In accordance with the known evidence that PS externalization is realized by the scramblase activated by an increase of intracellular Ca^{2+} content (Wesseling et al., 2016), we demonstrate a lower percent of RBCs with abnormal elevated intracellular Ca^{2+} together with a significant reduction in annexin V + RBCs in hypersplenic subjects.

The fluctuation in intracellular Ca^{2+} and the increased externalization of PS in RBCs may also contribute to hypercoagulability and the pathological clotting that was noted in the SEM analysis (Figure 7) (Hood et al., 2018; Swieringa et al., 2018; Toorn et al., 2019).

Red blood cells flow cytometry studies: F-cells

Another parameter used to monitor the severity and drug treatment response in SCD patients is the HbF level analyzed by HPLC, or the F-Cells measured by FC. Hydroxyurea (HU) treatment for SCD patients leads to an increase in HbF and the number of F-Cells RBC concomitant with the improvement of clinical symptoms (Hebert et al., 2020). Hydroxyurea is a safe and effective treatment for SCD, however a proportion of SCA

patients are not responding to HU treatment (Pule et al., 2015), in any case, it is important to evaluate patient's response to this treatment, titrate the dosage and prevent unnecessary overdose. It is known that the clinical response to HU treatment can be evident a few days after treatment initiation and on the opposite sudden stop of HU can provoke an acute pain crisis long before the HbF level drops (Pule et al., 2015).

Measurement of F Reticulocytes using FC, after a few days of HU treatment, will provide a fast understanding of each patient's response to HU treatment instead of the routinely used HbF measurement analyzed by HPLC, which shows HbF changes usually after 3–4 months (Steinberg et al., 2014). In our study, we found that F Reticulocytes count was significantly higher in hypersplenic subjects compared to asplenia/hyposplenism. We found that the percent of immature RBCs CD71⁺, reticulocytes expressing the transferrin receptor on the cell surface was lower in the hypersplenism vs. asplenia/hyposplenism group. These results correlate with a decreased trend in total reticulocyte count in the CBC suggesting an accelerated maturation of reticulocytes in hypersplenic subjects and less hemolysis (Lebman et al., 1982; Kono et al., 2009). The impact of the number of circulating reticulocytes as well as its influence on sickling and oxidative stress mechanism in SCD patients need further research.

In patients with functional spleen and hypersplenism the enhanced clearance of sickled RBC (especially due to its pathological morphological and rheological properties), together with the specific slow and open microcirculation in the spleen provides the best platform to favor deoxygenation, promoting RBC sickling and subsequent, accelerating RBC destruction (Brousse et al., 2014). Thus, despite the improvement in RBC rheology and metabolism, these features may be counteracted with aggravation of the anemia and anemia-related complications.

One of the study limitations is the relatively small number of patients studied and more than that this fact did not allow comparison inside each subgroup. In addition, the results of our study should be compared with other clinical parameters like age and clinical severity. The patients with hypersplenism are younger than the patients with asplenia/hyposplenism but they are in the second decade of age, beyond the age when usually asplenia develops in SCD patients. We also suggest, that in the future, a study that will use the power of electron microscopy at single cell level, to make a robust comparative RBCs morphological evaluation of asplenia/hyposplenism vs hypersplenism.

In conclusion, in addition to the known laboratory manifestations of hypersplenism such as severe pancytopenia, our results show some significant "beneficial" laboratory findings including lower HbS, CRP, and D-dimmer values and lower morphological and metabolic pathological properties of the RBCs. The results of this study may provide other tools to define more precisely the spleen function in SCD patients. Given our results, it is extremely important to make any efforts to preserve the spleen in patients with SCD and

preserve the immunological and hematological functions including the eradication of abnormal and senescent blood cells. New treatments should be focused on the prevention of functional asplenia and hypersplenism and avoid performing surgical splenectomy.

The benefits and risks of total splenectomy compared to chronic transfusion need to be evaluated in clinical trials and the standard approach to managing hypersplenism in SCD patients should be re-evaluated.

Data availability statement

The original contributions presented in the study are included in the article/Supplementary Material, further inquiries can be directed to the corresponding author.

Ethics statement

The studies involving human participants were reviewed and approved by the EMC Emek Medical Center Local Helsinki Committee. Written informed consent to participate in this study was provided by the participants' legal guardian/next of kin.

Author contributions

CL, AK, and MG contributed to the conception and design of the study. AK and CL treated and recruited the patients, and obtained the samples for the study, SP, LL, and EP performed the experiments; SP and LL organized the database and performed the statistical analysis. SP and LL wrote the first draft of the manuscript. AM, AB, and EP wrote sections of the manuscript. All authors contributed to manuscript revision, read, and approved the submitted version.

Acknowledgments

This project was partially funded by the Fondation Botnar as well as by the Baugarten Stiftung, Susanne & René Braginsky Stiftung and Ernst Göhner Stiftung and the Israeli Ministry for Development of the Negev and the Galilee. The authors thank the staff of Emek Medical Center's Hematology Laboratory Division for their technical help.

Conflict of interest

The authors declare that the research was conducted in the absence of any commercial or financial relationships that could be construed as a potential conflict of interest.

Publisher's note

All claims expressed in this article are solely those of the authors and do not necessarily represent those of their affiliated

organizations, or those of the publisher, the editors and the reviewers. Any product that may be evaluated in this article, or claim that may be made by its manufacturer, is not guaranteed or endorsed by the publisher.

References

- Adekile, A. D. (2013). What's new in the pathophysiology of sickle cell disease? *Med. Princ. Pract. Health Sci. Centre* 22, 311–312. doi:10.1159/0003502834
- al-Salem, A. H., Qaisaruddin, S., Nasserallah, Z., al Dabbous, I., and al Jam'a, A. (1996). Splenectomy in patients with sickle-cell disease. *Am. J. Surg.* 172 (3), 254–258. doi:10.1016/S0002-9610(96)00158-4
- Bain, B. J. (2008). *Haemoglobinopathy diagnosis. Hemoglobin and the genetic of hemoglobin synthesis*. Chapter 1 2nd Edition. John Wiley & Sons. Blackwell Publishing Ltd. 2nd ed. John Wiley & Sons. Blackwell publishing Ltd.
- Brousse, V., Buffet, P., and Rees, D. (2014). The spleen and sickle cell disease: The sick(led) spleen. *Br. J. Haematol.* 166 (2), 165–176. doi:10.1111/bjh.12950
- Brown, A. K., Sleeper, L. A., Miller, S. T., Pegelow, C. H., Gill, F. M., and Waclawiw, M. A. (1994). Reference values and hematologic changes from birth to 5 Years in patients with sickle cell disease. Cooperative study of sickle cell disease. *Arch. Pediatr. Adolesc. Med.* 148 (8), 796–804. doi:10.1001/archpedi.1994.02170080026005
- Costa, E., Rocha, S., Rocha-Pereira, P., Reis, F., Teixeira, F., Miranda, V., et al. (2008). Cross-talk between inflammation, coagulation/fibrinolysis and vascular access in hemodialysis patients. *J. Vasc. Access* 9 (4), 248–253. doi:10.1177/112972980800900405
- Diggs, L. W., and Memphis, Tenn (1935). Siderofibrosis of the spleen in sickle cell anemia. *J. Am. Med. Assoc.* 104, 538–541. doi:10.1001/jama.1935.02760070020005
- Eichner, E. R. (1979). Splenic function: Normal, too much and too little. *Am. J. Med.* 66 (2), 311–320. doi:10.1016/0002-9343(79)90554-0
- El Hoss, S., Cochet, S., Marin, M., Lapoumeroulie, C., Dussiot, M., et al. (2019). Insights into determinants of spleen injury in sickle cell anemia. *Blood Adv.* 3 (15), 2328–2336. doi:10.1182/bloodadvances.2019000106
- El Hoss, S., Dussiot, M., Renaud, O., Brousse, V., and El Nemer, W. (2018). A novel non-invasive method to measure splenic filtration function in humans. *Haematologica* 103 (10), e436–39. doi:10.3324/haematol.2018.188920
- Emond, A. M., Morais, P., Venugopal, S., Carpenter, R. G., and Serjeant, G. R. (1984). Role of splenectomy in homozygous sickle cell disease in childhood. *Lancet (London, Engl.)* 1 (8368), 88–91. doi:10.1016/s0140-6736(84)90014-x
- Fasola, F. A., and Adekanmi, A. J. (2019). Haematological profile And blood transfusion pattern of patients with sickle cell anaemia vary with spleen size. *Ann. Ib. Postgrad. Med.* 17 (1), 30
- Franceschi, Lucia de, Domenica Cappellini, Maria, and Olivieri, Oliviero (2011). Thrombosis and sickle cell disease. *Semin. Thromb. Hemost.* 37 (3), 226–236. doi:10.1055/s-0031-1273087
- Gibson, J. S., Speake, P. F., and Ellory, J. C. (1998). Differential oxygen sensitivity of the K⁺-Cl⁻ cotransporter in normal and sickle human red blood cells. *J. Physiol.* 511, 225–234. doi:10.1111/j.1469-7793.1998.225b1.x
- Girasole, M., Dinarelli, S., and Boumis, G. (2012). Structural, morphological and nanomechanical characterisation of intermediate states in the ageing of erythrocytes. *J. Mol. Recognit.* 25 (5), 285–291. doi:10.1002/jmr.2170
- Hänggi, P., Makhro, A., Gassmann, M., Schmugge, M., Goede, J. S., Speer, O., et al. (2014). Red blood cells of sickle cell disease patients exhibit abnormally high abundance of N-methyl D-aspartate receptors mediating excessive calcium uptake. *Br. J. Haematol.* 167 (2), 252–264. doi:10.1111/bjh.13028
- Hannemann, A., Rees, D. C., Tewari, S., and Gibson, J. S. (2015). Cation homeostasis in red cells from patients with sickle cell disease heterologous for HbS and HbC (HbSC genotype). *EBioMedicine* 2 (11), 1669–1676. doi:10.1016/j.ebiom.2015.09.026
- Hannemann, A., Rees, D. C., Brewin, J. N., Noe, A., Low, B., and Gibson, J. S. (2018). Oxidative stress and phosphatidylserine exposure in red cells from patients with sickle cell anaemia. *Br. J. Haematol.* 182 (4), 567–578. doi:10.1111/bjh.15441
- Harrod, V. L., Howard, T. A., Zimmerman, S. A., Dertinger, S. D., and RussellWare, E. (2007). Quantitative analysis of howell-jolly bodies in children with sickle cell disease. *Exp. Hematol.* 35 (2), 179–183. doi:10.1016/j.exphem.2006.09.013
- Hebert, N., Rakotoson, M. G., Bodivit, G., Audureau, E., Bencheikh, L., Kiger, L., et al. (2020). Individual red blood cell fetal hemoglobin quantification allows to determine protective thresholds in sickle cell disease. *Am. J. Hematol.* 95 (11), 1235–1245. doi:10.1002/ajh.25937
- Hood, J. E., Yesudasan, S., and Averett, R. (2018). Glucose concentration affects fibrin clot structure and morphology as evidenced by fluorescence imaging and molecular simulations. *Clin. Appl. Thromb. Hemost.* 24, 104S–116S–116S. doi:10.1177/1076029618792304
- el Hoss, S., and Brousse, V. (2019). Considering the spleen in sickle cell disease. *Expert Rev. Hematol.* 12 (7), 563–573. doi:10.1080/17474086.2019.1627192
- Iolascon, A., Andolfo, I., Barcellini, W., Corcione, F., Garçon, L., de Franceschi, L., et al. (2017). Recommendations regarding splenectomy in hereditary hemolytic anemias. *Haematologica* 102 (8), 1304–1313. doi:10.3324/haematol.2016.161166
- Izumo, H., Lear, S., Williams, M., Rosa, R., and Epstein, F. H. (1987). Sodium-potassium pump, ion fluxes, and cellular dehydration in sickle cell anemia. *J. Clin. Invest.* 79 (6), 1621–1628. doi:10.1172/JCI112998
- Kämpf, S., Seiler, E., Bujok, J., Hofmann-Lehmann, R., Riond, B., Makhro, A., et al. (2019). Aging markers in equine red blood cells. *Front. Physiol.* 10, 893. doi:10.3389/fphys.2019.00893
- Kono, M., Kondo, T., Takagi, Y., Wada, A., and Fujimoto, K. (2009). Morphological definition of CD71 positive reticulocytes by various staining techniques and electron microscopy compared to reticulocytes detected by an automated Hematology analyzer. *Clin. Chim. Acta.* 404 (2), 105–110. doi:10.1016/j.cca.2009.03.017
- Kuypers, F. A., Lewis, R. A., Hua, M., Schott, M. A., Discher, D., Ernst, J. D., et al. (1996). Detection of altered membrane phospholipid asymmetry in subpopulations of human red blood cells using fluorescently labeled annexin V. *Blood* 87 (3), 1179–1187. doi:10.1182/blood.v87.3.1179.bloodjournal8731179
- Kyaw, M. H., Holmes, E. M., Toolis, F., Wayne, B., Chalmers, J., Jones, I. G., et al. (2006). Evaluation of severe infection and survival after splenectomy. *Am. J. Med.* 119 (3), 276e1–e7. doi:10.1016/j.amjmed.2005.07.044
- Ladu, A. I., O Ayienigba, A., Adekunle, A., and Bates, I. (2021). The spectrum of splenic complications in patients with sickle cell disease in africa: A systematic review. *Br. J. Haematol.* 193 (1), 26–42. doi:10.1111/bjh.17179
- Laws, H. L., Burlingame, M. W., Carpenter, J. T., Prchal, J. T., and Conrad, M. E. (1979). Splenectomy for hematologic disease. *Surg. Gynecol. Obstet.* 149 (4), 509
- Lebman, D., Trucco, M., Bottero, L., Lange, B., Pessano, S., and Rovera, G. (1982). A monoclonal antibody that detects expression of transferrin receptor in human erythroid precursor cells. *Blood* 59 (3), 671–678. doi:10.1182/blood.v59.3.671.bloodjournal593671
- Leone, G., and Pizzigallo, E. (2015). Bacterial infections following splenectomy for malignant and nonmalignant hematologic diseases. *Mediterr. J. Hematol. Infect. Dis.* 7 (1), e2015057–e21. doi:10.4084/MJHID.2015.057
- Leshner, A. P., Ram, K., Glenn, J. B., Jackson, S. M., and Andre, H. (2009). Outcome of splenectomy in children younger than 4 Years with sickle cell disease. *J. Pediatr. Surg.* 44 (6), 1134–1138. doi:10.1016/j.jpedsurg.2009.02.016
- Lewis, S. M., Williams, A., and Eisenbarth, S. C. (2019). Structure and function of the immune system in the spleen. *Sci. Immunol.* 4 (33), eaau6085. doi:10.1126/sciimmunol.aau6085
- Lipinski, B., Pretorius, E., Oberholzer, H. M., and J van der Spuy, W. (2012). Interaction of fibrin with red blood cells: The role of iron. *Ultrastruct. Pathol.* 36 (2), 79–84. doi:10.3109/01913123.2011.627491
- Luthra, M. G., and Sears, D. A. (1982). Increased Ca⁺⁺, Mg⁺⁺, and Na⁺ + K⁺ ATPase activities in erythrocytes of sickle cell anemia. *Blood* 60 (6), 1332–1336. doi:10.1182/blood.v60.6.1332.bloodjournal6061332
- Luu, S., Spelman, D., and Woolley, I. J. (2019). Post-splenectomy sepsis: Preventative strategies, challenges, and solutions. *Infect. Drug Resist.* 12, 2839–2851. doi:10.2147/IDR.S179902
- Lv, Y., Lau, W. Y., Li, Y., Deng, J., Han, X., Gong, X., et al. (2016). Hypersplenism: History and current status. *Exp. Ther. Med.* 12 (4), 2377–2382. doi:10.3892/etm.2016.3683

- Makhro, A., Kaestner, L., and Anna, B. (2017). NMDA receptor activity in circulating red blood cells: Methods of detection. *Methods Mol. Biol.* 1677, 265–282. doi:10.1007/978-1-4939-7321-7_15
- Makhro, A., Pascal, H., Goede, J. S., Wang, J., Brüggemann, A., Gassmann, M., et al. (2013). N-Methyl-D-Aspartate receptors in human erythroid precursor cells and in circulating red blood cells contribute to the intracellular calcium regulation. *Am. J. Physiol. Cell Physiol.* 305 (11), c1123–38. doi:10.1152/ajpcell.00031.2013
- Mansoor, F., Bai, P., Kaur, N., Sultan, S., Sharma, S., Dilip, A., et al. (2021). Evaluation of serum electrolyte levels in patients with anemia. *Cureus* 13 (10), e18417. doi:10.7759/cureus.18417
- More, T. A., Dalal, B., Devendra, R., Warang, P., Shankarkumar, A., and Kedar, P. (2020). Applications of imaging flow cytometry in the diagnostic assessment of red cell membrane disorders. *Cytom. B Clin. Cytom.* 98 (3), 238–249. doi:10.1002/cyto.b.21857
- Niihara, Y., ScottMiller, T., Kanter, J., Lanzkron, S., Smith, W. R., Hsu, L. L., et al. (2018). A phase 3 trial of L-glutamine in sickle cell disease. *N. Engl. J. Med.* 379 (3), 226–235. doi:10.1056/NEJMoa1715971
- O'Brien, R. T., Sue McIntosh, G. T. A., Pearson, H. A., and Pearson, H. A. (1976). Prospective study of sickle cell anemia in infancy. *J. Pediatr.* 89 (2), 205–210. doi:10.1016/S0022-3476(76)80449-0
- Olumuyiwa-Akeredolu, O. O., Page, M. J., Soma, P., and Pretorius, E. (2019). Platelets: Emerging facilitators of cellular crosstalk in rheumatoid arthritis. *Nat. Rev. Rheumatol.* 15 (4), 237–248. doi:10.1038/s41584-019-0187-9
- Palta, S., Saroa, R., and Anshu, P. (2014). Overview of the coagulation system. *Indian J. Anaesth.* 58 (5), 515–523. doi:10.4103/0019-5049.144643
- Pandey, S., Sharma, A., Dahia, S., Shah, V., Sharma, V., Mishra, R. M., et al. (2012). Biochemical indicator of sickle cell disease: Preliminary report from India. *Indian J. Clin. biochem.* 27 (2), 191–195. doi:10.1007/s12291-011-0162-y
- Pearson, H. A., McIntosh, S., Ritchey, A. K., Lobel, J. S., Rooks, Y., and Johnston, D. (1979). Developmental aspects of splenic function in sickle cell diseases. *Blood* 53 (3), 358–365. doi:10.1182/blood.v53.3.358.358
- Pearson, H. A., Spencer, R. P., and Cornelius, E. A. (1969). Functional asplenia in sickle-cell anemia. *N. Engl. J. Med.* 281 (17), 923–926. doi:10.1056/NEJM196910232811703
- Piel, F. B., Hay, S. I., Gupta, S., Weatherall, D. J., and Williams, T. N. (2013). Global burden of sickle cell anaemia in children under five, 2010–2050: Modelling based on demographics, excess mortality, and interventions. *PLoS Med.* 10 (7), e1001484. doi:10.1371/journal.pmed.1001484
- Platt, O. S. (2000). The acute chest syndrome of sickle cell disease. *N. Engl. J. Med.* 342 (25), 1904–1907. doi:10.1056/NEJM200006223422510
- Pretorius, E., Swanepoel, A. C., DeVilliers, S., and Bester, J. (2017). Blood clot parameters: Thromboelastography and scanning electron microscopy in research and clinical practice. *Thromb. Res.* 154, 59–63. doi:10.1016/j.thromres.2017.04.005
- Pule, G. D., Mowla, S., Novitzky, N., Wysong, C. S., and Ambrose, W. (2015). A systematic review of known mechanisms of hydroxyurea-induced fetal hemoglobin for treatment of sickle cell disease. *Expert Rev. Hematol.* 8 (5), 669–679. doi:10.1586/17474086.2015.1078235
- Randeria, Shehan N., Thomson, Greig J. A., Timothy Roberts, Theo A. Nell, Pretorius, Etheresia, and Pretorius, E. (2019). Inflammatory cytokines in type 2 diabetes mellitus as facilitators of hypercoagulation and abnormal clot formation. *Cardiovasc. Diabetol.* 18 (1), 72. doi:10.1186/s12933-019-0870-9
- Romero, P. J., Romero, E. A., and Winkler, M. D. (1997). Ionic calcium content of light dense human red cells separated by Percoll density gradients. *Biochim. Biophys. Acta* 1323 (1), 23–28. doi:10.1016/s0005-2736(96)00141-1
- Roth, E. F., Grossman, H. A. H. T., and Nagel, R. L. (1979). Reticulocytes contain increased amounts of reduced glutathione except when produced by acetylphenylhydrazine. *Biochem. Med.* 21 (3), 333–341. doi:10.1016/0006-2944(79)90087-5
- Samuk, I., Seguer-Lipszyc, E., Baazov, A., Tamary, H., Nahum, E., Steinberg, R., et al. (2019). Emergency or urgent splenectomy in children for non-traumatic reasons. *Eur. J. Pediatr.* 178 (9), 1363–1367. doi:10.1007/s00431-019-03424-6
- Sato, S., Kozuma, Y., Hasegawa, Y., Kojima, H., Chiba, S., and Ninomiya, H. (2010). Enhanced expression of CD71, transferrin receptor, on immature reticulocytes in patients with paroxysmal nocturnal hemoglobinuria. *Int. J. Lab. Hematol.* 32, e137–43. doi:10.1111/j.1751-553X.2009.01148.x
- Serjeant, G. R., Sommereux, A. M., Stevenson, M., Mason, K., and Serjeant, B. E. (1979). Comparison of sickle cell-beta0 thalassaemia with homozygous sickle cell disease. *Br. J. Haematol.* 41 (1), 83–93. doi:10.1111/j.1365-2141.1979.tb03684.x
- Steinberg, M. H., Chui, D. H. K., GeorgeDover, J., Paola, S., and Alsultan, A. (2014). Fetal hemoglobin in sickle cell anemia: A glass half full? *Blood* 123 (4), 481–485. doi:10.1182/blood-2013-09-528067
- Swieringa, F., Spronk, H. M. H., Heemskerk, J. W. M., and van der Meijden, Paola E. J. (2018). Integrating platelet and coagulation activation in fibrin clot formation. *Res. Pract. Thromb. Haemost.* 2 (3), 450–460. doi:10.1002/rth2.12107
- Tahir, F., Ahmed, J., and Malik, F. (2020). Post-splenectomy sepsis: A review of the literature. *Cureus* 12 (2), e6898. doi:10.7759/cureus.6898
- Thiagarajan, P., Parker, C. J., and JosefPrchal, T. (2021). How do red blood cells die? *Front. Physiol.* 12, 655393. doi:10.3389/fphys.2021.655393
- Toorn, F. A. v. d., de Mutsert, R., WillemLijfering, M., FritsRosendaal, R., and Vlieg, A. v. H. (2019). Glucose metabolism affects coagulation factors: The NEO study. *J. Thromb. Haemost.* 17 (11), 1886–1897. doi:10.1111/jth.14573
- Vitoux, D., Olivieri, O., Garayt, R. P., Cragoe, E. J., Galacteros, F., and Beuzard, Y. (1989). Inhibition of K⁺ efflux and dehydration of sickle cells by [(dihydroindenyl) oxy]alkanoic acid: An inhibitor of the K⁺ Cl⁻ cotransport system. *Proc. Natl. Acad. Sci. U. S. A.* 86, 4273–4276. doi:10.1073/pnas.86.11.4273
- Warang, P., Gupta, M., Kedar, P., Ghosh, K., and Colah, R. (2011). Flow cytometric osmotic fragility—an effective screening approach for red cell membranopathies. *Cytom. B Clin. Cytom.* 80 (3), 186–190. doi:10.1002/cyto.b.20583
- Ware, R. E., de Montalembert, M., Tshilolo, L., and Abboud, M. R. (2017). Sickle cell disease. *Lancet (London, Engl.)* 390 (10091), 311–323. doi:10.1016/S0140-6736(17)30193-9
- Wesseling, M. C., Wagner-Britz, L., Huppert, H., Benjamin, H., Hertz, L., Nguyen, D. B., et al. (2016). Phosphatidylserine exposure in human red blood cells depending on cell age. *Cell. Physiol. Biochem.* 38 (4), 1376–1390. doi:10.1159/000443081
- Yacobovich, J., Barzilai-Birenboim, S., Steinberg-Shemer, O., Stark, P., Pazgal, I., and Tamary, H. (2020). Splenectomy in childhood for non-malignant hematologic disorders - long-term follow-up shows minimal adverse effects. *Br. J. Haematol.* 190 (6), 909–915. doi:10.1111/bjh.16657
- Zago, M. A., Costa, F. F., Freitas, T. C., and Bottura, C. (1980). Clinical, hematological and genetic features of sickle-cell anemia and sickle cell-beta thalassemia in a Brazilian population. *Clin. Genet.* 18 (1), 58–64. doi:10.1111/j.1399-0004.1980.tb01366.x
- Zerez, C. R., Lachant, N. A., Lee, S. J., and Tanaka, K. R. (1988). Decreased erythrocyte nicotinamide adenine dinucleotide redox potential and abnormal pyridine nucleotide content in sickle cell disease. *Blood* 71 (2), 512–515. doi:10.1182/blood.v71.2.512.bloodjournal712512

Frontiers in Physiology

Understanding how an organism's components work together to maintain a healthy state

The second most-cited physiology journal, promoting a multidisciplinary approach to the physiology of living systems - from the subcellular and molecular domains to the intact organism and its interaction with the environment.

Discover the latest Research Topics

[See more →](#)

Frontiers

Avenue du Tribunal-Fédéral 34
1005 Lausanne, Switzerland
frontiersin.org

Contact us

+41 (0)21 510 17 00
frontiersin.org/about/contact

